

# Rothamsted Repository Download

## F - Theses

Nitnavare, R. 2023. *Physiological and genetic variation in Nitrogen Use Efficiency of wheat*. F - Theses Rothamsted Research Sustainable Crops and Soils

The output can be accessed at:

<https://repository.rothamsted.ac.uk/item/991z7/physiological-and-genetic-variation-in-nitrogen-use-efficiency-of-wheat>.

© Please contact [library@rothamsted.ac.uk](mailto:library@rothamsted.ac.uk) for copyright queries.

# Physiological and genetic variation in Nitrogen Use Efficiency of wheat



**Rahul Nitnavare**

Thesis submitted to the University of Nottingham for the degree of  
*Doctor of Philosophy*

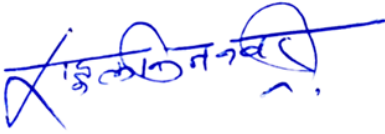
**July 2023**

Division of Plant and Crop Sciences  
School of Biosciences, University of Nottingham  
Sutton Bonington Campus  
LE12 5RD, UK

## Declaration

I hereby declare that the research work presented in this thesis, entitled "Identifying novel variation in Nitrogen Use Efficiency and its physiological and genetic basis in wheat", has been carried out by me at University of Nottingham and Rothamsted Research, UK under the supervision of Prof Malcolm Hawkesford and Dr John Foulkes. The work is composed solely by me no part of the thesis has been submitted, in whole or in part, earlier for any other degree of any University.

**Date:** 27<sup>th</sup> July 2023



**Rahul B Nitnavare**

## **Acknowledgements**

*I would like to express my sincere gratitude to my supervisor Prof Malcom Hawkesford, Discovery Leader, Rothamsted Research for giving me an opportunity to work with him and encouraging me to explore new avenues in research.*

*I am grateful to my University supervisor, Dr John Foulkes, Associate Professor, Division of Plant and Crop Sciences for teaching me basics of field plant physiology, statistics, and wheat field experiments.*

*Both have been always instrumental in advising me on designing experiments, analysing data and inputs while writing my thesis. Without both of their support, it would not have been possible to complete my PhD project and thesis.*

*I would like to thank our collaborators Dr Simon Griffiths and Dr. Luzie Wingen, John Innes Centre, UK, who have been helpful with providing information regarding QTLs and clearing doubts with generation of NILs.*

*I express my regards to Mr. Jayalath DeSilva and Dr. Minuka Warasinghe for their support and help to undertake my field trials work at University of Nottingham. Special thanks to Minuka for teaching me the gas exchange measurements.*

*I am indebted towards help received in field experiments and recording field data by Mr. Andrew Riche, Mr. March Castle (for recording UAV data and beautiful aerial images of the fields) and Mr. David Steele (for unconditional support, motivation, and help). I would like to thank Mr Chris Hall for help and advice while working at Jenkinson Laboratory.*

*I am thankful towards our lab members Dr Petros Sigalas, Mrs. Saroj Parmar and Dr. Peter Buchner for their help and co-operation during my tenure at Rothamsted Research.*

*I would like to thank my friends and colleagues Dr. Nicolas Virlet, Dr. Latifa Greche, Ms. Parul Sehrawat, Mr. Rohan Richards, Mr Daniel Cudjoe for their support during my PhD.*

*I would like to acknowledge my PhD Studentship grant NOS: 11015/137/2017-SCD-V provided by Government of India, without their financial support, it would have complete my PhD Studies*

*Last but not the least, I would like to thank my mother Manda Nitnavare, father Balasaheb Nitnavare, my mother-in-law Mrs Suniti Bhattacharya, sisters Kiran & Rohini, Prashant bhैया and partner Ms. Joorie Bhattacharya for her unconditional support, motivation, and love throughout this journey of PhD.*

## Table of Content

	List of Figures	
	List of Tables	
	List of Abbreviations	
	Abstract	1
<b>Chapter 1 Introduction and Literature Review</b>		
<b>1.1</b>	<b>Introduction</b>	<b>4</b>
<b>1.2</b>	<b>Traits affecting NUE</b>	<b>8</b>
<b>1.2.1</b>	<b>Nitrogen uptake efficiency traits</b>	<b>8</b>
<b>1.2.1.1</b>	<b>Root architecture</b>	<b>8</b>
<b>1.2.2</b>	<b>N-Utilisation Efficiency Traits</b>	<b>9</b>
<b>1.2.2.1</b>	<b>Photosynthesis</b>	<b>9</b>
<b>1.2.2.2</b>	<b>Leaf chlorophyll content</b>	<b>11</b>
<b>1.2.2.3</b>	<b>Stay-green trait</b>	<b>12</b>
<b>1.2.3</b>	<b>Nitrogen harvest index (NHI)</b>	<b>13</b>
<b>1.2.4</b>	<b>N remobilisation efficiency (NRE)</b>	<b>14</b>
<b>1.2.5</b>	<b>Nitrate assimilation</b>	<b>14</b>
<b>1.2.6</b>	<b>Grain Protein Deviation/Content/Concentration</b>	<b>16</b>
<b>1.3</b>	<b>Approaches for NUE improvement</b>	<b>19</b>
<b>1.3.1</b>	<b>High-throughput phenotyping</b>	<b>19</b>
<b>1.4</b>	<b>Genetic diversity in wheat landraces</b>	<b>22</b>
<b>1.5</b>	<b>Agronomic practices to increase NUE</b>	<b>25</b>
<b>1.5.1</b>	<b>Bio-fertilisers and nano-fertilisers</b>	<b>25</b>
<b>1.6</b>	<b>Genomics-assisted breeding approaches</b>	<b>28</b>
<b>1.6.1</b>	<b>QTL identification</b>	<b>28</b>
<b>1.6.2</b>	<b>GWAS studies</b>	<b>32</b>
<b>1.7</b>	<b>Biotechnological techniques for improving NUE</b>	<b>34</b>
<b>1.7.1</b>	<b>Transgenesis</b>	<b>34</b>
<b>1.7.2</b>	<b>Genome editing</b>	<b>34</b>
<b>1.8</b>	<b>Conclusions</b>	<b>35</b>
<b>Hypotheses and Objectives</b>		<b>38</b>
<b>Chapter 2 Overview of Materials and Methods</b>		
<b>2.1</b>	<b>Screening of germplasm Field Experiments: 2018-19 Sutton Bonington and Harpenden</b>	<b>41</b>
<b>2.1.1</b>	<b>Germplasm</b>	<b>42</b>
<b>2.1.2</b>	<b>Crop measurements at Sutton Bonington site</b>	<b>43</b>
<b>2.1.2.1</b>	<b>Growth stages and establishment</b>	<b>43</b>
<b>2.1.2.2</b>	<b>NDVI and leaf senescence</b>	<b>43</b>
<b>2.1.2.3</b>	<b>Physiological maturity and harvest growth analysis</b>	<b>46</b>
<b>2.1.3</b>	<b>Crop Measurements and harvest analysis at Harpenden site</b>	<b>46</b>
<b>2.1.4</b>	<b>Statistical Analysis</b>	<b>47</b>
<b>2.2</b>	<b>Field experiments on selected sub-set (20 NILs) at Rothamsted in 2020 and 2021</b>	<b>47</b>
<b>2.2.1</b>	<b>Experimental site and design</b>	<b>47</b>
<b>2.2.2</b>	<b>Crop measurements</b>	<b>47</b>
<b>2.3</b>	<b>RNAseq based transcriptomics field experiment 2022</b>	<b>49</b>
<b>2.3.1</b>	<b>RNA seq analysis</b>	<b>49</b>
<b>2.3.2</b>	<b>Read mapping to the reference genome</b>	<b>52</b>
<b>2.3.3</b>	<b>Differential gene expression analysis and quantification</b>	<b>52</b>

2.3.4	Gene Ontology analysis and KEGG enrichment analysis	53
2.3.5	Single Nucleotide Polymorphisms (SNP)	53
2.4	Statistical analysis	53
<b>Chapter 3 Genetic variation for Nitrogen Use Efficiency and associated traits in landraces, synthetic hexaploid wheat</b>		
3.1	Introduction	55
3.2	Materials and methods	57
3.2.1	Field sites	57
3.2.2	Germplasm	57
3.2.3	Crop Development measurements	59
3.2.3.1	Sutton Bonington measurements	59
3.2.3.2	Harpenden measurements	60
3.2.4	Physiological maturity and harvest analysis	60
3.2.5	Statistical Analysis	60
3.3	Results	61
3.3.1	Rothamsted Research, 2019	62
3.3.1.1	Grain yield, yield components and height	62
3.3.1.2	Nitrogen-use efficiency and NUE components	66
3.3.1.3	Association between yield and NUE and its components	70
3.3.1.4	Allelic variation among Paragon × Watkin NILs	73
3.3.1.5	Genetic variation among synthetic-derived lines	74
3.3.2	Harvest and NUE components Sutton Bonington, 2019	75
3.3.2.1	Genetic variation in grain yield, yield components and Nitrogen-use efficiency and NUE components	75
3.3.2.2	Genetic variation in photosynthesis traits	80
3.3.2.3	Association between photosynthesis traits and grain yield	83
3.3.2.4	Association between yield and NUE and its components	85
3.3.2.5	Allelic variation among Paragon × Watkin NILs	87
3.3.2.6	Genetic variation among synthetic lines	89
3.3.3	Effect of site on performance of NILs	91
3.4	Discussion	93
3.4.1	Evidence for genetic variation in grain yield and NUE	94
3.4.2	Evidence for genetic variation in N uptake efficiency (NUpE)	95
3.4.3	Evidence for genetic variation in N utilisation efficiency (NUE)	95
3.4.4	Associations between leaf photosynthesis traits and NUE	97
3.5	Summary	98
<b>Chapter 4- Genetic variation for NUE and associated traits in landraces and synthetic hexaploid wheat under high and low nitrogen conditions</b>		

4.1	Introduction	101
4.2	Materials and Methods	103
4.2.1	Field experiments on selected sub-set (17 NILs, Paragon and Robigus) at Rothamsted in 2020 and 2021	103
4.2.1.1	Experimental site and design	103
4.2.1.2	Crop measurements	103
4.2.2	Physiological maturity and harvest analysis	103
4.2.3	Statistical analysis	104
4.3	Results	105
4.3.1	Effects on NUE and related traits	106
4.3.1.1	NUE 2020-21	106
4.3.1.2	N-uptake efficiency in 2020 and 2021	107
4.3.1.3	N-utilisation efficiency in 2020 and 2021	108
4.3.2	Effects on Grain yield (GY), Above-ground biomass (AGDM) and Harvest Index (HI)	112
4.3.2.1	Grain yield	112
4.3.2.2	Above-ground Biomass (AGDM)	112
4.3.2.3	Harvest Index	113
4.3.3	Effects on Grain N Uptake (GNUP), Straw N Uptake (SNUP) and Nitrogen Harvest Index (NHI)	117
4.3.3.1	Grain N Uptake	117
4.3.3.2	Straw N Uptake	117
4.3.2.3	Nitrogen Harvest Index	118
4.3.4	Effects on Grain Protein Content (GPC) and Thousand Grain Weight (TGW)	122
4.3.4.1	Grain Protein Content	122
4.3.4.2	Thousand Grain Weight	122
4.3.5	Traits associations between HN and LN conditions	125
4.3.5.1	Association in Grain yield, Above-ground biomass and harvest index under HN and LN condition	125
4.3.5.2	Association between NUE under HN and LN conditions	127
4.3.5.3	Association between GY and NUE, NUpE, NUPE and AGBM across two-year mean	128
4.3.5.4	Associations between GY and ear m <sup>-2</sup> and Grains ear <sup>-1</sup> across two-year mean	129
4.3.5.5	Associations between GPC, and GY and NUE along with NUE and AGDM across two-year mean	129
4.3.5.6	Correlation between traits under HN and LN conditions	130
4.4	Discussion	132

4.4.1	Grain yield and Above-ground biomass performance of NILs under varying N condition	132
4.4.2	Genetic variation in NUE in relation to NUpE and NUtE components	133
4.5	Summary	135
<b>Chapter 5 RNA-Seq-based transcriptomics analyses of wheat near isogenic lines to identify candidate genes for Nitrogen Use Efficiency and related traits</b>		
5.1	Introduction	138
5.2	Materials and Methods	140
5.2.1	Field conditions and plant material sampling	140
5.2.2	Growth measurements and harvest analysis	140
5.2.3	RNA seq experiment	141
5.2.4	Reads mapping to the reference genome	141
5.2.5	Differential gene expression analysis and quantification	141
5.2.6	Gene Ontology analysis and KEGG enrichment analysis	142
5.2.7	Single Nucleotide Polymorphisms (SNP)	142
5.3	Results	143
5.3.1	Transcriptome Summary of NILs	143
5.3.1.1	RNA-seq data quality and mapping statistics	143
5.3.1.2	Transcriptome profiles of the NILs in response to high and low N application	144
5.3.2	Synthetic lines	149
5.3.2.1	RNA-seq data quality and mapping statistics	149
5.3.2.2	Analysis of differentially expressed genes (DEGs)	149
5.3.2.3	GO and KEGG Analysis of DEGs in synthetic hexaploid line	150
5.3.3	P x W lines	153
5.3.3.1	RNA-seq data quality and mapping statistics	153
5.3.3.2	Analysis of differentially expressed genes (DEGs)	153
5.3.3.3	GO Analysis of DEGs	155
5.3.3.4	KEGG analysis of DEGs	159
5.3.4	Identification of candidate DEG transcripts for improved NUE	163
5.3.5	SNP analysis	172
5.4	Discussion	173
5.4.1	Photosynthesis	173
5.4.2	Carbon metabolism	174
5.4.3	Nitrogen metabolism	174
5.4.4	Biosynthesis of amino acid	175
5.5	Summary	176
<b>Chapter 6 General Discussion</b>		
6.1	Hypothesis validation	179
6.2	Validation of QTLs for target traits and improved NUE (QTLs performance)	182



<b>6.3</b>	<b>Genetic diversity in traits and their association with NUE</b>	<b>184</b>
<b>6.4</b>	<b>Discovery of candidate gene markers</b>	<b>185</b>
<b>6.5</b>	<b>Application of traits and candidate genes for plant breeding for N-uptake efficiency and N-utilisation efficiency</b>	<b>186</b>
<b>Chapter 7 Conclusion and Future prospects</b>		
<b>7.1</b>	<b>Conclusion and Summary</b>	<b>190</b>
<b>7.2</b>	<b>Ongoing work</b>	<b>192</b>
<b>7.3</b>	<b>Future work</b>	<b>193</b>
	<b>References</b>	<b>195</b>
	<b>Appendix</b>	<b>214</b>

## List of Figs

<b>Fig 2.1</b>	Map view and geographic coordinates of the two locations of 4 field trials	41
<b>Fig 2.2</b>	Field image of the two sites, A) Sutton Bonington campus, University of Nottingham B) Rothamsted Research, Harpenden	42
<b>Fig 2.3</b>	Instruments used to measure senescence kinetics and photosynthesis related traits	45
<b>Fig 2.4</b>	Field image of the two experiments at Rothamsted Research, Harpenden, A) 2020 and B) 2021 C) aerial image taken by Unmanned aerial vehicle field trial 2021	48
<b>Fig 2.5</b>	30 RNA samples (400ng) extracted from flag leaf tissue of wheat plants of 5 near isogenic lines under 2 N treatments (N1= Low N (50 kg ha <sup>-1</sup> ) and N2= High N (200 kg ha <sup>-1</sup> ) and three biological replicates	50
<b>Fig 2.6</b>	RNaseq data quality control workflow	50
<b>Fig 2.7</b>	Overall outline of the RNaseq based transcriptomics experiment	52
<b>Fig 3.1</b>	Linear regression of (A) Nitrogen-Uptake Efficiency (NUpE (kg AGN kg <sup>-1</sup> N)) and (B) Nitrogen-Utilisation Efficiency (NUE (kg DM kg N <sup>-1</sup> ) on Grain Yield GY (t ha <sup>-1</sup> )	70
<b>Fig 3.2</b>	Linear regression of (A) Nitrogen Harvest Index (NHI) and on Grain Yield GY (t ha <sup>-1</sup> ) and (B) Harvest Index (HI) on Grain Yield GY (t ha <sup>-1</sup> )	71
<b>Fig 3.3</b>	Linear regression of (A) Above-ground N Uptake (AGNUP (kg AGN kg <sup>-1</sup> N), on Grain Yield GY (t ha <sup>-1</sup> ) and (B) Biomass (BM (t ha <sup>-1</sup> ) on Grain Yield GY (t ha <sup>-1</sup> )	71
<b>Fig 3.4</b>	Linear regression of (A) Ears m <sup>-2</sup> , on Grain Yield GY (t ha <sup>-1</sup> ) and (B) Grain Yield GY (t ha <sup>-1</sup> ) on Grain Protein Content (GPC)	72
<b>Fig 3.5</b>	Linear regression of (A) Nitrogen Use Efficiency (NUE (kg Grain DM kg <sup>-1</sup> N)) on Grain Protein Content (GPC %) and (B) Harvest Index (HI) on Nitrogen Use Efficiency (NUE (kg Grain DM kg <sup>-1</sup> N))	72
<b>Fig 3.6</b>	Bar chart represents (A) NUpE (kg AGN kg <sup>-1</sup> N) (B) NUtE (kg DM kg N <sup>-1</sup> ) (C) NUE (kg Grain DM kg <sup>-1</sup> N) (D) NHI of allelic groups for QTLs in Paragon ×Watkins landraces NILs and elite cultivar Paragon	73
<b>Fig 3.7</b>	Bar chart represents (A) NUpE (kg AGN kg <sup>-1</sup> N) (B) NUtE (kg DM kg N <sup>-1</sup> ) (C) NUE (kg Grain DM kg <sup>-1</sup> N) (D) NHI of seven synthetic-derived hexaploid wheat lines (grey) and Robigus parent (dark grey)	74
<b>Fig 3.8</b>	Bar chart of flag-leaf photosynthesis rate at (A) GS61 and (B) GS61+10d and stomatal conductance at (C) GS61 and (D) GS61+10d of 15 P × W near-isogenic lines, two synthetic derived lines and Paragon and Robigus parents	82
<b>Fig 3.9</b>	Linear regression of Grain Yield GY (t ha <sup>-1</sup> ) on (A) Photosynthesis Rate at GS61 and (B)GS61+10D, (C) Grain Yield GY (t ha <sup>-1</sup> ) vs Stomal Conductance at GS61 (D) GS61+10D	83
<b>Fig 3.10</b>	Linear regression of (A) Grain N Uptake (GNUP ( kg N ha <sup>-1</sup> ), on NUE (kg Grain DM kg <sup>-1</sup> N)and (B) Grain Yield GY (t ha <sup>-1</sup> ) on NHI	85
<b>Fig 3.11</b>	Linear regression of (A) Grain Yield GY (t ha <sup>-1</sup> ) on Grain Protein Content (GPC) and (B) Grain Yield GY (t ha <sup>-1</sup> ) on Grain N Uptake (GNUP ( kg AGN kg <sup>-1</sup> N))	85
<b>Fig 3.12</b>	Linear regression of Grain Protein Content (GPC) on NUE (kg Grain DM kg <sup>-1</sup> N)	86
<b>Fig 3.13</b>	Linear regression of (A) NDVI at GS61 Anthesis on NUE (kg Grain DM kg <sup>-1</sup> N ) and (B) Grain Yield GY (t ha <sup>-1</sup> ) on NDVI at GS61 anthesis	86
<b>Fig 3.14</b>	Bar chart represents (A) Grain Yield GY (t ha <sup>-1</sup> ) (B) Grain N Uptake (GNUP ( kg N ha <sup>-1</sup> ) of QTL allelic groupings for Paragon × Watkins landraces and parent Paragon	87
<b>Fig 3.15</b>	Bar chart represents (A) NUE (kg Grain DM kg <sup>-1</sup> N) (B) Grain Protein Content (GPC) of allelic groups for Watkins landraces × elite cultivar Paragon crosses near-isogenic lines and parent Paragon	88

<b>Fig 3.16</b>	Bar chart represents genetic variation among synthetic lines for (A) Grain Yield GY (t ha <sup>-1</sup> ), (B) Grain N UP (kg N ha <sup>-1</sup> ), (C)NUE (kg Grain DM kg <sup>-1</sup> N) and (D) Grain Protein Content (GPC)	89
<b>Fig 3.17</b>	Effect of two experiment sites i.e., Rothamsted Research (RR) and Sutton Bonington (SB) on performance of 66 NILs	92
<b>Fig 4.1</b>	Linear regression of Grain Yield (t ha <sup>-1</sup> ) at HN on Grain Yield at LN in (A) 2020 (B)2021 and (C) mean values of two years; Above-ground Biomass (AGBM t ha <sup>-1</sup> ) at HN on AGBM at LN in (D) 2020 (E)2021 and (F) mean values of two years; Harvest index (HI) at HN on HI at LN in (G) 2020 (H)2021 and (I) mean values of two years	126
<b>Fig 4.2</b>	Linear regression of Nitrogen Use Efficiency (NUE kg Grain DM kg <sup>-1</sup> N ) at HN on NUE at LN in (A) 2020 (B)2021 and (C) mean values of two years	127
<b>Fig 4.3</b>	Linear regression of (A) GY on NUpE (B) GY on NUE and (C) GY on NUtE and (D) GY on AGDM of mean across two years of 19 NILs	128
<b>Fig 4.4</b>	Linear regression of (A) GY on Ears m <sup>2</sup> and (B) GY on Grains Ear <sup>-1</sup> for 19 genotypes.	129
<b>Fig 4.5</b>	Linear regression of (A) GPC on GY, (B) GPC on NUE and (C) AGDM and NUE of mean across two years of 19 genotypes. Blue colour and green colour data points represents values of mean across 2020 and 2021 year at LN and HN, respectively	130
<b>Fig 4.6</b>	Correlation matrix of traits like GY: Grain Yield (t ha <sup>-1</sup> ), AGBM: Above-ground biomass (t ha <sup>-1</sup> ), Ears m <sup>2</sup> , GPC: Grain Protein Content (%), Grains Ear <sup>-1</sup> , HI: Harvest Index, NHI: Nitrogen Harvest Index, NUE, NUpE: Nitrogen-Uptake Efficiency (kg AGN kg <sup>-1</sup> N), NUE: Nitrogen-Use Efficiency (kg Grain DM kg <sup>-1</sup> N), NUtE: Nitrogen-Utilisation Efficiency (kg DM Kg N <sup>-1</sup> ) and TGW: Thousand Grain Weight (g) at (A)high N (200 kg ha <sup>-1</sup> ) (B) Low N (50 kg ha <sup>-1</sup> ) conditions. These values represent the mean across 2020 and 2021	131
<b>Fig5.1</b>	Co-relation matrix depicts the Pearson co-relation between 30 samples	144
<b>Fig 5.2</b>	Principal component analysis of 30 samples from 5 different genotypes	145
<b>Fig 5.3</b>	Venn diagram showing differential expressed genes across 5 different genotypes	146
<b>Fig 5.4</b>	Bar chart representing differential expressed genes counts across 5 different genotypes	147
<b>Fig 5.5:</b>	Heatmap of differential expression patterns of genes across 5 different genotypes	148
<b>Fig 5.6</b>	Details of differentially expressed genes (DEGs) (A) Volcano plot (B) Bar Graph showing significantly expressed DEGs	150
<b>Fig 5.7</b>	Gene ontology (GO) enrichment analysis (p<0.05) of synthetic hexaploid wheat	151
<b>Fig 5.8</b>	KEGG pathways DEGs enrichment analysis of synthetic hexaploid wheat	152
<b>Fig 5.9</b>	Volcano plot of Differentially expressed genes (DEGs)	154
<b>Fig 5.10</b>	Gene ontology (GO) enrichment analysis (p<0.05) of QTL AGDM	156
<b>Fig 5.11</b>	Gene ontology (GO) enrichment analysis (p<0.05) of QTL grain yield	157
<b>Fig 5.12</b>	Gene ontology (GO) enrichment analysis (p<0.05) of QTL straw yield	158
<b>Fig 5.13</b>	Gene ontology (GO) enrichment analysis (p<0.05) of parent Paragon	159
<b>Fig 5.14</b>	KEGG pathways DEGs enrichment analysis for QTL AGDM	161
<b>Fig 5.15</b>	KEGG pathways DEGs enrichment analysis for QTL grain yield	161
<b>Fig 5.16</b>	KEGG pathways DEGs enrichment analysis for QTL straw yield	162
<b>Fig 5.17</b>	KEGG pathways DEGs enrichment analysis for Paragon	163
<b>Fig 5.18</b>	SNP function of 5 genotypes with MISSENSE (a single nucleotide changes that missense mutation), NONSENSE (a single nucleotide change that does not cause mutation) and SILENT (a single nucleotide changes that synonymous mutation)	172

## List of Tables

<b>Table 1.1</b>	Definitions of selected NUE parameters	7
<b>Table 2.1</b>	Near isogenic lines used in two screening field experiments	43
<b>Table 2.2</b>	Near isogenic lines (2019-20) used at Harpenden site	48
<b>Table 2.3</b>	RNA quality control parameters, concentration (ng/ $\mu$ l), A260/280 and A260/230 values of 5 near isogenic lines under 2 N treatments (N1= Low N (50 kg ha <sup>-1</sup> ) and N2= High N (200 kg ha <sup>-1</sup> ) and three biological replicates	51
<b>Table 3.1</b>	List of 66 Near Isogenic Lines (NILs) in field trails 2018-19	57
<b>Table 3.2</b>	Available N from soil and N fertiliser applied at Rothamsted Research, Harpenden (RR) and Sutton Bonington (SB)	61
<b>Table 3.3</b>	Anthesis date and Plant Height (PH) in cm at Rothamsted Research (RR) and Sutton Bonington (SB) in year 2018-2019	61
<b>Table 3.4</b>	NILs, BM (Total Biomass ha <sup>-1</sup> ), Ears m <sup>-2</sup> , Grain Fill Rate (GFR), GY (Grain Yield t ha <sup>-1</sup> at 100% DM), Height (cm), HI (Harvest Index), Ears m <sup>-2</sup> and TGW (Thousand grain Weight) g at Rothamsted Research, Harpenden in 2019	63
<b>Table 3.5</b>	AGNUP (Above-ground N Uptake kg N ha <sup>-1</sup> ), NHI (Nitrogen Harvest Index), NUE (Nitrogen-Use Efficiency kg Grain DM kg <sup>-1</sup> N), NUPE (Nitrogen-Uptake Efficiency kg AGN kg <sup>-1</sup> N), NUtE (Nitrogen-Utilisation Efficiency kg DM kg N <sup>-1</sup> , Grain N UP (Grain N Uptake kg N ha <sup>-1</sup> ), GPC (Grain Protein Content %) at Rothamsted Research in 2019	67
<b>Table 3.6</b>	Genetic variation in harvest and NUE related traits at Rothamsted Research, Harpenden in 2019 in 66 near-isogenic line and synthetic-derived wheat lines and Paragon and Robigus parents	70
<b>Table 3.7</b>	Genotype, GY (Grain Yield t ha <sup>-1</sup> ), Grain N UP (kg N ha <sup>-1</sup> ), GPC (Grain Protein Content) TGW (Thousand grain Weight), Grain N% and Straw N% at Sutton Bonington in 2019	77
<b>Table 3.8</b>	Genetic variation in harvest and NUE related traits: GY (Grain Yield at 100% DM t ha <sup>-1</sup> ), TGW (Thousand grain Weight), NUE (Nitrogen-Use Efficiency kg Grain DM kg <sup>-1</sup> N), Straw N uptake (kg AGN kg <sup>-1</sup> N) at Sutton Bonington, Nottingham in 2019	80
<b>Table 3.9</b>	Genetic variation in photosynthesis flag-leaf traits: Photosynthesis Rate at GS61 and GS61+10D, Stomatal Conductance at GS61 and GS61+10D, SPAD (Chlorophyll Content) at GS61 at Sutton Bonington in 2019 in 15 P $\times$ W near-isogenic lines, two synthetic-derived lines and Paragon and Robigus parents	81
<b>Table 3.10</b>	Genetic variation in photosynthesis traits flag-leaf photosynthesis rate at GS61 and GS61+10d, stomatal conductance at GS61 and GS61+10D, SPAD (Chlorophyll Content) at Sutton Bonington	84
<b>Table 3.11</b>	Site variation variation of 64 NILs and Paragon and Robigus in GY (Grain Yield t ha <sup>-1</sup> ), Grain N%, Straw N%, Grain N UP (kg ha <sup>-1</sup> ), TGW (Thousand grain Weight), NHI (Nitrogen Harvest Index), NUE (Nitrogen-Use Efficiency kg Grain DM kg <sup>-1</sup> N) and GPC (Grain Protein Content) from the cross-site ANOVA at the two experiment sites i.e., Rothamsted Research (RR) and Sutton Bonington (SB)	93
<b>Table 3.12</b>	5 Shortlisted NILs for further experiments under varying N conditions	99
<b>Table 4.1</b>	List of Near Isogenic Lines (NILs) in field trails 2020 and 2021	105
<b>Table 4.2</b>	N fertiliser application and soil available N from soil at Rothamsted Research, Harpenden, year 2020 and 2021	105

<b>Table 4.3</b>	Weather data like Temperature (Min) °C, Temperature (Max) °C, Rain(mm), Relative Humidity (%), Solar Radiation (J cm <sup>-2</sup> ) at Rothamsted Research, site, year 2020 and 2021	106
<b>Table 4.4</b>	N-use efficiency (NUE), N-uptake efficiency (NUpE) and N-utilisation efficiency (NUE) in 15 P X W near-isogenic lines, two synthetic hexaploid-derived wheat lines and Paragon and Robigus lines in 20120, 2021 and mean of two years	110
<b>Table 4.5</b>	Grain Yield (GY t ha <sup>-1</sup> ) at 100% DM, Above-ground Biomass (AGBM t ha <sup>-1</sup> ) and Harvest Index (HI) in 15 P X W near-isogenic lines, two synthetic-derived hexaploid wheat lines and Paragon and Robigus lines in year 2020, 2021 and mean of two years	115
<b>Table 4.6</b>	Grain N Uptake (GNUP kg N ha <sup>-1</sup> ), Straw N Uptake (SNUP kg N ha <sup>-1</sup> ) and Nitrogen Harvest Index (NHI) in 15 P X W near-isogenic lines, 2 synthetic-derived hexaploid wheat lines and parents Paragon and Robigus in year 2020, 2021 and mean of two years	120
<b>Table 4.7</b>	Grain Protein Content (GPC %) and Thousand Grain Weight (TGW g) in 15 P X W near-isogenic lines, two synthetic-derived hexaploid wheat lines and parent Paragon and Robigus lines in year 2020, 2021 and mean of two years	123
<b>Table 4.8</b>	5 Shortlisted NILs and criteria used for selection	136
<b>Table 5.1</b>	Details of the germplasm used for RNAseq experiments; nitrogen treatment (N1 (50 kg ha <sup>-1</sup> ) and N2 (200 kg ha <sup>-1</sup> )), Group, Line accession and trait and background	140
<b>Table 5.2</b>	Quality control parameters of flag tissue RNA libraries of QTLs	143
<b>Table 5.3</b>	Mapping statistics of RNAseq data	143
<b>Table 5.4</b>	Quality control parameters and mapping statistics of RNA-seq data of hexaploid wheat line high and low N conditions	149
<b>Table 5.5</b>	Quality control parameters and mapping statistics of RNA-seq data of PxW lines and paragon at high and low N conditions	153
<b>Table 5.6</b>	Differentially Expressed Genes in SHW derived lines when compared with high and low N treatment	165
<b>Table 5.7</b>	Differentially Expressed Genes in AGDM QTL when compared with high and low N treatment.	166
<b>Table 5.8</b>	Differentially Expressed Genes in GY QTL when compared with high and low N treatment	167
<b>Table 5.9</b>	Differentially Expressed Genes in straw yield QTL when compared with high and low N treatment.	168
<b>Table 5.10</b>	Differentially Expressed Genes in Paragon when compared with high and low N treatment	169

## List of Abbreviations

$A_{max}$	Photosynthesis Rate
A	Adenine
AGDM	Above-Ground Dry Matter
ANOVA	Analysis of variance
AGN	Above Ground Nitrogen
BC	Back Cross
BM	Biomass
C	Cytosine
cm	centimetre
COMGRWT	Combine Grain Weight
COMSTR	Combine Straw Weight
DAE	Days after emergence
DEG	Differentially Expressed Gene
DEGs	Differentially Expressed Genes
DM	Dry Matter
DNA	Deoxyribonucleic acid
DW	Dry Weight
FAO	Food and Agriculture Organisation
FW	Fresh Weight
g	Grams
G	Genotype
G	Guanine
G	Genotype
GA	Green Area
GAI	Green Area Index
GFPTT	Grain Fill Period Thermal Time
GFR	Grain Fill Rate
GN	Grain Number
GO	Gene ontology
GPC	Grain Protein Content
GRYLD	Grain Yield
gs	Stomatal Conductance
GS	Growth Stage
GS65	Anthesis (Zadoks growth scale)
GS65+10 D	Ten days after anthesis (Zadoks growth scale)
GS65+12 D	Twelve days after anthesis (Zadoks growth scale)
GS87	Physiological Maturity (Zadoks growth scale)
GW	Grain Weight
GWAS	Genome-Wide Association Study
GY	Grain Yield
h	Hours
ha	Hectare
HI	Harvest Index
HN	High Nitrogen
KEGG	Kyoto Encyclopedia of Genes and Genomes
kg	Kilogram
L	Litre

Lam	Lamina
LN	Low Nitrogen
LSD	Least Significant Difference
m	Meters
MAS	Marker Assisted Selection
Max	Maximum
mg	Milligrams
Min	Minimum
mm	Millimetres
N	N Treatment
NDVI	Normalized Difference Vegetative Index
NHI	Nitrogen Harvest Index
NIL	Near-Isogenic Lines
NIRS	Near Infrared Spectroscopy Method
NRE	N remobilizationremobilisation efficiency
NUE	Nitrogen Use Efficiency
NU <sub>p</sub> E	Nitrogen Uptake Efficiency
NU <sub>t</sub> E	Nitrogen Utilisation Efficiency
P allele	Paragon Allele
PCA	Principal Component Analysis
PGR	Plant Growth Regulator
PH	Plant Height
PM	Physiological Maturity
P X W	Paragon X Watkins line
QTL	Quantitative Trait Loci
RIL	Recombinant Inbred Line
RNA	Ribonucleic acid
RR	Rothamsted Research
SB	Sutton Bonington
SG	Stay Green
SHW	Synthetic Hexaploid Wheat
SD	Synthetically Derived
SNP	Single Nucleotide Polymorphism
SPAD	Flag leaf relative chlorophyll content
T	Thymine
t	Tonne
TGW	Thousand-Grain Weight
UAV	Unmanned Aerial Vehicle
UK	United Kingdom
W allele	Watkins Allele
Y	Year
%	Percentage
°C	Degree centigrade

## Abstract

Wheat is one of the three main cereal crops in the world and its demand is increasing with increasing population. The excess use of nitrogen (N) fertilisers causes serious environmental impacts including nitrate leaching into ground water, eutrophication of water bodies, and global warming due to nitrous oxide emissions. Therefore, a key breeding target in wheat cultivation is enhancing Nitrogen-use efficiency (NUE). In wheat, there is relatively small genetic variation in adapted elite germplasm in N-uptake efficiency (NUpE) and N-utilisation efficiency (NUE), which are the two key components of the NUE. Therefore, this study aims to identify novel variation for traits and associated gene markers for NUE using more diverse germplasm.

The main objectives of the present study were: (i) Screening of diverse sets of hexaploid wheat genetic resources including landraces (from AE Watkins collection) x elite cultivar Paragon crosses, synthetic hexaploid wheat-derived lines, and elite cultivars for novel trait variation for improved NUE and (ii) the identification of haplotypes to enable development of markers for NUE and related traits. Initially, a diverse set of 64 Near-Isogenic Lines was screened for variation in NUE, NUpE, NUE and associated traits including Grain Yield (GY), Above-Ground Dry Matter (AGDM), Nitrogen Harvest Index (NHI), Grain N Uptake, Grain Protein Content (GPC) and photosynthesis traits, e.g. Flag-leaf Photosynthesis Rate ( $A_{max}$ ) and Stomatal Conductance ( $g_s$ ), in field experiments under optimal N supply at two locations, i.e., Rothamsted Research and Sutton Bonington in 2018-19. Several NILs having Watkins alleles for QTLs for traits such as Grain yield (GY), Above-Ground Dry Matter (AGDM) and Grain-Fill Period Thermal Time (GFPTT) showed higher values for NUE as compared to Paragon. The performance of the NILs for the photosynthesis traits flag-leaf  $A_{max}$  and  $g_s$  was also considered for the selection of a sub-set of lines as they directly influence biomass, GY and NUE. Therefore, 18 NILs along with parents (Paragon and Robigus) were shortlisted after evaluating performance at both the experimental sites for studying response to N availability in high N and low N treatments.

Phenotyping of the 18 shortlisted NILs under high and low N conditions (High N 200 kg N ha<sup>-1</sup> and Low N 50 kg N ha<sup>-1</sup> respectively) to determine lines suitable for carrying out a RNA-seq based transcriptomics study was then performed in field experiments at Rothamsted



Research for two consecutive years 2020 and 2021. These experiments were carried out and then five genotypes were shortlisted for the RNAseq-based transcriptomics field study. After analysing cross-year results, NILs which showed significant correlation with NUE, NHI, NUpE, GPC and NUtE traits when compared with the corresponding Paragon allele were shortlisted. The five genotypes shortlisted included three Paragon × Watkins landrace NILs for QTLs for above-ground dry matter (PW141-10-Q7D-AGDM-W), Grain Yield (PW468-1-Q5A-COMGRWT-W) and Straw Yield (PW292-1-Q3A-COMSTR-W), the Paragon parent and one synthetic hexaploid wheat (SHW) derived line 58.

(iii) To Identify candidate genes for NUE through transcriptomics of flag-leaf tissue at post-anthesis stage of the five selected genotypes under high N and low N conditions, RNA-seq based transcriptomics was performed with the flag leaves of these genotypes in a field experiment in 2021 at Rothamsted Research. The RNAseq data were analysed to identify the candidate genes having differential expression under the two N treatments. Several genes showed differential expression. However, Gene Ontology and Kyoto Encyclopedia of Genes and Genomes (KEGG) pathways enrichment analysis suggested the following key genes from various biological processes including photosynthesis: *chlorophyll a-b binding protein 1B*, *glyceraldehyde-3-phosphate dehydrogenase*, *cytochrome P450*, stress response: *proline-rich receptor-like protein kinase*, *BED zinc finger*, *FBD-associated F-box protein*, amino acid metabolism: *tryptophan decarboxylase 1*, *aspartic proteinase*, *LRR receptor-like serine/threonine-protein kinase*. These candidate genes may contribute to the development of precise SNP markers for NUE traits for deployment in marker-assisted selection in wheat breeding ultimately leading to new cultivars with higher NUE and grain yields.

## ***Chapter 1***

### ***Introduction and Literature Review***

## 1.1 Introduction

Wheat is consumed globally as a staple crop and is the third largest produced cereal after rice and maize, and second largest according to grain acreage. Due to its high carbohydrate content, it is a major source of nutrition in several countries. The most grown wheat are common wheat (*Triticum aestivum*), durum wheat (*T. durum*), and club wheat (*T. compactum*) (FAO, 2022). Wheat grain is used for various purposes such as in bread-making, food condiments like pasta, biscuits, as fodder (Sharma *et al.*, 2020), and the wheat straw is utilised as an alternative for bioethanol production (Talebnia *et al.*, 2010). The global wheat production as of 2020 was 760 million tonnes (FAO, 2022), 774 million tonnes in 2021 and is expected to decline in 2022 by 0.8% (Collier, 2022). Wheat is cultivated on more than 240 million ha globally (Martínez-Moreno *et al.*, 2022). The major wheat-producing countries are China, India, Russia, USA and France of which China and India account for 17% and 12.5% respectively (Rastogi and Ang, 2022). The 10 key wheat exporting regions are EU, Russia, Canada, USA, Ukraine, Australia, Kazakhstan, Argentina, Turkey and Brazil which account for 57% of global wheat production, 54% of global wheat producing area and 92% of global wheat exports (Trnka *et al.*, 2019). The current ongoing conflict between Russia and Ukraine has had significant impact on the global wheat production as both countries are major wheat producers as well as exporters. Owing to the rising demand of wheat, it is important to increase the production of wheat. The yield of wheat is greatly influence by the level of nitrogen present in the crop. Nitrogen is also one of the most important limiting factors for plant growth and is a key component in several metabolic pathways. The increasing demand for yield in cereals has led to the correlative rise in usage of nitrogen fertilisers over the past five decades (Dobermann, 2005, Dobermann and Cassman 2005). After the development of the Haber-Bosch process in the beginning of the 20th century, use of fertilisers accelerated (Hawkesford, 2014). In developing countries, use of nitrogen fertilisers increased exponentially increase post the Green Revolution. However, the nitrogen uptake in crops is lower despite the increase of nitrogen fertiliser use. With a sevenfold increase in fertiliser input, there was only a two-fold increase in nitrogen uptake since the late 1970s (Hirel *et al.*, 2007; Shrawat *et al.*, 2008). This is because nitrogen is lost due to several factors such as leaching, gaseous plant emission as NH<sub>3</sub> volatilisation via plant canopy, soil denitrification, soil runoff. Primary N absorption by roots takes place during the vegetative stage of the plant, such as the phase up to anthesis in case of wheat. Nitrogen is reduced to NH<sub>3</sub> and later

converted into amino acids like glutamine or asparagine by the process of catabolism. During this process of catabolism,  $\text{NH}_3$  is produced in the leaves which then escapes into the environment through open stomata which is the loss of N as  $\text{NH}_3$  via the plant canopy. (Raun and Johnson 1999, Fageria and Baligar 2005). Nitrogen may be present in the form of organic compounds such as urea, amines, and amides as well as in gaseous forms such as  $\text{NH}_3$  and  $\text{N}_2\text{O}$  which eventually contribute to air pollution (Galloway *et al.*, 1995, Dobermann 2005). This leads to a huge loss of resources, economically and environmentally (Hawkesford 2017).

The evolutionary set-up of crop plants is usually to conserve as much nitrogen as possible. The general approach to generating cultivars with improved N-use efficiency in plant breeding would be to evaluate the progeny of new crosses under varying N environments. This would help in identifying a genotype which has higher N absorption under low N environments as well as optimal conditions (Han *et al.*, 2015). Unfortunately, NUE has not been the major focus of most of the breeding programmes and larger focus has been placed on indirect selection of yield in environments targeted by breeding programmes, for the improvement of NUE. Breeding for an efficient use of N is an important aspect and objective which needs to be explored for enhancing NUE. In this context, factors like, role of root system, nitrate assimilation and its impact on photosynthesis and post-anthesis remobilisation, leaf and canopy structure, senescence dynamics have a direct influence on nitrogen uptake and use by the plant. Breeding for these components are being explored in the public domain like INRA (Institute national de la recherche agronomique, France) and CIMMYT (International Maize and Wheat Improvement Center, Mexico), and can be used for achieving enhanced NUE (Cormier *et al.*, 2016).

To understand plant responses to N limitation, NUE can be divided into two components (Hirel *et al.*, 2007) (Han *et al.*, 2015). NUE can be defined as the grain yield per unit of nitrogen supplied (from N fertiliser and soil) and is dependent on the following two key components.

1. Nitrogen (N) uptake efficiency (NUpE)
2. Nitrogen utilisation efficiency (NUtE)

NUE is the product of NUpE and NUtE (Moll *et al.*, 1982).  $\text{NUE} = \text{NUpE} \times \text{NUtE}$

The N-uptake efficiency is the nitrogen taken up by the above-ground crop as a fraction of the amount N supplied (Good *et al.*, 2004, Hawkesford 2014, Hans *et al.*, 2015). The NUpE is highly

dependent on the root system of the plant which is essential for supplementing the fast-depleting seed N reserve. There are two types of root systems, seminal roots (deepest roots) and crown roots (comprising of 70% of total root length density at anthesis). The seminal roots contribute towards the main stem while the crown roots serve the tillers and both systems are crucial for maximum grain yield (Kuhlmann and Barraclough, 1987). Selection for improved root system architecture traits like such can be used for resource-efficient use of N (Fradgley *et al.*, 2020). Nitrogen continues to be taken up by the crop after anthesis during grain filling. During grain filling, the role of nitrate transporters and amino acid transporters are crucial. Therefore, over-expression of such nitrate transporters would inevitably aid nitrogen transport. Studies pertaining to root system architecture are also pivotal for consideration. For example, a plant with high NUpE would tend to have longer roots and higher root length density, which can penetrate deeper into the soil in search of soil nitrogen reserves (Duncan *et al.*, 2018; Fernando *et al.*, 2021). However, higher root biomass may only be relevant in certain low N availability conditions and therefore, appropriate screening of root variation is necessary (Whalley *et al.*, 2017). At the crop level, NUpE is based on uptake of N fertiliser, and soil nitrogen including atmospherically deposited nitrogen (Hawkesford, 2017). Another essential parameter governing NUE is N harvest index (NHI).

NUtE on the other hand is the grain dry matter yield per amount of nitrogen taken up in the above-ground crop. This component is dependent on the photosynthesis rate of canopy and the N assimilation and N remobilisation capacity of the crop affecting canopy senescence (Good *et al.* 2004). Canopy green area (stem and lamina) is primarily responsible for nitrogen remobilisation as well as nitrogen assimilation during grain filling at maturity of the plant. However, delayed senescence leads to reduced photosynthetic activity limiting yield (Hawkesford, 2017) and an increase in grain protein concentration.

The Nitrogen harvest index (NHI) is the amount of nitrogen in grain as a proportion of that in grain and straw (Fageria 2010). NHI is also critical factor influencing grain yield, NUtE and grain protein content.

$$\text{NHI} = \frac{\text{Grain N}}{\text{Grain N} + \text{straw N}} \times 100 (\%)$$

The ability of a crop plant to assimilate and utilise nitrogen is dependent on the genotype (G), environment and location (E), and agronomic management (M). The interaction between

these factors leads to a sustainable and productive crop yield. The NUE is governed mainly by two key components; NUtE and NUPE, and these components are greatly influenced by genetic and environmental factors. The N uptake differs throughout the various developmental stages and assimilation efficiency then determines the grain yield and grain protein content. While most of the N is taken up by roots, some of the N is assimilated from the vegetative parts to the grain post flowering. NUE is a highly complex and polygenic trait due to which comprehending the underlying genetic and environmental effects will help dissect this trait.

**Table 1.1:** Definitions of selected NUE parameters (*Modified from Hawkesford and Griffiths, 2019*)

Abbreviation	Trait	Definition	Unit
NUE	Nitrogen use efficiency	Yield (grain) per unit total available nitrogen (fertiliser and mineral N); it is the product of NUPE × NUtE	kg Grain DM kg <sup>-1</sup> N available
NUPE	Nitrogen uptake efficiency	Nitrogen taken up by entire Above-ground biomass as a fraction of total nitrogen available to the crop	kg AGN kg <sup>-1</sup> N kg above-ground N (AGN) at harvest per kg N available
NUtE	Nitrogen utilisation efficiency	Yield as a function of the amount of nitrogen taken up	(kg DM kg <sup>-1</sup> N)kg grain DM per kg above-ground N at harvest
GPC	Grain protein content	The grain protein (content); often the N content (% concentration) × a standard factor to convert to protein (e.g., 5.7)	%
NHI	Nitrogen harvest index	The fraction of N in the grain compared to total N taken up, usually at harvest.	Fraction

## 1.2 Traits affecting NUE

### 1.2.1 Nitrogen uptake efficiency traits

#### 1.2.1.1 Root architecture

Nearly all N taken up by the plant is in the form of ammonium or nitrate. Taking into consideration the high proportion of fertiliser and soil N which the plant is unable to take up due to factors such as soil denitrification, soil runoff and volatilisation and nitrate leaching, it is important to effectively understand the mechanisms underlying N uptake through soil.

Since below-ground trait studies are difficult to carry out, relatively little research has been done on root architecture. However, it is crucial to understand the significance of root profiles in NUE. Improved cultivars which have a greater soil penetration and extensive root density at depth not only increase the uptake of N by crops but also reduce the loss of N to deeper water and soil layers subsequently improving NUE (Lynch, 2013, Peng, 2012). Additionally, a higher root length density (root length per unit volume; RLD) induces a greater ability of the crop to uptake nutrients. In the lower horizons of soil, the average RLD was found to be half of the critical value. Considering the critical RLD (cRLD) for water capture as  $1\text{cm cm}^{-3}$ , RLD has been found to be inadequate for complete water capture below a depth of 0.32m in wheat (White *et al.*, 2015).

Crops can regulate N uptake by modulating root architecture and growth. Different signalling pathways have been studied which trigger an overall change in root system to improve N uptake (Lima *et al.*, 2010). Under N-limited conditions the primary and lateral root systems are increased (Lopez-Bucio *et al.*, 2003, Gruber *et al.*, 2013). Increased N uptake has been seen to be associated with transporter systems such as kinases (Wall Associated Kinase 4 (WAK4)] and auxin (Multidrug Resistance 4/P-Glycoprotein 4 (MDR4/PGP4) in *Arabidopsis* (Terasaka *et al.*, 2005, Giehl *et al.*, 2014). Thus, it is evident that these transporter systems play an instrumental role in defining the root architecture of a crop and subsequent improved N acquisition. In most soils, the availability of water and thus N is greater in deeper soil strata over the growing season (Lynch, 2013). Therefore, one of the most important characteristics to improve is rooting depth. The construction of an ideotype to maximise nutrients and water capture in cereal crops has been widely proposed (Foulkes *et al.*, 2009; Lynch, 2013; Cormier *et al.*, 2016). These ideotypes includes a deeper relative distribution of roots. The primary

root traits that may contribute to rooting depth in cereal crops include (1) a large diameter of primary root with few but long laterals (2) many seminal roots with shallow growth angles, thin diameters, many lateral and long root hairs, (3) an intermediate number of crown roots with steep growth angles and few but long lateral branches, the growth angle of axial roots is a primary determinant of root foraging depth (Lynch, 2013).

To cope with scarce N, regulation of nitrogen acquisition efficiency is crucial. The nitrogen acquisition efficiency is dependent on the uptake activity of N transporters and root architecture. The N transporter genes have been studied and characterised in *Arabidopsis*. Additionally, due to high nitrate mobility in soil, the efficiency of root architecture for N uptake depends of other factors like species type, environment and soil type (Kiba and Krapp, 2016). An interesting outlook would be to explore these transporter systems for high affinity uptake of nitrogen in cereals and other monocots under varying environmental conditions and concentrations of N applied. Nitrate uptake is facilitated by specific transporters belonging to high affinity and low affinity transport systems (HATS and LATS, respectively) (Glass 2003; Fan *et al.*, 2017; Masclaux-Daubresse *et al.*, 2010). HATS are active when the concentration of  $\text{NO}_3^-$  in the soil is low  $<250 \mu\text{M}$ . LATS, by contrast, predominates at high soil  $\text{NO}_3^-$  concentration ( $>250 \mu\text{M}$ ).

## **1.2.2 N-Utilisation Efficiency Traits**

### **1.2.2.1 Photosynthesis**

Canopy architecture directly influences light penetration and radiation use efficiency (RUE) especially during stem elongation and anthesis periods which determine the yield of wheat. While the genetic increase in yield is either due to increase in harvest index and/or above-ground biomass (AGBM), we are reaching a limit in these two parameters. Therefore, it is important to explore the relation between canopy structure and yield. Erect canopies have demonstrated a linear relationship between canopy architecture and grain yield and an increase of 24% more grain than planophiles. This variation is due to enhanced AGBM and grain number (Richards *et al.*, 2019).

The effects of photosynthesis directly relate to grain yield and NUE. Nitrogen deficiency leads to reduced photosynthetic capacity and chlorophyll *a* content (Boussadia, 2010). An increased level of  $\text{CO}_2$  fixation and assimilation capacity, all things being equal, would consequently



improve N-use efficiency. An enhanced canopy area would contribute to achieving maximum light interception at anthesis hence improving the photosynthetic capacity and subsequently the NUE (Hawkesford, 2014). Additionally, it is also important to achieve full light interception at booting and during spike growth from booting to anthesis which helps in determining grains per unit area. The early and late light interception has been found to be associated with genetic improvement of wheat (Reynolds *et al.*, 2005). There are various other means of influencing the leaf photosynthesis rate. The Rubisco enzyme facilitates the carboxylation of ribulose-1, 5- biphosphate (RuBP) in CO<sub>2</sub> assimilation (Murchie *et al.*, 2009). After nitrate and ammonium assimilation, the photosynthetic tissues containing Rubisco proteins, and structural proteins for vascular connections, are developed. Rubisco accounts for a large portion of reserved N as well as photosynthetic N. Since Rubisco is a slow catalyst, amount required for photosynthetic rate sustenance is high and accounts for almost 25% of leaf N (Parry *et al.*, 2003; Pask *et al.*, 2012). Strategies implemented to enhance rubisco activity could in turn improve photosynthetic efficiency. Canopy architecture is an important factor which influences rubisco activity. In canopy structures with ample light penetrance, photosynthesis is restricted due to Rubisco activity, while in light-limited structures photosynthesis is limited due to electron transport rate. The Rubisco activity is dependent on factors like Rubisco active sites free of inhibitors and hence capable of catalysis and number of inhibitors. Under low light conditions, the electron carrier system in chloroplast is programmed to minimise the electron transfer in an uncontrolled and inappropriate manner (Murchie *et al.*, 2009). Increasing the rate of Rubisco catalysis in leaves with light, enhances the CO<sub>2</sub> assimilation and in shaded areas this becomes a limited value. Further, in certain situations, enhancing Rubisco activity may not contribute to increasing photosynthetic efficiency. At low light and high CO<sub>2</sub> conditions, the regeneration of RuBP limits photosynthetic efficiency. In such conditions, Rubisco amount and leaf N is seen to decrease which in turn enhances photosynthetic NUE (PNUE). The balance between RuBP consumption and regeneration for optimum Rubisco activity and maximum PNUE (Carmo-silva *et al.*, 2015, Hawkesford 2014). Similarly, avenues have been explored in introducing C<sub>4</sub> pathways in C<sub>3</sub> plants to obtain better yield. This would help in better CO<sub>2</sub> assimilation as crops with higher photosynthetic activity are able to capture solar radiation with better efficiency (Karki *et al.*, 2013). Concentration of CO<sub>2</sub> in the vicinity of the Rubisco molecule can also be achieved via cyanobacterial CO<sub>2</sub> assimilation mechanisms (Parry and Hawkesford, 2010). The C<sub>4</sub> plants

reduce the photorespiration by minimising the oxygenase function of Rubisco thereby reducing the loss of carbon. Atmospheric CO<sub>2</sub> is fixed by phosphoenolpyruvate carboxylase (PEPC) into the mesophyll cells and the resulting 4-C compound is moved to bundle sheaths where decarboxylation occurs. Therefore, CO<sub>2</sub> is present at the Rubisco site in bundle sheaths at higher concentration than oxygen. This leads to reduction in photorespiration and increase in photosynthetic activity in comparison to C<sub>3</sub> plants (Mallmann *et al.*, 2014).

Another enzyme which is crucial in photosynthesis and helps in storage of N is PEPC. Knockdown experiments carried out using RNAi technology has shown that N assimilation was reduced from NH<sub>4</sub><sup>+</sup>. As mentioned earlier, PEPC is the key enzyme in atmospheric N fixation on C<sub>4</sub> plants which eventually leads to decrease in photorespiration. In C<sub>3</sub> plants, PEPC plays a role in replenishing the tricarboxylic acid cycle. Increased levels of N assimilation and Pi starvation in C<sub>3</sub> plants can lead to elevated levels of PEPC (Masumoto *et al.*, 2010). However, over-expression studies did not lead to increased N assimilation due to inhibition by phosphates (Häusler *et al.*, 2010). PEPC may not have a direct impact on NUE, but it can be clumped up with other pathway related genes to develop a NUE strategy.

#### **1.2.2.2 Leaf chlorophyll content**

Chlorophyll *a* and chlorophyll *b* being the two major components of the photosynthetic apparatus are involved in photochemistry and stabilising the light-harvesting chlorophyll-binding proteins, respectively. Conversion of chlorophyll *a* to chlorophyll *b* is part of the chlorophyll cycle and are regulated by three major enzymes; chlorophyllide *a* oxygenase, chlorophyll *b* reductase, and 7-hydroxymethyl-chlorophyll reductase all of which further regulate construction and destruction of light-harvesting complexes (Tanaka and Tanaka, 2011). Chlorophyll meters have been widely used to study the status of N in crops and to estimate yield. SPAD readings are an effective means to quantify chlorophyll content per leaf area. This is also based on red and NIR light and the dependency of their absorption by chlorophyll (Xiong 2015). The SPAD readings are influenced by the application of N as fertilisers, and it was observed that plants receiving full inorganic fertiliser demonstrate higher SPAD reading as compared to those receiving lower reduced amount. There is a direct correlation of the SPAD readings and grain yield at different growth stages of the crop. Experiments performed on the *Sonalika* variety of wheat under varying fertiliser management options displayed increased SPAD reading and subsequently higher grain yield for plants

receiving inorganic fertilisers as compared to those receiving organic fertilisers. The SPAD reading were also observed to be positively correlated with grain yield at various growth stages with SPAD values of flag leaves up to 96 days after sowing are crucial for estimating the grain yield (Islam, 2014).

SPAD readings are however often affected by environmental factors and therefore it is essential to take into consideration the stress status of the crop. Light dependent chlorophyll movement greatly impacts this factor under high/low N supplements and thus it is vital to maintain the congruence between nitrogen supplements and NUE (Naus *et al.*, 2010, Xiong 2015). Novel genetic variations in hexaploid wheat under HN and LN conditions for landraces, modern and synthetic-derived cultivars demonstrated potential of enhanced leaf photosynthesis rate for improved adaptation of modern bread wheat under low N conditions. In modern and synthetic-derived cultivars of wheat, higher flag-leaf photosynthetic rate was associated with higher flag-leaf chlorophyll content implying towards higher N content in leaf and additionally, Rubisco content, as compared to the landraces. (Gaju *et al.*, 2016).

### **1.2.2.3 Stay-green trait**

The stay green trait refers to crops with delayed senescence (Thomas and Ougham 2014) and stay green is often associated with altered chlorophyll metabolism (Gregersen *et al.*, 2013). Various factors may contribute to precocious senescence such as temperature stress, pathogens, water stress causing the plant to remobilise nutrients (Fischer, 2012; Rapp *et al.*, 2015). Canopy of plants play an important role as their photosynthetic apparatus. The N stored in the canopy is used during grain filling for supplying grain N demand. Early canopy senescence may limit further photosynthetic activity but is required for remobilisation of the nitrogen. Hence, a larger canopy causing an increased N uptake per unit green area, having phased senescence, would cover all these aspects: continued photosynthesis, sufficient N concentration and hence increased NUE (Hawkesford 2014). Ideally, a stay green phenotype should extend grain filling and enhance grain yield. On the other hand, a delayed senescence may have detrimental effect on the N remobilisation of crops. Under optimal conditions, grain growth is likely to be sink -limited so stay-green may not improve yields, but under low N availability source-limited conditions should be correlated with yield (Bouchet 2016). A negative correlation has been observed between these phenotypes wherein the harvest index (HI) and nitrogen harvest index (NHI) were seen to be reduced in stay green phenotypes

(Hawkesford 2011). Increasing the rate of senescence using transcriptional factors saw an increase in grain protein concentration and nutrient remobilisation (Waters *et al.*, 2009). However, this may have a negative effect on the grain yield (Hawkesford 2011). Post anthesis N uptake (PANU) and stay green (indicated by onset of senescing phase, SEN<sub>ONSET</sub>) was not seen under LN. However, a negative correlation between N remobilisation efficiency and SEN<sub>ONSET</sub> was observed suggesting that differences in SEN<sub>ONSET</sub> is associated with post anthesis N remobilisation. Genetic differences in SEN<sub>ONSET</sub> were due to variation in anthesis date. The variation of SEN<sub>ONSET</sub> was further associated with phenotypic variation in NUtE and GY amongst the genotypes (Gaju *et al.*, 2011).

The NDVI tool is based on the concept of reflectance of red (680 nm) and near infrared (970 nm) bands (NIR) which are the most widely used bands (Inman *et al.*, 2007, Liu 2015). It has been shown to correlate with genetic variation in canopy N status and biomass and yield in wheat (Babar *et al.*, 2006). There is a positive correlation between crop N content and NDVI in wheat which helps in diagnosing the N status of the crop at various key developmental stages such as anthesis, booting, maturity and grain filling under varying agro climatic conditions (Sultana *et al.*, 2014, Sathisha and Desai *et al.*, 2016).

### **1.2.3 Nitrogen harvest index (NHI)**

The N recovery efficiency (RE) is defined as the proportion of nitrogen utilised and taken up by the crop from the N applied (Congreves *et al.*, 2021). A major limitation to NUE is the reduced RE due to several factors mentioned before. The N taken up by the crop is divided into that taken up by vegetative parts such as stem and leaf; and that taken up by the reproductive part such as grain (Chakwizira *et al.*, 2016), as represented by the NHI.

In the case of wheat, the NHI is affected by the translocation of stored N in vegetative parts into the grain (Fageria, 2010). The NHI is affected by the amount of grain produced and therefore improving the dry-matter harvest index of the crop will also improve the grain nitrogen uptake and N-utilisation efficiency (Chakwizira, 2016). The NHI is also found to be high in modern wheat and largely independent of N input. The N in grain comes mainly from the canopy N, which is remobilized during grain filling, and a relatively small amount remains in the straw. Therefore, increases in NHI seem to have limited scope for NUE improvement as little N is present in the straw biomass at harvest in modern wheat cultivars. (Hawkesford,

2017). Nonetheless, environmental factors, genotypic variation along with crop canopy maturation influence efficiency of the trait.

#### **1.2.4 N remobilisation efficiency (NRE)**

Some of the N taken up and stored by the plant is utilised for structural purposes. The N remobilisation efficiency (NRE) is defined as the amount of stored N during flowering which is not used for vegetative parts during maturity (Barbottin *et al.*, 2005). The variation of N remobilisation from vegetative organs to the grain is influenced by factors such as heat and drought stress, post-anthesis N uptake and low disease intensity. Further, the remobilisation of N from vegetative parts was found to be highest when the N availability was low during pre-flowering stage. In case of N uptake and N remobilisation during aforementioned environmental stages, the efficiency was insensitive to genotypic variation (Barbottin *et al.*, 2005). However, it must be noted that different crop plants have different nitrogen distribution amongst organs (Barraclough *et al.*, 2014).

High rates of NR have been observed when accelerated senescence takes place (Bogard *et al.*, 2010) leading to a high protein content, but may negatively impact grain yield due to the reduced C assimilation. There is a debate regarding how nitrogen remobilisation is regulated during grain filling period (Kong *et al.*, 2016). It has been suggested that the extent of remobilisation is dependent on N availability, environmental conditions and genotype and it is also influenced by the post anthesis N uptake (Martre *et al.*, 2003; Bancal, 2009; Ben Slimane *et al.*, 2013)

#### **1.2.5 Nitrate assimilation**

A series of enzyme-mediated reactions convert the absorbed nitrate into ammonium and then into amino compounds in the roots and leaves. These reactions may cause a bottleneck in NUtE and therefore modifications of these reactions in wheat can help improve N uptake. Another important enzyme which plays a key role in nitrogen metabolism is Glutamine synthetase (GS). This enzyme is essential for the assimilation of ammonia after nitrogen fixation. It additionally reassimilates ammonia which is released because of photorespiration. Glutamine synthetase/glutamate synthase (GS/ GOGAT) enzymes convert ammonium to glutamine and glutamate. This step is crucial for improvement of NUtE. During late leaf senescence stage ammonia accumulates at the leaf making them susceptible to volatilisation.

However, GS activity reduces these losses. The two cytosolic (GS1) and plastidic (GS2) isoforms of GS are critical for N assimilation and remobilisation as they play a role in leaf nitrate content, yield, root growth, grain N and grain filling (Foulkes *et al.*, 2009). GS isoforms have been over-expressed for generation of transgenics in wheat with improved NUE (Hu *et al.*, 2018). Habash *et al.*, (2001) demonstrated the role of GS in enhancing accumulation of nitrogen and root and grain biomass in transgenic wheat containing a *Phaseolous vulgaris* gene, GS1 driven by *rbcS* promoter. Schjoerring (2001) also performed experiments in oilseed rape wherein over-expression of GS1 was done with CaMV 35s promoter. Mutant lines generated for GS genes in rice, *OsGS1*, demonstrated stark reductions in growth rate and grain filling in adequate nitrogen conditions which demonstrated the role of GS in plant growth (Tabuchi *et al.*, 2005). The significance of GS has also been confirmed by Martin *et al.*, (2006) and Hirel *et al.*, (2007) in maize. Introduction of *TaGS2-2A<sub>pro</sub>::TaGS2-2A*, a favourable allele of *TaGS2-2A*, into Ji5265 variety of winter wheat significantly increased GS activity in leaves. Under high N and low N conditions, the transgenic events exhibited enhanced grain yield, spike number, TGW and grain number / spike as compared to the control. The transgenic expression of *TaGS2-2A* increased N uptake through root, NHI, N remobilisation and prolonged leaf function duration implying towards the significant role of *TaGS2-2A* in improving NUE in wheat through genetic engineering (Hu *et al.*, 2018).

Alanine on the other hand is essential for carbon and nitrogen metabolism in plants (Walters *et al.*, 1998). AlaAT was previously not known to be a key factor in nitrogen metabolism until recently (Miyashita *et al.*, 2007, Good and Beatty, 2011) when its role was specified in alanine anabolism which is a non-toxic stored form of nitrogen. Alanine aminotransferase (*AlaAT*) over-expression has also demonstrated improved NUE in cereals like rice (Shrawat *et al.*, 2008). Over-expression of the a barley *ALaAT* (*HvALaAT*) driven by stress inducible promoter *OsAnt1*, have been explored in rice, barley and also in wheat successfully enhancing NUE (Tiong *et al.*, 2021). These studies used homozygous lines of *Brassica napus* and *Arabidopsis thaliana* for the analysis and a barley *AlaAT* cDNA driven by a canola root specific promoter (*btg26*) was introduced in them. The *btg26* gene is a known regulator of osmotic and turgor pressure. The expression of *AlaAT:btg26* in comparison with control wildtype showed a clear increase in biomass and yield in nitrogen-limiting conditions (Good *et al.*, 2007). Similar experiments were performed in rice wherein, barley *AlaAT* cDNA driven by a rice tissue-

specific promoter (*OsAnt1*) was introduced, wildtype and transgenic plans showed comparable levels of nitrogen content (Shrawat *et al.*, 2008). However, in comparison to the canola root specific promoter, *btg26*, rice tissue-specific promoter *OsAnt1* demonstrated higher NUE phenotype in rice as well as stronger expression. Under the control of stress inducible promoter of rice, *OsAnt1*, an alanine aminotransferase of barley, *HvAlaAT*, was over-expressed in wheat to evaluate the effects on growth of the plant under two N conditions, 40 kg N ha<sup>-1</sup> (LN) and 80 kg N ha<sup>-1</sup> (HN) applied as urea. When grown under 80 kg N ha<sup>-1</sup> higher shoot biomass and yield against null and wild type was observed in GL45 line. In GL77 line, under HN conditions, higher grain yield only against wild type was observed. The altered expression of *AlaAT* has been seen to have an impact on glycolysis and TCA cycle that promotes N assimilation and utilisation consequently leading to greater biomass. Further studies may help unravel other underlying nitrate assimilation mechanisms for NUE improvement (Tiong *et al.*, 2021).

A significant number of over-expressing lines have been developed which show improved NUE, by increasing the activities of enzymes such as alanine aminotransferase and glutamine synthetase as well as knockout mutants which show the role of isoenzymes in amino acid metabolism (Lea and Azevedo, 2007). The generation of N uptake- efficient crops would reduce N fertiliser requirements and also would significantly reduce environmental impacts associated with N fertilisers. Alanine aminotransferase (*AlaAT*) is responsible for both production as well as degradation of alanine. While the role of these enzymes in NUtE, N accumulation in root, enhanced biomass has been demonstrated in several major cereals, exploring the effect on wheat remains to be done.

#### **1.2.6 Grain Protein Deviation/Content/Concentration**

The grain protein content is impacted by the nitrogen application rate and time, the variety and the interaction between them. Many studies have shown that the grain protein concentration increase with an increase in application of N (Haile *et al.*, 2012). Previous studies have shown decreased grain protein concentration upon early application of N at planting or tilling stage (Brian *et al.*, 2007). Wheat varieties having high grain percentage N tend to have low NUtE due to lower grain yield. Increasing fertiliser content up to 200 kg N ha<sup>-1</sup> showed a significant increase in grain protein. However, increased NHI have little to no impact on yield. The grain yield and NUtE are known to have an inverse relationship with the

grain percentage N and grain yield (grain N%) amongst genotypes (Hawkesford, 2012). This inverse relationship between yield and protein concentration can be attributed to dilution of protein at high yields, competition for energy and assimilation during the two processes and variation in accumulation rates of carbohydrates and proteins during grain filling. To overcome this, selection of genotypes which can have high  $N_{upMAT}$  (grain produced per unit of N uptake) while ensuring high yield at increased N uptake levels can be done. Although the negative correlation between yield and grain protein has been emphasised extensively, further exploration of this phenomenon is required (de Oliveira Silva *et al.*, 2020).

Studies conducted on two cultivars (Snowmass and Byrd) and 20 hard winter genotypes. with varying applications of N (0, 28, 56, 84, 112 kg ha<sup>-1</sup>). Showed variance for NUE was due to variation in  $NUE$  under high N conditions, while due to  $NUpE$  under limiting N conditions. However, enhanced  $NUE$  leads to decreased grain protein content along with high yield. Grain protein deviation (GPD) in multi-environments like these is determined by identifying genotypes exhibiting grain protein concentrations which deviate from expected value relative to their grain yield. A high yielding genotype, Brawl CL Plus, was identified among the 20 genotypes, with grain protein deviation of 6.7 g kg<sup>-1</sup> implying towards the possibility of superior lines, combining improved  $NUE$  and grain protein concentration, in a breeding population (Latshaw *et al.*, 2016). Enhanced levels of  $NUE$  is directly associated with increased N uptake and assimilation,  $PANU$  and grain protein content and are promising traits for selection by breeders (Foulkes *et al.*, 2009)

Several grain proteins correlate with the quality of baking bread particularly prolamins storage protein, gliadin, glutenin and albumin/globulin, all of which enhance or impact the dough one way or the other. Different landraces and cultivars contain these proteins in varying levels of the total grain protein concentration and influence the grain protein and baking quality of wheat. In this, it is crucial to also identify the grain proteins which are beneficial to the bread-making quality such a high molecular weight glutenins through modern genomics tools. Furthermore, grain N accumulation occurs through remobilisation of N accumulated in the canopy at anthesis and soil N uptake after anthesis. Therefore, boosting the post-anthesis N uptake by using application of N fertilisers at around anthesis can contribute to improving grain protein (Zörb *et al.*, 2018).



While deficiency of N is harmful for biomass growth, certain periods of N deficiency have no effect on the grain yield. In order to determine the exact N deficiency status of the crop, nitrogen nutrition index (NNI) has been taken up as an indicator (Justes *et al.*, 1994; Ziadi *et al.*, 2010). NNI is the minimal concentration of N required for maximum production of aerial dry matter. As mentioned previously as well, application of N fertiliser enhances NUE and early application of N lowers NUE. Application of N at later stages of can increase the NUE over a crop cycle. Analysis of NNI was carried out at different growth stages (GS30, GS32, GS39 and GS60) on the Zadoks scale of 14 wheat cultivars with varying fertilization strategies for two groups: with and without yield loss relative to maximum yield. It was observed that N deficiency during vegetative growth (four growth stages; GS30, GS32, GS39 and GS60 on the Zadoks scale) did not reduce the yield and grain protein, and enhanced the NUE. Therefore, NNI suggests that delaying N application during early stages can minimise unnecessary biomass and increase, yield, grain protein content and NUE (Ravier *et al.*, 2017).

Stay-green traits like leaf senescence timing and rate also effect the grain protein concentration and grain quality. During delayed senescence, N mobilisation is hindered thereby reducing grain protein concentration and grain quality. However, extending the duration of photosynthesis enhances the crop yield. A NAC transcription factor (TaNAC-S) was identified which showed expression in leaf/sheath tissues and decreased expression during post-anthesis leaf senescence. Over-expression of TaNAC-S in wheat showed a stay-green phenotype. While traits like grain yield, biomass, total grain N content and HI remained unaffected; grain protein content, grain N concentrations and total straw N content were found to be higher in the transgenics compared to the wild type. Thus, TaNAC-S is a negative regulator of leaf senescence leading to enhanced grain protein content at similar yields as non-transgenics. This may be due to enhanced N uptake in grain and in post-anthesis N uptake. (Zhao *et al.*, 2014). This result is in agreement with a previous study, where grain protein content and grain yield relation deviation were explained by variation in post-anthesis N uptake (PANU). The study carried out in a multi-environmental field trial with 27 European wheat cultivars across France under 4 different N treatments, for determining the relation between physiological processes related to genetic variability of GPD indicated the negative relation to PANU (Bogard *et al.*, 2010).

## 1.3 Approaches for NUE improvement

### 1.3.1 High-throughput phenotyping

High-throughput phenotypic methods through remote sensing techniques like unmanned aerial vehicles (UAVs), scan analysers, hyperspectral and multispectral radio imaging etc., provide a means of measuring NUE traits in large populations or panels of germplasm in terms of operability. Comprehending the N utilisation of crops would give a better knowledge of optimum application of fertilisers. For development of varieties with improved NUE, it is advantageous to have data the responses to N availability (Holman *et al.*, 2016). High-throughput phenotypic methods have been found to be beneficial to breeders and has helped reduce the genome-phenome gap as well (Jin *et al.*, 2020).

Unmanned aerial vehicles (UAV) or unmanned aerial systems (UAS) are an aerial platform wherein sensors are mounted and flown over vast areas collecting data. UAVs are utilized for various purposes such collecting multispectral and hyperspectral imagery, crop nitrogen efficiencies and determining crop growth rate (Holman *et al.*, 2016). UAVs carry sensors such as hyperspectral, multispectral and thermal cameras (Sozzi *et al.*, 2021). In a study by Yang *et al.*, (2020), UAV-based multispectral phenotyping was used to evaluate NUE in three cultivars of winter wheat (Zhongmai 895, Aikang 58, and Zhoumai 18) and assess the effectiveness of N fertiliser dosage for uptake by genotypes. The multispectral traits which include red normalized difference vegetation index (RNDVI), green normalized difference vegetation index (GNDVI), normalized difference red-edge index (NDRE), red-edge chlorophyll index (RECI) and normalized green-red difference index (NGRDI) were examined using UAV. RNDVI was used in prediction of phenotypic variation for NUE. Among the three cultivars, Zhongmai 895, was found to be efficient in NUE across the N treatments. Thereby, the study successfully demonstrated the effectiveness of UAV-based assessment of NUE for selection of superior genotypes (Yang *et al.*, 2020).

Hyperspectral, multispectral and digital imaging techniques can facilitate assessment of growth, biophysical changes of plant populations corresponding to varying N levels, eventually improving NUE (Jin *et al.*, 2020). These techniques allow for collecting high-quality phenotypic data among diverse germplasms. Estimation of chlorophyll levels, shoot biomass and growth parameters were derived using hyperspectral imaging-derived biomarkers at the

vegetative stage precluding the need for analysis at the mature stage of wheat. Phenotypic examination for N response traits like NUE at varying levels of N in a controlled environment was carried out using digital and hyperspectral image analysis. Further, in order to estimate biomarkers like chlorophyll and biomass content, these high-throughput phenotyping digital and hyperspectral imaging techniques proved to be useful for studying N response traits. The study conclusively derived a novel vegetation index (NDCl<sub>w</sub>) which was able to estimate chlorophyll levels more efficiently than previously reported vegetation indices using hyperspectral imagery. Additionally, digital coloured imagery was able to deduce shoot biomass. Therefore, the two techniques can be utilised for selection of superior germplasm for improving NUE using hyperspectral chlorophyll and digital biomass as biomarkers (Banerjee *et al.*, 2020). Crop improvement efforts targeting attributes like canopy height, biomass production, ABGM and GC for assessment in a temporal fashion is also done through the capacity of Light Detection and Ranging (LiDAR). Synergies between LiDAR and hyperspectral imaging can facilitate the development of multisensory indices and would help overcome challenges pertaining to changes in canopy density and allowing estimation of biomass across the various layers of a dense canopy (Jimenez-Berni *et al.*, 2018).

While high-throughput phenotyping techniques are labour-intensive and accurate, they often are time consuming and expensive which can be a bottleneck in crop breeding. Red-Green-Blue (RGB) imagery has been explored for its cost-effectiveness and high-throughput approach in wheat and the colour components and vegetation indices were associated with GY and canopy temperature depression (CTD) levels (Zhou *et al.*, 2015). RGB imagery has been utilized for assessment of biotic stress conditions in wheat (Zhou *et al.*, 2015) and leaf N concentration across varying N fertilisation condition (Vergara-Díaz *et al.*, 2016).

The review by Jin *et al.*, (2020) provides a comprehensive overview of the various sensors which can be utilised for estimation of NUE. Apart from UAVs, hyperspectral and multispectral cameras, photosynthetic sensors like LI-COR 6400 and fluorescence sensors like PlantExplorer are able to monitor NUE (Jin *et al.*, 2020). Leaf N content is a defining parameter for photosynthetic proteins as well as other traits like leaf-chlorophyll content, leaf mass per area, area-based canopy, leaf dry weight per unit soil area and leaf mass area. Prevalent phenotyping techniques monitor the leaf N content but are prone to non-specificity for N stress due to backgrounds. Sun-induced chlorophyll fluorescence (SIF) is a novel technique

developed to obtain PNUE as well as area/mass-based leaf N content in an accurate manner (Jia *et al.*, 2021). Apart from this, fluorescence sensors such as canopy fluorescence sensors have also been developed for estimation of winter wheat N and grain quality along with its spatial and temporal variability. Canopy fluorescence sensor measurements have also been used to investigate the spatial variability across various developmental stages in winter wheat of soil N on grain quality (Song *et al.*, 2017).

Enhanced root length density is directly correlated with improved N uptake and assimilation (Foulkes *et al.*, 2009). Technical constraints of high-throughput root phenotyping limits seedling screening usually on artificial media rather than on mature soil. To overcome this limitation of manually annotating images of root seedlings, a novel 2-D statistical data analyser software, RootNav, has been developed which allows automated analysis of images of seedling root system of wheat grown in growth pouches in controlled environment. Atkinson *et al.*, (2015) carried out a study for quantifying root system architecture traits in DH mapping populations to determine QTLs seedling root traits related to early vigour, which has an major influence of N uptake, using a high-throughput phenotyping pipeline. In a study by Kenobi *et al.*, (2017) related with root architecture, 300 wheat genotypes were taken and divided into two categories: high versus low NUpE and high versus low nitrate uptake in growth medium. The use of linear discriminant analysis has been adapted to examine differences in distribution patterns of root architecture (RAS) between wheat plants in the first category. Furthermore, among the low NUpE group distribution of RAS was also found to vary in the second category.

Root system architecture (RSA) is also crucial for gaining optimum N. A seedling root phenotyping pipeline has been utilised with RootNav 2.0 to quantify genetic variation in 30 landraces derived from parental Paragon cultivar for RSA traits under HN and LN conditions in hydroponic conditions. Further the study aimed to correlate genetic variation in leaf photosynthesis rate, N uptake, biomass and NUE traits in glasshouse conditions under HN and LN. Substantial variation was observed for seedling RSA in landrace derived lines above elite Paragon cultivar. Also, glasshouse experiments demonstrated genetic variation in flag-leaf photosynthesis rate in landrace derived genotypes (Kareem *et al.*, 2022). Intermediate scale root phenotyping such as X-ray computed tomography (Mooney *et al.*, 2012, Mairhofer *et al.*, 2013), magnetic resonance imaging (Schmittgen *et al.*, 2015), mini-rhizotrons (Poorter *et al.*,

2012), and rhizotron (Nagel *et al.*, 2009) methods have also been developed which offers promise.

#### **1.4 Genetic diversity in wheat landraces**

The domestication of wheat occurred about 8,000 years ago in the Southern part of Turkey by hybridisation of tetraploid *Triticum dicoccoides* (A and B genome donor) with wild, diploid *Aegilops tauschii* (D genome donor) (Salamini *et al.*, 2002). This domestication has caused the loss of genetic diversity which existed in the wild ancestors. These domesticated varieties, called landraces (LCs), also became adapted to environmental conditions and genetic drift and selection further reduced the genetic diversity. The modern elite cultivars (MCs) are also known to have a diminished genetic diversity (Kareem *et al.*, 2022). The A.E. Watkins bread wheat landrace collection was developed by A.E. Watkins based from many countries in Asia and Europe. He developed an astounding collection of 7000 accessions of which only 826 remain available today. This collection of bread wheat collection, the Watkins collection, holds potential for demonstrating genetic diversity before domestication and modern breeding (Wingen *et al.*, 2014). These landraces can be utilised to obtain enhanced biomass and other sustainable agronomic goals like water and N stress tolerance. This can be achieved through introgressing desirable traits from LCs into MCs (Winfield *et al.*, 2018). In a study to investigate genetic diversity of the Watkins collection and also the genetic structure, the collection was genotyped with 41 SSR microsatellite markers across all 21 chromosomes. This analysis was combined with the modern collection of European wheat cultivars, Gediflux collection. The Watkins collection exhibited a global geographic scale while the Gediflux collection had a much narrower geographic reach. Other trend differences observed were flowering time, plant height and grain characteristics (Wingen *et al.*, 2014). Exploring these LCs for introgressing novel traits and alleles into wheat varieties is an excellent means of overcoming the plateau reached in wheat yield.

In recent years, SNP markers have been detected which provide a genome-wide coverage (Winfield *et al.*, 2016). High-density, SNP-based genotyping was performed using 800,000 markers of bread wheat to characterise 120 core Watkins collection and 145 elite cultivars. This array revealed 258 605 polymorphic markers in which 218,106 belonged to Watkins and 188,441 to the elite collection. Of these 32.2% (70,164) of Watkins collection and 21.5% (40,499) of the elite accessions were unique. Similar to the previous study, the Watkins

collection demonstrated significantly enhanced genetic diversity compared to the elite cultivars (Winfield *et al.*, 2018).

To fully exploit landrace collections, identification of genetic variations and their impact on meiosis, sexual reproduction and fertility in populations need to be assessed. This would facilitate the understanding of underlying mechanism and consequences of adaptation, stress tolerance and performance of the crop system. Emphasising on post-domestication adaptive circumstances, a nested association mapping (NAM) population of 60 biparental sub-populations comprising mostly of crosses with core Watkins collection landraces was developed (Wingen *et al.*, 2017). An elite cultivar of spring wheat, Paragon, was taken as reference parent. Over 126,300 cross-over events from the NAM panel was assessed which gave about 1611 linkage groups. Further, a consensus map, called landrace consensus map (LRC) was developed which included 2406 SNP markers and 33 SSRs, and the map length and marker distance were compared between linkage maps. A positive correlation was found between number of linked markers and map length. Investigation of recombinant QTLs demonstrated over 126,300 cross-over events wherein the mean number of cross-overs showed variation within populations which was later found to be due to less influence of non-reference parent towards the recombinant rate. This study could be useful for selection of parents for crossing events in breeding programs (Carvalho and Foulkes 2018; Wingen *et al.*, 2017).

Synthetic hexaploid wheat (SHW) has been generated from tetraploid, *Triticum turgidum* (A and B genome) and its diploid wild relative, *Aegilops tauschii* (D genome) and are utilised for development of improved wheat with new characteristics. Various means have been employed to explore SHW in breeding programs mainly through phenotyping for evaluation of genetic variations for stress tolerance and disease resistance (Halloran *et al.*, 2008; Xie and Nevo 2008). Additionally, evaluation of genetic variation can also be achieved through crosses and backcrossing and advanced backcross-quantitative trait loci (AB-QTL) analysis. Further gains utilising SHW can be attained through development of introgression lines (ILs) which is essentially a complete/near complete genome of a wild relative in the background of an elite cultivar. ILs, however, are not able to dissect epistasis effects. SHWs have been explored for incorporation of disease resistance (also multiple disease resistance, MDR), environmental stress tolerance (salinity, nutrition), enhancing yield and productivity and quality

improvement (Ogbonnaya *et al.*, 2013). The first reported wheat cultivar derived from SHW backcrossing with synthetic backcross-derived line (SBL) was Chuanmai 42, which had an enhanced yield of 22.7% compared to other cultivars (Yang *et al.*, 2009). Since this cultivar has high potential, identification of loci harbouring important traits which have been introgressed in SHW has been done (Li *et al.*, 2011). Synthetic-derived lines have been observed to have higher grain yield and biomass under LN conditions as compared to recurrent parent Paragon. N stress adaptation traits mainly N uptake capacity was associated with improved root mass and length. In the Watkins collection, enhanced grain yield performance was seen under LN conditions in comparison to modern cultivars. Therefore, landraces have proven to possess a wide array of useful stress adaptive traits which can be further examined (Gaju *et al.*, 2016).

Approximately 4 high-yielding wheat varieties using primary SHW lines and 12 from SHW-derived lines have been developed. Polymorphism studies, genotype-phenotype and fingerprinting analysis has led to the development of elite varieties with characteristics such as greater spikes and grain per plant, large grain, and enhanced grain potential along with disease resistance (Li *et al.*, 2014) such as stripe rust resistance (Li *et al.*, 2006). Today about 1500 SHWs are catalogued globally. Populations derived from SHW using SSR and SNP markers would help in genetic mapping and trait identification occurring due to genetic variations (Ogbonnaya *et al.*, 2013).

While SHWs have been shown to demonstrate abiotic stress tolerance traits, they also have a few undesirable characteristics such as late maturity, tall plants, red seed coat colour and difficulty in threshing (Li *et al.*, 2014). The wild relatives *Triticum urartu* (wheat A genome donor) is known to be associated with photosynthetic capacity which directly has implications for NUE (Austin *et al.*, 1982). Synthetic lines (*Triticum durum* × *Aegilops tauschii*) along with synthetic derivatives created in CIMMYT by crossing with elite bread wheats have been shown to have greater leaf photosynthetic rate and yield than bread wheat parents. Additionally, primary synthetic spring wheat has been observed to demonstrate greater biomass as compared to recurrent parent (Dreccer *et al.*, 2004). In a study identifying novel wheat lines with improved higher biomass, NUE and leaf photosynthesis than the bread wheat parent under HN and LN, amphidiploid lines were characterised (Nehe *et al.*, 2022). These lines were generated by crossing wild relatives of wheat (*Amblyopyrum muticum*, *Aegilops speltoides*,

*Aegilops umbellalata*, *Aegilops comosa*, *Thinopyrum turcicum* and *Thinopyrum bessarbicum*) with bread wheat parents. Under LN conditions, the average grain yield was seen to reduce by 38% as compared to high N conditions. Positive transgressive segregation was observed at pre- and post-anthesis for flag-leaf photosynthesis under HN and LN conditions. Additionally, one amphidiploid line demonstrated positive transgressive segregation under LN conditions for N uptake. These results successfully exhibited the potential of diversity of wild relatives for improving NUE in modern bread wheat germplasm (Nehe *et al.*, 2022).

Studies investigating novel variation for NUE and associated traits have also been carried out in a panel of diverse hexaploid wheat germplasm comprising: (i) landraces from the AE Watkins collection, (ii) synthetic-derived hexaploid lines in a cv. Paragon spring wheat background and (iii) UK modern cultivars including cv. Paragon under HN and LN conditions. Physiological traits were assessed. Under low N conditions, synthetic derived lines had higher biomass than modern cultivars. In addition, under high N conditions, one synthetic-derived line had higher pre-anthesis flag-leaf photosynthesis rate than Paragon. Similarly, under LN conditions, one SD line and two SHW derived lines had greater yield and biomass respectively as compared to Paragon. The study concluded that trait introgression from synthetic-derived wheat lines into UK modern wheat cultivars has potential in improving yield and above-ground biomass under varying N conditions (Gaju *et al.*, 2016).

## **1.5 Agronomic practices to increase NUE**

### **1.5.1 Bio-fertilisers and nano-fertilisers**

A novel and interesting technology to raise the efficacy of nitrogen uptake is the soil inoculation with plant growth promoting bacteria (PGPB) and can be exploited as an aspect of integrated nitrogen management systems.

The PGPB comprise of genera of microorganisms such as *Azotobacter*, *Nitrobacter*, *Pseudomonas*, *Rhizobium*, *Arthrobacter*, *Enterobacter* and *Bacillus* species. Studies have shown that such microorganisms efficiently inhabit within the plant space and contribute by fixing nitrogen and facilitating the nodulation process (Bhattacharyya and Jha, 2012). To reduce the harmful effects of chemical fertilisers, bio fertilisers are a potential means to negate the detrimental effects on the environment.



There have been several documented events focussing on the use of PGPB as bio fertilisers in crops such as legumes, maize and wheat (Naiman *et al.*, 2009, Piccinin *et al.*, 2011, Saia *et al.*, 2015, Hassan Bano, 2016, Charousová *et al.*, 2016, Majeed *et al.*, 2018) wherein there has been an enhancing effect on the plant growth through mechanisms such as phosphate solubilisation, nitrogen fixation, production of antifungal/ antibiotic metabolites and an overall induced systemic resistance of the plant (Di Benedetto, 2017). These microorganisms were also seen to improve the growth, nitrogen uptake and grain quality (Saia *et al.*, 2015; Colla *et al.*, 2015)

Plant N uptake systems through  $\text{NO}_3^-$  and  $\text{NH}_4^+$  may be enhanced by interaction with arbuscular mycorrhizal fungi (AMF) (Cormier *et al.* 2016). The conversion of  $\text{N}_2$  into  $\text{NH}_3$  is performed by N-fixing bacteria present in the soil (Venieraki *et al.*, 2011) in the wheat rhizosphere. Similarly, many microorganisms regulate plant hormones such as cytokinins and auxins, and subsequently modifying the root structural system (Cassán *et al.*, 2009, Moubayidin *et al.*, 2009). However, there are still certain aspects to establish bio fertilisers such as PGPB as an alternate approach to increase NUE. Extensive phenotypic and genotypic studies to comprehend the interaction between host-pathogen would give a clearer picture of the best candidates and strains of PGPB (Di Benedetto *et al.*, 2017).

Nanotechnology is an emerging aspect of modern agricultural technologies utilizing the unique properties of nanoparticles. Nano-fertilisers are synthesized by fortifying cationic ( $\text{NH}_4^+$ ,  $\text{K}^+$ ,  $\text{Mg}_2^+$ ) and anionic ( $\text{NO}_3^-$ ,  $\text{PO}_4^-$ ) nutrients onto the plants with nano-dimensions (1-100nm). These nano-fertilisers are released into the soil at a slow pace to reduce loss of resources (Subramanian and Thirunavukkarasu, 2017). Nano-fertilisers have been used in a few studies focussing on major nutrients such as potassium and phosphorous (Bansiwal *et al.*, 2006, Liu *et al.*, 2006). The unique feature of these fertilisers is their slow release. Nitrate nitrogen nano-fertilisers are capable of releasing nitrogen for almost 50 days in contrast to chemical fertilisers which release for a maximum of 2 weeks (Subramanian and Rahale, 2009). This slow release reduces leaching to a great extent and provides the plant with a constant supply of nutrition for a comparatively extensive period.

Reduce uptake efficiency of N by plant is mainly attributed to nitrate leaching and denitrification of  $\text{NO}_3^-$  and di-nitrogen gas. Ammonium N ( $\text{NH}_4^+$ ) is less prone to denitrification and fertilisers are therefore used in this form. The oxidation of  $\text{NH}_4^+$  to  $\text{NO}_2^-$  is the first step to

nitrification followed by production of nitrate via ammonia oxidising bacteria. Commercial inhibitors are used to minimise the effect of these bacterial species. Production of nitrification inhibitors from plant roots has emerged to be a cost-effective alternative to commercial inhibitors. These, known as biological nitrification inhibition (BNI) have also been found in root exudates of certain wheat relatives such as *Leymus racemosus* and also more recently in *Triticum aestivum* (O'Sullivan *et al.*, 2016). The identification of BNIs in modern wheat cultivar suggests its potential for breeding into other elite cultivars.

Studies have been carried out to improve NUE using this revolutionary technology. Zeolite proved to be an excellent material for nano-fertilisers development due to its large surface area and sieving properties. Fertilisers amended with zeolite showed a 15% increase in NUE in wheat (Ahmed *et al* 2008). Comparison with commercial fertilisers also showed promising results (Fujinuma *et al.*, 2011).

While novel fertilisers have been developed, it is also important to ensure reduce loss of N, due to environmental factors such as irrigation, and subsequently increase NUE. The performance of neem-coated urea has been assessed with neem cake (NCU) and neem oil (NOCU) in increasing the yield of wheat. A study comparing the effect of neem-coated urea and ordinary urea to wheat at different levels in 3 and 2 split doses, demonstrated improved NUE when applied in 3 split doses ( $48+48+24 \text{ kg N ha}^{-1}$ ) or drilled between rows as single dose ( $96 \text{ kg N ha}^{-1}$ ) in coarse textured soil. In fine textured soil, however, the performance of urea and neem coated urea was at par probably due to reduced loss in nitrate leaching owing to texture of soil (Thind *et al.*, 2010).

In addition to this, early-season NDVI use for N estimation and guided input of fertiliser is another method to optimize fertiliser usage (Lukina *et al.*, 2001). A modified light reflectance sensor has been developed which allows for early estimation of N uptake and computes a NDVI based on this. The sensor can be used to correlate growth stages 4 and 6 with NDVI. Furthermore, this correlation also was related to grain yield which helped in estimation of potential N which could be removed between planting to sensing dates. This predicted the N requirements of the plants which can then be accurately supplemented using N fertiliser in an optimum dosage (Lukina *et al.*, 2001).

## **1.6 Genomics-assisted breeding approaches**

Physiological traits such as root length density, glutamine synthetase (GS) and Alanine aminotransferase (AlaAT) activity, post anthesis leaf photosynthetic rate, N remobilisation efficiency (NRE) post anthesis, post anthesis N uptake (PANU), root system architecture (RSA) and stay green trait are relevant to NUE improvement (Foulkes *et al.*, 2009). The growing need to reduce usage of nitrogen fertilisers and increase NUE has led researchers to explore the identification of key regions of chromosomes associated with NUE traits by genetic analysis to identify QTLs to develop markers for the key traits for application in marker-assisted breeding (MAS). Marker-assisted selection (MAS) has gained much focus in recent times and researchers have delved deeper into the question of optimum usage of variation in crop gene pools and also examining useful variations in wild relatives of the crop. Markers are essential in analysing crop traits and linking them with genomic regions (Miflin and Habash, 2002). Molecular breeding technologies such as genomic-assisted breeding involve the utilisation of molecular information to develop superior genotypes. For a complex and polygenic trait like NUE (Hawkesford and Griffiths, 2019), the regulatory pathways occurring at the transcriptional and post-transcriptional level are of utmost importance (Cormier *et al.*, 2016). Molecular markers also reduce the labour and time intensive phenotypic traits of NUE (Guttieri *et al.*, 2017) and therefore, discovering molecular markers related to NUE traits would help in enhancing N uptake.

### **1.6.1 QTL identification**

The identification of genes controlling NUE can be done through various means such as association genetics, QTL mapping using biparental (RIL and DH lines) and multi-parental populations, backcrossing and identification of variation in near-isogenic lines (NILs) (Hawkesford and Griffiths, 2019). The number of QTLs identified in a particular study depends on several factors such as environmental conditions, density of the genetic map and number of traits, and size and type of population etc.

The association of NUE and role of glutamine synthase (GS) has been demonstrated through correlation studies wherein this enzyme can be utilised for studying N levels in the plant (Kichey *et al.*, 2007). In addition to this, QTLs associated with grain yield and grain protein content encoded by cytosolic GS1 and/or plastidic GS2 have been identified contributing to wheat productivity. Gene families related to the amino acid biosynthesis (GOGAT and GS) and

nitrogen transporters have been studied due to their role in nitrate assimilation (Beatty *et al.*, 2013). NAD (P) H-GOGAT is involved in N assimilation and therefore is known to play a fundamental role in N uptake (Quraishi *et al.*, 2011; Beatty *et al.*, 2013). Additionally, studies in durum wheat have suggested that NADH-GOGAT expression and grain protein content are directly related with this enzyme and not cytosolic GS1 which is crucial for NUE in C3 cereals like wheat (Cormier *et al.*, 2016). The identification of QTLs co-localised with N uptake and assimilation enzymes provides insight into improving NUE (Hirel *et al.*, 2007). Mapping studies usually are carried out to identify regions in chromosome that are linked to a particular trait and are further developed into markers. Most of the regions that have been found associated with NUE-related traits are seen to be evolutionarily conserved regions. An excellent example of this is the GOGAT and GS genes (Quraishi *et al.*, 2011, Han *et al.*, 2015). However, it is crucial to consider the fact that such studies are not specific and are often imprecise about the genomic regions. There is the possibility of the existence of other genes which might be strongly correlated with NUE-related traits but do not fall in any such conserved regions, viz *Ppd*, *Vrn* (Habash *et al.*, 2007, Laperche 2007) and hence it is essential to consider co-segregation of such genes too (Han *et al.*, 2015).

As mentioned earlier, grain N is derived from two major sources, N remobilisation (NRE) and uptake post anthesis. In winter wheat, 76-80% of N may be derived from remobilisation of pre-anthesis N (Bogard *et al.*, 2010). While NRE and post-anthesis N uptake (PANU) both contribute significantly to NUE, they are often negatively correlated. GPD is directly influenced by GPD PANU which is an effective strategy in improving grain yield and protein in wheat (Guttieri *et al.*, 2015). Association mapping has led to findings where 32-380 small effect QTLs were indicated related to NUE traits in various studies in wheat (Cormier *et al.*, 2016).

A study performed in 8 environments testing 2 N levels in bread wheat led to noteworthy findings (Cormier *et al.*, 2014). 1010 significant SNPs defining 333 chromosomal regions with at least one NUE-related trait were found. Co-localisations for 39% of QTLs was determined. A network-based approach helped in analysing these co-localisations showing similarity with previously identified genes such as NADH-GOGAT and GSe (Cormier *et al.*, 2014).

Root system architecture has gained much importance in cereals leading to the development of RSA ideotypes as an important factor for improving N-uptake efficiency. Wheat is

predominantly grown in rain-fed regions where drought is the major stress concern. In these regions, the grain yield of wheat is only 10-50% of that reached under irrigation. Lack of QTLs pertaining to root traits has significantly hindered MAS for RSA in wheat. A study performed in tetraploid durum wheat has led to identification of QTLs associated with RSA (Maccaferri *et al.*, 2016). Association mapping for RSA in 2 recombinant inbred lines (RIL) and 183 elite durum wheat accessions identified 20 QTLs associated with root length and 30 for root growth angle (RGA). Among the 20 QTLs for root length, 15 overlapped with RSA traits reported previously in bread wheat. Additionally, out of the 30 QTLs for RGA, 6 have shown correspondence with reported bread wheat QTLs. Prioritisation of these overlapping QTLs on the basis of breeding value identified 3 QTL clusters for root length and number and 9 QTL clusters of significant value in QTL MAS or cloning of relevant causal genes (Maccaferri *et al.*, 2016). Studies on seedling seminal root traits such as vigorous early root growth and angle are known to have an impact on N uptake. A high-throughput phenotyping pipeline was used to characterise a Savannah × Rialto doubled-haploid population for RSA traits and identified 29 QTLs across chromosomes (chr) 1A,2B, 3B, 3D, 4D, 6D, 7A, and 7D. Out of these 7 QTLs were associated with GY QTLs and 9 with N uptake QTLs as identified for this DH population in field experiments. Two QTLs for GY and NUp co-localised with root QTLs on chr 2B and 7D. Additionally, 11 root QTLs were found to co-localise on 6D which suggests the major-gene effect of these regions on seedling root architecture (Atkinson *et al.*, 2015). A high density map generated using 184 RILs (Tainong 18 × Linmai 6) associated with 14 seedling and 17 maturity traits for NUE were examined in wheat under high N (HN), moderate N (MN) and low N (LN). A total of 121 and 130 QTLs were identified in a seedling screen (hydroponic culture trial) and at maturity stage, respectively, of which 47 were relatively high frequency QTLs (RHF-QTLs) and 16 clusters were found. The most important marker, C9 on chromosome 4B, was corresponded to QTLs for biomass, yield, NUpE and NUtE and comprised 9 and 11 QTLs for seedling and maturity stages. 7RHF-QTLs were mapped to this marker which makes this a valuable marker. Correlation analysis also indicated that biomass traits and yield traits can be considered as morphological indexes for NUE examination (Zhang *et al.*, 2019). In order to determine the underlying genetics of N response, 136 RILs and 138 DH lines of high NUE parent VA05W-151 × low NUE parent Yorktown and high NUE parent VA09W-52 × Yorktown, respectively, of winter wheat was investigated at four-site seasons under low and high N conditions. Sequencing using a genotyping-by sequencing platform determined around

3100 high quality single nucleotide polymorphisms (SNPs). A total of 130 QTLs were detected across 20 chromosomes, out of which 6 were directly related with NUE and N-related traits. While 2 of these 6 QTLs were associated with previously defined photoperiod (*Ppd-D1* on chromosome 2D) and disease resistance (*FHB-4A*) gene and prior investigations; one of the QTLs, *QNue.151-1D* was novel. This QTL was later shown to be linked with the *TaGW2* gene which impacts grain size (Brasier *et al.*, 2020).

The optimum root diameter, root number and lateral root hair length are important for N uptake from low N soil. Under low N conditions, the root length usually increases for greater penetration and enhanced uptake of N. Therefore, apart from RSA, RSA-related traits (RRTs) and their plasticity is crucial for enhanced NUE. In a study by Fan *et al.*, (2018) with 188 RILs of wheat (Kenong and Jing, 411) under control and low N conditions, 53 QTLs were identified for 7 RRTs and 14 QTLs for plasticity of RRTs. Out of these, 30 QTLs were located in 9 cluster chromosome 2B, 2D 3A, 3D, 6B, 6D, 7A and 7B of which 6 were found to be co-localized with loci for NUE-related traits. Clusters on chromosome (chr) 2B and 7B contributed towards optimal root system and on chr 6D influenced the RRT plasticity response to NUE. In addition to this, meta-QTL analysis has demonstrated that a cluster on chr 7B has the potential to impact root architecture under different genetic backgrounds (Fan *et al.*, 2018).

While several studies have been carried out identifying QTLs related to NUE, reproducibility is lacking owing to the quantitative nature of NUE traits. Thus, identifying QTLs with a potential to deploy in MAS is a challenge. As a result of this, meta-analysis of QTL (MQTL) has been carried out and has identified 11 major chromosomal regions, a meta-QTL associated with NUE. The QTL for NUE identified was *QNue.151-6A* located near QTL on 6A which was previously found to co-localize with glutamine synthetase gene (*GS1*) (Brasier *et al.*, 2020; Quraishi *et al.*, 2011). These MQTLs have reduced confidence intervals (CI) and enhanced phenotypic variation is explained (PVE%) which makes identification of candidate genes easier.

Wheat is of two types based on the vernalisation pattern; winter wheat which requires low temperature exposure during winter to accelerate vegetative to reproductive maturity and spring wheat which does not require vernalization. Winter wheat requires more N for yield as it has a longer duration growing season. A study using RILs (Jagger x 2174) of winter wheat under contrasting N fertilization regimes in a greenhouse for identification of QTL for N-

related agronomic traits was performed. Positional cloning of a major QTL demonstrated that the vernalisation gene *TaVRN-A1* was closely related to expression of *TaNUE1* gene which is known to influence NUE in wheat (Lei *et al.*, 2018).

RSA traits and RRTs related QTLs have been studied extensively and known to be related to N uptake and yield in wheat. Studying root morphology in soil and precision QTL mapping for many genotypes is a challenge and therefore hydroponic conditions are used which ensure evaluation of multiple genotypes with least error. Epistatic interactions between QTLs have also been studied in NUE trait in Indian wheat. Using 187 F<sub>2</sub> and F<sub>2:3</sub> population derived from nitrogen-responsive contrasting trait parents, linkage map was developed using SSR markers. The parental lines demonstrated variation for most of the NUE-traits. Root dry weight, N uptake and utilisation were assessed through phenotyping under high N conditions. QTL analysis was then performed for 103 SSR loci using mean phenotypic data of 8 NUE related traits (shoot dry weight (SDW), root dry weight (RDW), total dry weight (TDW), root: shoot (R: S), N% in shoot, NUpE, NUtE and NUE). A total of 27 QTLs were identified across 14 chromosomes for the 8 traits. Out of these 2 QTLs have been detected as significant for SDW and/or NUE. The major part of phenotypic variation was contributed by QTLs for NUtE (32.39%) and R: S (21.48%). Chromosome 2A, 4A and 7A harboured QTLs for maximum NUE-traits. In addition to this, the QTLs were found to have epistatic interactions influenced by additive and non-additive genes. This was mainly observed in QTLs in chromosome 2A for traits SDW, RDW, TDW, R: S, %N, NUtE, and NUpE including epistasis. Owing to the complexity of the trait, dissection of epistasis QTLs can prove to be useful for breeding programs in improving NUE (Ranjan *et al.*, 2021).

### **1.6.2 GWAS studies**

GWAS have gained popularity in recent times for genetic research and is an excellent addition to QTL analysis. On one hand, QTL analysis contains linked genes, GWAS gives us unlinked genes and sometimes even nucleotides. While GWAS comes with its limitations including false positives and unavailability of genomic resources, combining QTL analysis and GWAS can produce promising and robust results (Miles and Wayne, 2008).

In the Great Plains of the United States 299 genotypes (258 hard red winter, 41 hard white winter) were grown in a span of two years at two levels of N fertility in a GWAS study (Guttieri

*et al.*, 2017). A total of 224 unique significant marker associations were identified for the traits GY, GPD, NHI, NUpE, NUtE, NRE and PANU involving 183 unique SNPs spanning over 5 chromosomes (1A, 1D, 2B, 2D, and 4B). It was also found that the minor alleles of the significant SNPs have an impact on the NUE traits and increasing the frequency of these alleles will eventually lead to improvement of NUE (Guttieri *et al.*, 2017). Another NUE study was done by Xu *et al.*, (2014) where 182 RILs (Xiaoyan 54 × Jing 411) of wheat was studied for NUE and yield traits, at varying N levels, in 6 environments for determination of QTLs. Eighteen QTLs for NUE were found to be conserved across environments and 3 major QTLs identified on chromosomes 2D, 4B and 6A. N fertilisers affected N concentration and uptake efficiency (Xu *et al.*, 2014).

Meta-analysis of QTLs for NUE and RSA in wheat along with ortho-MQTL analysis of wheat and maize has been performed (Saini *et al.*, 2021). The meta-analysis results were compared with GWAS and integrated with a transcriptomics study to reveal candidate genes affecting NUE and RSA. Out of the total 118 MQTLs, 1991 candidate genes were identified encoding kinase domains, F-box like domains, cytochrome P450 proteins, glycoside hydrolase, UDP-glucosyltransferases, NAC TFs, expansins, early nodulin-93 protein, GRAS TFs and ABC transporter-like proteins. All of these genes and gene families have been reported to be associated with NUE and/or RSA. The ortho-MQTL data demonstrated 60 rice genes where 35 of these were used for identifying 49 wheat orthologues. These wheat orthologues were found to encode genes which are involved in stress signalling, N assimilation, amino acid biosynthesis, TFs involved in NRE and NUE, and transporters (Saini *et al.*, 2021). Utilisation of one major MQTL and ortho-MQTL analysis can help improve marker assisted breeding (MAB) by determination of potential candidate genes which can then be further used for biotechnological techniques such as transgenesis and genome editing for improving NUE. GWAS has proven to be a useful tool for understanding complex traits such as NUE and NUE-related traits. However, QTLs for NUE identified at the mature stage in wheat is still lacking. In a GWAS of agronomic traits related to NUE in wheat, 389 cultivars were phenotyped in 5 environments (in various experimental stations across China) under HN and LN for 8 NUE-related agronomic traits: PH, GYP, plant height (PH), spike length (SL), grain number per spike (Gns), tiller number (TN), thousand kernel weight (TKW), and shoot biomass per plant (BpP) (Shi *et al.*, 2022). A total of 347 QTLs for low N tolerance indices were detected including 11



stable QTLs. In addition, 69 candidate genes were predicted for low N tolerance and four novel TFs. The study provided some promising markers and candidate genes for improvement of NUE in wheat.

## **1.7 Biotechnological techniques for improving NUE**

### **1.7.1 Transgenesis**

While enzymes such as alanine aminotransferase and glutamine synthetase have been examined through over-expression studies in wheat forming an integral part of nitrate assimilation, nitrate signalling is also crucial for NUE improvement, and several factors are known to be involved in nitrate sensing and signalling in crops. A NAC [NAM (no apical meristem), ATAF (*Arabidopsis* transcription activation factor), CUC (cup-shaped cotyledon)] transcription factor, *TaNAC2-5A* was isolated and identified in wheat which binds to promoter region of genes governing a nitrate transporter and glutamine synthetase. Transgenic events developed through over-expression of *TaNAC2-5A* demonstrated improved nitrate influx due to enhanced root growth. The transgenics also showed greater yield, N accumulation in aerial parts and greater grain N content compared to the non-transgenic, wild type. Therefore, this TF holds potential for enhanced N accumulation and allocation eventually contributing to improved NUE and yield (He *et al.*, 2015). The *Altered Meristem Program 1 (AMP1)* gene encodes a glutamate carboxypeptidase and amp1 mutants have been known to effect plant development (Shi and Tong, 2021). Its paralog *LAMP1 (LIKE AMP1)* has similar effects on plant development in *Arabidopsis*. In wheat, *TaLAMP1* was found to be induced by N deficit conditions and alteration in its expression influences root growth and N uptake at the seedling stage. Over-expression and knockdown studies of *TaLAMP1* was observed to reduce grain yield and yield response to application of N. These transgenics also demonstrated altered root morphology and changes in spike number and grain per spike. Further dissection of role of *TaLAMP1* would help in comprehending the underlying mechanism of altered root morphology and plant architecture (Shi and Tong, 2021).

### **1.7.2 Genome editing**

Additional factors have been identified in rice which influences NUE. The abnormal cytokinin response1 repressor1 (are1) mutants have been found to behave as a suppressor of fd-GOGAT mutants which cause defects in N assimilation. Loss-of function mutations in rice *ARE1*

cause delayed senescence, enhanced grain yield and NUE under LN conditions (Wang *et al.*, 2018). Three wheat homeologs of *ARE1* was identified and isolated from Chinese winter wheat cultivar ZhengMai 7698. CRISPR/Cas9-mediated targeted mutagenesis was performed for generation of mutant-lines with partial/ triple *taare1* alleles. The generated mutants, especially AABBdd and aabbDD lines, exhibited delayed senescence, prolonged photosynthesis and improved yield under LN condition (Zhang *et al.*, 2021). CRISPR/Cas9 mediated mutagenesis has also been done in winter wheat variety, Kenong 199, wherein *taare1* mutants were seen to enhance grain yield and NUE duly exemplifying the importance of *TaARE1* gene for NUE improvement (Guo *et al.*, 2021). While genome editing has been carried out in wheat for traits such as male sterility and haploid induction (Zhang *et al.*, 2021), studies based on NUE, and associated trait improvement are few and needs to be explored further.

## 1.8 Conclusion

Over the last 5 decades, a tremendous increase in demand of cereal crops has been seen, following which wheat production has doubled to meet the increased demand (Islam *et al.*, 2021). This is in part due to the dwarfing genes discovered during the green revolution and an increase in N input. However, the external application of N has gradually become unsustainable due to its negative effects on the environment. N is lost into the environment in the form of harmful greenhouse gas N<sub>2</sub>O or leached into the soil. Cereals in general take up only 33% of the N applied in the grain at the global scale (Hawkesford, 2017a). Therefore, exploration of NUE in cereals, especially a major cereal like wheat is of utmost importance. The increase in wheat production has been steady over the years at approximately 0.5 – 1% per year with improvement in technologies and agronomic solutions. Several agronomic traits govern NUE and N uptake such as leaf photosynthesis rate, chlorophyll content, senescence, canopy and root architecture, grain protein content all of which directly/indirectly influence N uptake. Further evaluation of these traits and their impacts can be done through modern biotechnological technologies like QTL analysis and mapping, transgenesis and genome editing. Approaches for studying NUE and its components have evolved over the years and span a wide range of techniques such as high throughput phenotyping, nitrate assimilation, exploring landraces and synthetic germplasm and marker-assisted breeding studies. A major difficulty often faced in deploying markers for NUE traits in plant breeding is the inconsistency

of QTL effects in contrasting environments and germplasm. The limitation can also be overcome through meta-analysis of multiple studies through which relationship between N uptake, yield and NUE can be deduced through multiple germplasm and environments (Hawkesford and Riche, 2020). Numerous NUE and related genes have been determined in major cereal systems like barley and rice; however, due to the complex ploidy of wheat, characterisation of NUE is challenging. Modern sequencing platforms as well as gene technologies will facilitate overcoming these limitations.

Amongst these, evaluation of wild germplasm offers a major contribution in overcoming yield-limiting biotic and abiotic stress and excessive exposure to N through fertilisers. Suitable genetic material with desired traits is found in landraces, synthetic hexaploids or wild relative introgressed into modern, elite cultivars. Since modern wheat cultivars lack genetic variation due to domestication over the years, exploring variations in agro-ecological contexts in association mapping would help in identification of diverse gene pools. Wheat improvement programs worldwide are adopting this strategy to dissect NUE and its component factors.

In addition to this, cis-regulatory elements such as transcription factors hold strong transcriptional control over N uptake, assimilation and remobilisation. Identification and characterisation of transcription factors associated with NUE, RSA have been done and help in providing insight of the underlying mechanism of regulation of NUE. Furthermore, genes involved in N metabolism such as enzymes (GS, GOGAT) have been individually examined and are known to contribute towards enhancement of NUE and their related traits. However, these genes are not key regulatory factors which calls for the need of stacking multiple regulatory genes which would give a more satisfactory effect of NUE improvement in the field (Islam *et al.*, 2021).

Future progress in terms of NUE improvement lies in an integrated approach from physiology, agronomy to determining the molecular regulation of key component traits across developmental stages, contrasting environments and N conditions. Preliminary data collection with the help of bioinformaticians and data analysts would give an insight about taking about large population studies. In addition to this, crop simulation models can prove to be useful (Foulkes *et al.*, 2009), time-intensive and would also give a more precise perception about the task in hand.

An increase in productivity to ensure food security through a sustainable means is the key idea of NUE. An integrated and multifaceted approach for maximum resource use by exploring related traits, their interactions and impact through existing technologies will be critical in attaining the much-required global food demand.

## **Hypotheses and Objectives**

A major gap identified in the literature review was that there is a lack of information on genetic variation of NUE and its physiological and genetic basis particularly in wider wheat germplasm. Also, to date, there are only a few studies on genetic variation in NUE in landrace-derived and synthetic-derived bread wheat material. Therefore, the present study aimed to identify genetic diversity and candidate genes for NUE in crosses of the elite spring wheat cultivar Paragon and landrace bread wheats, and the elite winter wheat cultivar Robigus and synthetic bread wheats, in field experiments carried out at Rothamsted Research and Sutton Bonington in four years 2018-19 to 2021-22. The candidate genes which were differentially expressed in QTLs of near-isogenic lines were selected as potential genes governing NUE and related traits.

Therefore, specific hypotheses of this thesis were:

1. There is genetic variation for N-use efficiency and its component traits that is related to NUpE and NUtE in the landrace-derived lines above the parent Paragon.
2. There is genetic variation for N-use efficiency and its component traits that is related to NUpE and NUtE in synthetic-derived lines above the parent Robigus.
3. There is genetic variation for grain yield and NUE which can be explained by physiological traits.
4. Genes expressed in the flag-leaf in the post-anthesis period will positively influence NUtE, NUE and grain yield.
5. Candidate genes with potential SNPs marker associating with NUE and NUE traits will be identified and confirmed with reference to previous literature.

The PhD project will focus on genetic analysis of traits determining biomass and N-Use efficiency (NUE) of wheat. A major focus of the project will be to investigate the genetic regulation of traits determining N uptake and N-Utilisation efficiency in wheat near-isogenic lines based on landrace x elite wheat cultivar crosses

**Specific major objectives will include:**

1. Screen diverse sets of hexaploid wheat genetic resources including landrace x elite crosses, synthetic derivatives, and elite cultivars for novel haplotypes to enable development of markers for NUE and related traits.
2. Phenotyping shortlisted near-isogenic lines under high and low N conditions to determine lines suitable for carrying out RNA-seq based transcriptomic studies.
3. Identify candidate genes for NUE through transcriptomics of flag-leaf tissue of near-isogenic lines at post-anthesis stage under high N and low N conditions.

## ***Chapter 2***

### ***Overview of Materials and Methods***

## 2.1 Screening of germplasm: Field Experiments: 2018-19 Sutton Bonington and Harpenden

In 2018-19, two field experiments were carried out at two sites (University of Nottingham, Sutton Bonington Sutton Bonington, UK (52°50'N, 1°14'W) and Rothamsted Research, Harpenden, (51° 48'N, 0° 21'E) (Fig 2.1 and 2.2). The experiments were sown on 4<sup>th</sup> and 2<sup>nd</sup> October at Sutton Bonington and in early October at Harpenden 2018 respectively. The Sutton Bonington and Harpenden field trial site soil type were, a sandy loam soil (Dunnington Heath series) and clay loam, respectively. Nitrogen fertiliser was applied as ammonium nitrate prills; the amount applied was 160 kg N ha<sup>-1</sup> at Sutton Bonington and 250 kg N ha<sup>-1</sup> at Harpenden. The previous crop was winter oats at Sutton Bonington and Harpenden. The seed rate was 350 seeds per m<sup>2</sup> at both sites. Herbicides, fungicides and pesticides were applied as necessary to minimised effects of weeds, diseases and pests at both sites.

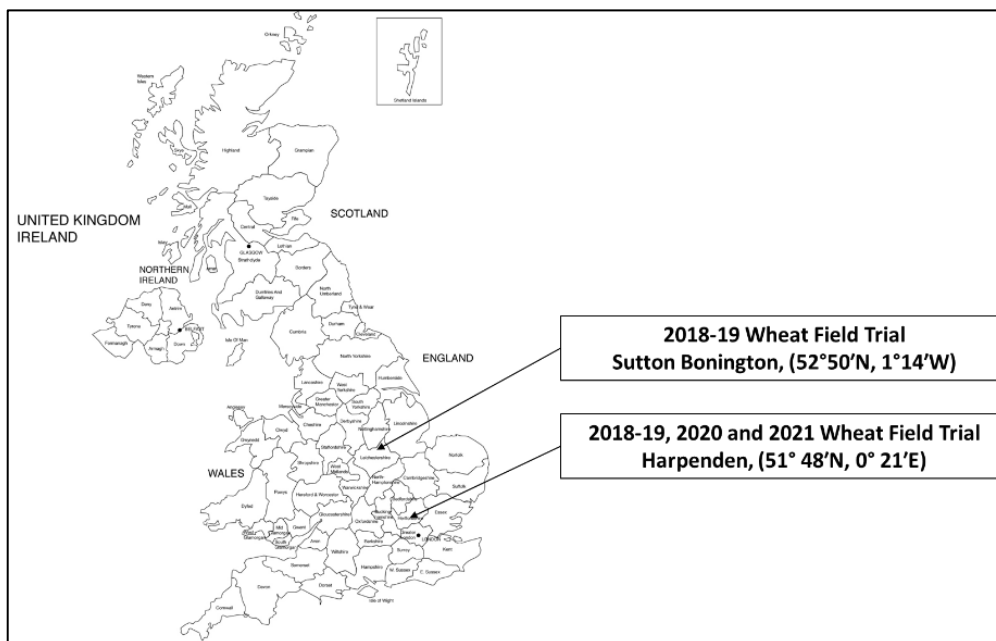


**Fig 2.1:** Map view and geographic coordinates of the two locations of 4 field trials





**Fig 2.2:** Field image of the two sites, A) Sutton Bonington campus, University of Nottingham  
B) Rothamsted Research, Harpenden

### 2.1.1 Germplasm

The selected germplasm for this project was taken from BBSRC Designing Future Wheat (DFW) Breeder's Toolkit. This toolkit was comprised of the bread wheat landrace NAM (nested association mapping) panel and was developed as a set of bi-parental segregating F4 single-seed populations from crosses of spring wheat accession 'Paragon' with diverse wheat germplasm, particularly from the AE Watkins core set (Wingen *et al.*, 2014). Populations were genotyped, mostly employing KASPar SNP markers, and genetic maps were developed (Wingen *et al.*, 2017). Selected Quantitative Trait Loci (QTLs) regions were introgressed by Marker Assisted Selection (MAS) into UK reference cultivar 'Paragon', which is also the common parent of the NAM panel. Back-crossing was started from a RIL (recombinant inbred line) of the NAM panel. Final BC2F2 NILs are BC3 equivalents (since the donor of the Watkins allele is a Paragon x Watkins RIL chosen to have high Paragon background). Homozygotes were selected from selfed BC2 and were multiplied in pots and then as bulk seed that went into 1m plot. The BC2 NILs have approximately 87% Paragon background. Performance of BC2F2 NIL pairs, which were selected by MAS to have opposing parental alleles in the targeted QTL region, is compared in field trial. [Example of PXW lines accession name for reference PW141-41-2-21-Q5B-NDVI-P where P-Paragon, W141- Watkins's landrace, 41-2-21- Plant selected after back crossing, Q5B-Chromosome no, NDVI- Trait and P-paragon allele].

A sub-set of these 66 Near-Isogenic Lines (NILs) (Table 2.1) was selected based on QTLs related to NUE and related traits from the BBSRC Designing Future Wheat (DFW) Breeder’s Toolkit 2018-19 comprising 229 genotypes. The Near-Isogenic Lines were derived from: i) Watkins landraces and ii) synthetic hexaploid wheat derivatives (SD introgressed into a Paragon and Robigus background, respectively). The sub-set comprised of NILs for QTLs specific for NUE-related traits: Above-ground dry matter (AGDM), thousand grain weight (TGW), Grain filling period thermal time (GFPTT), Grainfill rate (GFR), Grain yield (GRYLD) and Normalised Difference Vegetative Index (NDVI). In each experiment, the recurrent spring wheat parents Paragon and winter wheat Robigus were also included. The NILs were arranged in plots in a randomised block design (plot size 6 x 1.65 m at SB and 6 x 2 m at RR) with each genotype having three replicates. Both the field experiments were winter sown (October 2018)

## 2.1.2 Crop measurements at Sutton Bonington site

### 2.1.2.1 Growth stages and establishment

Growth stages were assessed visually once per week and twice per week during anthesis period by using the Zadoks wheat growth scale (Zadoks *et al.*, 1974). At GS20, plant establishment count was recorded in a 1m x 1 m quadrat. The key growth stages of anthesis (GS65) and physiological maturity (GS87) were recorded when 50% of the visible shoots in a plot were observed to be at the relevant stage.

### 2.1.2.2 NDVI and leaf senescence

The canopy development and senescence kinetics were observed in each plot by Normalised Difference Vegetative Index (NDVI) measurements, flag-leaf visual senescence score and flag leaf relative chlorophyll content (SPAD) carried out weekly from GS65 to maturity. NDVI was measured by a Trimble handheld Greenseeker (Trimble Agriculture, USA) (Fig. 2.3A), scanning the crop canopy from 50 cm above.

**Table 2.1:** Near isogenic lines used in two field experiments. P = Paragon, R = Robigus.

Sr No	Accession Name	Germplasm type
1	PW141-41-2-21-Q5B-NDVI-P	P x Landrace
2	PW141-41-2-13-Q5B-NDVI-W	P x Landrace
3	PW141-41-2-14-Q5B-NDVI-W	P x Landrace
4	PW141-41-2-17-Q5B-NDVI-W	P x Landrace
5	PW141-41-2-20-Q5B-NDVI-W	P x Landrace

6	PW141-58-7-20-Q7D-AGDM-P	P x Landrace
7	PW141-58-7-10-Q7D-AGDM-W	P x Landrace
8	PW141-58-7-7-Q7D-AGDM-W	P x Landrace
9	PW292-9-5-7-Q4B-GFPTT-P	P x Landrace
10	PW292-9-5-14-Q4B-GFPTT-P	P x Landrace
11	PW292-9-5-15-Q4B-GFPTT-P	P x Landrace
12	PW292-9-5-18-Q4B-GFPTT-P	P x Landrace
13	PW292-9-5-6-Q4B-GFPTT-W	P x Landrace
14	PW292-9-5-8-Q4B-GFPTT-W	P x Landrace
15	PW292-9-5-10-Q4B-GFPTT-W	P x Landrace
16	PW292-22-9-16-Q3A-COMSTR-P	P x Landrace
17	PW292-22-9-19-Q3A-COMSTR-P	P x Landrace
18	PW292-22-9-1-Q3A-COMSTR-W	P x Landrace
19	PW292-22-9-7-Q3A-COMSTR-W	P x Landrace
20	PW292-22-9-8-Q3A-COMSTR-W	P x Landrace
21	PW352-5-1-10-Q1B-GRYLD-P	P x Landrace
22	PW352-5-1-13-Q1B-GRYLD-W	P x Landrace
23	PW352-5-1-16-Q1B-GRYLD-W	P x Landrace
24	PW352-23-4-14-Q1A-NDVI-P	P x Landrace
25	PW352-23-4-17-Q1A-NDVI-P	P x Landrace
26	PW352-23-4-18-Q1A-NDVI-P	P x Landrace
27	PW352-23-4-20-Q1A-NDVI-P	P x Landrace
28	PW352-23-4-6-Q1A-NDVI-W	P x Landrace
29	PW352-23-4-7-Q1A-NDVI-W	P x Landrace
30	PW352-26-4-10-Q2A-GFR-P	P x Landrace
31	PW352-26-4-17-Q2A-GFR-P	P x Landrace
32	PW352-26-4-19-Q2A-GFR-P	P x Landrace
33	PW352-26-4-20-Q2A-GFR-P	P x Landrace
34	PW352-26-4-2-Q2A-GFR-W	P x Landrace
35	PW352-26-4-3-Q2A-GFR-W	P x Landrace
36	PW352-26-4-4-Q2A-GFR-W	P x Landrace
37	PW352-26-4-14-Q2A-GFR-W	P x Landrace
38	PW468-10-1-2-Q2A-NDVI-P	P x Landrace
39	PW468-10-1-21-Q2A-NDVI-P	P x Landrace
40	PW468-10-1-5-Q2A-NDVI-W	P x Landrace
41	PW468-10-1-17-Q2A-NDVI-W	P x Landrace
42	PW468-77-3-9-Q7B-AGDM-P	P x Landrace
43	PW468-77-3-16-Q7B-AGDM-P	P x Landrace
44	PW468-77-3-20-Q7B-AGDM-P	P x Landrace
45	PW468-77-3-10-Q7B-AGDM-W	P x Landrace
46	PW468-77-3-11-Q7B-AGDM-W	P x Landrace
47	PW468-77-3-14-Q7B-AGDM-W	P x Landrace
48	PW468-77-3-19-Q7B-AGDM-W	P x Landrace
49	PW468-84-4-4-Q5A-COMGRWT-P	P x Landrace
50	PW468-84-4-12-Q5A-COMGRWT-P	P x Landrace
51	PW468-84-4-1-Q5A-COMGRWT-W	P x Landrace
52	PW729-55-3-6-Q6B-AGDM-P	P x Landrace
53	PW729-55-3-8-Q6B-AGDM-P	P x Landrace
54	PW729-55-3-13-Q6B-AGDM-P	P x Landrace
55	PW729-55-3-15-Q6B-AGDM-P	P x Landrace
56	PW729-55-3-1-Q6B-AGDM-W	P x Landrace

57	PW729-55-3-21-Q6B-AGDM-W	P x Landrace
58	Paragon	parental control
59	Robigus	parental control
60	SEL56	R x Synthetic Hexaploid
61	SEL57	R x Synthetic Hexaploid
62	SEL58	R x Synthetic Hexaploid
63	SEL63	R x Synthetic Hexaploid
64	SEL64	R x Synthetic Hexaploid
65	SEL65	R x Synthetic Hexaploid
66	SEL69	R x Synthetic Hexaploid

The flag-leaf light-saturated photosynthetic rate ( $A_{max}$ ), stomatal conductance ( $g_s$ ), intercellular carbon dioxide concentration ( $C_i$ ) and maximum efficiency of PSII ( $F_v'/F_m'$ ) were measured using a Li-Cor LI-6400XT Portable Photosynthesis System (Lincoln, NE, USA) in the experiment at SB (Fig. 2.3B). For gas-exchange measurements a sub-set of 20 lines from the larger sub-set of 65 NILs was selected. The basis of this selection for the NILs was QTLs related to above-ground dry matter (AGDM) and NDVI. Three shoots with healthy flag leaf per plot were selected for taking LICOR-6400 measurements. The flag-leaf chlorophyll fluorescence (Quantum yield) was measured by Fluorpen FP100 (PSI, Brno, Czech Republic) (Fig. 2.3C). The relative chlorophyll content was measured using a SPAD meter (Konika Minolta-502, Japan) (Fig. 2.3D) at GS41 and GS65 in 2 replicates. Three fertile shoots per plot were selected randomly and a single measurement per flag leaf was taken. The flag-leaf senescence score was assessed visually using a key as described by Pask *et al.* (2012).

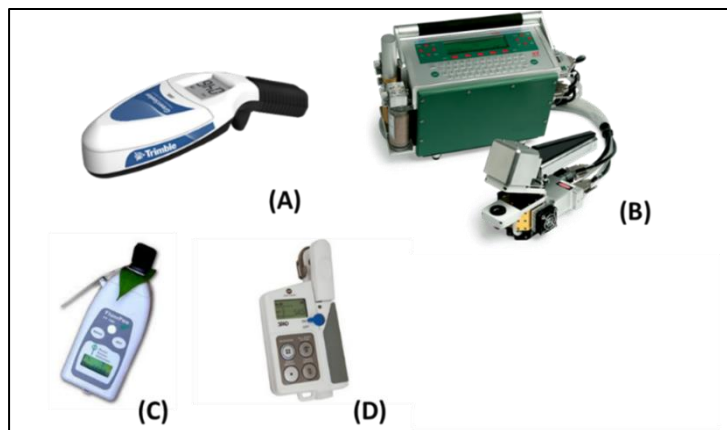


**Fig 2.3:** Instruments used to measure senescence kinetics and photosynthesis related traits (A) Trimble handheld Greenseeker (B) Li-Cor LI-6400XT Portable Photosynthesis System (C) Fluorpen FP100 (D) Konika Minolta-502 SPAD meter.

### **2.1.2.3 Physiological maturity and harvest growth analysis**

The plant height was measured from ground level to the tip of ear using a ruler at five random positions per plot in the field. The lodging scoring of all the lines was also done pre-harvest. At GS94, samples of 70 fertile shoots per plot were collected from 4 corners of the plot for analysis. While sampling, shoots were not taken from outer rows or ends of the plot to avoid edge/border effect. To calculate the following traits, the detailed partitioning and yield component analysis was carried out in the laboratory: Grain yield (GY).

The lodging scoring of all the lines was also done per-harvest. At GS94 stage, samples of 100 fertile shoots per plot were collected for analysis. The ears were threshed, and the grain collected and counted in a digital seed counter. The dry weight of the grain and straw was recorded after drying for 48 h at 80°C. The N% from harvested grain and stem samples were estimated by NIRS (Near Infrared Spectroscopy Method) by using ASD FieldSpec 4 Hi-Res NG spectrometer, Analytik Ltd, UK. Total N estimated values were used to calculate the NUE, NUpE, NUtE, and GPC. Grain yield per plot was recorded by machine harvesting the plot and values were further adjusted to moisture percentage measured in each plot. From the data obtained ears m<sup>-2</sup>, grains m<sup>-2</sup>, harvest index, above-ground biomass m<sup>-2</sup> and NUE components were calculated.

### **2.1.3 Crop Measurements and harvest analysis at Harpenden site**

The plant height was measured by an Unmanned Aerial vehicle (UAV) as well as manually. The visual flag-leaf senescence score was recorded every 3-4 days from GS71 to GS93. The lodging scoring of all the lines was done at GS88. At GS94 stage, samples of 100 fertile shoots per plot were collected for analysis. To calculate the Nitrogen, Use Efficiency (NUE), Nitrogen Uptake Efficiency (NUpE) and Nitrogen Utilisation Efficiency (NUtE); N Quantification analysis was carried out in the laboratory using the NIRS (Near Infrared Spectroscopy Method) by using ASD FieldSpec 4 Hi-Res NG spectrometer, Analytik Ltd, UK. The moisture content and dry matter analysis was performed on 100 shoots harvested samples. The plant material was separated into the spikes and stems (leaf lamina, true stem and leaf sheath). Ear number and weight was recorded then samples were dried for 48 hours at 80°C. Dry weights of both components were then recorded. The ears were then threshed to collect the grains. Grain samples were counted in a digital seed counter and dry weights recorded after 48 hours drying at 80°C. Chaff weight was calculated by the difference between grain weight and ear

weight. Grain yield per plot was recorded by machine harvesting the plot and values were further adjusted to moisture percentage measured in each plot. From the data obtained ears  $\text{m}^{-2}$ , grains  $\text{m}^{-2}$ , harvest index, above-ground biomass  $\text{m}^{-2}$  were calculated.

#### **2.1.4 Statistical Analysis**

ANOVA and generation of least significant differences (LSDs) was performed using Genstat 22 with genotype as a fixed effect and replicate and environment as random effects. Linear regressions and correlations were calculated using the treatment means from ANOVA using the Genstat 22.

### **2.2 Field experiments on selected sub-set (18 NILs and Paragon and Robigus) at Rothamsted in 2020 and 2021**

#### **2.2.1 Experimental site and design**

Based on the two- experiments from 2018-19 (results described in Chapter 3), 20 genotypes (Table 2.2) were selected for further field experiments at the Rothamsted site, Hertfordshire (51° 48' 19.79" N 0° 21' 11.39" E). The field experiment used a randomised block design with plot size of 4.15 x 1.8 m and three replicates of each genotype. There were two N treatments, N1 (50 kg  $\text{ha}^{-1}$ ) and N2 (200 kg  $\text{ha}^{-1}$ ), applied as ammonium nitrate prills. The soil type at field experiment site was silty clay loam (Fig 2.4). The seed rate was 350 seeds per  $\text{m}^2$ . Herbicides, fungicides and pesticides were applied as necessary to minimised effects of weeds, diseases and pests at both sites. The two experiments were spring-sown crops, sown in the second half of March in each year.

#### **2.2.2 Crop measurements**

The plant height was measured by an Unmanned Aerial vehicle (UAV) (Holman *et al.*, 2016). The visual flag-leaf senescence score was recorded every 3-4 days from GS71 to GS93 (Zadoks 0-99 scale). The lodging score of all the lines was done at GS88. At GS94 stage, samples of 100 fertile shoots (those with an ear) per plot were collected for analysis by cutting at ground level. Ears were separated from straw and the dry weight recorded after drying for 48 h at 80°C. The ears were then threshed, and the grain collected, and the dry weight recorded after drying for 48 h at 80°C. N estimation was carried out by NIRS (Near Infrared Spectroscopy Method) by using ASD FieldSpec 4 Hi-Res NG spectrometer, Analytik Ltd, UK to calculate N-

Use Efficiency (NUE), N-Uptake Efficiency (NUpE) and N Utilisation Efficiency (NUtE), the analysis of which is described in Chapter 4.



**Fig 2.4:** Field image of the two experiments at Rothamsted Research, Harpenden, A) 2020 and B) 2021 C) Aerial image taken by Unmanned aerial vehicle field trial 2021.

**Table 2.2:** Near isogenic lines (2020 and 2021) used at Harpenden site.

Sr No	Accession Name	Background
1	Paragon	parental control
2	PW141-58-7-10-Q7D-AGDM-W	Landrace X Paragon
3	PW141-58-7-20-Q7D-AGDM-P	Landrace X Paragon
4	PW292-22-9-19-Q3A-COMSTR-P	Landrace X Paragon
5	PW292-22-9-1-Q3A-COMSTR-W	Landrace X Paragon
6	PW292-22-9-7-Q3A-COMSTR-W	Landrace X Paragon
7	PW292-22-9-8-Q3A-COMSTR-W	Landrace X Paragon
8	PW292-9-5-18-Q4B-GFPTT-P	Landrace X Paragon
9	PW292-9-5-6-Q4B-GFPTT-W	Landrace X Paragon
10	PW468-77-3-10-Q7B-AGDM-W	Landrace X Paragon
11	PW468-77-3-10-Q7B-AGDM-W	Landrace X Paragon
12	PW468-77-3-14-Q7B-AGDM-W	Landrace X Paragon

13	PW468-77-3-20-Q7B-AGDM-P	Landrace X Paragon
14	PW468-84-4-12-Q5A-COMGRWT-P	Landrace X Paragon
15	PW468-84-4-1-Q5A-COMGRWT-W	Landrace X Paragon
16	PW729-55-3-15-Q6B-AGDM-P	Landrace X Paragon
17	PW729-55-3-1-Q6B-AGDM-W	Landrace X Paragon
18	Robigus	parental control
19	SEL58	Synthetic Hexaploid
20	SEL63	Synthetic Hexaploid

### 2.3 RNAseq based transcriptomics field experiment 2021

Based on the two experiments from 2020 and 2021 (results described in Chapter 4), the wheat synthetic hexaploid derivative line SEL58, the Paragon parent and 3 near-isogenic lines (PW141-58-7-10-Q7D-AGDM-W, PW468-84-4-1-Q5A-COMGRWT-W and PW292-22-9-1-Q3A-COMSTR-W) were selected for the RNAseq experiment. The field experiment used a randomised block design with plot size of 4.15 x 1.8 m and three replicates of each genotype. There were two N treatments N1 (50 kg ha<sup>-1</sup>) and N2 (200 kg ha<sup>-1</sup>) applied as ammonium nitrate prills. The soil type at field experiment site was silty clay loam.

Flag leaf sample at anthesis (GS61) + 12 days was collected from each plot for these genotypes in the low N and high N treatments in this field experiment at Rothamsted Research, Harpenden, Hertfordshire (51° 48' 19.79" N 0° 21' 11.39" E) in 2020-21.

#### 2.3.1 RNA seq analysis

Main shoots (flag leaf) were tagged at anthesis (GS65) and the flag leaves of the same shoots were collected at 12 days post-anthesis. The total RNA of the 30 samples was isolated by using the Qiagen RNeasy kit method. The isolated RNA was purified by using the Sodium Acetate (NaOAc) precipitation method. The concentration of purified RNA was measured by NanoDrop™ 2000/2000c Spectrophotometers. The RNA samples with the ratio of absorbance at 260 nm and 280 nm is used to assess the purity of RNA and samples with ratio ~2.0 were run on 1% agarose gel to visualise any degradation and presence of DNA contamination (Table 2.3) (Fig 2.5).



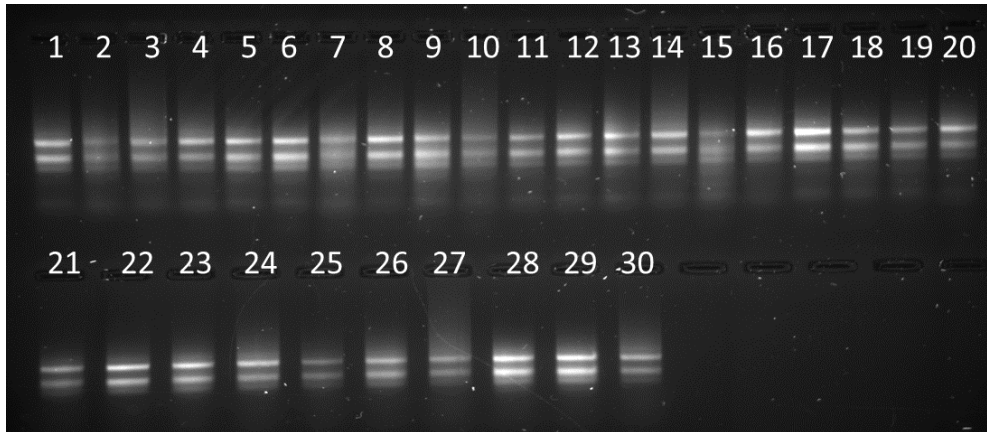


**Fig 2.5:** 30 RNA samples (400ng) extracted from flag leaf tissue of wheat plants of 5 near isogenic lines under 2 N treatments (N1= Low N (50 kg ha<sup>-1</sup>) and N2= High N (200 kg ha<sup>-1</sup>) and three biological replicates

The purified RNA samples were submitted to Novogene UK Pvt Ltd, Cambridge for Illumina next gen RNAseq Pair End 150bps (12 G raw data per sample). The samples were sequenced and analysed at the service provider facility. Raw data (raw reads) of FASTQ format were firstly processed through Perl scripts. In this step, clean data (clean reads) were obtained by removing reads containing adapter, reads containing poly-N and low-quality reads from raw data. At the same time, the clean data of Q20, Q30 and GC content were calculated. All the downstream analyses were based on the clean data with high quality (Fig 2.6). A summarised overview of the RNAseq-based workflow is given in Fig 2.7.

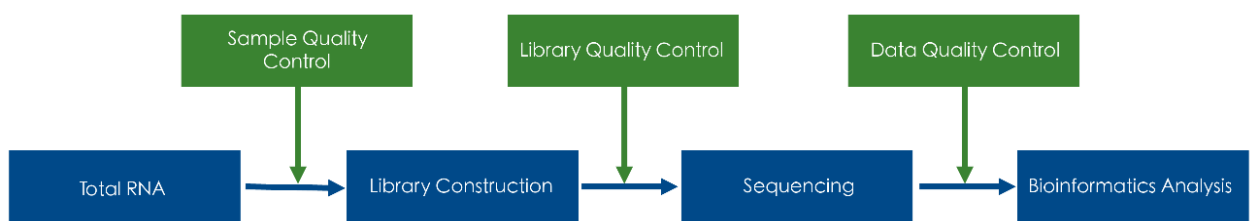


**Fig 2.6:** RNAseq data quality control workflow

**Table 2.3:** RNA quality control parameters, concentration ( $\text{ng } \mu\text{l}^{-1}$ ), A260/280 and A260/230 values of 5 near isogenic lines under 2 N treatments (N1= Low N ( $50 \text{ kg ha}^{-1}$ ) and N2= High N ( $200 \text{ kg ha}^{-1}$ ) and three biological replicates.

NILs	Nitrogen Treatment	RNA conc. ( $\text{ng } \mu\text{l}^{-1}$ )	A260/280	A260/230
AGDM_N1_R1	Low N	71	2.05	2.2
AGDM_N1_R2	Low N	123	2.1	2.08
AGDM_N1_R3	Low N	170.4	2.12	2.23
AGDM_N2_R1	High N	127.9	2.07	2.2
AGDM_N2_R2	High N	175.2	2.11	2.23
AGDM_N2_R3	High N	83.6	2.03	2.22
CMGRWT_N1_R1	Low N	36.4	2.03	2.09
CMGRWT_N1_R2	Low N	98.5	2.05	2.23
CMGRWT_N1_R3	Low N	133.6	2.12	2.24
CMGRWT_N2_R1	High N	75.1	2.02	2.21
CMGRWT_N2_R2	High N	183.5	2.11	2.23
CMGRWT_N2_R3	High N	93.5	2.08	2.2
COMSTR_N1_R1	Low N	76.7	2.07	2.18
COMSTR_N1_R2	Low N	51.3	2.02	2.19
COMSTR_N1_R3	Low N	185.3	2.06	2.23
COMSTR_N2_R1	High N	98.7	2.05	2.21
COMSTR_N2_R2	High N	82.1	2.06	2.2
COMSTR_N2_R3	High N	172.7	2.11	2.25
Para_N1_R1	Low N	38.8	2	2.05
Para_N1_R2	Low N	165.9	2.09	2.26
Para_N1_R3	Low N	150.5	2.13	2.27
Para_N2_R1	High N	136	2.08	2.2
Para_N2_R2	High N	227.9	2.14	2.26
Para_N2_R3	High N	124.8	2.07	2.27
SEL58_N1_R1	Low N	145.3	2.11	2.19
SEL58_N1_R2	Low N	70.4	2.1	2.25
SEL58_N1_R3	Low N	190	2.08	2.23
SEL58_N2_R1	High N	88.9	2.06	2.19
SEL58_N2_R2	High N	119.4	2.06	2.25
SEL58_N2_R3	High N	148.6	2.09	2.22

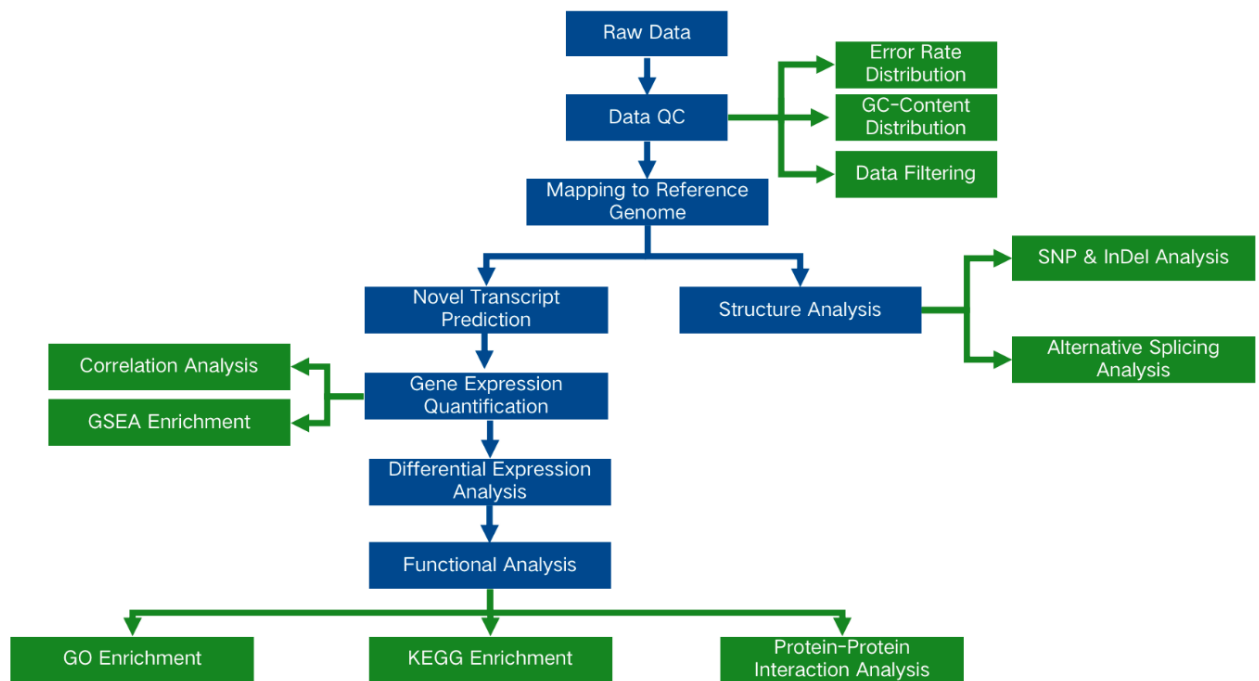


**Fig 2.7:** Overall outline of the RNAseq based transcriptomics experiment.

### 2.3.2 Read mapping to the reference genome

Reference genome and gene model annotation files were downloaded from NCBI. ([https://ftp.ncbi.nlm.nih.gov/genomes/all/GCF/018/294/505/GCF\\_018294505.1\\_IWGSC\\_CS\\_RefSeq\\_v2.1/GCF\\_018294505.1\\_IWGSC\\_CS\\_RefSeq\\_v2.1\\_genomic.fna.gz](https://ftp.ncbi.nlm.nih.gov/genomes/all/GCF/018/294/505/GCF_018294505.1_IWGSC_CS_RefSeq_v2.1/GCF_018294505.1_IWGSC_CS_RefSeq_v2.1_genomic.fna.gz)). Index of the reference genome was built using Hisat2 v2.0.5 and paired-end clean reads were aligned to the reference genome using Hisat2 v2.0.5.

### 2.3.3 Differential gene expression analysis and quantification

The mapped reads of each sample were assembled by StringTie (v1.3.3b) (Pertea *et al.*, 2015) in a reference-based approach to predict the novel transcripts. The software feature Counts v1.5.0-p3 was used to count the read numbers mapped to each gene. The FPKM (fragments per kilo base per million reads mapped) of each gene was then calculated based on the length of the gene and reads count mapped to this gene.

Differential expression analysis of two conditions/groups (two biological replicates per condition) was performed using the DESeq2Rpackage (1.20.0). DESeq2 provides statistical routines for determining differential expression in digital gene expression data using a model based on the negative binomial distribution. The resulting P-values were adjusted using the

Benjamini and Hochberg's approach for controlling the false discovery rate (Benjamini and Hochberg, 1995). Genes with an adjusted P-value <0.05 found by DESeq2 were reassigned as differentially expressed (for edgeR without biological replicates). Prior to differential gene expression analysis, for each sequenced library, the read counts were adjusted by edgeR program package through one scaling normalised factor. Differential expression analysis of two conditions was performed using the edgeR R package (3.22.5). The P values were adjusted using the Benjamini and Hochberg method. Corrected P-value of 0.001 and absolute fold change of > 2 were set as the threshold for significant differential expression.

#### **2.3.4 Gene Ontology analysis and KEGG enrichment analysis**

GO (Gene ontology) and KEGG (Kyoto Encyclopedia of Genes and Genomes) enrichment analysis of differentially expressed genes was performed. GO enrichment analysis of differentially expressed genes was implemented by the cluster Profiler R package, in which gene length bias was corrected. GO terms with corrected p-value less than 0.05 were considered significantly enriched by differential expressed genes. We have used cluster Profiler R package to test the statistical enrichment of differential expression genes in KEGG pathways.

#### **2.3.5 Single Nucleotide Polymorphisms (SNP)**

SNP analysis GATK (v4.1.1.0) software was used to perform SNP calling. Raw vcf files were filtered with GATK standard filter method and other parameters (cluster:3; WindowSize:35; QD 30.0; DP < 10).

#### **2.4 Statistical analysis**

Analysis of variance (ANOVA) procedures for a split-plot design were used to analyse N treatment, genotype effects, site, year and test their interaction in the experiments in 2019-20, 2020 and 2021 using Genstat version 22 ([www.genstat.com](http://www.genstat.com); VSN International Ltd, Hemel Hempsted, UK), where replicates were regarded as random effects and N treatment, genotype and site as fixed effects. Pearson's correlation coefficient and linear regression were calculated using mean data for replicates using Genstat version 22 (VSN International, Hemel Hempstead UK).

## ***Chapter 3***

***Genetic variation for Nitrogen-Use Efficiency and associated traits in near-isogenic lines derived from crosses between Paragon, Watkins landraces and synthetic hexaploid wheat***

### 3.1 Introduction

The global demand for cereals is estimated to double by 2050 which places producers under severe pressure (Jha *et al.*, 2023). Wheat being one of the three primary cereals consumed globally, also expects enhanced production in future years (Semenov *et al.*, 2007). The current wheat production is uncertain due to changes in trade policies, rising international prices, the ongoing Ukraine war as well as reduced production in major wheat producing countries like Ukraine, Australia, and India. The global wheat production declined in 2022 by 0.8 percent resulting in approximately 771 million tonnes (Collier, 2022). It is therefore crucial to enhance wheat production and yield to meet the growing demand globally. The production of wheat is greatly influenced by nitrogen (N) of which nitrate is the common form found in the cell vacuole of the plant. The nitrogen use efficiency (NUE) is the ability of the plant to convert available N into the economic form, grain yield. High supply of N, however, can be detrimental for the environment as well as cause economic loss. While optimum application of N fertilisers can enhance the NUE, thousand-grain weight and protein content of the plant; their extensive use can cause lodging stress and subsequently economic losses (Ghafoor *et al.*, 2021). Enhancing NUE ensures increased production and yield of crop, reduced fertiliser costs and possibility of nitrate leaching into the soil, and limits greenhouse gas emission of N<sub>2</sub>O produced by denitrification of nitrate by soil bacteria.

Wheat was domesticated over 10,000 years ago (Shewry, 2009) and the current wheat genome has been derived from a cross between tetraploid, *Triticum dicoccoides* and wild diploid, *Aegilops tauschii* (Salamini *et al.*, 2002). The process of domestication of wheat landraces, over the years, has led to the reduction in genetic diversity as compared to wild ancestors. This might have also caused loss in valuable traits relating to NUE in the germplasm. This brings in the requirement of examining a wide range of germplasm for selection of NUE and related traits like, nitrogen-uptake efficiency (NUpE), nitrogen-utilisation efficiency (NUtE), nitrogen harvest index (NHI), grain protein deviation (GPD) and grain protein content (GPC) (Hawkesford, 2017a). The Watkins collection showcases the genetic diversity present before modern breeding and domestication events. The Watkins collection contains nine ancestral geographical groupings which possibly led to exchange of genetic material between these groups and consequently led to immense genetic diversity (Wingen *et al.*, 2014). The wild cultivars of wheat have been found to have higher leaf

photosynthetic rate as compared to the modern elite cultivars implying towards the reduction in this important NUE trait. The landraces have also demonstrated increased penetration of the root biomass towards deeper profiles of the soil, in order to enhance moisture uptake, as compared to modern wheat varieties (Jaradat, 2013). Additionally, synthetic hexaploid wheat (SHW), derived from *Triticum durum* and *Aegilops tauschii* in pre-breeding programmes has been found to demonstrate enhanced levels of leaf photosynthetic rate and grain yield (Del Blanco *et al.*, 2000; Ogbonnaya *et al.*, 2003). Therefore, studying the wheat landraces and synthetically-derived lines of wheat and their derivatives can help in identifying bread wheat lines with important traits of NUE such as plant biomass, photosynthetic capacity, grain yield (GY) under varying N conditions (Gaju *et al.*, 2011). Genetic variation studies carried out in hexaploid wheat panels consisting of landrace cultivars, SHW and modern elite cultivars for physiological traits associated with NUE like normalised difference vegetative index (NDVI), leaf chlorophyll content (SPAD), leaf senescence duration and rate, can also prove to be invaluable in determining important target for breeding cultivars with enhanced NUE (Nehe *et al.*, 2022).

The current study focusses on field phenotyping at two sites of near-isogenic lines (NILs) developed by backcrosses between Watkins' wheat landraces and the elite spring wheat cultivar Paragon for QTLs governing NUE contributing traits and crosses between synthetic hexaploid wheats and winter wheat cultivar Robigus. The traits we have primarily targeted are above-ground dry matter (AGDM), combined thousand grain weight (CTGW), grain filling period thermal time (GFPTT), grainfill rate (GFR), grain yield (GY) and normalised difference vegetative index (NDVI). The two-site screening of this diverse set of wheat germplasm is carried out to identify novel genetic variation in NUE and related traits.

## 3.2 Material and Methods

### 3.2.1 Field sites

In 2018/19, two field experiments were carried out at two sites, one each at University of Nottingham, Sutton Bonington, UK (52°50'N, 1°14'W) and Rothamsted Research (RR), Harpenden, (51° 48'N, 0° 21'E). The experiments were sown on 4<sup>th</sup> October 2018. At the Sutton Bonington and Harpenden sites, the soil type was a silty clay loam (Duningron Heath Series) and clay loam soil, respectively. The weather data including Temperature (Min) °C, Temperature(Max) °C, Rain (mm), Relative Humidity (%), Solar Radiation (J cm<sup>-2</sup>) at Rothamsted Research and Sutton Bonington, site, in the year 2018-19 were recorded (Appendix Table 5 and 6).

### 3.2.2 Germplasm

A sub-set of 66 near-isogenic lines (NILs) (Table 3.1) was selected based on Quantitative Trait Loci (QTLs) related to NUE and related traits from the BBSRC Designing Future Wheat (DFW) Breeder's Toolkit 2018-19 comprising 229 genotypes. The NILs were mostly derived from Watkins collection landraces introgressed into a spring wheat cv. Paragon background (57 NILs). These were comprised of NILs for QTLs for specific NUE-related traits: above-ground dry matter (AGDM), thousand grain weight (TGW), grain filling period thermal time (GFPTT), grain fill rate (GFR), grain yield (GRYLD) and Normalised Difference Vegetative Index (NDVI). Additionally, seven synthetic hexaploid wheat derivatives developed by National Institute of Agricultural Botany (NIAB), Cambridge, UK were also part of the sub-set (Table 3.1). These synthetic hexaploid wheats are in Robigus background. Therefore, in each experiment, the spring wheat parent Paragon (for comparing with P × W landraces NILs) and UK winter wheat cultivar Robigus for comparing with synthetic wheat derivatives) were included in each field trial. The NILs were arranged in plots in a randomised block design (plot size 6 x 1.65 m at SB and 6 x 2 m at RR) with each genotype having three replicates.

**Table 3.1:** List of 66 Near Isogenic Lines (NILs) and Paragon (P) and Robigus (R) parents in field trials 2018-19

Sr No	Code	Accession Name	Germplasm type
1	WL 136	PW141-41-2-21-Q5B-NDVI-P	P x Landrace
2	WL 142	PW141-41-2-13-Q5B-NDVI-W	P x Landrace
3	WL 143	PW141-41-2-14-Q5B-NDVI-W	P x Landrace
4	WL 144	PW141-41-2-17-Q5B-NDVI-W	P x Landrace
5	WL 145	PW141-41-2-20-Q5B-NDVI-W	P x Landrace
6	WL 146	PW141-58-7-20-Q7D-AGDM-P	P x Landrace
7	WL 147	PW141-58-7-10-Q7D-AGDM-W	P x Landrace



8	WL 148	PW141-58-7-7-Q7D-AGDM-W	P x Landrace
9	WL 153	PW292-9-5-7-Q4B-GFPTT-P	P x Landrace
10	WL 154	PW292-9-5-14-Q4B-GFPTT-P	P x Landrace
11	WL 155	PW292-9-5-15-Q4B-GFPTT-P	P x Landrace
12	WL 156	PW292-9-5-18-Q4B-GFPTT-P	P x Landrace
13	WL 157	PW292-9-5-6-Q4B-GFPTT-W	P x Landrace
14	WL 158	PW292-9-5-8-Q4B-GFPTT-W	P x Landrace
15	WL 159	PW292-9-5-10-Q4B-GFPTT-W	P x Landrace
16	WL 163	PW292-22-9-16-Q3A-COMSTR-P	P x Landrace
17	WL 164	PW292-22-9-19-Q3A-COMSTR-P	P x Landrace
18	WL 165	PW292-22-9-1-Q3A-COMSTR-W	P x Landrace
19	WL 166	PW292-22-9-7-Q3A-COMSTR-W	P x Landrace
20	WL 167	PW292-22-9-8-Q3A-COMSTR-W	P x Landrace
21	WL 194	PW352-5-1-10-Q1B-GRYLD-P	P x Landrace
22	WL 195	PW352-5-1-13-Q1B-GRYLD-W	P x Landrace
23	WL 196	PW352-5-1-16-Q1B-GRYLD-W	P x Landrace
24	WL 215	PW352-23-4-14-Q1A-NDVI-P	P x Landrace
25	WL 216	PW352-23-4-17-Q1A-NDVI-P	P x Landrace
26	WL 217	PW352-23-4-18-Q1A-NDVI-P	P x Landrace
27	WL 218	PW352-23-4-20-Q1A-NDVI-P	P x Landrace
28	WL 219	PW352-23-4-6-Q1A-NDVI-W	P x Landrace
29	WL 220	PW352-23-4-7-Q1A-NDVI-W	P x Landrace
30	WL 228	PW352-26-4-10-Q2A-GFR-P	P x Landrace
31	WL 230	PW352-26-4-17-Q2A-GFR-P	P x Landrace
32	WL 231	PW352-26-4-19-Q2A-GFR-P	P x Landrace
33	WL 232	PW352-26-4-20-Q2A-GFR-P	P x Landrace
34	WL 233	PW352-26-4-2-Q2A-GFR-W	P x Landrace
35	WL 234	PW352-26-4-3-Q2A-GFR-W	P x Landrace
36	WL 235	PW352-26-4-4-Q2A-GFR-W	P x Landrace
37	WL 236	PW352-26-4-14-Q2A-GFR-W	P x Landrace
38	WL 251	PW468-10-1-2-Q2A-NDVI-P	P x Landrace
39	WL 252	PW468-10-1-21-Q2A-NDVI-P	P x Landrace
40	WL 253	PW468-10-1-5-Q2A-NDVI-W	P x Landrace
41	WL 254	PW468-10-1-17-Q2A-NDVI-W	P x Landrace
42	WL 275	PW468-77-3-9-Q7B-AGDM-P	P x Landrace
43	WL 276	PW468-77-3-16-Q7B-AGDM-P	P x Landrace
44	WL 277	PW468-77-3-20-Q7B-AGDM-P	P x Landrace
45	WL 278	PW468-77-3-10-Q7B-AGDM-W	P x Landrace
46	WL 279	PW468-77-3-11-Q7B-AGDM-W	P x Landrace
47	WL 281	PW468-77-3-14-Q7B-AGDM-W	P x Landrace
48	WL 283	PW468-77-3-19-Q7B-AGDM-W	P x Landrace
49	WL 290	PW468-84-4-4-Q5A-COMGRWT-P	P x Landrace
50	WL 291	PW468-84-4-12-Q5A-COMGRWT-P	P x Landrace
51	WL 292	PW468-84-4-1-Q5A-COMGRWT-W	P x Landrace
52	WL 311	PW729-55-3-6-Q6B-AGDM-P	P x Landrace
53	WL 312	PW729-55-3-8-Q6B-AGDM-P	P x Landrace
54	WL 314	PW729-55-3-13-Q6B-AGDM-P	P x Landrace
55	WL 315	PW729-55-3-15-Q6B-AGDM-P	P x Landrace
56	WL 316	PW729-55-3-1-Q6B-AGDM-W	P x Landrace
57	WL 317	PW729-55-3-21-Q6B-AGDM-W	P x Landrace
58	Paragon	Paragon, parental control	

59	Robigus	Robigus, parental control	
60	DFWSEL56	SEL56	R x Synthetic Hexaploid
61	DFWSEL57	SEL57	R x Synthetic Hexaploid
62	DFWSEL58	SEL58	R x Synthetic Hexaploid
63	DFWSEL63	SEL63	R x Synthetic Hexaploid
64	DFWSEL64	SEL64	R x Synthetic Hexaploid
65	DFWSEL65	SEL65	R x Synthetic Hexaploid
66	DFWSEL69	SEL69	R x Synthetic Hexaploid

### 3.2.3 Crop Development measurements

Growth stages were assessed visually once per week and twice per week during anthesis period by using the Zadoks wheat growth scale (Zadoks *et al.*, 1974). At GS20, plant establishment count was recorded in a 1m x 1 m quadrat. The key growth stages of GS31, GS41, GS51, GS55, GS65, GS71, GS83 and GS91 were recorded when 50% of the visible shoots in a plot were observed to be at the relevant stage at both sites.

#### 3.2.3.1 Sutton Bonington measurements

The canopy development and senescence kinetics were observed in each plot by Normalised Difference Vegetative Index (NDVI) measurements and flag-leaf visual senescence score carried out weekly from GS31 to maturity. NDVI at Sutton Bonington site was measured by a Trimble handheld GreenSeeker (Trimble Agriculture, USA) by scanning the canopy from 50 cm above the crop. The relative chlorophyll content was measured using a SPAD meter (Konika Minolta-502, Japan) from GS41 to GS65 in 2 replicates. Three fertile shoots per plot were selected randomly and a single measurement per flag leaf was taken. The flag-leaf senescence score was assessed visually using a key as described by Pask *et al.*, (2012).

The flag-leaf photosynthetic rate ( $A_{max}$ ), stomatal conductance ( $g_s$ ), intercellular carbon dioxide concentration ( $C_i$ ) and maximum efficiency of PSII ( $F_v'/F_m'$ ) of the flag-leaf were measured using a Li-Cor LI-6400XT Portable Photosynthesis System (Licor, NE, USA). For Licor measurements a sub-set of 20 lines from the larger sub-set of 66 NILs was selected for which QTLs related to above-ground dry matter (AGDM) and NDVI. Three fertile shoots per plot were selected for taking all the measurements. The flag-leaf Quantum yield was also measured by Fluorpen FP100 (PSI, Brno, Czech Republic). Hyperspectral spectro-radiometer measurements (FieldSpec Pro2, Analytik, Cambridge, UK) were also taken to quantify the light interception during the crop cycle at key growth stages, GS55, GS65 and GS71.

At GS94, samples of 100 fertile shoots per plot were collected for analysis. Total N from harvested grain and straw samples were estimated by NIRS (Near Infrared Spectroscopy Method) using ASD FieldSpec 4 Hi-Res NG spectrometer, Analytik Ltd, UK. Total N estimated values were then used to calculate the NUE, NUpE, NUtE, GPC and other NUE related derived traits.

### **3.2.3.2 Harpenden measurements**

### **3.2.4 Physiological maturity and harvest analysis**

The plant height was measured from ground level to the tip of ear using a ruler at five random positions per plot in the field. The visual flag-leaf senescence score was recorded every 3-4 days from GS71 to GS93. The lodging scoring of all the lines was also done per-harvest. At GS94 stage, samples of 100 fertile shoots per plot were collected for analysis. Total N from harvested grain and stem samples were estimated by NIRS (Near Infrared Spectroscopy Method) using ASD FieldSpec 4 Hi-Res NG spectrometer, Analytik Ltd, UK. The estimated total N values were then used to calculate the NUE, NUpE, NUtE, GPC and other NUE related derived traits.

### **3.2.5 Statistical Analysis**

Analysis of variance for all the traits and harvest components were performed by using Genstat 21 (VSN International, United Kingdom) for a randomised split-plot design considering genotypes and site as fixed effects and replicates as a random effect. For the combined cross-site analysis an ANOVA model was used considering genotypes as fixed effects and site and replicates as random effects. Linear regression analysis was performed using the mean values across replicates using Genstat 21.

### 3.3 Results

The results section of this chapter has been divided into two sub-sections where first summarises the harvest and NUE components field data from Rothamsted Research and second the data from Sutton Bonington.

**Table 3.2:** Available N from soil and N fertiliser applied at Rothamsted Research, Harpenden (RR) and Sutton Bonington (SB)

Parameter/Site	Rothamsted Research (RR)	Sutton Bonington (SB)
N Fertiliser (kg ha <sup>-1</sup> )	250	160
Soil type	Silty clay loam	Clay loam
Soil Mineral N (kg ha <sup>-1</sup> )	103	27

To calculate NUE and its components, soil mineral N to 90 cm soil depth was measured by taking soil cores and submitting soil samples to analytical laboratories for chemical analysis at respective site. RR site's soil type was silty clay loam whereas SB site had clay loam soil. N fertiliser applied was 250 and 160 kg N ha<sup>-1</sup> at RR and SB, respectively (Table 3.2).

**Table 3.3:** Anthesis date and Plant Height (PH) in cm at Rothamsted Research (RR) and Sutton Bonington (SB) in year 2018-2019.

Parameter/Site		Rothamsted Research (RR)	Sutton Bonington (SB)
Anthesis Date	Minimum	03 June 2019	10 June 2019
	Maximum	17 June 2019	16 June 2019
	Mean	06 June 2019	12 June 2019
		P<0.001	P<0.001
Plant Height (PH) (cm)	Minimum	70.5	82
	Maximum	143.5	135.29
	Mean	106.73	100.89
		P<0.001	P<0.001

The mean anthesis date for both experiments in 2018-2019 was in a difference of 6 days, RR on 6<sup>th</sup> June 2019 and SB at 12<sup>th</sup> June 2019. It ranged from 3<sup>rd</sup> June to 17<sup>th</sup> June for RR and 10<sup>th</sup> June to 16<sup>th</sup> June for SB. The plant height trait showed a significant variation at each site (P<0.001). At RR site, maximum plant height measured was 143.5 cm whereas SB recorded 135.29 cm. The mean plant height at RR and SB was 106.73 and 100.89 cm (Table 3.3) respectively.

### **3.3.1 Rothamsted Research, 2019**

#### **3.3.1.1 Grain yield, yield components and height**

The overall mean biomass was 16.7 t ha<sup>-1</sup>. Across the 66 genotypes, the biomass showed genetic variation ranging from 11.1-18.4 t ha<sup>-1</sup> (P=0.207; Table 3.4). Among the synthetic-derived lines, the BM ranged from 11.1-17.8 t ha<sup>-1</sup> in comparison to Robigus which had a BM of 14.5 t ha<sup>-1</sup>. Further, in the P × W NILs, the BM ranged from 15.5-18.4 t ha<sup>-1</sup> and Paragon had a BM of 16.4 t ha<sup>-1</sup>.

Grain yield had an overall mean of 9.18 t ha<sup>-1</sup> ranging among genotypes between 6.94-10.58 t ha<sup>-1</sup> (P=0.084). The minimum and maximum grain yield were observed in the synthetic-derived lines while the GY of Robigus was 9.47 t ha<sup>-1</sup>. In the P × W NILs grain ranged from 8.35-10.37 t ha<sup>-1</sup> and that of Paragon was 9.34 t ha<sup>-1</sup>. Additionally, the height of the NILs ranged from 74.3- 133.9 cm (P<0.001). The P × W NILs had a comparatively higher range 100.8-133.9 cm) as compared to the synthetic-derived lines (74.3-89.5 cm). The height of Robigus and Paragon cultivars were 77.8 cm and 103.6 cm, respectively.

The Harvest Index (HI) ranged from 0.42 (PW352-26-4-10-Q2A-GFR-P) - 0.56 (Robigus) and was significant (P<0.001) (Table 3.4).

**Table 3.4:** NILs, BM (Above-ground Biomass t ha<sup>-1</sup>), Ears m<sup>-2</sup>, Grain Fill Rate (GFR), GY (Grain Yield t ha<sup>-1</sup> at 100% DM), Height (cm), HI (Harvest Index), Ears m<sup>-2</sup> and TGW (Thousand grain Weight) g at Rothamsted Research, Harpenden in 2018-19 for 64 near-isogenic line and synthetic-derived wheat lines with Paragon and Robigus parents

NILs	BM (t ha <sup>-1</sup> )	GFR (g m <sup>-2</sup> dy <sup>-1</sup> )	GY (t ha <sup>-1</sup> )	Height (cm)	HI	Ears m <sup>-2</sup>	TGW (g)
DFW SEL 0056	11.1*	11.75*	6.94*	84.46	0.53	422.4	35
DFW SEL 0057	14.2	15.44	8.81	74.33	0.53	501.4	33.3*
DFW SEL 0058	16.5	16.1	10.04	89.46*	0.52	478.3	41.9*
DFW SEL 0063	17	16.88	10.58	81.99	0.53	448.1	42*
DFW SEL 0064	17.1*	15.08	9.61	87.5*	0.48*	515.7*	40.2*
DFW SEL 0065	15.3	15.22	9.49	82.91	0.53	520*	37.8*
DFW SEL 0069	17.8*	17.25	10.42	76.49	0.50	636.8**	35.1
Robigus	14.5	16.78	9.47	77.83	0.56*	437.1	35
Paragon	16.4	15.49	9.34	103.75	0.47	408.7	35.5
PW141-41-2-13-Q5B-NDVI-W	16.6	15.66	9.31	108.91	0.48	410.1	37.9*
PW141-41-2-14-Q5B-NDVI-W	15.5	14.19	8.52	108.24	0.47	374.4	38.5*
PW141-41-2-17-Q5B-NDVI-W	16.9	14.49	9.04	101.58	0.46	371	40.7*
PW141-41-2-20-Q5B-NDVI-W	16.5	16.84	9.25	106.74	0.4	367.8	38.8*
PW141-41-2-21-Q5B-NDVI-P	16.6	14.99	9.12	105.83	0.47	401.2	38.7*
PW141-58-7-10-Q7D-AGDM-W	16.6	14.57	9.18	108.41	0.47	429.2	34.3
PW141-58-7-20-Q7D-AGDM-P	16.9	16.4	9.39	106.99	0.47	409.6	37.1*
PW141-58-7-7-Q7D-AGDM-W	16.4	15.42	9.06	105.08	0.47	423.8	34.8
PW292-22-9-16-Q3A-COMSTR-P	15.6	15.37	8.74	104.16	0.48	416.5	35.7
PW292-22-9-19-Q3A-COMSTR-P	16.3	15.17	8.79	107.33	0.46	413.3	36.3
PW292-22-9-1-Q3A-COMSTR-W	16.4	16.32	8.93	108.91	0.46	455.4	36.6
PW292-22-9-7-Q3A-COMSTR-W	16.4	14.28	8.87	107.74	0.46	441.3	37.4*
PW292-22-9-8-Q3A-COMSTR-W	17.1	16.1	9.33	104.49	0.46	445.7	35.7*
PW292-9-5-10-Q4B-GFPTT-W	17.1	16.67	9.34	111.24	0.46	425.2	37.7*

PW292-9-5-14-Q4B-GFPTT-P	15.5	15.68	8.50	102.41	0.47	414.1	35.8
PW292-9-5-15-Q4B-GFPTT-P	17.3	16.21	9.23	104.91	0.46	438.1	37.4*
PW292-9-5-18-Q4B-GFPTT-P	16.6	14.85	9.04	106.74	0.46	408.6	36.8*
PW292-9-5-6-Q4B-GFPTT-W	17.5	18.17	9.43	115.91	0.46	409.7	37*
PW292-9-5-7-Q4B-GFPTT-P	16.6	15.7	9.19	102.16	0.47	413.7	35.5
PW292-9-5-8-Q4B-GFPTT-W	16.2	14.79	8.91	110.24	0.47	366.8	39.4*
PW352-23-4-14-Q1A-NDVI-P	17.7	15.71	9.40	104.16	0.45	493.2	35.1
PW352-23-4-17-Q1A-NDVI-P	17.1	16.59	9.44	105.58	0.47	458.7	35.8
PW352-23-4-18-Q1A-NDVI-P	16.2	15.1	8.99	101.74	0.47	426.3	34.8
PW352-23-4-20-Q1A-NDVI-P	16.9	15.41	9.28	103.83	0.47	433.3	34.4
PW352-23-4-6-Q1A-NDVI-W	17.2	15.65	9.46	111.58	0.47	450.1	36.1
PW352-23-4-7-Q1A-NDVI-W	16.9	17.42	9.06	112.16	0.46	472.8	35.4
PW352-26-4-10-Q2A-GFR-P	17.1	15.11	8.94	121.58*	0.45	403	37.3*
PW352-26-4-14-Q2A-GFR-W	16.2	16.93	9.67	115.33*	0.52*	368.3	37.7*
PW352-26-4-17-Q2A-GFR-P	17.5	15.53	9.40	115.24*	0.46	435.2	37
PW352-26-4-19-Q2A-GFR-P	16.9	14.88	9.28	103.83	0.47	412.7	36
PW352-26-4-20-Q2A-GFR-P	17.3	16.76	8.94	116.08*	0.44	425.1	34.6
PW352-26-4-2-Q2A-GFR-W	17.6	16.27	9.57	114.74*	0.46	447.6	35.9
PW352-26-4-3-Q2A-GFR-W	17.7	15.74	9.48	120.49*	0.46	429.7	39.1
PW352-26-4-4-Q2A-GFR-W	16.4	16.26	8.65	113.41*	0.45	383.7	35.4
PW352-5-1-10-Q1B-GRYLD-P	17	15.65	9.47	101.83	0.48	428.9	33.9*
PW352-5-1-13-Q1B-GRYLD-W	17.4	17.08	9.87	104.24	0.48	477.7	36.1
PW352-5-1-16-Q1B-GRYLD-W	16.5	14.81	9.01	100.83	0.46	449.6	33.9
PW468-10-1-17-Q2A-NDVI-W	17.8	15.93	9.74	114.41*	0.47	367.3	37.5
PW468-10-1-21-Q2A-NDVI-P	17.8	15.67	9.52	117.91*	0.46	445.2	34.3
PW468-10-1-2-Q2A-NDVI-P	17.3	14.91	9.35	113.91*	0.46	435.5	37
PW468-10-1-5-Q2A-NDVI-W	15.9	14.12	8.80	114.91*	0.47	354.1	36.2
PW468-77-3-10-Q7B-AGDM-W	17.8	14.96	9.16	129.91**	0.44	387.3	42.5*
PW468-77-3-11-Q7B-AGDM-W	15.7	13.17*	7.92*	130.58**	0.43*	361.5	40.5*
PW468-77-3-14-Q7B-AGDM-W	17.2	13.84	8.86	128.91*	0.44	365	40.7*
PW468-77-3-16-Q7B-AGDM-P	17.6	14.62	9.06	125.08*	0.44	440.5	38.1*

PW468-77-3-19-Q7B-AGDM-W	16	13.82	8.92	109.91	0.47	377.3	36.7
PW468-77-3-20-Q7B-AGDM-P	16.8	13.79	8.35	133.08**	0.42*	405	42.1*
PW468-77-3-9-Q7B-AGDM-P	17.7	15.1	8.92	130.66**	0.43*	373.1	41.3*
PW468-84-4-12-Q5A-COMGRWT-P	17.1	14.24	9.34	108.83	0.46	409	38*
PW468-84-4-1-Q5A-COMGRWT-W	18.4	17.48	10.33	108.74	0.48	426.1	42.1*
PW468-84-4-4-Q5A-COMGRWT-P	16.9	14.19	8.96	110.91	0.45	372.1	40.7*
PW729-55-3-13-Q6B-AGDM-P	16.1	15.23	8.70	106.49	0.46	442.1	33.9
PW729-55-3-15-Q6B-AGDM-P	16.1	14.58	8.91	107.41	0.47	402.5	35.7
PW729-55-3-1-Q6B-AGDM-W	16.9	15.02	9.35	106.49	0.47	523**	34.8
PW729-55-3-21-Q6B-AGDM-W	16.9	16.03	9.21	107.58	0.46	457.7	34.7
PW729-55-3-6-Q6B-AGDM-P	16.9	15.85	9.28	108.08	0.47	438.1	35.3
PW729-55-3-8-Q6B-AGDM-P	17.9	15.53	9.75	103.99	0.46	461.9	35.3
<b>Mean</b>	<b>16.7</b>	<b>15.47</b>	<b>9.18</b>	<b>107.37</b>	<b>0.5</b>	<b>426.8</b>	<b>36.9</b>
<b>LSD (Genotype) (5%)</b>	<b>2.58</b>	<b>3.08</b>	<b>1.22</b>	<b>9.14</b>	<b>0.03</b>	<b>75.54</b>	<b>1.54</b>
<b>P value</b>	<b>0.207</b>	<b>0.618</b>	<b>0.084</b>	<b>&lt;0.001</b>	<b>&lt;0.001</b>	<b>&lt;0.001</b>	<b>&lt;0.001</b>

\*Significance at the 5% ( $P = 0.05$ ) level. \*\*1% ( $P = 0.01$ ) level. \*\*\*0.1% ( $P = 0.001$ )

The NILs showing values higher than Paragon for PxW lines and Robigus for SHW lines have been marked with \* according to the degree of significance.



### 3.3.1.2 Nitrogen-use efficiency and NUE components

The average NUE across the genotypes was 22.11 kg Grain DM kg<sup>-1</sup> N (P=0.084; Table 3.5) with synthetic lines ranging from 16.72-25.09 kg Grain DM kg<sup>-1</sup> N and P × W NILs between 34.1-36.76 kg Grain DM kg<sup>-1</sup> N. The NUE of Robigus and Paragon cultivars were 22.79 and 22.5 kg Grain DM kg<sup>-1</sup> N, respectively.

The average NHI of the NILs was 0.81 and ranged among the NILS from 0.77-0.83 (P = 0.034; Table 3.5). The maximum variation was seen in the synthetic lines. The NHI of Robigus was 0.80 while that of Paragon was 0.81. Further the other NUE components of NUpE and NUtE had significant P values of 0.051 and <0.001 for the genotype effect. The NUpE ranged from 0.47-0.72 kg AGN kg<sup>-1</sup> N and overall NUpE was 0.63 kg AGN kg<sup>-1</sup> N across the genotypes. The average NUtE was 35.12 kg DM kg N<sup>-1</sup> ranging between 33.19-38.12 kg DM kg N<sup>-1</sup> in the synthetic lines and 32.38-38.19 kg DM kg N<sup>-1</sup> in the P × W NILs. The NUpE and NUtE of Robigus were 0.58 kg AGN kg<sup>-1</sup> N and 38.87 kg DM kg N<sup>-1</sup> and of Paragon were 0.64 kg AGN kg<sup>-1</sup> N and 35.33 kg DM kg N<sup>-1</sup>, respectively.

The grain protein content did not show large variation and ranged between 12.8-15.63% (P=<0.001) across the 66 NILs with overall GPC being 14.39%. The GPC of Robigus and Paragon were 12.8 and 14.37%, respectively (Table 3.5).

The above-ground N uptake ranged between 166.2-246.1 kg N ha<sup>-1</sup> in the synthetic lines in comparison to Robigus which had an AGNUP of 206.5 kg N ha<sup>-1</sup>. In the P × W NILs, the AGNUP ranged from 203.6- 253.2 kg N ha<sup>-1</sup> and that of Paragon was 224.8 kg N ha<sup>-1</sup>. The mean AGNUP across all the NILs was 222.42 kg N ha<sup>-1</sup> (P=0.051) (Table 3.5).

A summary table of the genetic variation for the traits is given in Table 3.6. The highest genotype significance was seen in height, ears, grain NUP, TGW, HI, NUtE and GPC traits with P value <0.001.

**Table 3.5:** AGNUP (Above-ground N Uptake kg N ha<sup>-1</sup>), NHI (Nitrogen Harvest Index), NUE (Nitrogen-Use Efficiency kg Grain DM kg<sup>-1</sup> N ), NUpE (Nitrogen-Uptake Efficiency kg AGN kg<sup>-1</sup> N), NUtE (Nitrogen-Utilisation Efficiency kg DM kg N<sup>-1</sup>, Grain N UP (Grain N Uptake kg N ha<sup>-1</sup>), GPC (Grain Protein Content %) at Rothamsted Research in 2019 for 66 near-isogenic line and synthetic-derived wheat lines and Paragon and Robigus parents

Genotype	AGNUP (kg N ha <sup>-1</sup> )	NHI	NUE	NUpE	NUtE	Grain N UP (kg N ha <sup>-1</sup> )	GPC %
DFW SEL 0056	166.19*	0.78*	16.72*	0.47*	35.55*	129.21*	13.68
DFW SEL 0057	196.54	0.79	21.22	0.56	38.12	156.09	13.03
DFW SEL 0058	229.68	0.81	24.18	0.65	37.21	186.25	13.63
DFW SEL 0063	242.38*	0.82*	25.47	0.69*	37.12	199.85*	13.92*
DFW SEL 0064	246.05*	0.77*	23.14	0.7*	33.19*	189.37*	14.5*
DFW SEL 0065	221.07	0.80	22.85	0.63	36.53	177.13	13.72*
DFW SEL 0069	242.35*	0.81	25.09	0.69*	36.52	195.35*	13.83*
Robigus	206.48	0.80	22.79	0.58	38.87	164.25	12.8
Paragon	224.82	0.81	22.5	0.64	35.33	182.39	14.37
PW141-41-2-13-Q5B-NDVI-W	232.79	0.83*	22.43	0.66	34.01	192.11	15.17
PW141-41-2-14-Q5B-NDVI-W	218.3	0.82	20.5	0.62	33.16*	178.28	15.4
PW141-41-2-17-Q5B-NDVI-W	235.81	0.81	21.78	0.67	32.59*	191.41	15.63*
PW141-41-2-20-Q5B-NDVI-W	225.63	0.81	22.26	0.64	34.88	182.18	14.51
PW141-41-2-21-Q5B-NDVI-P	223.75	0.81	21.96	0.63	34.57	180.47	14.61
PW141-58-7-10-Q7D-AGDM-W	220.46	0.80	22.11	0.62	35.5	176.74	14.14
PW141-58-7-20-Q7D-AGDM-P	219.96	0.82	22.61	0.62	36.28	180.12	14.1
PW141-58-7-7-Q7D-AGDM-W	213.87	0.81	21.83	0.61	36.05	173.7	14.1
PW292-22-9-16-Q3A-COMSTR-P	211.05	0.82	21.05	0.6	35.08	172.95	14.68
PW292-22-9-19-Q3A-COMSTR-P	212.36	0.81	21.15	0.6	35.22	172.66	14.44
PW292-22-9-1-Q3A-COMSTR-W	215.41	0.82	21.5	0.61	35.16	177.32	14.62
PW292-22-9-7-Q3A-COMSTR-W	229.64	0.81	21.37	0.65	32.81*	186.29	15.48*
PW292-22-9-8-Q3A-COMSTR-W	228.97	0.81	22.46	0.65	34.64	185.41	14.62
PW292-9-5-10-Q4B-GFPTT-W	218.54	0.83	22.48	0.62	36.28	181.74	14.33
PW292-9-5-14-Q4B-GFPTT-P	204.87	0.82	20.47	0.58	35.33	168.89	14.6
PW292-9-5-15-Q4B-GFPTT-P	223.83	0.82	22.21	0.63	35.14	184.12	14.67

PW292-9-5-18-Q4B-GFPTT-P	220.74	0.82	21.76	0.63	34.82	180.93	14.72
PW292-9-5-6-Q4B-GFPTT-W	223.12	0.81	22.71	0.63	35.94	181.83	14.21
PW292-9-5-7-Q4B-GFPTT-P	220.87	0.82	22.13	0.63	35.38	180.71	14.45
PW292-9-5-8-Q4B-GFPTT-W	214.67	0.81	21.46	0.61	35.25	174.08	14.42
PW352-23-4-14-Q1A-NDVI-P	236.69	0.80	22.64	0.67	33.77	190.08	14.86
PW352-23-4-17-Q1A-NDVI-P	231.04	0.81	22.72	0.65	34.69	186.87	14.58
PW352-23-4-18-Q1A-NDVI-P	217.6	0.82	21.65	0.62	35.17	177.62	14.53
PW352-23-4-20-Q1A-NDVI-P	225.23	0.81	22.35	0.64	35.02	182.17	14.45
PW352-23-4-6-Q1A-NDVI-W	225.67	0.80	22.77	0.64	35.68	180.13	14.01
PW352-23-4-7-Q1A-NDVI-W	222.92	0.81	21.82	0.63	34.66	181.09	14.69
PW352-26-4-10-Q2A-GFR-P	213.82	0.81	21.53	0.61	35.63	172.24	14.17
PW352-26-4-14-Q2A-GFR-W	215.38	0.83*	23.28	0.61	38.19	178.14	13.56
PW352-26-4-17-Q2A-GFR-P	223.9	0.80	22.63	0.63	35.59	179.95	14.15
PW352-26-4-19-Q2A-GFR-P	225.38	0.81	22.34	0.64	34.97	183.39	14.55
PW352-26-4-20-Q2A-GFR-P	222.26	0.81	21.52	0.63	34.21	179.31	14.75
PW352-26-4-2-Q2A-GFR-W	225.74	0.81	23.05	0.64	36.06	181.98	13.97
PW352-26-4-3-Q2A-GFR-W	229.28	0.81	22.83	0.65	35.21	185.32	14.37
PW352-26-4-4-Q2A-GFR-W	206.56	0.82	20.84	0.59	35.61	168.71	14.35
PW352-5-1-10-Q1B-GRYLD-P	231.38	0.82	22.81	0.66	34.79	190.39	14.79
PW352-5-1-13-Q1B-GRYLD-W	242.44	0.81	23.78	0.69	34.63	196.18	14.61
PW352-5-1-16-Q1B-GRYLD-W	220.75	0.82	21.69	0.63	34.68	180.21	14.73
PW468-10-1-17-Q2A-NDVI-W	225.33	0.78*	23.44	0.64	36.82	176.61	13.33*
PW468-10-1-21-Q2A-NDVI-P	221.42	0.79	22.92	0.63	36.59	174.52	13.48
PW468-10-1-2-Q2A-NDVI-P	231.02	0.81	22.51	0.65	34.53	185.72	14.59
PW468-10-1-5-Q2A-NDVI-W	203.63	0.80	21.2	0.58	36.76	162.04	13.54
PW468-77-3-10-Q7B-AGDM-W	237	0.79	22.06	0.67	32.87*	186.45	15.01
PW468-77-3-11-Q7B-AGDM-W	208	0.79	19.07*	0.59	32.38	165	15.32
PW468-77-3-14-Q7B-AGDM-W	223.92	0.79	21.34	0.63	33.64	177.34	14.74
PW468-77-3-16-Q7B-AGDM-P	220.2	0.79	21.81	0.62	35.05	174	14.13
PW468-77-3-19-Q7B-AGDM-W	216.01	0.81	21.48	0.61	35.07	174.01	14.37
PW468-77-3-20-Q7B-AGDM-P	210.62	0.78*	20.09	0.6	33.6	165.11	14.63

PW468-77-3-9-Q7B-AGDM-P	221.98	0.78*	21.47	0.63	34.1	173.27	14.33
PW468-84-4-12-Q5A-COMGRWT-P	230.16	0.79	22.48	0.65	34.48	181.32	14.31
PW468-84-4-1-Q5A-COMGRWT-W	253.21*	0.80	24.87	0.72	34.69	202.57	14.46
PW468-84-4-4-Q5A-COMGRWT-P	224.66	0.80	21.57	0.64	33.92	179.17	14.7
PW729-55-3-13-Q6B-AGDM-P	215.17	0.80	20.94	0.61	34.31	171.52	14.55
PW729-55-3-15-Q6B-AGDM-P	219.39	0.81	21.46	0.62	34.53	178.53	14.73
PW729-55-3-1-Q6B-AGDM-W	234.74	0.81	22.5	0.66	33.86	189.66	14.92
PW729-55-3-21-Q6B-AGDM-W	223.77	0.80	22.18	0.63	34.94	178.29	14.27
PW729-55-3-6-Q6B-AGDM-P	223.86	0.82	22.35	0.63	35.21	183.36	14.54
PW729-55-3-8-Q6B-AGDM-P	234.78	0.81	23.48	0.67	35.32	190.07	14.36
<b>Mean</b>	<b>222.42</b>	<b>0.81</b>	<b>22.11</b>	<b>0.63</b>	<b>35.12</b>	<b>179.46</b>	<b>14.39</b>
<b>LSD (Genotype) (5%)</b>	<b>28.22</b>	<b>0.02</b>	<b>2.95</b>	<b>0.08</b>	<b>2.02</b>	<b>20.35</b>	<b>0.9</b>
<b>P value</b>	<b>0.051</b>	<b>0.034</b>	<b>0.084</b>	<b>0.051</b>	<b>&lt;0.001</b>	<b>&lt;0.001</b>	<b>&lt;0.001</b>

\*Significance at the 5% ( $P = 0.05$ ) level. \*\*1% ( $P = 0.01$ ) level. \*\*\*0.1% ( $P = 0.001$ )

The NILs showing values higher than Paragon for PxW lines and Robigus for SHW lines have been marked with \* according to the degree of significance.

**Table 3.6:** Genetic variation in harvest and NUE related traits: BM (Above-ground Biomass ha<sup>-1</sup>), Ears (m<sup>-2</sup>), Grain Fill Rate (GFR), GY (Grain Yield t ha<sup>-1</sup>), Height (cm), HI (Harvest Index) and TGW (Thousand grain Weight), AGNUP (Above-ground N Uptake kg N ha<sup>-1</sup>), NHI (Nitrogen Harvest Index), NUE (Nitrogen Use Efficiency kg Grain DM kg<sup>-1</sup> N), NUpE (Nitrogen Uptake Efficiency kg AGN kg<sup>-1</sup> N), NutE (Nitrogen Utilisation Efficiency kg DM kg N<sup>-1</sup>), Straw N uptake (kg N ha<sup>-1</sup>) at Rothamsted Research, Harpenden in 2019 in 64 near-isogenic line and synthetic-derived wheat lines with Paragon and Robigus parents

Trait	Maximum	Minimum	Mean	P value
Height (cm)	133.08	74.33	107.37	<0.001
BM (t ha <sup>-1</sup> )	18.4	11.1	16.7	0.207
GY (t ha <sup>-1</sup> )	10.58	6.94	9.20	0.084
Ears (m <sup>-2</sup> )	636.8	354.1	426.8	<0.001
GFR (g m <sup>-2</sup> dy <sup>-1</sup> )	18.17	11.75	15.47	0.68
Grain N UP (kg N ha <sup>-1</sup> )	202.57	129.21	179.46	<0.001
AGNUP (kg N ha <sup>-1</sup> )	253.21	166.19	222.42	0.051
TGW g	42.5	33.3	36.9	<0.001
HI	0.6	0.4	0.5	<0.001
NHI	0.83	0.77	0.81	0.034
NUE	36.76	16.72	22.11	0.084
NUpE	0.72	0.47	0.63	0.051
NUtE	38.87	32.38	35.12	<0.001
GPC %	15.63	12.8	14.39	<0.001

### 3.3.1.3 Association between yield and NUE and its components

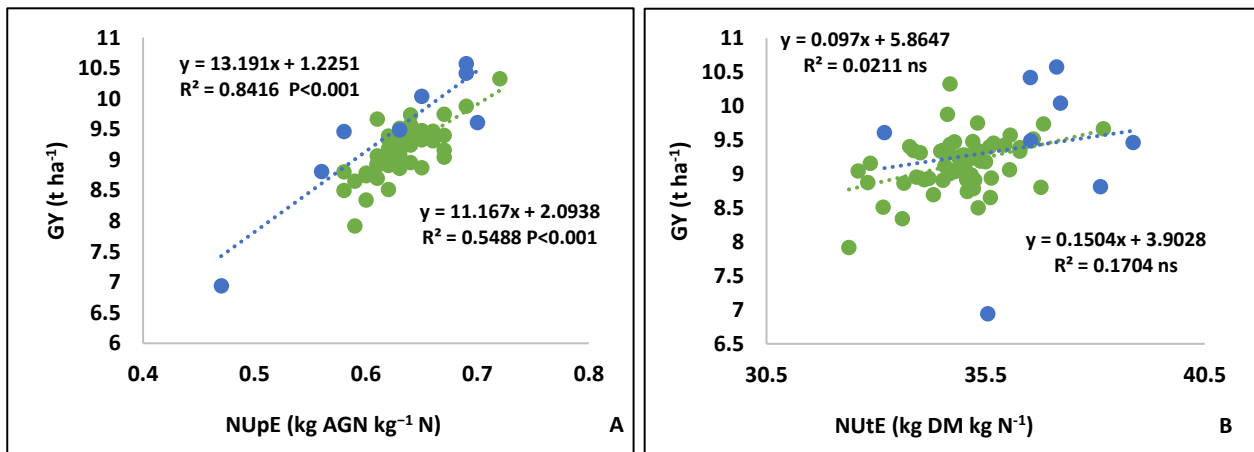
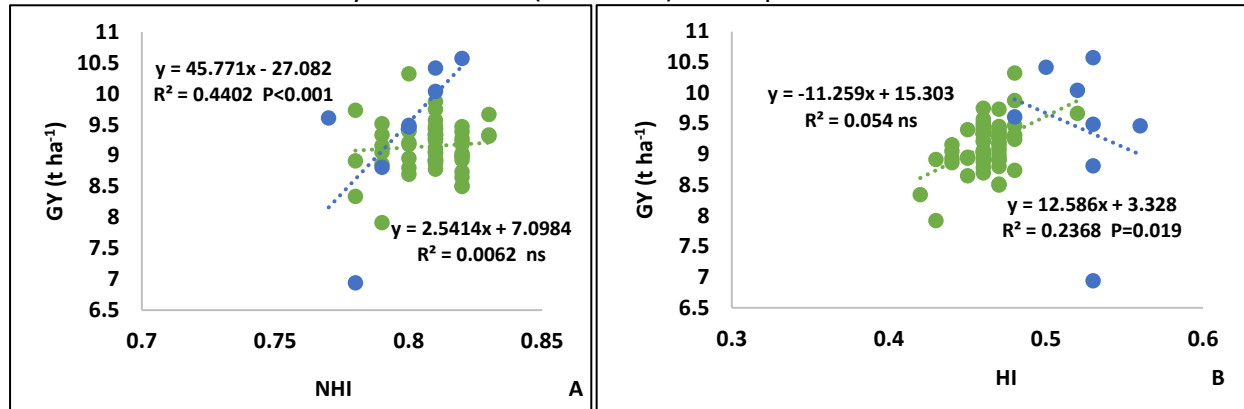


**Fig 3.1:** Linear regression of (A) Nitrogen-Uptake Efficiency (NUpE (kg AGN kg<sup>-1</sup> N)) and (B) Nitrogen-Utilisation Efficiency (NUtE (kg DM kg N<sup>-1</sup>)) on Grain Yield GY (t ha<sup>-1</sup>). Blue colour data points represent synthetic-derived hexaploid wheat lines and green colour points near isogenic lines developed by crossing Paragon and Watkins landraces. ns, denotes non significant.

A positive association was observed among the NILs between NUpE and GY in synthetic-derived lines ( $R^2 = 0.84$ ) and P x W NILs ( $R^2 = 0.54$ ) (Fig 3.1). Further, there was no association

between NUTe and GY in synthetic lines ( $R^2 = 0.021$ ) but a positive linear association in P × W



lines ( $R^2 = 0.17$ ) (Fig 3.1).

**Fig 3.2:** Linear regression of (A) Nitrogen Harvest Index (NHI) on Grain Yield GY (t ha<sup>-1</sup>) and (B) Harvest Index (HI) on Grain Yield GY (t ha<sup>-1</sup>). Blue colour data points represents data of synthetic hexaploid wheat lines and green colour points represents near isogenic lines developed by crossing Paragon and Watkins landraces.

Positive linear associations were seen between GY and each of NHI and HI as well. In the synthetic-derived lines there was an association between GY and NHI ( $R^2 = 0.44$ ) while no association ( $R^2 = 0.0002$ ) was seen between GY and HI. Additionally, in the P × W NILs there was no association ( $R^2 = 0.0062$ ) between GY and NHI but, a positive association was observed between GY and HI ( $R^2 = 0.1982$ ) (Fig 3.2).

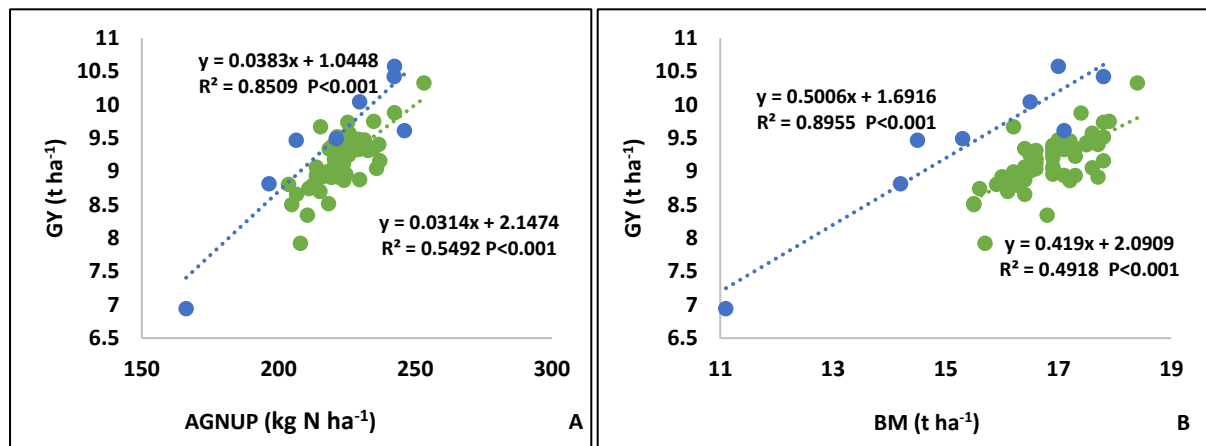


**Fig 3. 3:** Linear regression of (A) Above-ground N Uptake (AGNUP ( kg AGN kg<sup>-1</sup> N), on Grain Yield GY (t ha<sup>-1</sup>) and (B) Biomass (BM (t ha<sup>-1</sup>) on Grain Yield GY (t ha<sup>-1</sup>). Blue colour data points represents data of synthetic hexaploid wheat lines and green colour points represents near-isogenic lines developed by crossing Paragon and Watkins landraces.

There was positive linear association between AGNUP and GY in the synthetic-derived lines ( $R^2=0.85$ ) as well as for the  $P \times W$  NILs ( $R^2 = 0.54$ ). There was also a linear association between BM and GY in the synthetic-derived lines ( $R^2=0.89$ ) and  $P \times W$  NILs ( $R^2=0.49$ ) (Fig 3.3).

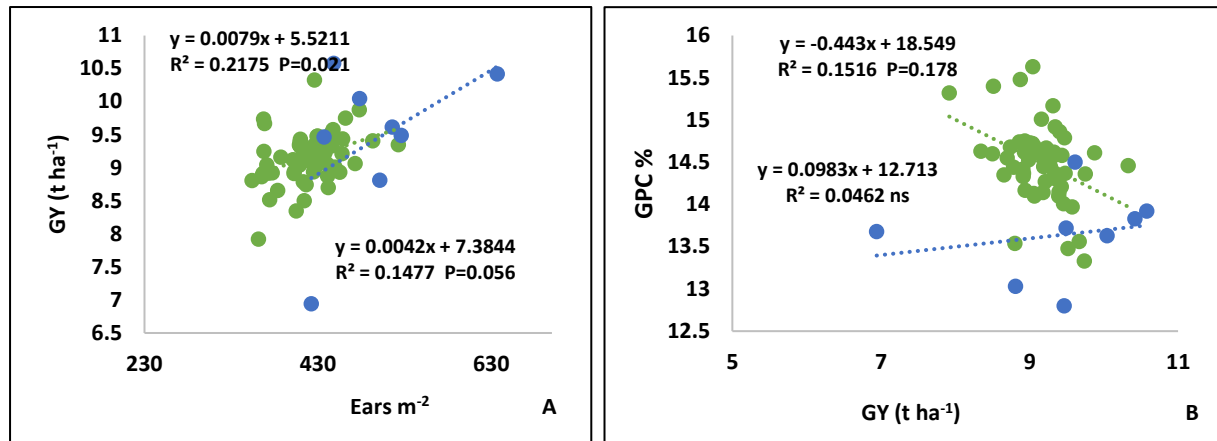


**Fig 3.4:** Linear regression of (A) Ears  $m^{-2}$ , on Grain Yield GY ( $t\ ha^{-1}$ ) and (B) Grain Yield GY ( $t\ ha^{-1}$ ) on Grain Protein Content (GPC). Blue colour data points represent data of synthetic-derived hexaploid wheat lines and green colour points represent near-isogenic lines developed by crossing Paragon and Watkins landraces

Ears  $m^{-2}$  was also positively associated with GY (Fig 3.4) in the synthetic-derived lines ( $R^2=0.2175$ ) and the  $P \times W$  NILs ( $R^2=0.147$ ). No association was found between grain protein content and GY in synthetic-derived lines ( $R^2=0.046$ ). However, in the  $P \times W$  NILs a negative correlation was observed between GPC and GY ( $R^2=0.15$ ).

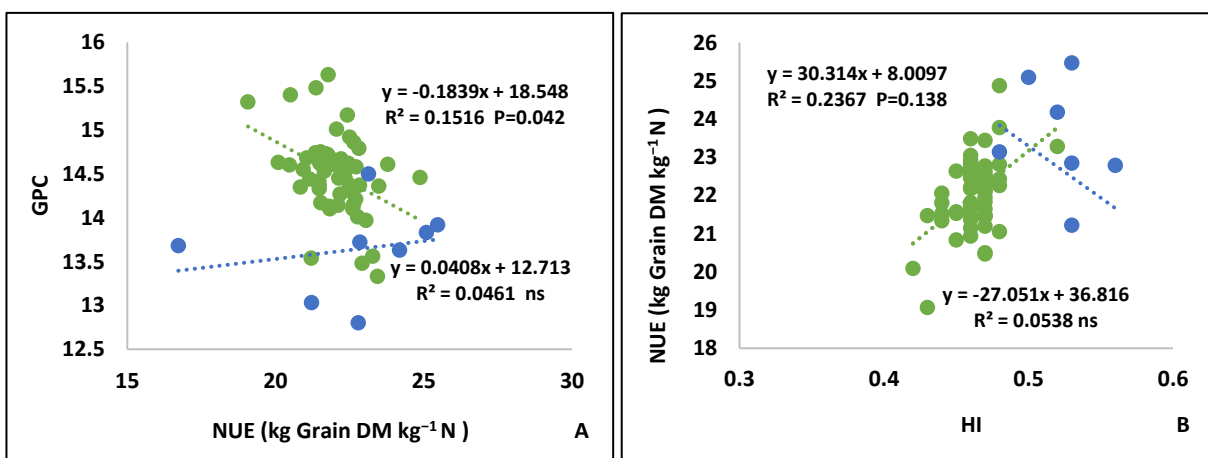


**Fig 3.5:** Linear regression of (A) Nitrogen Use Efficiency (NUE ( $kg\ Grain\ DM\ kg^{-1}\ N$ )) on Grain Protein Content (GPC %) and (B) Harvest Index (HI) on Nitrogen Use Efficiency (NUE ( $kg\ Grain\ DM\ kg^{-1}\ N$ )). Blue colour data points represents data of synthetic-derived hexaploid wheat

lines and green colour points represents near-isogenic lines developed by crossing Paragon and Watkins landraces

There was a negative correlation amongst P x W lines ( $R^2=0.15$ ) but no correlation among P x W NILs ( $R^2=0.046$ ) between NUE and GPC. A positive linear relationship was observed between NUE and HI in the synthetic-derived lines ( $R^2=0.198$ ) but no association amongst the P x W NILs ( $R^2=0.0002$ ) (Fig 3.5).

### 3.3.1.4 Allelic variation among Paragon x Watkin NILs

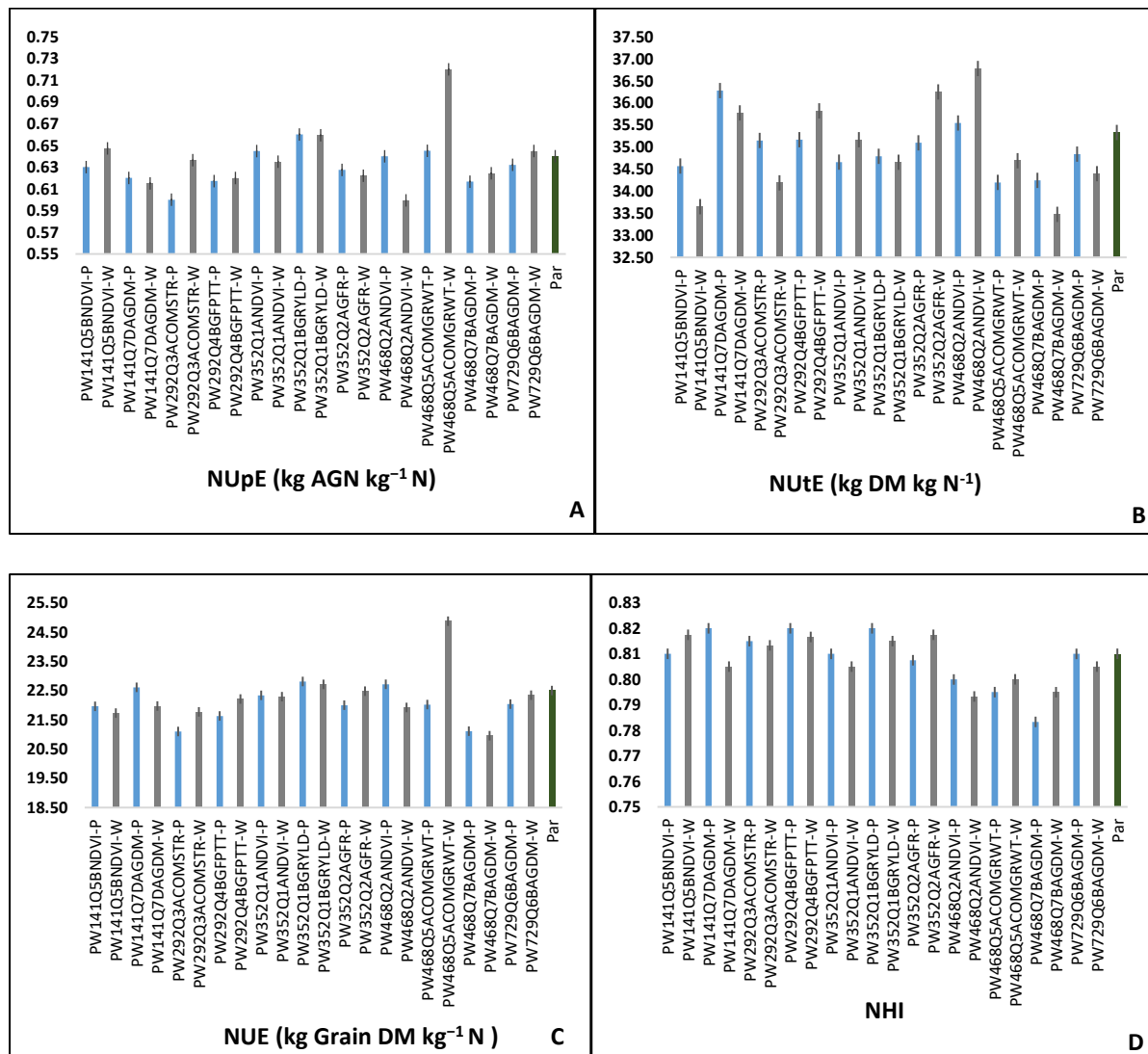


**Fig 3.6:** Bar graph represents (A) NUpE (kg AGN kg<sup>-1</sup> N) (B) NUtE (kg DM kg N<sup>-1</sup>) (C) NUE (kg Grain DM kg<sup>-1</sup> N) (D) NHI of allelic groups for QTLs in Paragon x Watkins landraces NILs and elite cultivar Paragon. Grey and blue colour represent near-isogenic lines with Watkins allele in the QTL and Paragon allele, respectively, whereas green colour bar corresponds to Paragon cultivar. Error bar represent standard +/- of the mean.



Landraces possess wide allelic variation for most key QTL traits. In the present study, significant variation was observed between Paragon and Watkins alleles in the P x W NILs in traits including NUpE, NUtE, NUE and NHI.

For the QTLs for GRWT on chr 5A and NDVI on chr 5B the Watkins allele showed a trend for higher NUpE compared to the Paragon allele of the same QTL. Similarly, for the QTLs for AGFR on chr 2A, NDVI on chr 2A and GFPTT on chr 4B the Watkins allele showed higher NUtE relative to Paragon. However, for the AGDM QTL on chr 7B, the Paragon allele showed higher NUtE. For NUE, the QTL for GRWT on chr 5A showed a higher value in the Watkins allele compared to the Paragon allele. Finally, there was not much allelic variation observed among the QTLs in NHI, with the AGFR QTL-Watkin allele showing slightly higher NHI than AGFR QTL-Paragon allele (Fig 3.6).

### 3.3.1.5 Genetic variation among synthetic-derived lines

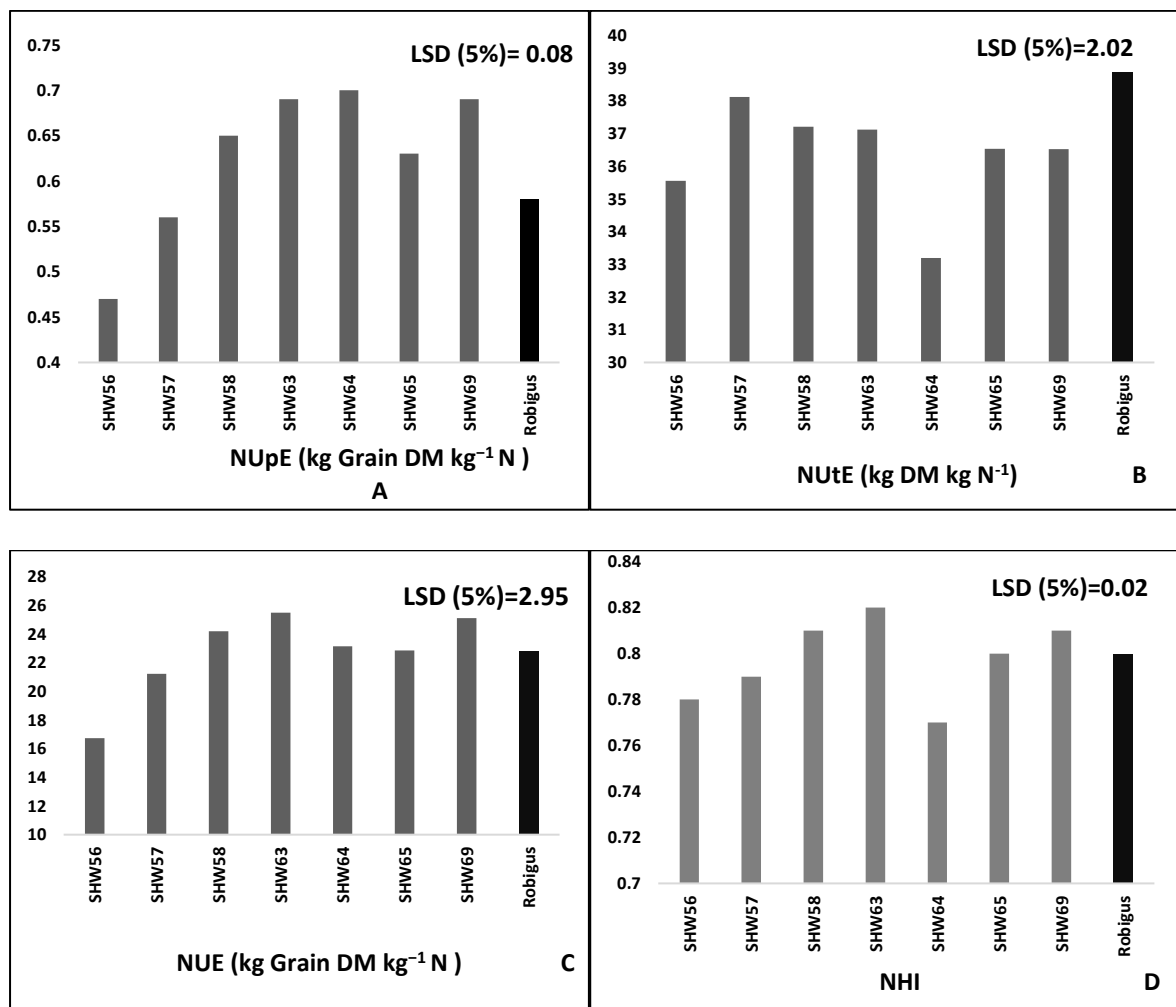


**Fig 3. 7:** Bar chart represents (A) NUpE (kg AGN kg<sup>-1</sup> N) (B) NUtE (kg DM kg N<sup>-1</sup>) (C) NUE (kg

Grain DM kg<sup>-1</sup> N) (D) NHI of seven synthetic-derived hexaploid wheat lines (grey) and Robigus parent (dark grey)

The synthetic-derived lines SHW58, SHW63, SHW64, SHW65 and SHW69 were observed to have higher NUpE, NHI, NUE and NUtE values. However, taking into consideration the LSD, the lines were not highly significant for these traits (Fig 3.7).

### **3.3.2 Harvest and NUE components Sutton Bonington, 2019**

The harvest and NUE components field results from the Sutton Bonington 2019 field trial are included in this section.

#### **3.3.2.1 Genetic variation in grain yield, yield components, N-use efficiency and NUE components**

Various NUE related traits including grain yield (GY), Grain N uptake (GNUP), Grain Protein Content (GPC) along with Thousand Grain Weight (TGW), Grain N% and Straw N% were analysed across the 66 genotypes (Table 3.7). The overall mean GY was 7.55 t ha<sup>-1</sup> (P<0.001). Among the P × W NILs, genetic variation ranged from 4.79-8.24 t ha<sup>-1</sup> compared to Paragon at 7.52 t ha<sup>-1</sup>. In the synthetic-derived lines, the GY was overall higher than the P × W NILs ranging from 7.95-8.80 t ha<sup>-1</sup> and that of Robigus was the highest (8.95 t ha<sup>-1</sup>).

The grain N uptake overall had a mean value of 166.3 kg N ha<sup>-1</sup>. The minimum as well as maximum GNUP was observed in the P × W NILs and ranged from 109.8- 213.3 kg N ha<sup>-1</sup> and that of Paragon was 173 kg N ha<sup>-1</sup> (P=0.041, Table 3.7) The genetic variation in GNUP observed in the synthetic-derived lines ranged from 167.6-194.1 kg N ha<sup>-1</sup> while that of Robigus was 178.4 kg N ha<sup>-1</sup> (Table 3.7).

The grain protein content (GPC) across the NILs and synthetic-derived lines was seen to be consistent with a mean value of 13.75% (P=0.676). The GPC showed non-significant genetic variation of 12.78- 17.11% in the NILs while Paragon had a GPC of 14.36%. In the synthetic-derived lines, the GPC showed non-significant variation from 12.76-13.77% and that of Robigus was 12.47%. The mean thousand grain weight (TGW) was 43.5 g and showed genetic variation (P<0.001). In the P × W NILs, the TGW ranged from 33.3-50.9 g and that of Paragon was 40.7 g. On the other hand, the TGW of synthetic-derived lines ranged between 39.3-44.8 g while Robigus was 37.6 g (Table 3.7).

Finally, the NUE (kg Grain DM kg<sup>-1</sup> N) showed a mean value of 40.37 (P=<.001). Among the NILs, the NUE ranged between 25.63-44.08 kg Grain DM kg<sup>-1</sup> N with Paragon at 40.22 kg Grain DM kg<sup>-1</sup> N. In the synthetic-derived lines, the NUE ranged from 42.5-47.08 kg Grain DM kg<sup>-1</sup> N and that of Robigus was 47.88 kg Grain DM kg<sup>-1</sup> N. Among all these lines, Robigus demonstrated the highest NUE (47.88 kg Grain DM kg<sup>-1</sup> N) followed by SEL65 (47.08 kg Grain DM kg<sup>-1</sup> N) (Table 3.7). However, NUE for Robigus was only significantly higher than SEL63 line (42.5 kg Grain DM kg<sup>-1</sup> N) (P< 0.05).

A summary of the genetic variation in traits is given in Table 3.8. The highest significances were observed for GY, NUE and TGW with P value <0.001.

**Table 3.7:** Genotype, GY (Grain Yield t ha<sup>-1</sup>), Grain N UP (kg N ha<sup>-1</sup>), GPC (Grain Protein Content) TGW (Thousand grain Weight), Grain N% and Straw N% at Sutton Bonington in 2019 for in 66 near-isogenic line and synthetic-derived wheat lines and Paragon and Robigus parents

NILs	GY (t ha <sup>-1</sup> )	Grain N UP (kg N ha <sup>-1</sup> )	NUE (kg Grain DM kg <sup>-1</sup> N)	GPC %	TGW (g)	Grain Number (Grains m <sup>-2</sup> )	Straw N%	Grain N%
Paragon	7.52	173	40.22	14.36	40.68	23336	0.62	2.3
PW141-41-2-13-Q5B-NDVI-W	7.2	152.8	38.5	13.23	44.83	18881	0.64	2.12
PW141-41-2-14-Q5B-NDVI-W	7.44	161.2	39.79	13.49	45.8	19103	0.44	2.16
PW141-41-2-17-Q5B-NDVI-W	7.4	164.8	39.58	13.92	44.93	19423	0.64	2.23
PW141-41-2-20-Q5B-NDVI-W	7.73	175.3	41.33	14.17	44.6	20465	0.86	2.27
PW141-41-2-21-Q5B-NDVI-P	6.97	159.5	37.26	14.29	45.1	18202	0.66	2.29
PW141-58-7-10-Q7D-AGDM-W	7.74	166.4	41.41	13.44	36.3	25573	1.08*	2.15
PW141-58-7-20-Q7D-AGDM-P	7.52	174.7	40.23	14.60	43.27	20455	0.72	2.34
PW141-58-7-7-Q7D-AGDM-W	7.55	157.6	40.4	13.03	41.77	21288	0.64	2.08
PW292-22-9-1-Q3A-COMSTR-W	7.28	166.6	38.93	14.28	43.7	19749	0.47	2.28
PW292-22-9-16-Q3A-COMSTR-P	7.22	155.9	38.61	13.47	42.7	20344	0.85	2.16
PW292-22-9-19-Q3A-COMSTR-P	7.39	163.8	39.52	13.82	43.63	19979	1*	2.21
PW292-22-9-7-Q3A-COMSTR-W	7.93	174.3	42.41	13.74	43.93	21247	0.48	2.2
PW292-22-9-8-Q3A-COMSTR-W	7.3	166	39.06	14.14	42.13	20413	0.5	2.26
PW292-9-5-10-Q4B-GFPTT-W	7.59	165.6	40.57	13.64	45.1	19801	0.9	2.18
PW292-9-5-14-Q4B-GFPTT-P	7.48	164.9	40.03	13.80	43.5	20238	0.85	2.21
PW292-9-5-15-Q4B-GFPTT-P	7.93	173.9	42.38	13.70	45.37	20580	0.69	2.19
PW292-9-5-18-Q4B-GFPTT-P	7.75	175.5	41.43	14.17	41.97	21737	0.62	2.27
PW292-9-5-6-Q4B-GFPTT-W	7.83	173.7	41.9	13.87	43.47	21197	0.85	2.22
PW292-9-5-7-Q4B-GFPTT-P	8.23	184.1	44.01	13.99	43.63	22217	0.84	2.24
PW292-9-5-8-Q4B-GFPTT-W	7.65	166.3	40.88	13.59	45.6*	19750	0.65	2.17
PW352-23-4-14-Q1A-NDVI-P	7.95	172.3	42.49	13.55	43	21758	0.54	2.17
PW352-23-4-17-Q1A-NDVI-P	8.06	164.5	43.09	12.77*	43.13	21980	0.73	2.04*
PW352-23-4-18-Q1A-NDVI-P	7.74	173	41.37	14.12	41.8	21867	1.02*	2.26
PW352-23-4-20-Q1A-NDVI-P	7.29	152.4	38.96	13.05	42.1	20367	0.82	2.09

PW352-23-4-6-Q1A-NDVI-W	7.79	179.6	41.67	14.43	44.43	20629	0.68	2.31
PW352-23-4-7-Q1A-NDVI-W	7.58	163.4	40.52	13.46	43.83	20350	0.45	2.15
PW352-26-4-10-Q2A-GFR-P	7.3	158.6	39.02	13.59	44.57	19243	0.64	2.17
PW352-26-4-14-Q2A-GFR-W	8.24	188.9	44.08	14.34	45.33	21416	0.84	2.29
PW352-26-4-17-Q2A-GFR-P	7.42	170.2	39.68	14.39	44.43	19699	0.63	2.3
PW352-26-4-19-Q2A-GFR-P	7.53	157.3	40.28	13.07	43.17	20532	0.73	2.09
PW352-26-4-2-Q2A-GFR-W	7.68	163.6	41.09	13.35	43.9	20618	0.82	2.14
PW352-26-4-20-Q2A-GFR-P	7.14	159.6	38.19	13.95	39.93	21033	1.01*	2.23
PW352-26-4-3-Q2A-GFR-W	6.67*	144.1**	35.69**	13.52	47.4**	16570**	0.7	2.16
PW352-26-4-4-Q2A-GFR-W	7.67	175.8	41.04	14.32	44.2	20436	0.72	2.29
PW352-5-1-10-Q1B-GRYLD-P	7.34	160.2	39.26	13.63	42.07	20509	0.7	2.18
PW352-5-1-13-Q1B-GRYLD-W	6.88	152.9	36.77	13.92	41.63	19443	0.68	2.23
PW352-5-1-16-Q1B-GRYLD-W	7.71	213.3	41.25	17.11**	33.3	33683**	0.76	2.74*
PW468-10-1-17-Q2A-NDVI-W	7.54	165.9	40.32	13.75	43.07	20645	0.82	2.2
PW468-10-1-2-Q2A-NDVI-P	8.03	168.1	42.93	13.05	44	21464	0.67	2.09
PW468-10-1-21-Q2A-NDVI-P	7.36	166.3	39.36	14.13	41.77	20735	0.46	2.26
PW468-10-1-5-Q2A-NDVI-W	7.86	171.4	42.03	13.66	41.73	22155	0.45	2.19
PW468-77-3-10-Q7B-AGDM-W	6.13**	129.6	32.8**	13.23	46.07	15686**	0.84	2.12
PW468-77-3-11-Q7B-AGDM-W	4.79**	109.8	25.63**	14.20	48.93	11625**	0.62	2.27
PW468-77-3-14-Q7B-AGDM-W	7.1	151	37.96	13.28	47.13*	17758**	0.58	2.13
PW468-77-3-16-Q7B-AGDM-P	8.07	178.5	43.14	13.82	47.17*	20132	0.65	2.21
PW468-77-3-19-Q7B-AGDM-W	7.73	164.7	41.31	13.34	44.87	20243	0.62	2.13
PW468-77-3-20-Q7B-AGDM-P	5.82	127.6	31.1**	13.64	50.87**	13478**	0.66	2.18
PW468-77-3-9-Q7B-AGDM-P	7.89	181.2	42.18	14.30	49.53**	18770	0.76	2.29
PW468-84-4-1-Q5A-COMGRWT-W	7.09	165.7	37.9	14.60	41.9	21321	0.68	2.34
PW468-84-4-12-Q5A-COMGRWT-P	7.71	172.9	41.22	13.97	46.17*	19640	0.85	2.24
PW468-84-4-4-Q5A-COMGRWT-P	6.08	155.7	32.53**	15.68	42.63	16773**	0.55	2.51
PW729-55-3-1-Q6B-AGDM-W	7.87	174.9	42.07	13.85	44.4	20891	0.64	2.22
PW729-55-3-13-Q6B-AGDM-P	7.07	148.5	37.81	13.15	43.6	19088	0.72	2.1
PW729-55-3-15-Q6B-AGDM-P	7.58	172	40.55	14.17	44.67	19969	0.55	2.27
PW729-55-3-21-Q6B-AGDM-W	7.79	166.8	41.68	13.38	42.77	21443	0.9	2.14
PW729-55-3-6-Q6B-AGDM-P	7.67	158.3	41	12.91	44.3	20375	0.81	2.07

PW729-55-3-8-Q6B-AGDM-P	8.04	177.5	42.98	13.80	42.67	22164	0.75	2.21
Robigus	8.95	178.4	47.88	12.47	37.6	28120	0.44	1.99
SEL56	8.49	182	45.39	13.38	43.2*	23153	0.64	2.14
SEL57	8.76	178.7	46.85	12.76	39.3	26251	0.52	2.04
SEL58	8.71	191.3	46.59	13.72	48.97*	20924**	0.45	2.19
SEL63	7.95	167.6	42.5**	13.17	44.43*	21054**	0.84*	2.11
SEL64	8.27	173.8	44.24	13.13	44.77*	21737**	0.68	2.1
SEL65	8.8	194.1	47.08	13.77	43.23*	23929	0.8*	2.2
SEL69	8.66	186.3	46.34	13.44	40.27	25311	0.48	2.15
<b>Mean</b>	<b>7.55</b>	<b>166.29</b>	<b>40.37</b>	<b>13.76</b>	<b>43.54</b>	<b>20535.6</b>	<b>0.68</b>	<b>2.20</b>
<b>LSD (Genotype) (5%)</b>	<b>0.80</b>	<b>27.84</b>	<b>4.26</b>	<b>1.58</b>	<b>4.49</b>	<b>5543.3</b>	<b>0.35</b>	<b>0.25</b>
<b>P value</b>	<b>&lt;0.001</b>	<b>0.041</b>	<b>&lt;0.001</b>	<b>0.676</b>	<b>&lt;0.001</b>	<b>0.051</b>	<b>0.628</b>	<b>0.676</b>

\*Significance at the 5% ( $P = 0.05$ ) level. \*\*1% ( $P = 0.01$ ) level. \*\*\*0.1% ( $P = 0.001$ )

The NILs showing values higher than Paragon for PxW lines and Robigus for SHW lines have been marked with \* according to the degree of significance.

**Table 3.8:** Genetic variation in harvest and NUE related traits: GY (Grain Yield at 100% DM t ha<sup>-1</sup>), TGW (Thousand grain Weight), NUE (Nitrogen-Use Efficiency kg Grain DM kg<sup>-1</sup> N), Straw N uptake (kg AGN kg<sup>-1</sup> N) at Sutton Bonington, Nottingham in 2019 in 66 near-isogenic line and synthetic-derived wheat lines with Paragon and Robigus parents

Trait	Minimum	Maximum	Mean	LSD (Genotype) (5%)	P value
GY (t ha <sup>-1</sup> )	4.79	8.95	7.55	0.80	<0.001
Grain N UP kg N ha <sup>-1</sup> )	109.8	213.3	166.29	27.84	0.041
NUE (kg G DM N kg N <sup>-1</sup> )	25.63	47.88	40.37	4.26	<0.001
GPC (%)	12.47	17.11	13.76	1.58	0.676
TGW (g)	33.3	50.87	43.55	4.49	<0.001
Grain Number (m <sup>-2</sup> )	11625	33683	20536	5543	0.051
Straw N%	0.44	1.08	0.68	0.35	0.628
Grain N%	1.99	2.74	2.20	0.25	0.676

### 3.3.2.2 Genetic variation in photosynthesis traits

Photosynthetic traits including light-saturated flag-leaf photosynthesis rate ( $A_{max}$ ) and stomatal conductance at GS61 and at GS61+10d, flag-leaf SPAD at anthesis were measured across 19 NILs and synthetic-derived wheat lines (Table 3.9 and 3.10). For flag-leaf photosynthesis rate at GS61, the mean across these genotypes was 24.1  $\mu\text{mol m}^{-2} \text{s}^{-1}$  ( $P < 0.001$ ). While the two synthetic lines (SEL 58 and SEL 63) showed photosynthesis rate of 19.14 and 25.06  $\mu\text{mol m}^{-2} \text{s}^{-1}$ , respectively, and Robigus demonstrated a value of 24.74  $\mu\text{mol m}^{-2} \text{s}^{-1}$ . The NILs ranged between 21.12-27.45  $\mu\text{mol m}^{-2} \text{s}^{-1}$  and the photosynthetic rate of Paragon was observed as 21.31  $\mu\text{mol m}^{-2} \text{s}^{-1}$  (Table 3.10).

The flag-leaf photosynthetic rate at GS61+10d had a mean value of 24.52  $\mu\text{mol m}^{-2} \text{s}^{-1}$  ( $P = 0.002$ ) (Table 3.9). The NILs ranged between 16.76-29.96  $\mu\text{mol m}^{-2} \text{s}^{-1}$  and Paragon was 28.47  $\mu\text{mol m}^{-2} \text{s}^{-1}$ . In the two synthetic lines, the photosynthetic rate at GS61+10d was 26.21 and 28  $\mu\text{mol m}^{-2} \text{s}^{-1}$  while Robigus was 25.55  $\mu\text{mol m}^{-2} \text{s}^{-1}$  (Table 3.10).

The stomatal conductance at GS61 showed a mean value of 0.26  $\text{mol m}^{-2} \text{s}^{-1}$  ( $P < 0.001$ ) (Table 3.9). The NILs ranged between 0.12-0.42  $\text{mol m}^{-2} \text{s}^{-1}$  and Paragon showed stomatal conductance of 0.381  $\text{mol m}^{-2} \text{s}^{-1}$ . The two synthetic lines did not show much genetic variation (0.3309 and 0.3145) with Robigus (0.3077) (Table 3.10).

For stomatal conductance at GS61+10d, the mean was observed as 0.36 ( $P = 0.069$ ) (Table 3.9). The 19 lines did not demonstrate much genetic variation. While the synthetic lines showed

stomatal conductance of 0.2142 and 0.37, Robigus was found to be around 0.36. The NILs ranged between 0.316-0.4217 and Paragon was seen to be 0.3201 (Table 3.10).

The flag-leaf SPAD analysis for chlorophyll content at GS61 showed a mean value of 54.18 ( $P < 0.001$ ) (Table 3.9). The highest SPAD was observed in the NIL PW292-9-5-6-Q4B-GFPTT-W of 57.18. The two synthetic lines showed SPAD of 51.8 and 56.4 with Robigus at 55.7. The NILs ranged from 51.7-57.17 and Paragon was at 54.12 (Table 3.10).

Overall, photosynthesis rate at GS61, stomatal conductance at GS61 and SPAD at GS61 demonstrated significant genetic variation with P value at  $< 0.001$  (Table 3.9).

**Table 3.9:** Genetic variation in photosynthesis flag-leaf traits: Photosynthesis Rate at GS61 and GS61+10D, Stomal Conductance at GS61 and GS61+10D, SPAD (Chlorophyll Content) at GS61 at Sutton Bonington in 2019 in 15 P × W near-isogenic lines, two synthetic-derived lines and Paragon and Robigus parents

Traits	Mean	Minimum	Maximum	P Value
Photosynthesis Rate at GS61 $\mu\text{mol m}^{-2} \text{s}^{-1}$	24.14	19.14	27.45	$< 0.001$
Photosynthesis Rate at GS61+10d $\mu\text{mol m}^{-2} \text{s}^{-1}$	24.52	16.76	29.96	0.002
Stomatal Conductance at GS61 $\text{mol m}^{-2} \text{s}^{-1}$	0.26	0.12	0.42	$< 0.001$
Stomatal Conductance at GS61+10d $\text{mol m}^{-2} \text{s}^{-1}$	0.36	0.21	0.42	0.069
SPAD (Chlorophyll Content) at GS61	54.18	51.7	57.17	$< 0.001$



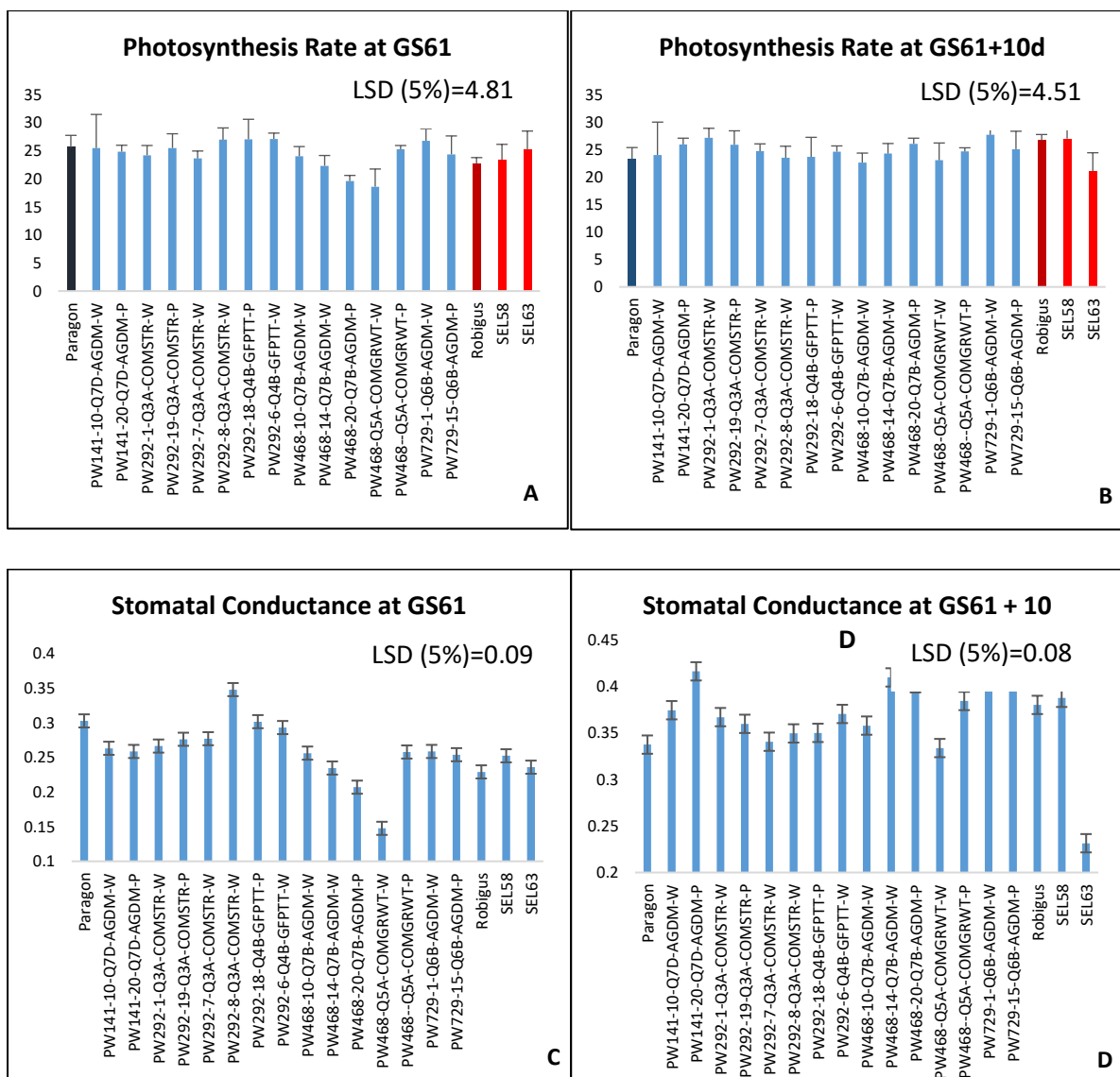


**Fig 3.8** Bar chart of flag-leaf photosynthesis rate at (A) GS61 and (B) GS61+10d and stomatal conductance at (C) GS61 and (D) GS61+10d of 15 P × W near-isogenic lines, two synthetic derived lines and Paragon and Robigus parents. Black colour bar corresponds to Paragon, dark red colour to Robigus, synthetic lines with red colour and light blue colour bars represent P × W near-isogenic lines. The error bars represent the standard deviation of the mean value.

The flag-leaf  $A_{max}$  of GS61 demonstrated genetic variation between NILs with the Watkins and Paragon allele. The Paragon allele demonstrated higher  $A_{max}$  for QTLs for AGDM on chr 7B, COMGRWT on chr 5A and COMSTR QTL on chr 3A compared to the Watkins allele. While both SEL58 and SEL63 showed high  $A_{max}$  compared to Robigus. In case of stomatal conductance, the Watkins allele showed higher  $A_{max}$  compared to the Paragon allele for QTLs for AGDM, COMSTR, GFPTT and COMGRWT QTL (Fig 3.8)

### 3.3.2.3 Association between photosynthesis traits and grain yield

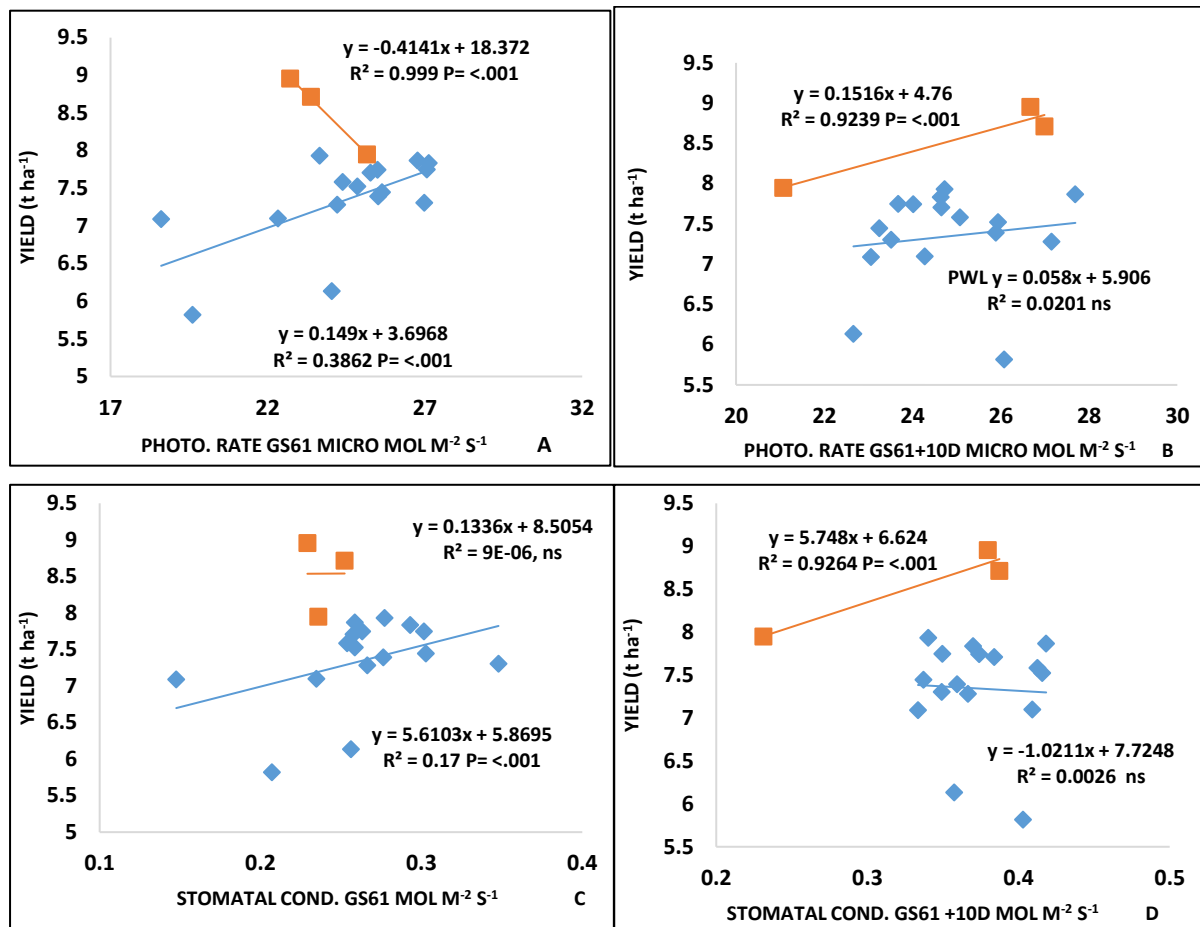


**Fig 3.9:** Linear regression of Grain Yield GY (t ha<sup>-1</sup>) on (A) Photosynthesis Rate at GS61 and (B)GS61+10D, (C) Grain Yield GY (t ha<sup>-1</sup>) vs Stomal Conductance at GS61 (D) GS61+10D. Orange colour data points represent data of synthetic-derived hexaploid wheat lines and Robigus and blue colour points represent near-isogenic lines developed by crossing Paragon and Watkins landraces and Paragon.

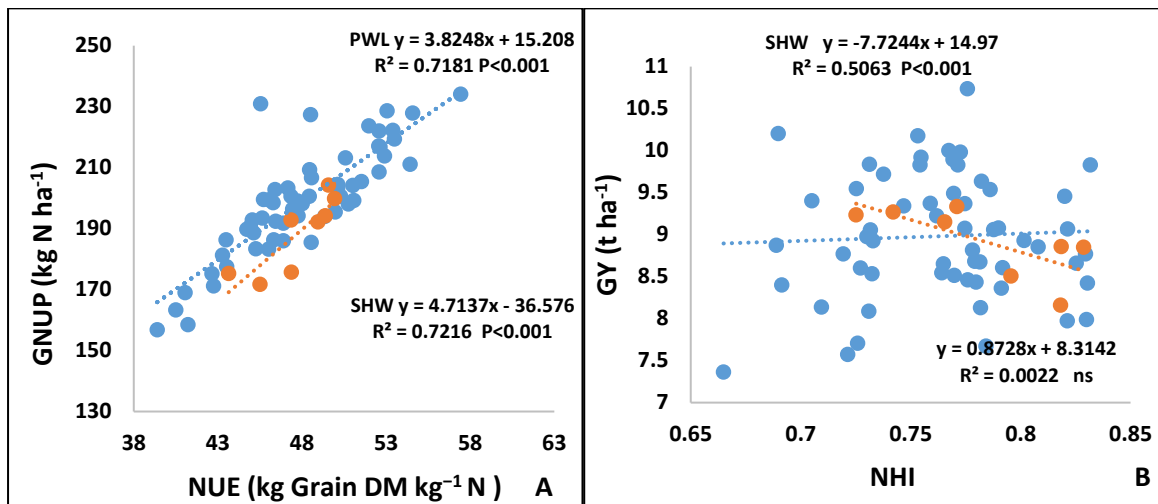
A positive correlation was observed in the P × W lines between each of photosynthesis rate and stomatal conductance at GS61 and grain yield,  $R^2 = 0.39$  and  $0.17$ , respectively ( $P < 0.001$ , Fig. 3.9). These linear association, however, were not significant at GS61+10d.

**Table 3.10:** Genetic variation in photosynthesis traits flag-leaf photosynthesis rate at GS61 and GS61+10d, stomatal conductance at GS61 and GS61+10D, SPAD (Chlorophyll Content) at Sutton Bonington in 15 P × W near-isogenic lines, two synthetic derived lines with Paragon and Robigus parents

NILs	Photosynthesis Rate at GS61	Photosynthesis Rate at GS61+10D	Stomatal Conductance at GS61	Stomatal Conductance at GS61+10D	SPAD (Chlorophyll Content)
DFW SEL 58	25.06	26.21	0.33	0.37	51.8**
DFW SEL 63	19.14	28	0.31	0.21**	56.4*
Paragon	21.31	28.47	0.38	0.32	54.12
PW141-58-7-10-Q7D-AGDM-W	25.39	22.64*	0.18*	0.38	52.73
PW141-58-7-20-Q7D-AGDM-P	24.01	27.69	0.34	0.40	54.6
PW292-22-9-1-Q3A-COMSTR-W	25.22	27.05	0.34	0.35	56.07
PW292-22-9-19-Q3A-COMSTR-P	27.26*	22.65	0.19**	0.36	55.67
PW292-22-9-7-Q3A-COMSTR-W	26.1	20.8*	0.19**	0.35	51.7**
PW292-22-9-8-Q3A-COMSTR-W	21.59	29.83	0.43**	0.33	55.3
PW292-9-5-18-Q4B-GFPTT-P	25.05	24.21	0.22*	0.36	53.3
PW292-9-5-6-Q4B-GFPTT-W	22.71	29.96	0.37**	0.35	55.3
PW468-77-3-10-Q7B-AGDM-W	24.03	21.19*	0.17**	0.36	57.17**
PW468-77-3-14-Q7B-AGDM-W	22.35	25.17	0.31*	0.39	52.43
PW468-77-3-20-Q7B-AGDM-P	27.45*	16.76**	0.12***	0.41*	54.4
PW468-84-4-1-Q5A-COMGRWT-W	21.12	21.45*	0.22*	0.31	54.23
PW468-84-4-12-Q5A-COMGRWT-P	26.03	22.42*	0.17**	0.39	51.8
PW729-55-3-1-Q6B-AGDM-W	25.75	29.6	0.33	0.40	53.33
PW729-55-3-15-Q6B-AGDM-P	26.45*	21.52*	0.17**	0.42**	53.97
Robigus	24.74	25.55	0.30	0.36	55.7
<b>LSD (5%)</b>	<b>4.81</b>	<b>4.51</b>	<b>0.09</b>	<b>0.08</b>	<b>1.97</b>
<b>Mean</b>	<b>24.14</b>	<b>24.52</b>	<b>0.26</b>	<b>0.36</b>	<b>54.18</b>
<b>P Value</b>	<b>&lt;0.001</b>	<b>0.002</b>	<b>&lt;0.001</b>	<b>0.069</b>	<b>&lt;0.001</b>

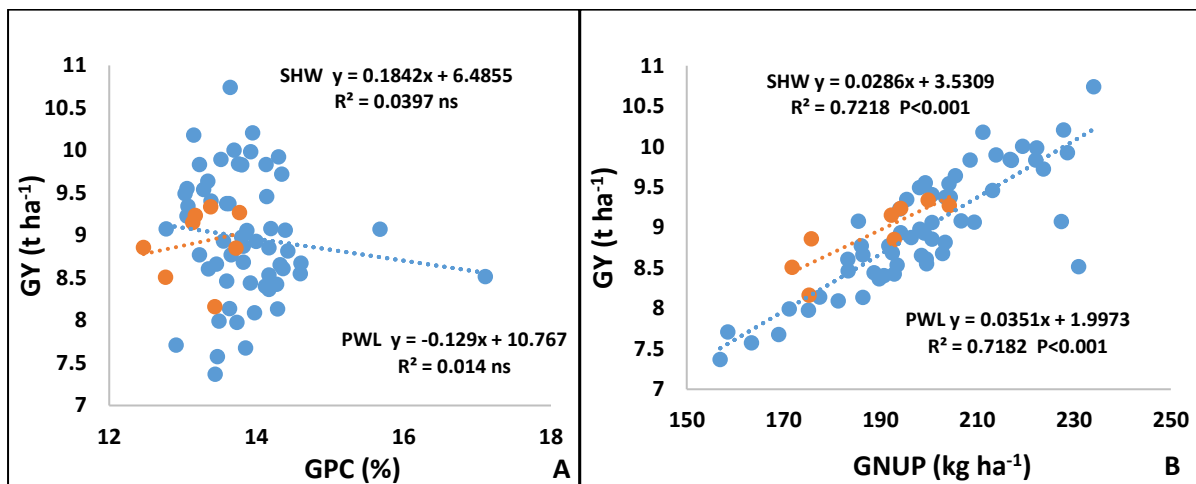
\*Significance at the 5% ( $P = 0.05$ ) level. \*\*1% ( $P = 0.01$ ) level. \*\*\*0.1% ( $P = 0.001$ ) The NILs showing values higher than Paragon for PxW lines and Robigus for SHW lines have been marked with \* according to the degree of significance.

### 3.3.2.4 Association between yield and NUE and its components



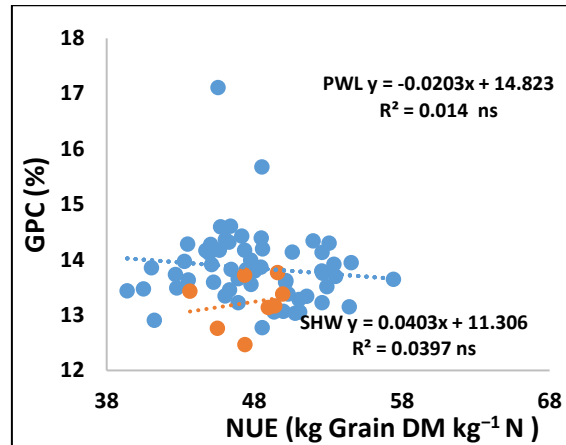
**Fig 3.10:** Linear regression of (A) Grain N Uptake (GNUP ( kg N ha<sup>-1</sup>), on NUE (kg Grain DM kg<sup>-1</sup> N) and (B) Grain Yield GY (t ha<sup>-1</sup>) on NHI. Orange colour data points represents data of synthetic hexaploid wheat lines and Blue colour points represents near-isogenic lines developed by crossing Paragon and Watkins landraces.

A strong positive correlation was observed between GNUP and NUE in P × W NILs ( $R^2=0.7216$ ) and synthetic-derived lines ( $R^2=0.7181$ ). Further, a negative linear relationship was seen between NHI and GY in synthetic-derived lines ( $R^2=0.50$ ; Fig 3.10).



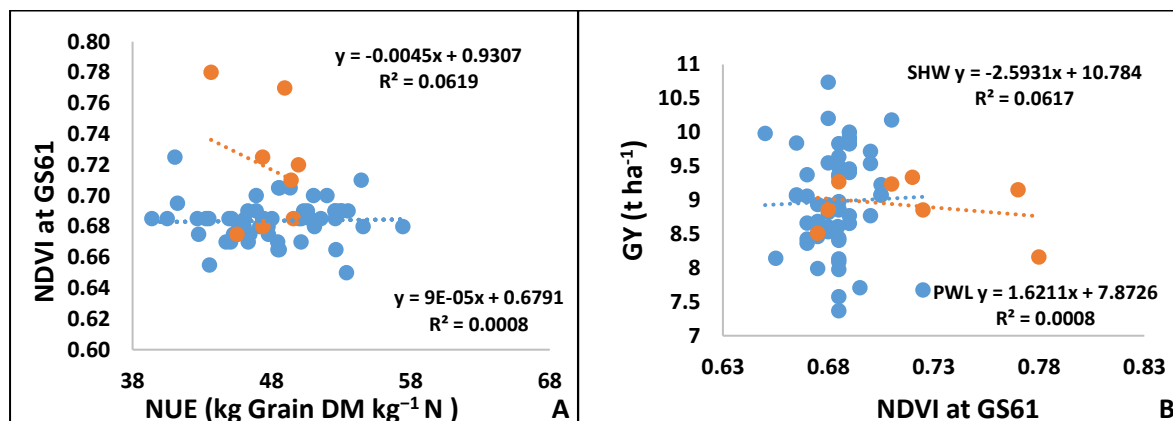
**Fig 3.11:** Linear regression of (A) Grain Yield GY (t ha<sup>-1</sup>) on Grain Protein Content (GPC) and (B) Grain Yield GY (t ha<sup>-1</sup>) on Grain N Uptake (GNUP ( kg AGN kg<sup>-1</sup> N). Orange colour data points represents data of synthetic hexaploid wheat lines and Blue colour points represents P × W near-isogenic lines developed by crossing Paragon and Watkins landraces.

For GPC and GY, no association was seen among the NILs ( $R^2= 0.014$ ) as well as the synthetic lines ( $R^2= 0.039$ ). However, there was a positive linear association between GNUP and GY for the synthetic lines  $R^2$  at 0.721 and NILs at  $R^2$  at 0.718 (Fig 3.11).



**Fig 3.12:** Linear regression of Grain Protein Content (GPC) on NUE (kg Grain DM  $\text{kg}^{-1}$  N). Orange colour data points represents data of synthetic-derived heaxaploid wheat lines and Robigus and Blue colour points represents P  $\times$  W near-isogenic lines developed by crossing Paragon and Watkins landraces and Paragon.

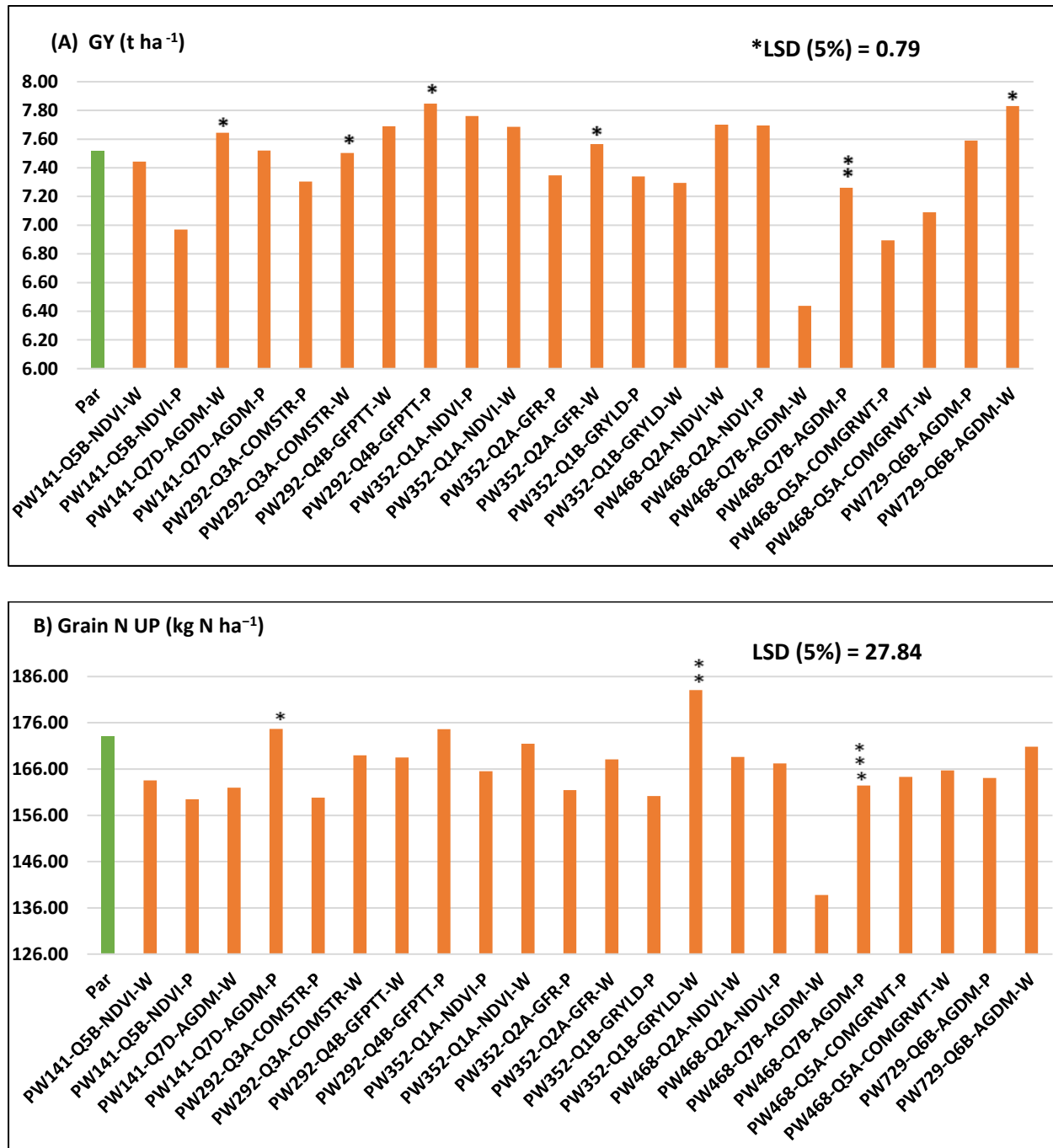
GPC was also found not to be associated with NUE in the synthetic derived lines ( $R^2=0.014$ ) and NILs ( $R^2=0.039$ ; Fig. 3.12). However, a strong positive association was seen between GNUP and NUE in synthetic-derived lines ( $R^2=0.718$ ) as well as NILs ( $R^2=0.721$ ) (Fig 3.12).



**Fig 3.13:** Linear regression of (A) NDVI at GS61 Anthesis on NUE (kg Grain DM  $\text{kg}^{-1}$  N) and (B) Grain Yield GY ( $\text{t ha}^{-1}$ ) on NDVI at GS61 anthesis. Orange colour data points represents data of synthetic-derived heaxaploid wheat lines and Robigus and blue colour points represents P  $\times$  W near-isogenic lines developed by crossing Paragon and Watkins landraces and Paragon.

In the case of NDVI at GS61 versus NUE and yield, the linear regressions were not statistically significant (Fig. 3.13).

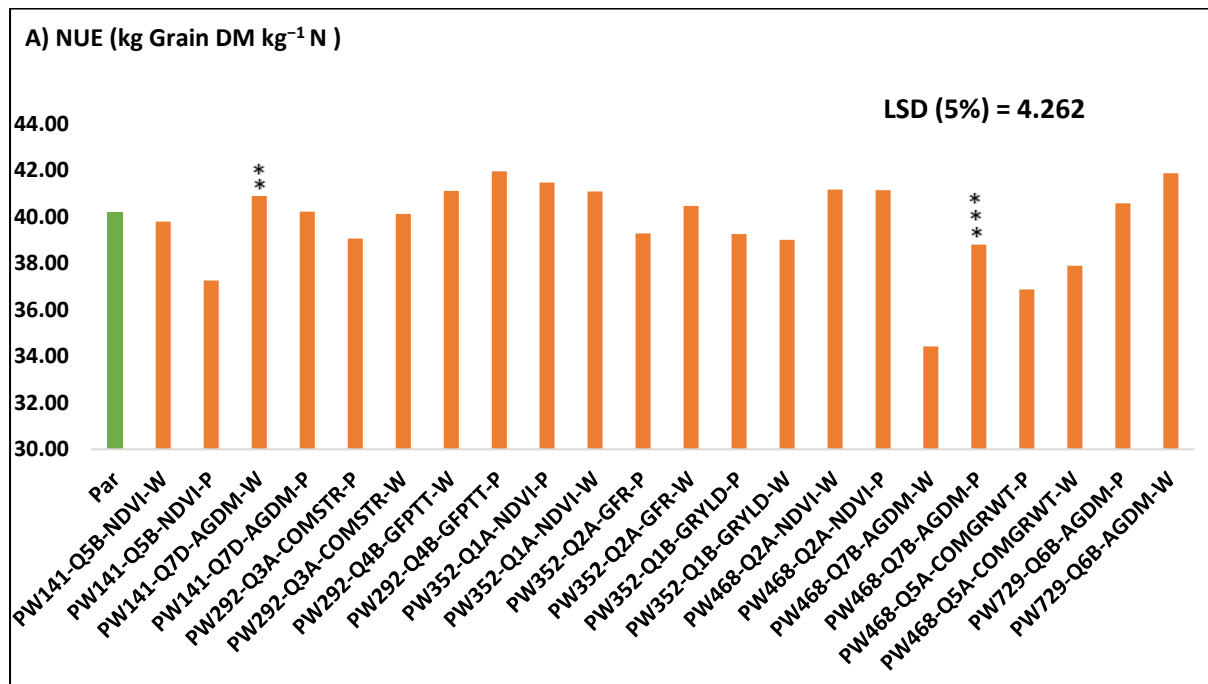
### 3.3.2.5 Allelic variation among Paragon × Watkin NILs

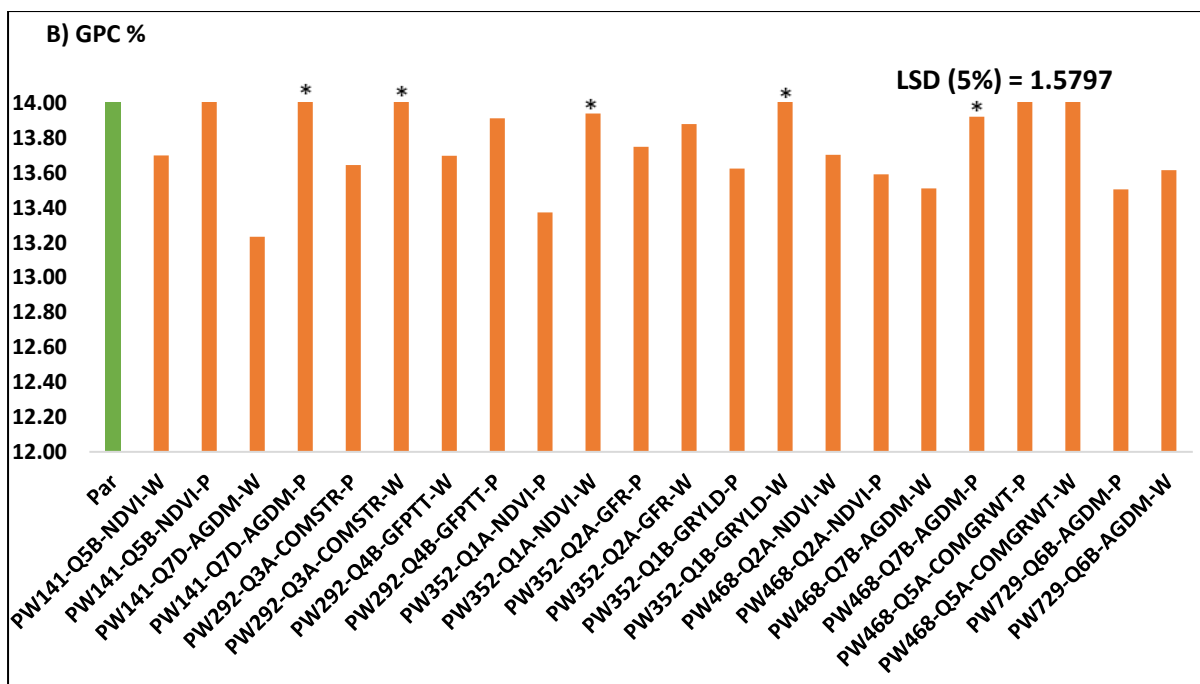


**Fig 3.14:** Bar graph represents (A) Grain Yield GY (t ha<sup>-1</sup>) (B) Grain N Uptake (GNUP ( kg N ha<sup>-1</sup>) of QTL allelic groupings for Paragon × Watkins landraces and parent Paragon. Orange colour represents QTL allelic groupings, whereas green colour bar corresponds to Paragon cultivar. \* represents significant difference for Watkins versus Paragon allele (P < 0.05), \*\* 1% (P = 0.01) level and \*\*\* 0.1% (P = 0.001)

In the present study, variation was observed between the Paragon and Watkins alleles for QTLs in the NILs. In case of GY, the QTL for GY on chr 1B, demonstrated a higher value in the Watkins allele compared to the Paragon allele and compared to Paragon. While the QTL for AGDM on 7B showed a higher value in Paragon allele compared to the Watkins allele. In addition, the QTL for AGDM on 7D showed a higher value in the Paragon allele than the Watkins allele (Fig 3.14).

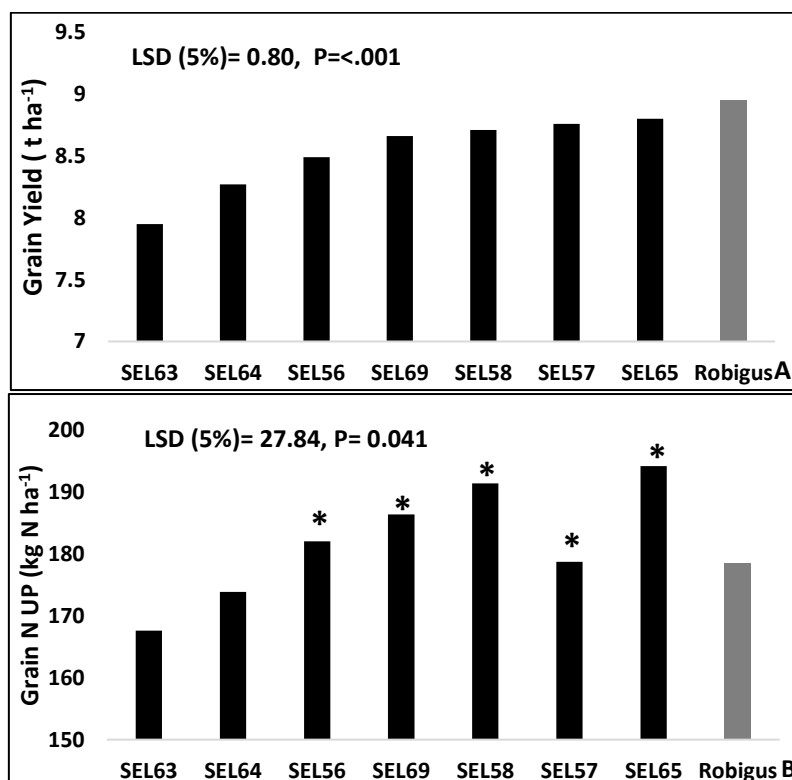
For NUE similar effects as for grain yield were observed. Further, for GPC, QTLs for COMSTRW on Chr 3A and NDVI on chr 1A and GRYLD on chr 1B showed higher values for the Watkins allele compared to the Paragon allele (Fig. 3.15). On the other hand, the QTL for AGDM on chr 7B demonstrated a significantly higher value for the Paragon compared to the Watkins allele.





**Fig 3.15:** Bar graph represents (A) NUE (kg Grain DM kg<sup>-1</sup> N) (B) Grain Protein Content (GPC) of allelic groups for Watkins landraces × elite cultivar Paragon crosses near-isogenic lines and parent Paragon. Orange colour represents near-isogenic lines with Watkins allele in the QTL and Paragon allele, whereas green colour bar corresponds to Paragon cultivar. \* represents significant difference for Watkins versus Paragon allele (P < 0.05), \*\*1% (P = 0.01) level and \*\*\*0.1% (P = 0.001)

### 3.3.2.6 Genetic variation among synthetic lines





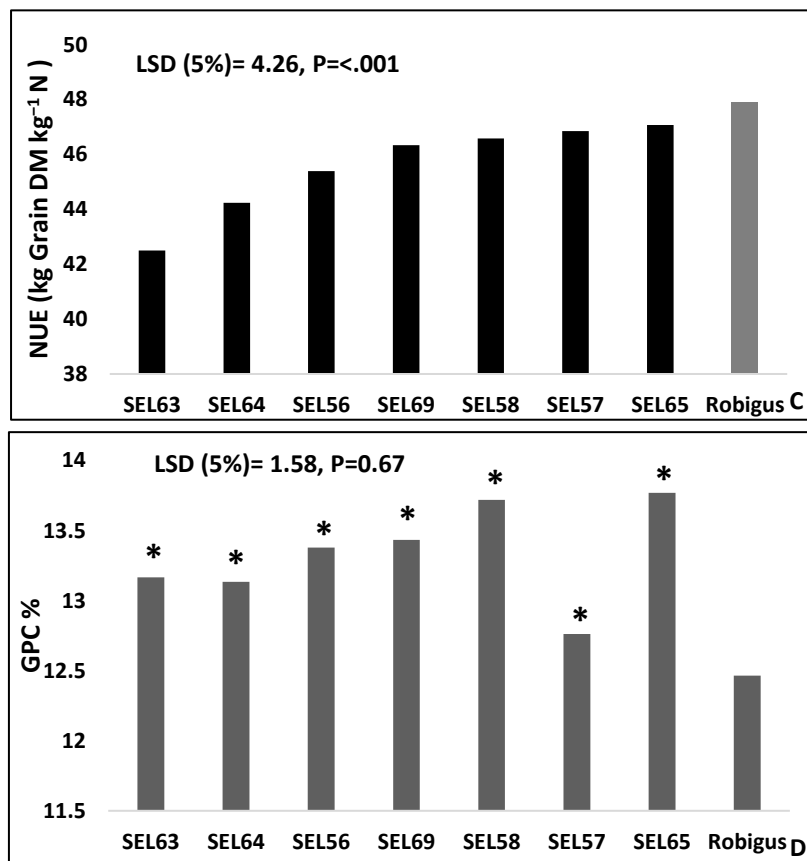


**Fig 3.16:** Bar graph represents genetic variation among synthetic lines for (A) Grain Yield GY (t ha<sup>-1</sup>), (B) Grain N UP (kg N ha<sup>-1</sup>), (C) NUE (kg Grain DM kg<sup>-1</sup> N) and (D) Grain Protein Content (GPC).

Significant genetic variation was observed among the synthetic-derived lines for GY, GNUP, NUE and GPC traits. None of the SHW derived lines showed high GY as compared to Robigus. However, genetic variation was observed between the SHW derived lines (P<0.001) (Fig 3.16 A). In the case of GNUP, SEL58 and SEL65 demonstrated a trend for higher grain N uptake than Robigus (P=0.041) (Fig 3.16 B).

The SHW derived lines did not show higher NUE compared to Robigus, although significant variation was seen within the lines (P<0.001) (Fig 3.16 C). Finally, none of the SHW derived lines showed significantly higher GPC compared to Robigus (; Fig 3.16 D).

Among the synthetic-derived lines, SEL65 and SEL58 exhibited a trend for higher GY, GNUP, NUE and GPC compared to the other synthetic derived lines.

The GNUP trait was found to show the most novel variation among all the NUE traits in the SHW derived lines compared to Robigus.

### **3.3.3 Effect of site on performance of NILs**

Among the 64 NILs studied across the two sites, as expected a statistically significant site effect was seen for GY, NUE, GPC, straw N %, GNUP, and TGW (Table 3.11). For GY overall the SB site had a higher value of 8.39 t ha<sup>-1</sup> compared to the RR at 7.83 t ha<sup>-1</sup>. A similar trend was seen in NUE where SB overall had a higher value (47.88 kg Grain DM kg<sup>-1</sup> N ) than RR (22.17 kg Grain DM kg<sup>-1</sup> N ) (LSD=6.10) (Fig 3.17).

On the other hand, for NHI the NILs at RR (0.80) did not differ significantly compared to NILs at SB (0.76) (LSD=0.066). Further, for GPC NILs at the RR site show greater mean value of 14.39 % compared to SB site at 13.80 (LSD=1.16) (Fig 3.17).

This data demonstrates the variation seen between the two sites which can be due to the varying soil type as well as differences in soil mineral N and supplied N. The Site X Genotype interaction was not found significant for any of the traits like GY, NUE, Grain N%, Straw N%, GPC but TGW (P<0.001).

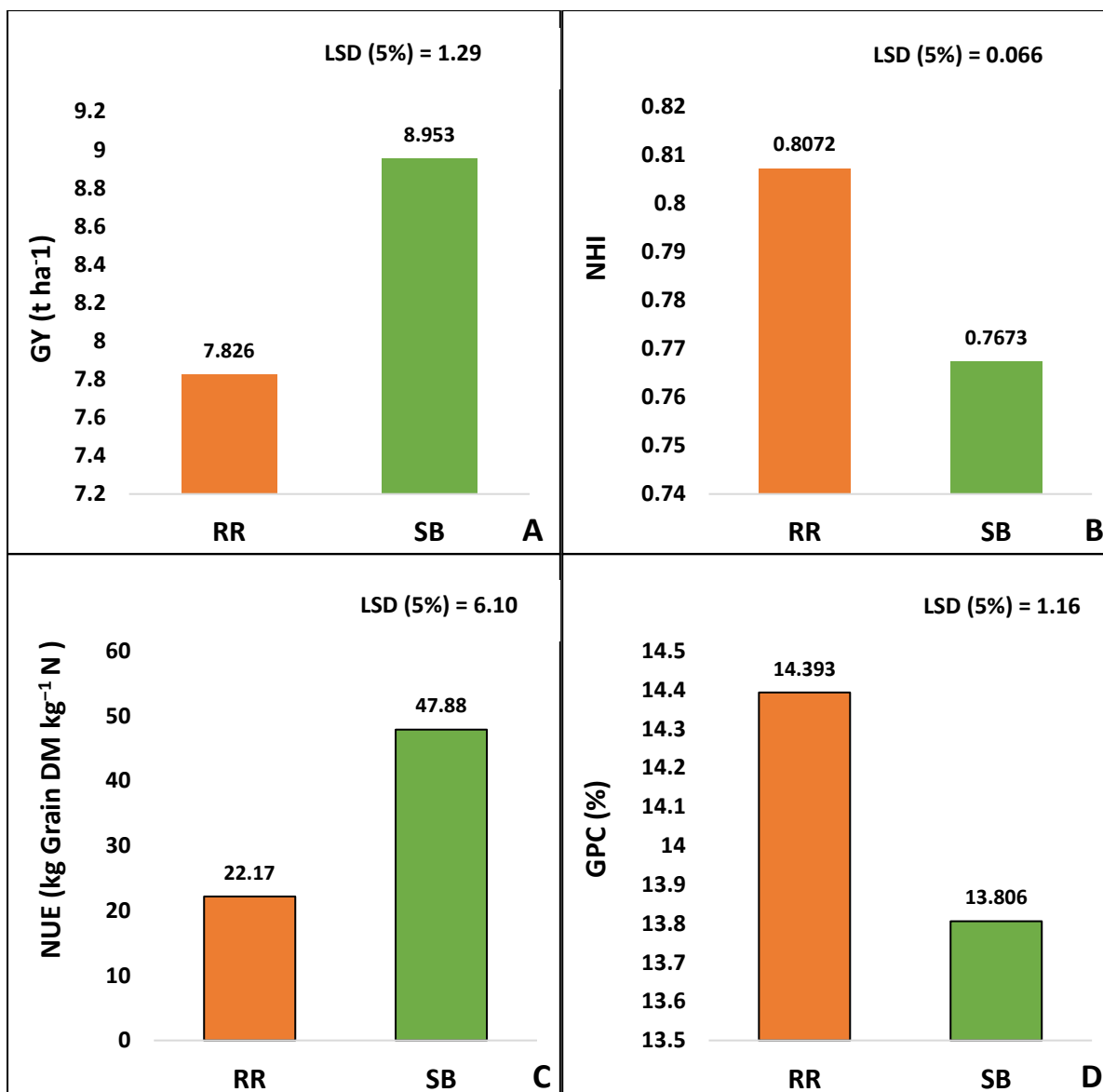


**Fig 3.17:** Effect of two experiment sites i.e., Rothamsted Research (RR) and Sutton Bonington (SB) on performance of 66 NILs. The LSD represents the interaction of site X NILs. Orange and Green colour represents individual values of (A) GY (t ha<sup>-1</sup>) (B) NHI (C) NUE (kg Grain DM kg<sup>-1</sup> N ) and (D) GPC at RR and SB site respectively.

**Table 3.11:** Site variation variation of 64 NILs and Paragon and Robigus in GY (Grain Yield t ha<sup>-1</sup>), Grain N%, Straw N%, Grain N UP (kg ha<sup>-1</sup>), TGW (Thousand grain Weight), NHI (Nitrogen Harvest Index), NUE (Nitrogen-Use Efficiency kg Grain DM kg<sup>-1</sup> N) and GPC (Grain Protein Content) from the cross-site ANOVA at the two experiment sites i.e., Rothamsted Research (RR) and Sutton Bonington (SB).

Trait	RR	SB	Mean	P value
GY (t ha <sup>-1</sup> )	7.826	8.953	8.389	0.005
Grain N%	2.303	2.209	2.256	0.060
Straw N%	0.488	0.691	0.589	0.001
Grain N UP (kg ha <sup>-1</sup> )	179.9	197.7	188.8	0.166
TGW g	36.95	43.47	40.21	0.002
NHI	0.8072	0.7673	0.7873	0.004
NUE	22.17	47.88	35.03	0.002
GPC %	14.393	13.806	14.100	0.060

### 3.4 Discussion

The Watkins NILs derived from landrace cultivars of *Triticum aestivum* L. demonstrate a high level of genetic diversity as compared to adapted winter wheat varieties. The modern adapted varieties exhibit lower genetic diversity in comparison to landraces consisting of a total of 826 accessions, the Watkins collection gives a snippet of the genetic diversity which existed prior to domestication and modern wheat breeding. With the changing climatic conditions and the need for sustainable means of enhancing crop yield, it is essential to employ strategies for increasing genetic diversity. This is where the Watkins collection has come into play. For example, the Watkins collection has been employed to identify genes and/or alleles pertaining to disease and pest resistance (Wingen *et al.*, 2014). In the present study this germplasm can be further utilised to identify genes associated with NUE and NUE related traits. Significant genetic variation was observed among the synthetic-derived lines for GY, GNUP, NUE and GPC traits. While distinct genetic variation was observed among the SHW derived lines in NUE and GY, significant variation ( $P < 0.001$ ) was observed in GNUP (LSD 5%=27.84) and GPC (LSD 5%= 1.58)

While there are many NUE related traits, the one trait which is directly linked with NUE is grain yield which in turn is dependent on the amount of N taken up and utilized by the crop. Additionally, the efficiency of N use further effects grain protein content which in turn impacts the grain quality. The present study emphasises on NUE related traits particularly, grain yield, grain protein content, biomass, nitrogen harvest index along with photosynthesis related traits like stomatal conductance and photosynthesis rate post anthesis. A greater part of the

N accumulated prior to anthesis is utilized for grain protein content enhancement. This gives us N remobilisation efficiency (NRE) which is essentially the fraction of N accumulated up to anthesis in the grain at harvest. This accumulation and subsequent remobilisation of N is crucial for grain yield and grain protein content which eventually impacts the quality. It is to be noted that while most of the remobilisation of N is dependent on genetic diversity, it is also greatly impacted by environmental factors like soil N concentrations and climatic conditions. Interestingly, while GPC and grain yield are correlated, there exists a negative association which makes the improvement of both these traits simultaneously difficult. However, choosing cultivars with high grain protein deviation and GPC is an important strategy owing to their direct association and impact on grain quality (Sharma *et al.*, 2023).

A more specific overview of the traits associated underlying NUE and their genetic variation across the two sites is given below.

#### **3.4.1 Evidence for genetic variation in grain yield and NUE**

At Rothamsted Research (RR), 17 and 15 PxW lines demonstrated higher GY and NUE than Paragon, respectively. At Sutton Bonington (SB) site, 28 and 32 PxW lines showed higher GY and NUE, respectively. These were found to be NILs related to NDVI, AGDM, COMSTR, GFPTT, GFR, GRYLD and COMGRWT. However, none of the NILs were significantly higher than Paragon although one line at RR (PW468-84-4-1-Q5A-COMGRWT-W); and two lines at SB (PW352-26-4-14-Q2A-GFR-W and PW292-9-5-7-Q4B-GFPTT-P) approached statistical significance. This is likely due to the presence of many unadapted genes in the NILs compared to Paragon.

From the allelic perspective, at SB site the Watkins allele showed increased GY and NUE compared to Paragon allele for the NDVI QTLs on 5B and 1A, for the AGDM QTLs on 7D, 6B and 7B, for the COMSTR QTL on 3A, for the GFPTT QTL on 4B, for the GFR QTL on 2A, and for the GRYLD QTL on 1B. On the other hand, the Paragon allele showed increased GY and NUE compared to Watkins for the NDVI QTL on 2A. At the RR site, Paragon allele showed increased GY and NUE for the AGDM QTL on 7D. While the Watkins allele demonstrated higher GY and NUE for the NDVI QTL on 1A, the GFR QTL on 2A, the GRYLD QTL on 1B and the COMGRWT QTL on 5A.

At RR site, among the synthetic-derived (SD) lines, most of the lines (SEL 0058, SEL 0063, SEL 0064, SEL 0065 and SEL 0069) showed higher GY and NUE than the parent Robigus. However, at SB none of these lines demonstrated significance as compared to Robigus. Nonetheless, variations were observed within the lines. The synthetic-derived line SEL63 exhibits significantly lower GY and NUE compared to Robigus.

These lines showing evidence for novel allelic variation for GY and NUE were therefore highlighted for further investigation in the field experiments in 2020 and 2021 (see Chapter 4).

#### **3.4.2. Evidence for genetic variation in N-uptake efficiency**

At the RR site, the N-uptake efficiency (NUpE) was seen to be higher in 14 PxW lines as compared to Paragon. However, the variation among these lines compared to Paragon was not statistically significant. Among these lines, the Watkins allele showed increased NUpE as compared to Paragon allele for the NDVI QTL on 5B, the COMSTRW QTL on 3A, the GFR QTL on 2A, the GRYLD QTL on 1B, the AGDM QTL on 7B and the COMGRWT QTL on 5A. On the other hand, the Paragon allele demonstrated higher NUpE than Watkin for AGDM QTL on 6B and, NDVI QTL on 2A and 1A.

Among the synthetic-derived lines, the lines (SEL 0058, SEL 0063, SEL 0064, SEL 0065 and SEL 0069) showed significantly higher NUpE than Robigus. All these five lines were also statistically significant in association with GY and NUE at RR site, implying their importance.

For SB site, above-ground N uptake was not estimated but for grain N uptake one line (PW352-5-1-16-Q1B-GRYLD) was significantly higher than Paragon. Three alleles showed significantly higher Grain N uptake compared to their contrasting allele: the Paragon allele for AGDM on 7D, the Watkins allele for grain yield on chr 1B and the Paragon allele for AGDM on chr 7B. These lines showing evidence for novel allelic variation for N uptake were therefore highlighted for further investigation in the field experiments in 2020 and 2021 (see Chapter 4).

#### **3.4.3 Evidence for genetic variation in N utilisation efficiency (NUtE)**

At the RR site, 15 PxW lines showed increased NUtE compared to the parent Paragon; however, none was significantly higher than Paragon. Within these lines, the Paragon allele

demonstrated higher NUtE as compared to Watkins for the AGDM QTL on 7D. While the Watkins allele showed increased NUtE compared to Paragon for the NDVI QTL on 2A and 1A, the GFR QTL on 2A, and the GFPTT QTL on 4B.

SHW derived lines did not differ significantly in NUtE compared to Robigus. However, significant variation was observed within the lines and SEL64 showed lowered NUtE compared to Robigus.

Plants accumulate N in the leaves and stems in the pre-anthesis stage after which it is distributed to the grains. This N remobilisation to the grain continues during senescence causing reduced photosynthetic activity and grain yield but high GPC (Hawkesford, 2017a). When ample N is available in soil, N uptake continues during grain filling as well (Desai and Bhatia, 1978).. In most of the NILS with a Watkins allele showing increased NUtE, the GPC content is observed to be lower than the parent Paragon. Therefore, lower GPC may be a desirable trait for higher NUtE and NUE. This may be feasible in feed varieties but could cause issues with the requirement for GPC of ca. 13% in bread-making varieties for bread-making quality. Linear regression demonstrated the negative association between GPC and GY as well in the P × W NILs.

Before grain filling, N is used for canopy establishment. During grain filling, any extra N taken up is redirected to the grain, however, most of the grain N is obtained from redistribution after canopy establishment. These processes determine the N harvest index (NHI) which is largely independent of N fertiliser supply and dependent on environmental factors (Barraclough *et al.*, 2010). To achieve improved NHI and NUtE, grain % N, therefore, is an important parameter. A simultaneous increase in all of these three parameters is a practically difficult feat to achieve (Hawkesford, 2012). Genetic variation for NHI in wheat has been observed (Desai and Bhatia, 1978) and is associated with efficient utilisation of N (Fageria, 2014). Due to this, NHI variation is genotype dependent and is associated with genotypes with high GY. In wheat, the amount of N present post-anthesis is extremely high and typically forms 75-85% of total N. High NHI is thereby also associated with high NUtE. In our study, the Watkins alleles showing high NUtE also generally demonstrated significantly higher NHI compared to the Paragon allele further confirming the correlation between NHI and NUtE.

#### 3.4.4 Associations between leaf photosynthesis traits and NUE

The association between leaf photosynthetic rate and grain yield has been established in wheat in recent decades (Gaju *et al.*, 2016) and therefore efforts are being taken to improve leaf photosynthesis rate which is essential for increase in yield potential in wheat. Studies have demonstrated that synthetic-derived lines show higher GY and biomass under LN conditions as compared to Paragon (Gaju *et al.*, 2016) Landraces and synthetic-derived lines are known to possess a higher adaptation to stress and genetic variation compared to modern bread wheat varieties (Nehe *et al.*, 2022).

In the present study also, synthetic-derived lines as well as NILs derived from Watkins and Paragon lines exhibited genetic variation in flag-leaf leaf photosynthesis rate which was positively related with grain yield and NUE. This paves the way for identifying specific genes and alleles associated with leaf photosynthesis rate traits to improve NUE.

Among the 15 PxW NILs, higher flag-leaf photosynthesis rate ( $A_{\max}$ ) at GS61 was observed in 9 lines as well as significant genetic variation within the PxW lines, but again there was not significant variation above the Paragon parent. However, the Paragon allele showed increased photosynthesis rate for the AGDM QTLs on 6B and 7B, the GFPTT QTL on 4B, and the COMSTR on 3A compared to Watkins allele. Moreover, the Watkins allele showed high  $A_{\max}$  compared to the Paragon for the AGDM QTL on 7D. The SD line SEL58 showed high  $A_{\max}$  compared to Robigus among the two SHW derived lines analysed.

Further, for stomatal conductance at GS61 the Watkins allele showed higher stomatal conductance compared to the Paragon allele for the AGDM QTLs on 6B and 7B, the GFPTT QTL on 4B and the COMSTR QTL on 3A.

The genetic variation observed in flag-leaf  $A_{\max}$  and stomatal conductance was positively correlated at GS61 with grain yield in both PxW NILs which signifies the scope of  $A_{\max}$  and stomatal conductance in UK wheat breeding programs. Similar results were obtained in a previous study by Gaju *et al.* (2016) wherein positive correlation was found between flag-leaf  $A_{\max}$  and GY among 15 genotypes (5 modern cultivars, 5 landraces and 5 SD wheat genotypes). Therefore, leaf photosynthesis rate is an important target trait for breeders. Plant breeding over the years has led to significant improvement in flag-leaf  $A_{\max}$  and continuous efforts are required to improve pre-anthesis flag-leaf  $A_{\max}$  which is a crucial governing factor of grain



number per unit area and GY. Leaf chlorophyll content assessed using a SPAD meter has been used as a parameter to assess leaf N content in wheat and may be related to leaf photosynthesis rate and grain yield (Xiong *et al.*, 2015; Gaju *et al.*, 2016). While SPAD readings are greatly influenced by N fertiliser application, genetic variation in the parameter has been shown to be directly associated with grain yield (Islam *et al.*, 2021). Additionally, leaf chlorophyll SPAD readings are known to be affected by environmental conditions including heat and drought causing genotypic variation along with variation in GY (Barutçular *et al.*, 2016). The Watkins allele for COMSTR QTL on 3A demonstrated high  $A_{max}$  and stomatal conductance at GS61 along with a high SPAD reading compared to the Paragon parent. Previous studies have shown that, the association between SPAD and GY is stronger during grain filling compared to previous stages. Thus, another perspective which can be explored for leaf chlorophyll content is the relation between cultivar-specific SPAD and  $A_{max}$  and GY for a more accurate analysis of N (Monostori *et al.*, 2016).

Evidently, there is much variation observed in the NILs. Previous studies have demonstrated that landraces have relatively low GY and NHI which makes higher NUE according to standard definitions challenging. The ultimate target for wheat breeders is to combine high yield and protein content. This can be achieved by emphasising on NUE at high N and ensuring optimum uptake of this high N in the grains (NHI) as well (Hawkesford and Griffiths, 2019). The wide repository available to breeders in the form of modern and the more diverse germplasm pools, e.g., the Watkins landrace collection, will allow for the identification of significant NUE-related alleles. Screening of these materials in multiple, contrasting locations using appropriate screening strategies and crop phenotyping indices such as NDVI, and leaf SPAD etc. will facilitate future exploitation of these resources.

### **3.5 Summary**

The variation in the GY, NHI, Grain N UP and GPC were used as the main basis for the NILs selection for the further experiments (see Chapters 4 and 5). Individually, several NILs having Watkins alleles for QTLs for traits like yield, above-ground DM and grain-fill period thermal time showed higher values as compared to Paragon; however, QTL performance contributing to photosynthesis traits like flag-leaf  $A_{max}$  and  $g_s$  were also considered for the selection as they directly influence biomass, GY and NUE. Therefore, the following 20 genotypes were

shortlisted after evaluating performance at both experimental sites for furthermore detailed experiments under high and low N treatments.

Shortlisted NILs for field experiments at Rothamsted Research (RR) site under varying N conditions in 2020 – 2021.

**Table 3.12** : 5 Shortlisted NILs for further experiments under varying N conditions

<b>NILs</b>	<b>Background</b>
Paragon	parental control
PW141-58-7-10-Q7D-AGDM-W	P X W Line
PW141-58-7-20-Q7D-AGDM-P	P X W Line
PW292-22-9-19-Q3A-COMSTR-P	P X W Line
PW292-22-9-1-Q3A-COMSTR-W	P X W Line
PW292-22-9-7-Q3A-COMSTR-W	P X W Line
PW292-22-9-8-Q3A-COMSTR-W	P X W Line
PW292-9-5-18-Q4B-GFPTT-P	P X W Line
PW292-9-5-6-Q4B-GFPTT-W	P X W Line
PW468-77-3-10-Q7B-AGDM-W	P X W Line
PW468-77-3-10-Q7B-AGDM-W	P X W Line
PW468-77-3-14-Q7B-AGDM-W	P X W Line
PW468-77-3-20-Q7B-AGDM-P	P X W Line
PW468-84-4-12-Q5A-COMGRWT-P	P X W Line
PW468-84-4-1-Q5A-COMGRWT-W	P X W Line
PW729-55-3-15-Q6B-AGDM-P	P X W Line
PW729-55-3-1-Q6B-AGDM-W	P X W Line
Robigus	parental control
SEL58	Synthetic Hexaploid
SEL63	Synthetic Hexaploid

## **Chapter 4**

***Genetic variation for NUE and associated traits in landraces and synthetic hexaploid wheat under high and low nitrogen conditions***

#### 4.1 Introduction

The global demand for cereals is estimated to double by the year 2050 which places the producers under severe pressure. Wheat being one of the primary cereals consumed globally, also expects enhanced production (Semenov *et al.*, 2007). The current wheat production market is uncertain due to changes in trade policies, rising international prices, the ongoing Ukraine war as well as reduced production in major wheat producing countries like Ukraine, Australia, and India. The global wheat production is predicted to decline in 2022 by 0.8 percent which gives approximately 771 million tonnes (Collier, 2022). It is therefore crucial to enhance wheat production and yield to meet the growing demand globally. The production of wheat is greatly influenced by nitrogen (N) of which nitrate is the common form found in the cell vacuole of the plant. The nitrogen use efficiency (NUE) is the ability of the plant for N uptake and change into the economic form. High content of N, however, can be detrimental for the environment as well as cause economic loss. While optimum application of N fertilisers can enhance the NUE, thousand-grain weight and protein content of the plant; their extensive use can cause lodging stress and subsequently economic losses (Ghafoor *et al.*, 2021). Enhancing NUE ensures increased production and yield of crop, reduced fertiliser costs and possibility of nitrate leaching into the soil, and limits greenhouse gas emission.

Wheat was domesticated over 10,000 years ago (Shewry 2009) and the current wheat genome has been derived from cross between tetraploid, *Triticum dicoccoides* and wild diploid, *Aegilops tauschii* (Salamini *et al.*, 2002). The process of domestication of wheat landraces, over the years, has led to the reduction in genetic diversity as compared to wild ancestors. This might have also caused loss in valuable traits relating to NUE in the germplasms. This brings in the requirement of examining a wide range of germplasms for selection of NUE and related traits like, nitrogen uptake efficiency (NUpE), nitrogen utilisation efficiency (NUtE), nitrogen harvest index (NHI), grain protein deviation (GPD) and grain protein content (GPC) (Hawkesford, 2017a). The Watkins collection established by A.E. Watkins consists of wheat germplasm of over 7000 accessions of which 826 bread wheat landrace cultivars remain today. This collection showcases the genetic diversity present before modern breeding and domestication events. The Watkins collection contains nine ancestral geographical groupings which possibly led to exchange of genetic material between these groups and consequently led to immense genetic diversity (Wingen *et al.*, 2014). The wild cultivars of wheat have been

found to have higher leaf photosynthetic rate as compared to the modern elite cultivars implying towards the reduction in this important NUE trait. Additionally, synthetic hexaploid wheat (SHW), derived from *Triticum durum* and *Aegilops tauschii*, has been found to also demonstrate enhanced levels of leaf photosynthetic rate and grain yield (Del Blanco *et al.*, 2000; Ogbonnaya *et al.*, 2003). Therefore, studying wheat landraces and synthetically-derived lines of wheat can help in identifying bread wheat cultivars with important traits of NUE such as plant biomass, photosynthetic capacity, grain yield (GY) under varying N conditions (Gaju *et al.*, 2011). Genetic variation studies carried out in hexaploid wheat panel consisting of landrace cultivars, SHW and modern elite cultivars for physiological traits like Normalised Difference Vegetative Index (NDVI), SPAD, leaf senescence, can also prove to be invaluable in determining important cultivars (Nehe *et al.*, 2022).

Among the 66 NILs analysed in the previous chapter (chapter 3), 19 NILs were selected for further studies. These 19 NILs included 15 near isogenic lines (NILs) developed by crosses between Watkins's wheat landraces and the elite cultivar, Paragon (PxW lines), two synthetic hexaploid wheat (SHW) lines, with parents Robigus and Paragon. These NILs were subjected to high N (HN) and low N (LN) conditions of concentration 200 kg AGN kg<sup>-1</sup> N and 50 kg AGN kg<sup>-1</sup> N respectively, at Rothamsted Research (RRes) experimental fields, UK. The two-year consecutive field trials of these 19 near isogenic lines under HN and LN conditions is carried out to validate their performance for NUE and related traits. The traits we have primarily emphasised on are above-ground dry matter (AGDM), grain N uptake (GNUP), nitrogen utilisation efficiency (NUtE), N uptake efficiency (NUpE), nitrogen harvest index (NHI), thousand grain weight (TGW), grain yield (GY) and Normalised Difference Vegetative Index (NDVI). Apart from this, the association studies between these traits, under varying N conditions, over 2 years has also been carried out. These two years field trials data will be primarily used to shortlist the NILs for further experimentation like RNAseq based transcriptomics studies to identify candidate gene markers for breeding for NUE and related traits.

## **4.2 Material and Methods**

### **4.2.1 Field experiments on selected sub-set (17 NILs, Paragon and Robigus) at Rothamsted in 2020 and 2021**

#### **4.2.1.2 Experimental site and design**

Based on the two- experiments from 2018-19 (results described in Chapter 3), 19 genotypes were selected for further field experiments at the Rothamsted site, Hertfordshire (51° 48' 19.79" N 0° 21' 11.39" E) during 2020 and 2021. The field experiment used a randomised block design with plot size of 4.15 x 1.8 m and three replicates of each genotype. There were two N treatments, N1 (50 kg ha<sup>-1</sup>) and N2 (200 kg ha<sup>-1</sup>), applied as ammonium nitrate prills. The soil type at field experiment site was silty clay loam (Fig 2.4). The seed rate was 350 seeds per m<sup>2</sup>. Herbicides, fungicides and pesticides were applied as necessary to minimised effects of weeds, diseases and pests. The two experiments were spring-sown crops, sown in the second half of March in each year. The experiments in 2021 and 2020 were on sown on 3<sup>rd</sup> March 2021 and 24<sup>th</sup> February 2020.

#### **4.2.1.2 Crop measurements**

Growth stages were assessed visually once per week and twice per week during anthesis period by using the Zadoks wheat growth scale (Zadoks *et al.*, 1974). At GS20, plant establishment count was recorded in a 1m x 1 m quadrat. The key growth stages of GS31, GS41, GS51, GS55, GS65, GS71, GS83 and GS91 were recorded when 50% of the visible shoots in a plot were observed to be at the relevant stage. At GS94 stage, samples of 100 fertile shoots (those with an ear) per plot were collected for post-harvest analysis by cutting at ground level. Ears were separated from straw and the dry weight recorded after drying for 48 h at 80°C. The ears were then threshed, the grain collected, and the dry weight recorded after drying for 48 h at 80°C. Similarly straw dry matters were recorded after drying for 48 h at 80°C. These grain and straw fresh and dry weights were used to calculate grain yield, NUpE, NUtE and NUE.

#### **4.2.2 Physiological maturity and harvest analysis**

The plant height was measured from ground level to the tip of ear using a ruler at five random positions per plot in the field. The visual flag-leaf senescence score was recorded every 3-4

days from GS71 to GS93. The lodging scoring of all the lines was also done pre-harvest. At GS94 stage, samples of 100 fertile shoots per plot were collected for analysis. Total N from harvested grain and stem samples were estimated by NIRS (Near Infrared Spectroscopy Method) and using ASD FieldSpec 4 Hi-Res NG spectrometer, Analytik Ltd, UK to calculate N-Use Efficiency (NUE), N-Uptake Efficiency (NUpE) and N Utilisation Efficiency (NUE). Total N estimated values were used to calculate the NUE, NUpE, NUE, and GPC.

#### **4.2.3 Statistical Analysis**

Analysis of variance for all the traits and harvest components were performed by using Genstat 22 (VSN International, United Kingdom) for a randomised split-plot design considering genotype and N as fixed effects and replicates as a random effect. For the combined cross-year analysis an ANOVA model was used considering genotype and N as fixed effects and year and replicate as random effects.

### 4.3 Results

A total of 19 genotypes were selected for the study including 15 PxW lines, 2 synthetic hexaploid wheat-derived lines, with the Robigus and Paragon parental lines (Table 4.1). The genotypes were subjected to 2 N treatments, high N (HN) and low N (LN) with N concentrations of 50 kg ha<sup>-1</sup> N in LN and 200 kg ha<sup>-1</sup> N in HN conditions. The two field sites in RRes had a silty clay loam soil type. In 2020, the soil mineral was estimated at 42.27 N kg ha<sup>-1</sup> N and in the year 2021, the soil mineral was recorded as 88 N kg ha<sup>-1</sup> N (Table 4.2). The weather data for parameters like temperature, Relative Humidity, Precipitation (Rain), and Solar Radiation data was recorded (Table 4.3) throughout the two trials.

**Table 4.1:** List of Near Isogenic Lines (NILs) in field trials 2020 and 2021

Sr No	Accession Name	Germplasm type
1	PW468-77-3-10-Q7B-AGDM-W	Paragon X Watkins Landrace crossed NIL
2	PW141-58-7-10-Q7D-AGDM-W	Paragon X Watkins Landrace crossed NIL
3	PW141-58-7-20-Q7D-AGDM-P	Paragon X Watkins Landrace crossed NIL
4	PW292-22-9-19-Q3A-COMSTR-P	Paragon X Watkins Landrace crossed NIL
5	PW292-22-9-1-Q3A-COMSTR-W	Paragon X Watkins Landrace crossed NIL
6	PW292-22-9-7-Q3A-COMSTR-W	Paragon X Watkins Landrace crossed NIL
7	PW292-22-9-8-Q3A-COMSTR-W	Paragon X Watkins Landrace crossed NIL
8	PW292-9-5-18-Q4B-GFPTT-P	Paragon X Watkins Landrace crossed NIL
9	PW292-9-5-6-Q4B-GFPTT-W	Paragon X Watkins Landrace crossed NIL
10	PW468-77-3-14-Q7B-AGDM-W	Paragon X Watkins Landrace crossed NIL
11	PW468-77-3-20-Q7B-AGDM-P	Paragon X Watkins Landrace crossed NIL
12	PW468-84-4-12-Q5A-COMGRWT-P	Paragon X Watkins Landrace crossed NIL
13	PW468-84-4-1-Q5A-COMGRWT-W	Paragon X Watkins Landrace crossed NIL
14	PW729-55-3-15-Q6B-AGDM-P	Paragon X Watkins Landrace crossed NIL
15	PW729-55-3-1-Q6B-AGDM-W	Paragon X Watkins Landrace crossed NIL
16	Robigus	Parental Control
17	Paragon	Parental Control
18	SEL58	Hexaploid Synthetic wheat Derivatives
19	SEL63	Hexaploid Synthetic wheat Derivatives

**Table 4.2:** N fertiliser application and soil available N from soil at Rothamsted Research, Harpenden, year 2020 and 2021

Parameter	2020	2021
N Fertiliser kg ha <sup>-1</sup>	50 and 200	50 and 200
Soil type	Silty clay loam	Silty clay loam
Soil Mineral N kg ha <sup>-1</sup>	42.27	88



**Table 4.3:** Weather data Temperature (Min) °C, Temperature (Max)°C, Rain (mm), Relative Humidity (%), Solar Radiation (J cm<sup>-2</sup>) at Rothamsted Research, site, year 2020 and 2021

<b>2020 Month</b>	<b>Temperature (Mean Max) °C</b>	<b>Temperature (Mean Min) °C</b>	<b>Rain (mm)</b>	<b>Solar Radiation (J cm<sup>-2</sup>)</b>	<b>Relative Humidity (%)</b>
March	10.33	2.73	1.41	878.54	77.72
April	16.01	4.74	1.71	1666.15	68.93
May	18.29	6.98	0.10	2244.08	60.66
June	20.02	10.95	2.91	1690.43	69.58
July	21.24	11.90	2.62	1635.78	69.21
August	22.42	13.84	5.55	1255.71	77.01
September	19.12	9.32	1.09	1174.10	77.11
<b>2021 Month</b>	<b>Temperature (Mean Max) °C</b>	<b>Temperature (Mean Min) °C</b>	<b>Rain (mm)</b>	<b>Solar Radiation (J cm<sup>-2</sup>)</b>	<b>Relative Humidity (%)</b>
March	10.68	3.47	0.89	843.55	83.61
April	11.56	1.14	0.05	1602.82	66.53
May	14.74	6.21	3.05	1505.31	78.52
June	20.29	11.82	2.59	1726.05	79.17
July	22.28	13.35	1.65	1731.26	79.42
August	20.47	11.68	1.51	1478.02	80.82

#### 4.3.1 Effects on NUE and related traits

The NUE, NU<sub>p</sub>E and NU<sub>t</sub>E of the 15 PxW lines, 2 synthetic-derived hexaploid wheat (SHW) lines along with parent lines, Paragon and Robigus have been analysed for two trials under high N (HN) and low N (LN).

##### 4.3.1.1 NUE 2020-21

In the 2020 experiment, the NUE was observed to be greater across all the PxW lines in LN conditions, ranging from 40.72-52.06 kg Grain DM kg<sup>-1</sup> N, as compared to the HN condition (12.68- 18.87 kg Grain DM kg<sup>-1</sup> N) with Paragon having an NUE of 52.27 kg Grain DM kg<sup>-1</sup> N (Table 4.3). Similarly, in the synthetic-derived hexaploid wheat lines, the NUE was higher under LN conditions (48.17 and 51.6 kg Grain DM kg<sup>-1</sup> N) than HN conditions (16.8 and 16.97 kg Grain DM kg<sup>-1</sup> N). In the parent Robigus, the NUE was higher than the SHW lines under LN condition (55.11 kg Grain DM kg<sup>-1</sup> N). The mean NUE observed under HN conditions was 15.39 kg Grain DM kg<sup>-1</sup> N while that of LN was 47.83 kg Grain DM kg<sup>-1</sup> N (Table 4.4)

However, in the 2021 experiment, while a similar trend was observed with NUE showing higher values under LN conditions, the NUE was significantly lower than in 2020. This can be

due to varying SMN at both the field sites. Also, while in the 2020 trials the difference between the NUE under HN and LN conditions was high, the difference between the treatments in 2021 was much less. Nevertheless, the NUE for PxW lines under LN ranged between 9.74-13.59 kg Grain DM kg<sup>-1</sup> N compared to Paragon at 12.85 kg Grain DM kg<sup>-1</sup> N. Further, the NUE of the SHW-derived lines under LN was 10.95 and 15.71 kg Grain DM kg<sup>-1</sup> N and that of Robigus was 13.59 kg Grain DM kg<sup>-1</sup> N. Under HN conditions, the NUE of the PxW lines ranged between 6.79-9.55 kg Grain DM kg<sup>-1</sup> N and that of the SHW-derived lines was 5.59 and 9.75 kg Grain DM kg<sup>-1</sup> N (Table 4.4). The mean observed for NUE under LN and HN conditions was 12.11 and 7.54 kg Grain DM kg<sup>-1</sup> N which is lower than the previous year.

The cross-year analysis demonstrated an average of 30.01 kg Grain DM kg<sup>-1</sup> N under LN conditions and that of 11.49 kg Grain DM kg<sup>-1</sup> N under HN conditions. The NUE ranged from 26.09- 34.35 under LN conditions across the NILs while under HN conditions it ranged between 9.74-13.59 kg Grain DM kg<sup>-1</sup> N which was evidently low implying towards the significant influence of N across the NILs (Table 4.4).

Significant N treatment (N) and year effect (Y) were observed across all the genotypes (P value <0.001. Additionally, because of this, the interaction between N and Y (N\*Y) was also observed to be highly significant with P value <0.001 (Table 4.4). The main effect for genotype was significant (P=0.08), but the N × G and the year × N × G interactions were not statistically significant

#### **4.3.1.2 N-uptake efficiency in 2020 and 2021**

The NUpE saw a similar trend as that of NUE with higher values under LN conditions than in HN conditions as well as relatively lower values in 2021 as compared to 2020.

In 2020, the NUpE observed for the PxW lines demonstrated a range of 1.09-1.65 kg Grain DM kg<sup>-1</sup> N under LN conditions compared to Paragon with 1.43 kg AGN kg<sup>-1</sup> N. The NUpE under HN conditions ranged between 0.34-0.57 kg AGN kg<sup>-1</sup> N with Paragon having an NUpE of 0.38 kg AGN kg<sup>-1</sup> N. In the case of the SHW-derived lines under HN, the NUpE was 0.51 and 0.42 kg AGN kg<sup>-1</sup> N and was comparable to Robigus at 0.50 kg AGN kg<sup>-1</sup> N. Further, under LN conditions, the NUpE was significantly higher than the HN counterparts with NUpE of 1.35 and 1.78 kg AGN kg<sup>-1</sup> N, respectively, and that of parent Robigus was 1.42 kg AGN kg<sup>-1</sup> N

(Table 4.4). The mean observed for the 2020 experiment of NUpE under LN and HN was 1.43 and 0.45 kg AGN kg<sup>-1</sup> N, respectively (Table 4.4).

In 2021, the NUpE was higher under LN conditions than the HN conditions for all the genotypes. Similar to the NUE effect, the NUpE for 2021 was notably lower than for 2020. In the PxW lines, the NUpE ranged between 0.24-0.33 kg AGN kg<sup>-1</sup> N and that of Paragon was 0.30 kg AGN kg<sup>-1</sup> N under LN conditions. Under HN conditions, the NUpE ranged between 0.19-0.29 kg AGN kg<sup>-1</sup> N which is comparable with LN but slightly lower. Further, in case of the SHW-derived lines, the NUpE was 0.34 and 0.25 kg AGN kg<sup>-1</sup> N under LN conditions and that under HN was 0.28 and 0.16 kg AGN kg<sup>-1</sup> N, respectively. For the parent line Robigus, NUpE was 0.31 and 0.22 kg N kgN<sup>-1</sup> under LN and HN conditions, respectively (Table 4.4). The mean observed for 2021 under LN and HN was 0.28 and 0.21 kg AGN kg<sup>-1</sup> N, respectively (Table 4.4).

The cross-year analysis demonstrated that the mean of NUpE for all the NILs under LN conditions was 0.86 kg AGN kg<sup>-1</sup> N and that under HN was 0.33 kg AGN kg<sup>-1</sup> N. Additionally, the NUpE ranged among genotypes between 0.27-0.42 kg AGN kg<sup>-1</sup> N under HN and 0.69-1.01 kg AGN kg<sup>-1</sup> N under LN circumstances showing the variation in N-uptake efficiency although the genotype effect was not statistically significant (Table 4.4).

The effect of N and Y was clearly seen across all the genotypes demonstrating high significance (P=0.001 for N and <0.001 for Y). The interaction between N and Y also showed significance at P=0.002 (Table 4.4).

#### **4.3.1.3 N-utilisation efficiency in 2020 and 2021**

In the case of NUtE, a contrasting trend was observed in both the experiments under varying N conditions. In the 2020, the NUtE was lower in all the genotypes under LN conditions compared to the HN conditions except for the lines, SEL58, PW729-1-Q6B-AGDM-W, PW468-20-Q7B-AGDM-P, PW468-1-Q5A-COMGRWT-W, PW468-12-Q5A-COMGRWT-P, PW292-6-Q4B-GFPTT-W, PW292-8-Q3A-COMSTR-W and Robigus. The mean NUtE was similar in LN (34.02 kg DM kg N<sup>-1</sup>) and HN (35.13 kg DM kg N<sup>-1</sup>). The NUtE ranged between 28.18-40.60 kg DM kg N<sup>-1</sup> under LN conditions and under HN conditions between 28.83-42.20 kg DM kg N<sup>-1</sup> (Table 4.4).

In contrast, in 2021, all the genotypes saw increased NUtE under LN conditions compared to the HN conditions. In the PxW lines under LN conditions, NUtE ranged between 42.23-46.68 kg DM kg N<sup>-1</sup> and that of Paragon was 44.25 kg DM kg N<sup>-1</sup>. Under HN conditions, the PxW lines ranged between 35.51-41.03 kg DM kg N<sup>-1</sup>. In case of the two SHW-derived lines, the NUtE under LN was 47.73 and 46.25 kg DM kg N<sup>-1</sup> and under HN was 37.45 and 39.28 kg DM kg N<sup>-1</sup>, respectively. The Robigus parent NUtE was 45.54 kg DM kg N<sup>-1</sup> and 37.30 kg DM kg N<sup>-1</sup> under LN and HN conditions, respectively. (Table 4.4).

The cross-year analysis exhibited an overall higher NUtE under LN conditions except for a few lines (SEL63, PW292-19-Q3A-COMSTR-P and PW468-10-Q7B-AGDM-W). However, the NUtE saw a higher average under LN condition of 39.41 kg DM kg N<sup>-1</sup> as compared to HN condition of 36.97 kg DM kg N<sup>-1</sup>. Additionally, the NUtE ranged between 36.68-42.41 kg DM kg N<sup>-1</sup> under LN and 34.56-41.71 kg DM kg N<sup>-1</sup> under HN conditions (Table 4.4).

However, the effect of N application on NUtE was not significant in contrast to NUE and NUpE. Moreover, no significance was seen for genotype or for the interaction between N and genotype (G) for NUtE (Table 4.4).

**Table 4.4:** N-use efficiency (NUE), N-uptake efficiency (NUpE) and N-utilisation efficiency (NUE) in 15 P X W near-isogenic lines, two synthetic hexaploid-derived wheat lines and Paragon and Robigus lines in 2020, 2021 and mean of two years. N: N treatment, Y: Year, G: Genotype, N\*Y: Nitrogen Treatment X Year, N\*G: Nitrogen X Genotype, Y\*G: Year X Genotype, N\*Y\*G: Nitrogen X Year X Genotype

Genotype	NUE (kg Grain DM kg <sup>-1</sup> N)						NUpE (kg AGN kg <sup>-1</sup> N)						NUE (kg DM kg N <sup>-1</sup> )					
	2020		2021		Mean		2020		2021		Mean		2020		2021		Mean	
	HN	LN	HN	LN	HN	LN	HN	LN	HN	LN	HN	LN	HN	LN	HN	LN	HN	LN
Paragon	15.25	52.27	7.5	12.85	11.37	32.56	0.38	1.43	0.21	0.30	0.30	0.87	40.68	37.54	38.85	44.25	39.76	40.90
PW141-10-Q7D-AGDM-W	14.75	49.69	7.67	12.15	11.21	30.92	0.44	1.65	0.23	0.28	0.33	0.96	35.28	30.04	36.34	46.63	35.81	38.34
PW141-20-Q7D-AGDM-P	14.97	45.69	7.7	13.08	11.34	29.39	0.42	1.32	0.22	0.31	0.32	0.82	36.99	35.39	38.85	44.29	37.92	39.84
PW292-1-Q3A-COMSTR-W	15.7	46.14	7.74	13.04	11.72	29.59	0.46	1.31	0.21	0.32	0.33	0.82	34.48	35.40	40.52	42.42	37.50	38.91
PW292-19-Q3A-COMSTR-P	14.39	49.88	7.39	10.22	10.89	30.05	0.34	1.49	0.20	0.24	0.27	0.87	42.40	34.62	41.03	44.71	41.71	39.67
PW292-7-Q3A-COMSTR-W	18.87	47.05	7.15	12.35	13.01	29.70	0.57	1.47	0.20	0.29	0.39	0.88	33.77	32.63	39.46	44.15	36.61	38.39
PW292-8-Q3A-COMSTR-W	14.25	52.06	6.94	13.37	10.60	32.72	0.45	1.67	0.19	0.30	0.32	0.98	31.91	32.72	38.65	46.68	35.28	39.70
PW292-18-Q4B-GFPTT-P	17.64	46.86	9.55	11.33	13.59	29.09	0.54	1.58	0.29	0.27	0.42	0.92	33.95	29.72	35.51	44.09	34.73	36.91
PW292-6-Q4B-GFPTT-W	16.76	46.92	7.71	10.7	12.23	28.81	0.52	1.25	0.21	0.25	0.37	0.75	33.81	38.00	40.30	44.17	37.06	41.08
PW468-10-Q7B-AGDM-W	14.87	46.65	7.6	13.87	11.23	30.26	0.39	1.65	0.22	0.33	0.30	0.99	37.79	28.18	37.16	45.18	37.47	36.68
PW468-14-Q7B-AGDM-W	12.68	40.72	6.79	11.46	9.74	26.09	0.36	1.18	0.19	0.27	0.27	0.73	37.39	35.11	40.13	43.81	38.76	39.46
PW468-20-Q7B-AGDM-P	13.47	42.92	7.86	12.42	10.67	27.67	0.39	1.09	0.22	0.29	0.31	0.69	34.27	40.60	38.86	44.21	36.57	42.41
PW468-1-Q5A-COMGRWT-W	14.77	47.21	7.24	10.69	11.00	28.95	0.46	1.37	0.20	0.27	0.33	0.82	34.06	36.54	39.34	43.15	36.70	39.85

<b>PW468-12-Q5A-COMGRWT-P</b>	14.46	46.54	7.82	10.6	11.14	28.57	0.47	1.40	0.22	0.25	0.35	0.83	31.09	33.59	38.03	42.23	34.56	37.91
<b>PW729-1-Q6B-AGDM-W</b>	13.25	49.35	7.42	11.43	10.33	30.39	0.46	1.55	0.20	0.25	0.33	0.90	28.83	31.77	40.79	46.58	34.81	39.18
<b>PW729-15-Q6B-AGDM-P</b>	16.34	46.06	7.22	11.74	11.78	28.90	0.52	1.38	0.21	0.28	0.36	0.83	33.68	33.50	38.26	43.33	35.97	38.42
<b>Robigus</b>	17.91	55.11	7.63	13.59	12.77	34.35	0.50	1.42	0.22	0.31	0.36	0.87	36.32	38.95	37.30	45.54	36.81	42.24
<b>SEL58</b>	16.8	48.17	9.75	15.71	13.27	31.94	0.51	1.35	0.28	0.34	0.39	0.85	34.03	36.04	37.45	47.73	35.74	41.88
<b>SEL63</b>	16.97	51.6	5.59	10.95	11.28	31.27	0.42	1.78	0.16	0.25	0.29	1.01	39.56	29.23	39.28	46.25	39.42	37.74
<b>Minimum</b>	<b>12.68</b>	<b>40.72</b>	<b>5.59</b>	<b>10.22</b>	<b>9.74</b>	<b>26.09</b>	<b>0.34</b>	<b>1.09</b>	<b>0.16</b>	<b>0.24</b>	<b>0.27</b>	<b>0.69</b>	<b>28.83</b>	<b>28.18</b>	<b>35.51</b>	<b>42.23</b>	<b>34.56</b>	<b>36.68</b>
<b>Maximum</b>	<b>18.87</b>	<b>55.11</b>	<b>9.75</b>	<b>15.71</b>	<b>13.59</b>	<b>34.35</b>	<b>0.57</b>	<b>1.78</b>	<b>0.29</b>	<b>0.34</b>	<b>0.42</b>	<b>1.01</b>	<b>42.40</b>	<b>40.60</b>	<b>41.03</b>	<b>47.73</b>	<b>41.71</b>	<b>42.41</b>
<b>Mean</b>	<b>15.39</b>	<b>47.83</b>	<b>7.54</b>	<b>12.11</b>	<b>11.49</b>	<b>30.01</b>	<b>0.45</b>	<b>1.43</b>	<b>0.21</b>	<b>0.28</b>	<b>0.33</b>	<b>0.86</b>	<b>35.13</b>	<b>34.02</b>	<b>38.71</b>	<b>44.68</b>	<b>36.97</b>	<b>39.41</b>
			<b>LSD</b>	<b>P value</b>	<b>df</b>						<b>LSD</b>	<b>P value</b>	<b>df</b>			<b>LSD</b>	<b>P value</b>	<b>df</b>
<b>N</b>			3.94 ***	<0.001	4						0.17 ***	0.001	4			14.00 ns	0.66	4
<b>Y</b>			3.69 ***	<0.001	4						0.11 ***	<0.001	4			1.18 ***	<0.001	4
<b>G</b>			2.50 ns	0.08	156						0.10 ns	0.26	156			3.27 ns	0.35	156
<b>N*Y</b>			4.49 ***	<0.001	7.97						0.18 **	0.002	6.88			13.98 ns	0.51	4.06
<b>N*G</b>			4.58 ns	0.52	22.41						0.20 ns	0.28	21.63			13.66 ns	0.73	5.77
<b>Y*G</b>			4.43 ns	0.23	25.81						0.17 ns	0.19	56.94			4.54 ns	0.43	159.40
<b>N*Y*G</b>			6.22 ns	0.86	45.25						0.26 ns	0.37	50.98			13.84 ns	0.33	7.9

*\*Significance at the 5% (P = 0.05) level. \*\*1% (P = 0.01) level. \*\*\*0.1% (P = 0.001) level. LSD, least significance difference (5%); df, degree of freedom; ns, not significant.*

#### **4.3.2 Effects on Grain yield (GY), Above-ground biomass (AGBDM) and Harvest Index (HI)**

##### **4.3.2.1 Grain yield**

In 2020, the mean grain yield was similar under LN conditions (4.41 t ha<sup>-1</sup>) compared to HN conditions (3.73 t ha<sup>-1</sup>). Under LN conditions, GY of the 15 PxW lines ranged from 3.76- 4.80 t ha<sup>-1</sup> and that of Paragon was higher than all the lines 4.82 t ha<sup>-1</sup>. Further, under HN conditions, the GY of the 15 lines ranged between 3.26-4.57 t ha<sup>-1</sup>. Additionally, the two SHW lines showed a GY of 4.44 and 4.76 t ha<sup>-1</sup> under LN which was lower than the of Robigus (5.08 t ha<sup>-1</sup>). Under HN conditions, the GY of the 2 SHW lines was 4.07 and 4.11 t ha<sup>-1</sup> and that of parent Robigus was 4.34 t ha<sup>-1</sup> (Table 4.5).

In the year 2021, the GY under LN conditions was significantly lower for all the 19 genotypes compared to HN. The overall GY under LN conditions was 1.70 t ha<sup>-1</sup> and GY under HN conditions was 2.12 t ha<sup>-1</sup>. In the PxW lines, the GY ranged between 1.43-1.96 t ha<sup>-1</sup> and under HN conditions between 1.92-2.69 t ha<sup>-1</sup>. Paragon under LN and HN conditions was 1.82 and 2.10 t ha<sup>-1</sup> e, respectively. The two SHW-derived lines were 2.18 and 1.52 t ha<sup>-1</sup> under LN, and 2.76 and 1.56 t ha<sup>-1</sup> , respectively, under HN conditions. The GY of Robigus under LN and HN conditions were 1.89 and 2.17 t ha<sup>-1</sup> respectively (Table 4.5).

The cross-year analysis showed no significant effect of N treatment on grain yield with an average of 3.06 t ha<sup>-1</sup> under LN conditions and 2.93 t ha<sup>-1</sup>. The GY ranged between 2.68-3.49 t ha<sup>-1</sup> among the 19 genotypes under LN while under HN, it ranged between 2.50-3.48 t ha<sup>-1</sup>.

In the case of GY, a significant effect on GY was observed for year (p<0.001) and genotype (p=0.02) (Table 4.5); the N x genotype interaction was not significant.

##### **4.3.2.2 Above-ground Biomass (AGBM)**

In 2020, average AGGM observed for all the genotypes under LN conditions was slightly higher (7.69 t ha<sup>-1</sup>) than under HN conditions (6.61 t ha<sup>-1</sup>), although not significantly so. In 2021, the AGDM was higher under HN (4.14 t ha<sup>-1</sup>) than LN conditions (3.31 t ha<sup>-1</sup>). However, the cross-year analysis showed that overall the AGBDM for all 19 NILs was similar under LN conditions (5.51 t ha<sup>-1</sup>) and HN conditions (5.39 t ha<sup>-1</sup>) (Table 4.5).

In 2020, the AGBDM for PxW lines ranged from 5.37-8.27 t ha<sup>-1</sup> (6.75 t ha<sup>-1</sup>) in HN conditions. However, under LN conditions, the Paragon showed highest AGDM at 8.35 compared to the 15 PxW lines which ranged between 6.57-8.25 t ha<sup>-1</sup>. For the 2 SHWs, the AGDM was 7.91 and 8.59 t ha<sup>-1</sup> under LN conditions and 7.45 and 7.17 t ha<sup>-1</sup> under HN conditions, respectively. Robigus had AGDM of 7.74 t ha<sup>-1</sup> under HN conditions while under LN conditions it had highest value of 8.79 t ha<sup>-1</sup> among all the 19 genotypes (Table 4.5).

In 2021, however, overall AGBDM was higher under HN conditions. In the PxW lines, AGDM ranged between 3.73-5.24 t ha<sup>-1</sup> under HN conditions and between 2.91 to 3.82 t ha<sup>-1</sup> under low N conditions while Paragon had an AGBM of 3.53 and 4.06 t ha<sup>-1</sup> under LN and HN, respectively. The two SHW-derived lines showed a similar trend of low AGBM under LN (4.44 and 2.89 t ha<sup>-1</sup>) as compared to HN (5.69 and 3.06 t ha<sup>-1</sup>) conditions. Robigus showed an AGDM value of 3.57 and 4.41 t ha<sup>-1</sup> under LN and HN conditions, respectively.

The cross-year analysis showed that the AGBM ranged between 4.89-6.18 t ha<sup>-1</sup> under LN conditions between 4.60-6.58 t ha<sup>-1</sup> under HN conditions (Table 4.5). Overall, there was no significant effect of N treatment.

The effects of year and genotype were significant (Y, p=0.002 and G, p=0.005) (Table 4.5). However, the N X genotype interaction was not significant.

#### **4.3.2.3 Harvest Index**

In 2020, mean HI was 0.57 under LN conditions and 0.56 under HN conditions. Similarly in 2021 under HN and LN conditions do not differ (0.51). In the cross-year analysis no effect of N was observed (HN 0.54 and LN 0.54) (Table 4.5).

In 2020, the PxW lines under LN conditions ranged between 0.56-0.58 with Paragon having HI of 0.58. Under HN conditions the HI of PxW lines ranged between 0.54-0.60 with Paragon having HI of 0.55 (Table 4.5). The two SHW lines had an HI of 0.57 and 0.56 under LN and 0.55 and 0.57 under HN conditions while Robigus had 0.58 and 0.56 (Table 4.5). respectively.

In 2021, for PxW lines HI ranged from 0.50-0.53 under LN and 0.50-0.54 under HN with Paragon showing no change under both conditions (0.51). The two SHW lines showed a HI of 0.50 and 0.53 under LN and 0.49 and 0.51 under HN conditions. Robigus also showed slightly higher HI under LN (0.53) than HN (0.50) conditions (Table 4.5).



The cross-year analysis showed that under LN conditions, the HI ranged between 0.53-0.55 among the 19NILs while under HN conditions it ranged between 0.52-0.56.

The year effect showed high significance ( $p < 0.001$ ) and there was a trend for a genotype effect ( $P = 0.09$ ) (Table 4.5).

**Table 4.5:** Grain Yield (GY t ha<sup>-1</sup>) at 100% DM, Above-ground Biomass (BM t ha<sup>-1</sup>) and Harvest Index (HI) in 15 P X W near-isogenic lines, two synthetic-derived hexaploid wheat lines and Paragon and Robigus lines in year 2020, 2021 and mean of two years. N: N treatment, Y: Year, G: Genotype, N\*Y: Nitrogen Treatment X Year, N\*G: Nitrogen X Genotype, Y\*G: Year X Genotype, N\*Y\*G: Nitrogen X Year X Genotype

Genotype	GY (t ha <sup>-1</sup> ) at 100 DM						BM (t ha <sup>-1</sup> )						HI					
	2020		2021		Mean		2020		2021		Mean		2020		2021		Mean	
	HN	LN	HN	LN	HN	LN	HN	LN	HN	LN	HN	LN	HN	LN	HN	LN	HN	LN
Paragon	3.70	4.82	2.10	1.82	2.90	3.32	6.75	8.35	4.06	3.53	5.40	5.94	0.55	0.58	0.51	0.51	0.53	0.55
PW141-10-Q7D-AGDM-W	3.57	4.59	2.14	1.72	2.86	3.15	6.35	7.84	4.13	3.35	5.24	5.60	0.56	0.58	0.51	0.51	0.54	0.55
PW141-20-Q7D-AGDM-P	3.63	4.22	2.15	1.86	2.89	3.04	6.32	7.35	4.22	3.69	5.27	5.52	0.57	0.57	0.51	0.50	0.54	0.54
PW292-1-Q3A-COMSTR-W	3.80	4.26	2.17	1.86	2.99	3.06	6.88	7.43	4.03	3.58	5.45	5.51	0.55	0.57	0.54	0.51	0.55	0.54
PW292-19-Q3A-COMSTR-P	3.49	4.60	2.10	1.43	2.79	3.01	5.84	8.08	3.94	2.77	4.89	5.42	0.60	0.57	0.53	0.51	0.56	0.54
PW292-7-Q3A-COMSTR-W	4.57	4.34	2.01	1.73	3.29	3.04	8.27	7.51	3.85	3.32	6.06	5.42	0.56	0.58	0.52	0.52	0.54	0.55
PW292-8-Q3A-COMSTR-W	3.45	4.80	1.94	1.85	2.70	3.33	6.07	8.25	3.73	3.51	4.90	5.88	0.57	0.58	0.52	0.53	0.55	0.55
PW292-18-Q4B-GFPTT-P	4.27	4.32	2.69	1.60	3.48	2.96	7.91	7.68	5.24	3.16	6.58	5.42	0.54	0.56	0.51	0.50	0.53	0.53
PW292-6-Q4B-GFPTT-W	4.06	4.33	2.18	1.49	3.12	2.91	7.19	7.74	4.17	2.98	5.68	5.36	0.57	0.56	0.52	0.50	0.54	0.53
PW468-10-Q7B-AGDM-W	3.60	4.30	2.12	1.96	2.86	3.13	6.27	7.42	4.09	3.82	5.18	5.62	0.57	0.58	0.51	0.51	0.54	0.54
PW468-14-Q7B-AGDM-W	3.07	3.76	1.92	1.61	2.50	2.68	5.37	6.57	3.83	3.20	4.60	4.89	0.58	0.58	0.50	0.50	0.54	0.54
PW468-20-Q7B-AGDM-P	3.26	3.96	2.20	1.72	2.73	2.84	5.68	6.87	4.42	3.38	5.05	5.12	0.57	0.58	0.50	0.51	0.54	0.54

<b>PW468-1-Q5A-COMGRWT-W</b>	3.58	4.36	2.06	1.53	2.82	2.94	6.28	7.53	3.98	2.93	5.13	5.23	0.57	0.58	0.52	0.52	0.54	0.55
<b>PW468-12-Q5A-COMGRWT-P</b>	3.50	4.29	2.21	1.45	2.86	2.87	6.48	7.40	4.43	2.91	5.45	5.16	0.54	0.58	0.50	0.50	0.52	0.54
<b>PW729-1-Q6B-AGDM-W</b>	3.21	4.55	2.08	1.57	2.65	3.06	5.61	7.84	3.97	3.13	4.79	5.48	0.57	0.58	0.52	0.50	0.55	0.54
<b>PW729-15-Q6B-AGDM-P</b>	3.96	4.25	2.03	1.64	3.00	2.95	6.92	7.38	4.00	3.17	5.46	5.28	0.57	0.58	0.51	0.51	0.54	0.55
<b>Robigus</b>	4.34	5.08	2.17	1.89	3.25	3.49	7.74	8.79	4.41	3.57	6.07	6.18	0.56	0.58	0.50	0.53	0.53	0.55
<b>SEL58</b>	4.07	4.44	2.76	2.18	3.42	3.31	7.45	7.91	5.69	4.44	6.57	6.17	0.55	0.57	0.49	0.50	0.52	0.53
<b>SEL63</b>	4.11	4.76	1.56	1.52	2.84	3.14	7.17	8.59	3.06	2.89	5.11	5.74	0.57	0.56	0.51	0.53	0.54	0.54
<b>Minimum</b>	<b>3.07</b>	<b>3.76</b>	<b>1.56</b>	<b>1.43</b>	<b>2.50</b>	<b>2.68</b>	<b>5.37</b>	<b>6.57</b>	<b>3.06</b>	<b>2.77</b>	<b>4.60</b>	<b>4.89</b>	<b>0.54</b>	<b>0.56</b>	<b>0.49</b>	<b>0.50</b>	<b>0.52</b>	<b>0.53</b>
<b>Maximum</b>	<b>4.57</b>	<b>5.08</b>	<b>2.76</b>	<b>2.18</b>	<b>3.48</b>	<b>3.49</b>	<b>8.27</b>	<b>8.79</b>	<b>5.69</b>	<b>4.44</b>	<b>6.58</b>	<b>6.18</b>	<b>0.60</b>	<b>0.58</b>	<b>0.54</b>	<b>0.53</b>	<b>0.56</b>	<b>0.55</b>
<b>Mean</b>	<b>3.73</b>	<b>4.41</b>	<b>2.12</b>	<b>1.70</b>	<b>2.93</b>	<b>3.06</b>	<b>6.61</b>	<b>7.69</b>	<b>4.14</b>	<b>3.31</b>	<b>5.39</b>	<b>5.51</b>	<b>0.56</b>	<b>0.57</b>	<b>0.51</b>	<b>0.51</b>	<b>0.54</b>	<b>0.54</b>
				<b>LSD</b>	<b>P value</b>	<b>df</b>				<b>LSD</b>	<b>P value</b>	<b>df</b>				<b>LSD</b>	<b>P value</b>	<b>df</b>
<b>N</b>				1.13ns	0.75	4				2.07ns	0.872	4				0.02	0.69	4
<b>Y</b>				0.68***	<0.001	4				1.26**	0.002	4				0.01***	<0.001	4
<b>G</b>				0.33*	0.02	156				0.62**	0.005	156				0.01ns	0.09	156
<b>N*Y</b>				1.14ns	0.24	6.55				2.09ns	0.27	6.61				0.02ns	0.57	5.27
<b>N*G</b>				1.11ns	0.45	6.98				2.03ns	0.43	7.16				0.02ns	0.51	14.36
<b>Y*G</b>				0.72ns	0.14	14.12				1.34ns	0.079	14.37				0.02ns	0.69	96.59
<b>N*Y*G</b>				1.24ns	0.88	14.11				2.28ns	0.923	14.63				0.03ns	0.77	32.23

\*Significance at the 5% ( $P = 0.05$ ) level. \*\*1% ( $P = 0.01$ ) level. \*\*\*0.1% ( $P = 0.001$ ) level. LSD, least significance difference (5%); df, degree of freedom; ns, not significant.

### **4.3.3 Effects on Grain N Uptake (GNUP), Straw N Uptake (SNUP) and Nitrogen Harvest Index (NHI)**

#### **4.3.3.1 Grain N Uptake**

In 2020, the mean observed for GNUP under LN was 116.27 kg N ha<sup>-1</sup> while that under HN was 94.32 kg N ha<sup>-1</sup>. However, in 2021, the GNUP under LN was 33.26 kg N ha<sup>-1</sup> but higher under HN at 47.31 kg N ha<sup>-1</sup>. The cross-year analysis, however, demonstrated similar GNUP under LN conditions (74.95 kg N ha<sup>-1</sup>) and HN conditions (71.01 kg ha<sup>-1</sup>) (Table 4.6).

In 2020 the PxW lines under LN conditions ranged from 88.94-137.62 kg N ha<sup>-1</sup> compared to Paragon at 113.84 kg N ha<sup>-1</sup>. Under HN PxW lines ranged from 89.94 – 137.62 kg N ha<sup>-1</sup> compared to 77.59 kg N ha<sup>-1</sup> for Paragon. Similarly, the 2 SHW lines at LN were 110.64 and 148.48 kg ha<sup>-1</sup> compared to 107.01 and 85.51 kg N ha<sup>-1</sup>, respectively. Robigus was 112.85 kg N ha<sup>-1</sup> at LN and 107.31 kg N ha<sup>-1</sup> at HN (Table 4.6).

In 2021, the GNUP was consistently lower in all the 19 genotypes under LN conditions compared to HN conditions. In the 15 PxW lines, GNUP ranged between 42.60-63.10 kg N ha<sup>-1</sup> under HN conditions and under LN conditions from 28.06-39.04 kg N ha<sup>-1</sup>. The parent Paragon also had a higher GNUP of 47.68 kg N ha<sup>-1</sup> at HN conditions and 37.12 kg N ha<sup>-1</sup> at LN conditions. Similarly, SHW, SEL58 and SEL63 lines had GNUP of 38.40 and 28.58 kg N ha<sup>-1</sup> under LN which was lower than under HN (57.18 and 34.03 kg N ha<sup>-1</sup>), respectively. Likewise, Robigus showed higher GNUP values at HN (45.22 kg N ha<sup>-1</sup>) in comparison to LN conditions (34.74 kg N ha<sup>-1</sup>) (Table 4.6).

The cross-year analysis showed overall no significant effect of N treatment; GNUP was 74.95 kg N ha<sup>-1</sup> and 71.01 kg N ha<sup>-1</sup> under HN conditions (Table 4.6).

The influence of year showed high significance (p<0.001), but other effects were not statistically different (Table 4.6).

#### **4.3.3.2 Straw N Uptake**

In 2020, overall SNUP was similar under LN (15.26 kg N ha<sup>-1</sup>) and HN conditions (13.98 kg N ha<sup>-1</sup>). However, in 2021 as well as for the cross-year analysis SNUP was greater under HN conditions (11.99 and 13.15 kg N ha<sup>-1</sup>, respectively) than LN conditions (7.34 and 11.39 kg N ha<sup>-1</sup>, respectively) (Table 4.6).

In 2020 SNUP of PxW lines ranged between 7.83-23.69 kg N ha<sup>-1</sup> under HN and 10.00-22.65 kg N ha<sup>-1</sup> under LN conditions; Paragon was 17.88 kg N ha<sup>-1</sup> under LN conditions and 13.62 kg N ha<sup>-1</sup> under HN conditions. The SHW lines had higher SNUP of 15.34 and 17.38 kg N ha<sup>-1</sup> under HN conditions 13.67 and 15.57 kg N ha<sup>-1</sup>, under LN conditions Robigus at LN was 18.40 kg N ha<sup>-1</sup> and at HN was 14.00 kg N ha<sup>-1</sup> (Table 4.6).

In 2021, all the genotypes had consistently lower SNUP at HN than at LN conditions. Among the 15 PxW lines, SNUP ranged from 9.70-18.07 kg N ha<sup>-1</sup> with Paragon at 12.00 kg N ha<sup>-1</sup> under HN conditions. Further, under LN conditions, SNUP ranged from 5.82-9.18 kg N ha<sup>-1</sup> with Paragon at 6.72 kg N ha<sup>-1</sup>. The SHW-derived lines also had a lower SNUP (10.79 and 7.07 kg N ha<sup>-1</sup>) under LN than HN (22.22 and 9.49 kg N ha<sup>-1</sup>). Correspondingly, Robigus also exhibited lower SNUP of 9.90 kg N ha<sup>-1</sup> under LN compared to HN at 17.23 kg N ha<sup>-1</sup> (Table 4.6).

The cross-year analysis showed SNUP was lower in LN than HN conditions ranging between 8.45-14.82 kg N ha<sup>-1</sup> under LN and 10.12-18.78 kg N ha<sup>-1</sup> with an overall average of 11.39 and 13.15 kg N ha<sup>-1</sup> respectively (Table 4.6). The genotype effect was significant at p=0.005 (Table 4.6).

#### **4.3.2.3 Nitrogen Harvest Index**

The NHI did not show any difference for the year and genotype effect. The NHI did not differ under LN and HN conditions (0.82 in both N treatments) (Table 4.6).

In 2020, NHI ranged between 0.78-0.88 among the PxW lines under HN conditions and between 0.80-0.89 under LN conditions. Paragon had NHI at LN of 0.83 and 0.81 at HN. The two SHW-derived lines had NHI of 0.87 and 0.89 at LN conditions and 0.85 and 0.78, at HN conditions. Robigus had NHI at HN of 0.86 and at LN of 0.82 (Table 4.6).

In 2021, NHI was higher under LN than HN conditions for all genotypes except PW292-1-Q3A-COMSTR-W. In the PxW lines, NHI ranged between 0.78-0.82 under HN and 0.79-0.84 under LN conditions. Paragon had NHI of 0.84 and 0.80 respectively. The two SHW-derived lines and Robigus parent also showed a trend for higher NHI at LN at 0.81, 0.80 and 0.77, respectively, than at HN at 0.75, 0.78 and 0.74 (Table 4.6).

The cross-year analysis showed NHI ranged between 0.78-0.85 among the 19 genotypes under LN while under HN conditions it ranged between 0.77-0.84 (Table 4.6). However, the effect of genotype was not statistically significant.

**Table 4.6:** Grain N Uptake (GNUP kg N ha<sup>-1</sup>), Straw N Uptake (SNUP kg N ha<sup>-1</sup>) and Nitrogen Harvest Index (NHI) in 15 P X W near-isogenic lines, 2 synthetic-derived hexaploid wheat lines and parents Paragon and Robigus in year 2020, 2021 and mean of two years. N: N treatment, Y: Year, G: Genotype, N\*Y: Nitrogen Treatment X Year, N\*G: Nitrogen X Genotype, Y\*G: Year X Genotype, N\*Y\*G: Nitrogen X Year X Genotype

	GNUP (kg N ha <sup>-1</sup> )						SNUP (kg N ha <sup>-1</sup> )						NHI					
	2020		2021		Mean		2020		2021		Mean		2020		2021		Mean	
	HN	LN	HN	LN	HN	LN	HN	LN	HN	LN	HN	LN	HN	LN	HN	LN	HN	LN
Paragon	77.59	113.84	47.68	37.12	62.63	75.48	13.62	17.88	12.00	6.72	12.81	12.30	0.81	0.83	0.80	0.84	0.81	0.83
PW141-10-Q7D-AGDM-W	90.11	135.90	49.49	34.01	69.80	84.95	15.71	16.29	13.66	6.20	14.68	11.24	0.81	0.86	0.78	0.84	0.80	0.85
PW141-20-Q7D-AGDM-P	95.09	107.08	49.38	37.58	72.24	72.33	7.83	14.98	12.41	8.20	10.12	11.59	0.89	0.84	0.81	0.83	0.85	0.84
PW292-1-Q3A-COMSTR-W	98.65	106.14	48.88	37.88	73.76	72.01	12.16	14.55	9.79	9.18	10.98	11.86	0.87	0.85	0.82	0.79	0.84	0.82
PW292-19-Q3A-COMSTR-P	71.87	119.99	45.54	28.06	58.70	74.03	10.65	17.50	9.70	6.37	10.17	11.94	0.82	0.84	0.81	0.81	0.81	0.83
PW292-7-Q3A-COMSTR-W	115.57	120.89	45.67	35.01	80.62	77.95	23.69	15.00	10.13	7.33	16.91	11.17	0.80	0.86	0.81	0.81	0.80	0.84
PW292-8-Q3A-COMSTR-W	95.08	131.07	42.95	35.21	69.02	83.14	14.63	22.65	10.38	6.99	12.50	14.82	0.84	0.80	0.80	0.82	0.82	0.81
PW292-18-Q4B-GFPTT-P	117.75	131.33	63.10	31.78	90.42	81.55	13.51	14.20	18.07	6.76	15.79	10.48	0.89	0.88	0.78	0.83	0.83	0.85
PW292-6-Q4B-GFPTT-W	116.48	99.13	48.03	29.79	82.25	64.46	10.65	16.13	10.54	5.82	10.60	10.98	0.89	0.83	0.81	0.84	0.85	0.83
PW468-10-Q7B-AGDM-W	77.53	137.62	48.33	39.04	62.93	88.33	16.71	14.85	11.79	8.41	14.25	11.63	0.78	0.87	0.80	0.82	0.79	0.85
PW468-14-Q7B-AGDM-W	75.25	97.10	42.60	31.47	58.92	64.29	11.39	11.85	10.16	7.26	10.78	9.56	0.84	0.86	0.81	0.82	0.83	0.84
PW468-20-Q7B-AGDM-P	78.79	88.94	49.94	33.17	64.36	61.05	16.43	11.17	12.46	7.34	14.44	9.26	0.78	0.85	0.81	0.81	0.79	0.83
PW468-1-Q5A-COMGRWT-W	97.61	109.18	45.06	32.21	71.33	70.69	13.68	17.24	10.77	6.85	12.23	12.05	0.84	0.82	0.80	0.82	0.82	0.82

<b>PW468-12-Q5A-COMGRWT-P</b>	97.02	119.14	49.47	28.69	73.25	73.92	16.53	10.00	12.83	6.91	14.68	8.45	0.83	0.89	0.81	0.81	0.82	0.85
<b>PW729-1-Q6B-AGDM-W</b>	96.32	123.60	46.10	29.72	71.21	76.66	15.19	19.53	9.70	6.22	12.45	12.88	0.83	0.82	0.82	0.84	0.82	0.83
<b>PW729-15-Q6B-AGDM-P</b>	112.58	113.67	46.55	32.95	79.56	73.31	13.46	13.64	11.16	7.05	12.31	10.35	0.88	0.86	0.81	0.82	0.84	0.84
<b>Robigus</b>	107.31	112.85	45.22	34.74	76.26	73.80	14.00	18.40	17.23	9.90	15.62	14.15	0.86	0.82	0.74	0.77	0.80	0.80
<b>SEL58</b>	107.01	110.64	57.18	38.40	82.09	74.52	15.34	13.67	22.22	10.79	18.78	12.23	0.85	0.87	0.75	0.81	0.80	0.84
<b>SEL63</b>	85.51	148.48	34.03	28.58	59.77	88.53	17.38	15.57	9.49	7.07	13.44	11.32	0.78	0.89	0.78	0.80	0.78	0.84
<b>Minimum</b>	<b>71.87</b>	<b>88.94</b>	<b>34.03</b>	<b>28.06</b>	<b>58.70</b>	<b>61.05</b>	<b>7.83</b>	<b>10.00</b>	<b>9.49</b>	<b>5.82</b>	<b>10.12</b>	<b>8.45</b>	<b>0.78</b>	<b>0.80</b>	<b>0.74</b>	<b>0.77</b>	<b>0.78</b>	<b>0.80</b>
<b>Maximum</b>	<b>117.75</b>	<b>148.48</b>	<b>63.10</b>	<b>39.04</b>	<b>90.42</b>	<b>88.53</b>	<b>23.69</b>	<b>22.65</b>	<b>22.22</b>	<b>10.79</b>	<b>18.78</b>	<b>14.82</b>	<b>0.89</b>	<b>0.89</b>	<b>0.82</b>	<b>0.84</b>	<b>0.85</b>	<b>0.85</b>
<b>Mean</b>	<b>94.32</b>	<b>116.27</b>	<b>47.31</b>	<b>33.26</b>	<b>71.01</b>	<b>74.95</b>	<b>13.98</b>	<b>15.26</b>	<b>11.99</b>	<b>7.34</b>	<b>13.15</b>	<b>11.39</b>	<b>0.84</b>	<b>0.85</b>	<b>0.80</b>	<b>0.82</b>	<b>0.82</b>	<b>0.83</b>
				<b>LSD</b>	<b>P value</b>	<b>df</b>				<b>LSD</b>	<b>P value</b>	<b>df</b>				<b>LSD</b>	<b>P value</b>	<b>df</b>
<b>N</b>				34.39ns	0.75	4				9.51ns	0.62	4				0.04ns	0.33	4
<b>Y</b>				16.62***	<0.001	4				5.18ns	0.052	4				0.01*	0.006	4
<b>G</b>				12.33ns	0.19	156				3.37*	0.005	156				0.02ns	0.38	156
<b>N*Y</b>				33.99ns	0.21	5.77				9.47ns	0.41	6.18				0.04ns	0.79	5.27
<b>N*G</b>				34.24ns	0.12	8.64				9.45ns	0.39	8.53				0.05ns	0.24	24.15
<b>Y*G</b>				21.2ns	0.27	33.19				6.15ns	0.17	24.72				0.04ns	0.12	132.61
<b>N*Y*G</b>				38.49ns	0.45	17.67				10.74ns	0.58	17.83				0.07ns	0.19	56.3

\*Significance at the 5% ( $P = 0.05$ ) level. \*\*1% ( $P = 0.01$ ) level. \*\*\*0.1% ( $P = 0.001$ ) level. LSD, least significance difference (5%); df, degree of freedom; ns, not significant.



#### **4.3.4 Effects on Grain Protein Content (GPC) and Thousand Grain Weight (TGW)**

##### **4.3.4.1 Grain Protein Content**

Averaging across genotypes, in 2020 GPC was similar under LN conditions (16.49%) compared to HN conditions (15.86%). However, in 2021 GPC was significantly higher under HN (13.34%) compared to LN conditions (11.83%) (Table 4.7).

In 2020, for the PxW GPC under LN conditions ranged between 12.87-18.75% under LN and between 13.99-20.00% under HN. Paragon was 14.81% and 13.18%, under LN and HN respectively. The 2 SHW-derived lines, however, showed GPC at LN of 15.71 and 19.47%; and GPC at HN of 16.91 and 13.09%(Table 4.7). Robigus had GPC at high N of 15.68% and at low N of 13.87%.

In 2021, all the 19 genotypes had lower grain protein content under low N conditions ranging from 10.77-12.33% than under high N conditions ranging between 12.64-14.09%. Paragon had GPC at LN of 12.17% compared to HN of 13.37%. Moreover, the SHW-derived lines also showed lower GPC at LN of 10.77 and 11.40% than at HN of 12.64 and 12.96%, respectively. Robigus showed the same trend with GPC at LN 11.22% and at HN 12.79% (Table 4.7).

From the cross-year analysis, GPC ranged between 12.54-15.90% under LN and between 12.96-15.90% but the genotype effect and the N × genotype interaction were not significantly different. (Table 4.7).

##### **4.3.4.2 Thousand Grain Weight**

Following the previous trends, the TGW in 2020 also exhibited similar levels under LN conditions at 46.29 g compared to HN conditions at 45.57 g. In 2021 TGW was also similar under LN (36.74 g) and HN (37.4 g) conditions. Cross-year analysis showed no significant effect of N treatment at 41.57 g under LN and 41.47 g under HN conditions (Table 4.7).

In 2020, the TGW under LN condition for PxW lines ranged between 42.50-50.57 g and under HN from 41.53-49.50 g. Paragon had TGW at LN of 45.93 g and at HN of 44.32 g. Both the SHW-derived lines had higher TGW than Robigus under LN at 48.63, 49.00 and 43.60 g, respectively, and also at HN conditions at 47.00, 47.57 and 43.47 g(Table 4.7).

In 2021, the TGW ranged between 33.67-39.23 g under LN while under HN it ranged between 32.17-41.90 g. (Table 4.7). Cross-year analysis showed the  $p < 0.001$  (Table 4.7).

**Table 4.7:** Grain Protein Content (GPC %) and Thousand Grain Weight (TGW g) in 15 P X W near-isogenic lines, two synthetic-derived hexaploid wheat lines with parent Paragon and Robigus in year 2020, 2021 and mean of two years. N: N treatment, Y: Year, G: Genotype, N\*Y: Nitrogen Treatment X Year, N\*G: Nitrogen X Genotype, Y\*G: Year X Genotype, N\*Y\*G: Nitrogen X Year X Genotype

	GPC (%)						TGW (g)					
	2020		2021		Mean		2020		2021		Mean	
	HN	LN	HN	LN	HN	LN	HN	LN	HN	LN	HN	LN
<b>Paragon</b>	13.18	14.81	13.37	12.17	13.28	13.49	44.32	45.93	36.22	35.83	40.27	40.88
<b>PW141-10-Q7D-AGDM-W</b>	15.58	18.67	13.74	11.67	14.66	15.17	41.53	42.50	34.57	34.30	38.05	38.40
<b>PW141-20-Q7D-AGDM-P</b>	16.14	15.97	13.52	11.98	14.83	13.98	43.87	44.57	35.37	37.00	39.62	40.78
<b>PW292-1-Q3A-COMSTR-W</b>	16.87	15.88	13.33	11.98	15.10	13.93	46.00	46.60	37.13	38.40	41.57	42.50
<b>PW292-19-Q3A-COMSTR-P</b>	12.87	16.25	13.06	11.88	12.96	14.06	45.97	46.90	37.97	35.47	41.97	41.18
<b>PW292-7-Q3A-COMSTR-W</b>	15.70	17.44	13.41	12.06	14.55	14.75	46.07	45.20	37.73	35.97	41.90	40.58
<b>PW292-8-Q3A-COMSTR-W</b>	17.52	16.77	13.32	11.56	15.42	14.16	45.00	45.17	35.93	35.33	40.47	40.25
<b>PW292-18-Q4B-GFPTT-P</b>	17.21	19.00	14.09	11.96	15.65	15.48	46.03	46.60	37.17	36.83	41.60	41.72
<b>PW292-6-Q4B-GFPTT-W</b>	17.32	14.21	13.25	12.23	15.29	13.22	49.17	48.77	40.33	38.03	44.75	43.40
<b>PW468-10-Q7B-AGDM-W</b>	13.88	20.00	13.68	11.79	13.78	15.90	48.00	49.47	41.90	38.77	44.95	44.12
<b>PW468-14-Q7B-AGDM-W</b>	15.17	16.17	13.35	11.84	14.26	14.00	46.27	46.67	39.90	38.10	43.08	42.38
<b>PW468-20-Q7B-AGDM-P</b>	15.34	13.99	13.34	11.85	14.34	12.92	49.50	50.57	40.30	39.23	44.90	44.90
<b>PW468-1-Q5A-COMGRWT-W</b>	16.72	15.38	13.36	12.33	15.04	13.85	46.57	47.77	38.10	36.87	42.33	42.32
<b>PW468-12-Q5A-COMGRWT-P</b>	17.63	17.39	13.54	12.28	15.59	14.84	44.87	46.23	37.30	37.97	41.08	42.10
<b>PW729-1-Q6B-AGDM-W</b>	18.75	17.12	13.06	11.71	15.90	14.41	41.97	44.17	35.57	33.67	38.77	38.92
<b>PW729-15-Q6B-AGDM-P</b>	17.50	16.87	13.69	12.18	15.60	14.52	43.60	44.00	37.40	35.50	40.50	39.75
<b>Robigus</b>	15.68	13.87	12.79	11.22	14.23	12.54	43.47	43.60	32.17	34.70	37.82	39.15
<b>SEL58</b>	16.91	15.71	12.64	10.77	14.78	13.24	47.00	48.63	37.13	38.33	42.07	43.48
<b>SEL63</b>	13.09	19.47	12.96	11.40	13.03	15.44	47.57	49.00	38.80	38.43	43.18	43.72
<b>Minimum</b>	<b>12.87</b>	<b>13.87</b>	<b>12.64</b>	<b>10.77</b>	<b>12.96</b>	<b>12.54</b>	<b>41.53</b>	<b>42.50</b>	<b>32.17</b>	<b>33.67</b>	<b>37.82</b>	<b>38.40</b>
<b>Maximum</b>	<b>18.75</b>	<b>20.00</b>	<b>14.09</b>	<b>12.33</b>	<b>15.90</b>	<b>15.90</b>	<b>49.50</b>	<b>50.57</b>	<b>41.90</b>	<b>39.23</b>	<b>44.95</b>	<b>44.90</b>
<b>Mean</b>	<b>15.86</b>	<b>16.49</b>	<b>13.34</b>	<b>11.83</b>	<b>14.62</b>	<b>14.18</b>	<b>45.57</b>	<b>46.39</b>	<b>37.35</b>	<b>36.74</b>	<b>41.47</b>	<b>41.57</b>
				<b>LSD</b>	<b>P value</b>	<b>df</b>			<b>LSD</b>	<b>P value</b>	<b>df</b>	
<b>N</b>				3.83ns	0.78	4			2.18ns	0.89	4	

<b>Y</b>	0.27***	<0.001	4	0.92***	<.001	4
<b>G</b>	1.52ns	0.28	156	1.31***	<.001	156
<b>N*Y</b>	3.83ns	0.47	4.04	2.15ns	0.39	5.38
<b>N*G</b>	3.87ns	0.44	9.93	2.5ns	0.85	20.83
<b>Y*G</b>	2.09ns	0.47	158.27	1.91ns	0.73	118.4
<b>N*Y*G</b>	4.274ns	0.26	18.19	3.108ns	0.88	48.7

\*Significance at the 5% ( $P = 0.05$ ) level. \*\*1% ( $P = 0.01$ ) level. \*\*\*0.1% ( $P = 0.001$ ) level. LSD, least significance difference (5%); df, degree of freedom; ns, not significant.

### **4.3.5 Traits associations between HN and LN conditions**

#### **4.3.5.1 Association in Grain yield, Above-ground biomass and harvest index under HN and LN condition**

The associations between traits including GY, AGDM and HI have been analysed under high N and low N conditions in 2020, 2021 and for the mean of the two years.

In the case of grain yield, in 2020, no association was observed between LN and HN conditions ( $R^2=0.1245$   $P=0.138$ ) (Fig 4.1 A). In the 2021, GY under HN and LN showed a strong trend for a positive association ( $R^2=0.1492$ ,  $P=0.102$ ) (Fig 4.1 B). However, the two years mean of GY under HN and LN, did not show a significant association ( $R^2= 0.1124$  and  $P=0.161$ ) (Fig 4.1 C).

Under HN and LN conditions, the AGDM showed a trend for a linear correlation ( $R^2=0.1572$  and  $P=0.093$ ) in 2020 (Fig 4.2 D). Similarly, in the year 2021, AGDM under HN and LN exhibited positive linear association ( $R^2=0.2843$ ,  $P=0.019$ ) (Fig 4.2 E). Averaging over the two years, AGDM under HN and LN conditions showed a trend for a positive amongst the genotypes ( $R^2=0.179$  and  $P$  value at 0.071) (Fig 4.1 F).

The harvest index did not show an association between LN and HN conditions ( $R^2=0.0687$ ,  $P=0.856$ ) in 2020 (Fig 4.1 G) or in 2021 ( $R^2=0.002$ ,  $p=0.153$ ) (Fig 4.1 H). The two-year means also did not show a linear association between the two N treatments ( $R^2=0.1163$ ,  $p=0.278$ ) (Fig 4.1 I).

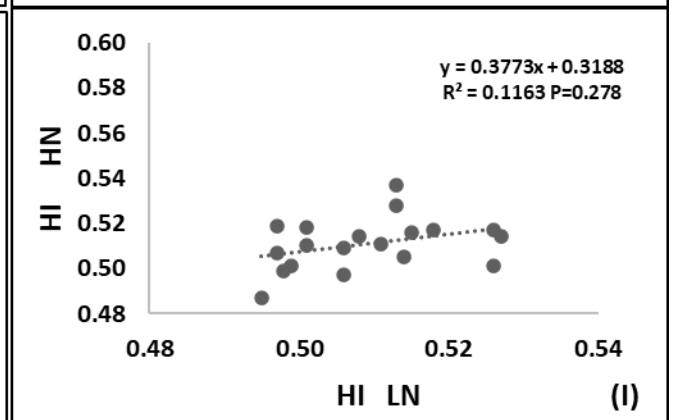
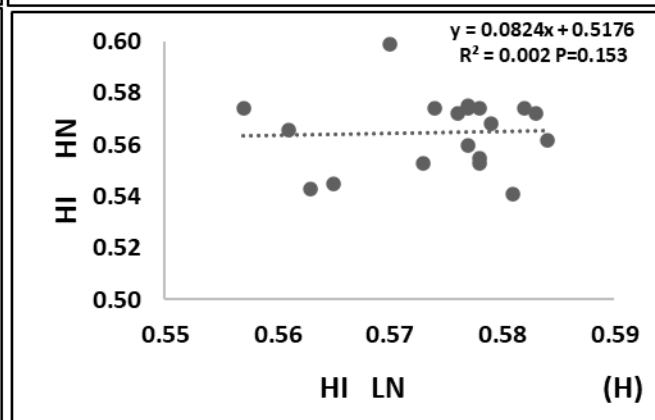
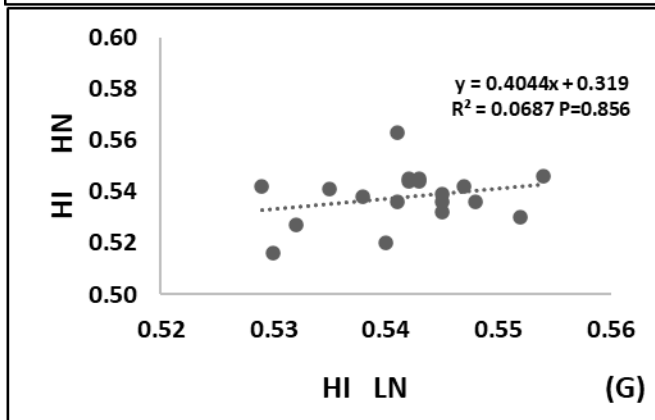
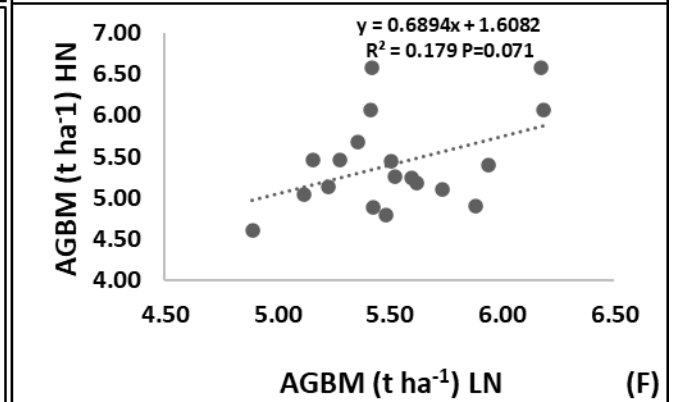
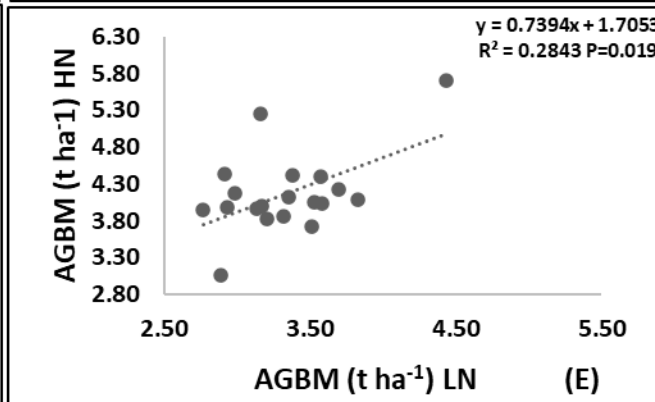
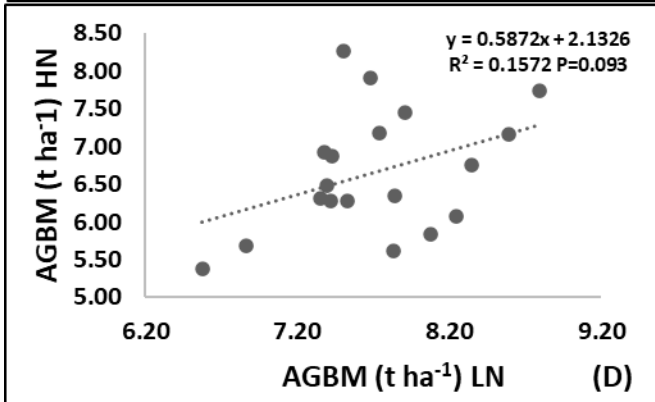
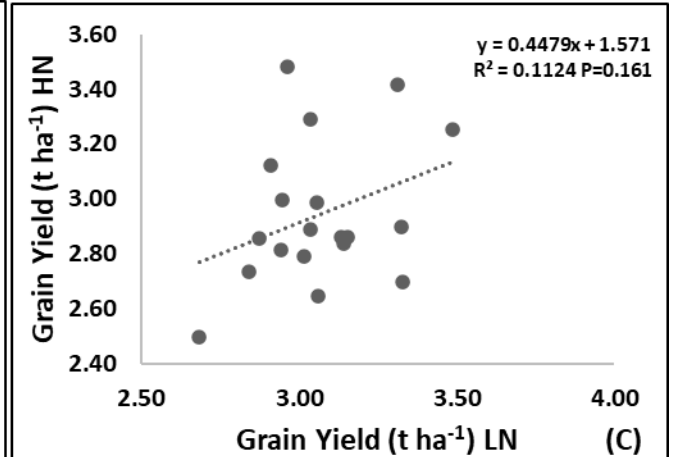
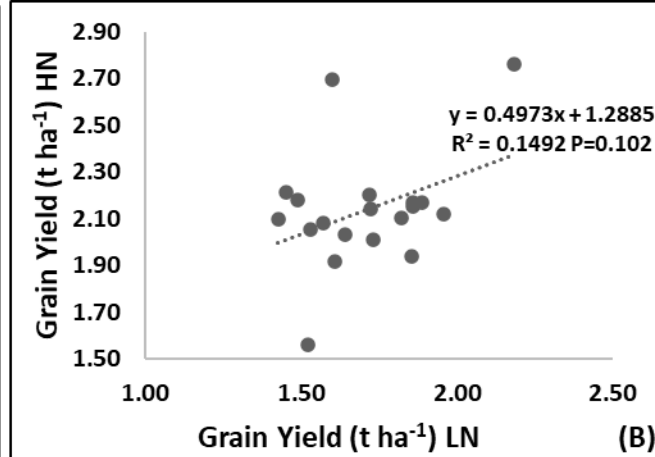
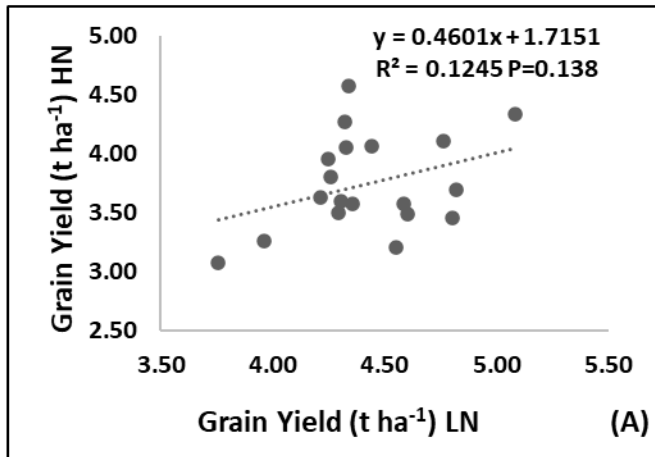


**Fig 4.1:** Linear regression of Grain Yield ( $t\ ha^{-1}$ ) at HN on Grain Yield at LN in (A) 2020 (B)2021 and (C) mean values of two years; Above-ground Biomass (AGBM  $t\ ha^{-1}$ ) at HN on AGBM at LN in (D) 2020 (E)2021 and (F) mean values of two years; Harvest index (HI) at HN on HI at LN in (G) 2020 (H)2021 and (I) mean values of two years

#### 4.3.5.2 Association between NUE under HN and LN conditions

The linear regression of Nitrogen-use efficiency was analysed under high N and low N conditions across the genotypes in the two experiments as well as for the mean of the two experiments. No significant association between NUE at HN and NUE at LN was observed in 2020 ( $R^2=0.1248\ p=0.138$ ) (Fig 4.2 A). In 2021, there was a trend for positive correlation ( $R^2=0.1658\ p=0.084$ ) (Fig 4.2 B). The mean NUE of the two years under HN and LN showed a weak linear correlation with less significant positive association ( $R^2=0.1012\ p=0.185$ ) (Fig 4.2 C)

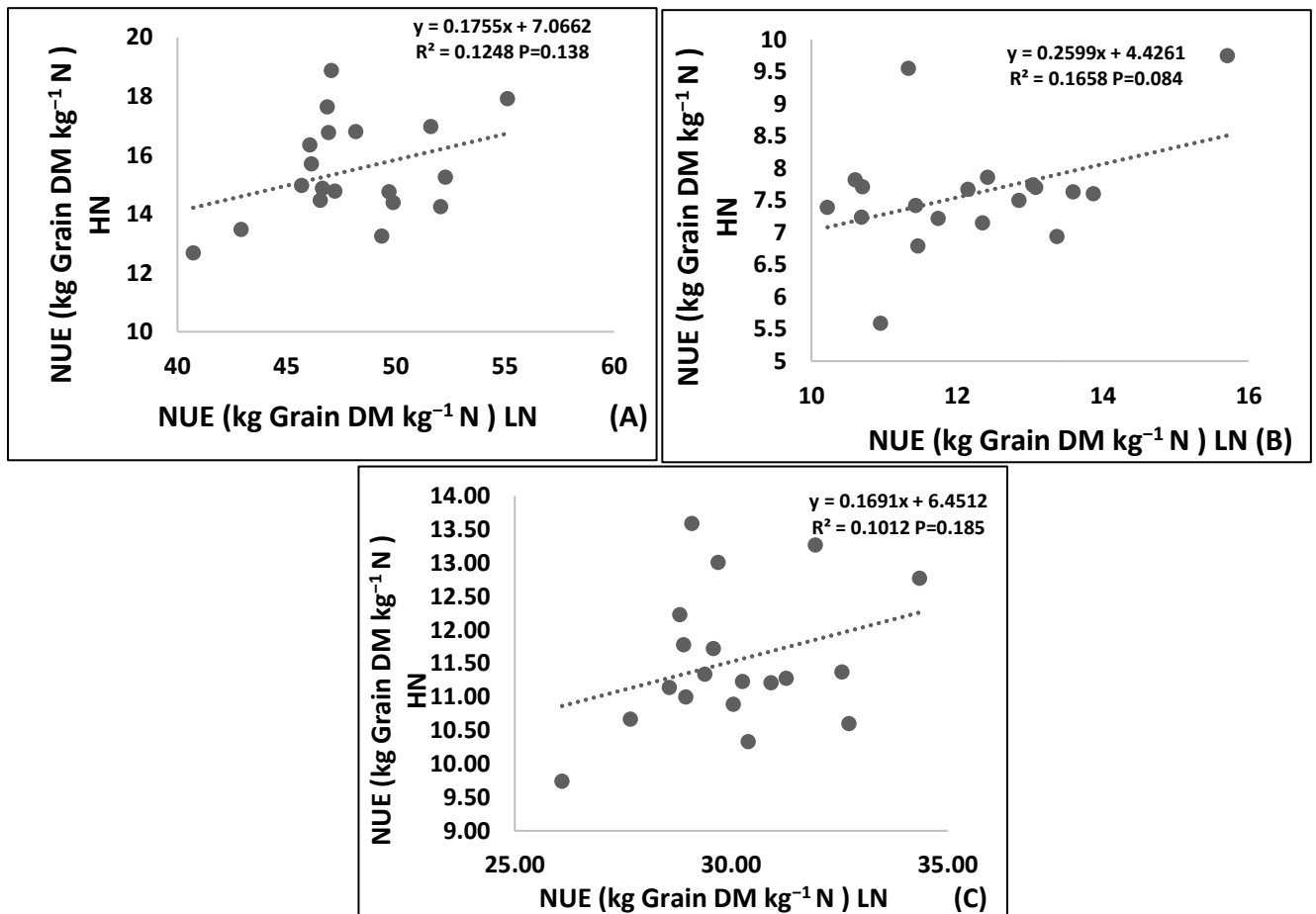


**Fig 4.2:** Linear regression of Nitrogen Use Efficiency (NUE kg Grain DM kg<sup>-1</sup> N ) at HN on NUE at LN in (A) 2020 (B)2021 and (C) mean values of two years.

#### 4.3.5.3 Association between GY and NUE, NUtE, NUPE and AGBM across two-year mean

Among the 19 genotypes, the association of GY with traits including NUE, NUtE, NUPE and AGDM was examined for the two-year means.

A strong positive linear correlation was seen between GY and NUPE ( $R^2=0.7321$ ,  $P < 0.001$ ) under HN. Similarly, a linear association was seen between GY and NUPE under LN ( $R^2=0.3299$ ,  $P=0.010$ ) (Fig 4.3 A). As expected, a strong positive association was observed between GY and NUE under LN ( $R^2 = 0.9734$ ,  $P < 0.001$ ) and HN ( $0.9962$ ,  $P < 0.001$ ) conditions (Fig 4.3 B). GY and NUtE, however, did not show a positive association under LN ( $R^2=0.07$ ,  $P=0.290$ ) or HN ( $R^2 = 0.082$ ,  $P=0.243$ ) conditions (Fig 4.3 C). Averaging across the two years, the 19 genotypes showed a significantly high and positive linear correlation between GY and AGDM under HN ( $R^2 = 0.9671$ ,  $P < 0.001$ ) as well as LN ( $R^2 = 0.948$ ,  $P < 0.001$ ) conditions (Fig 4.3 D).

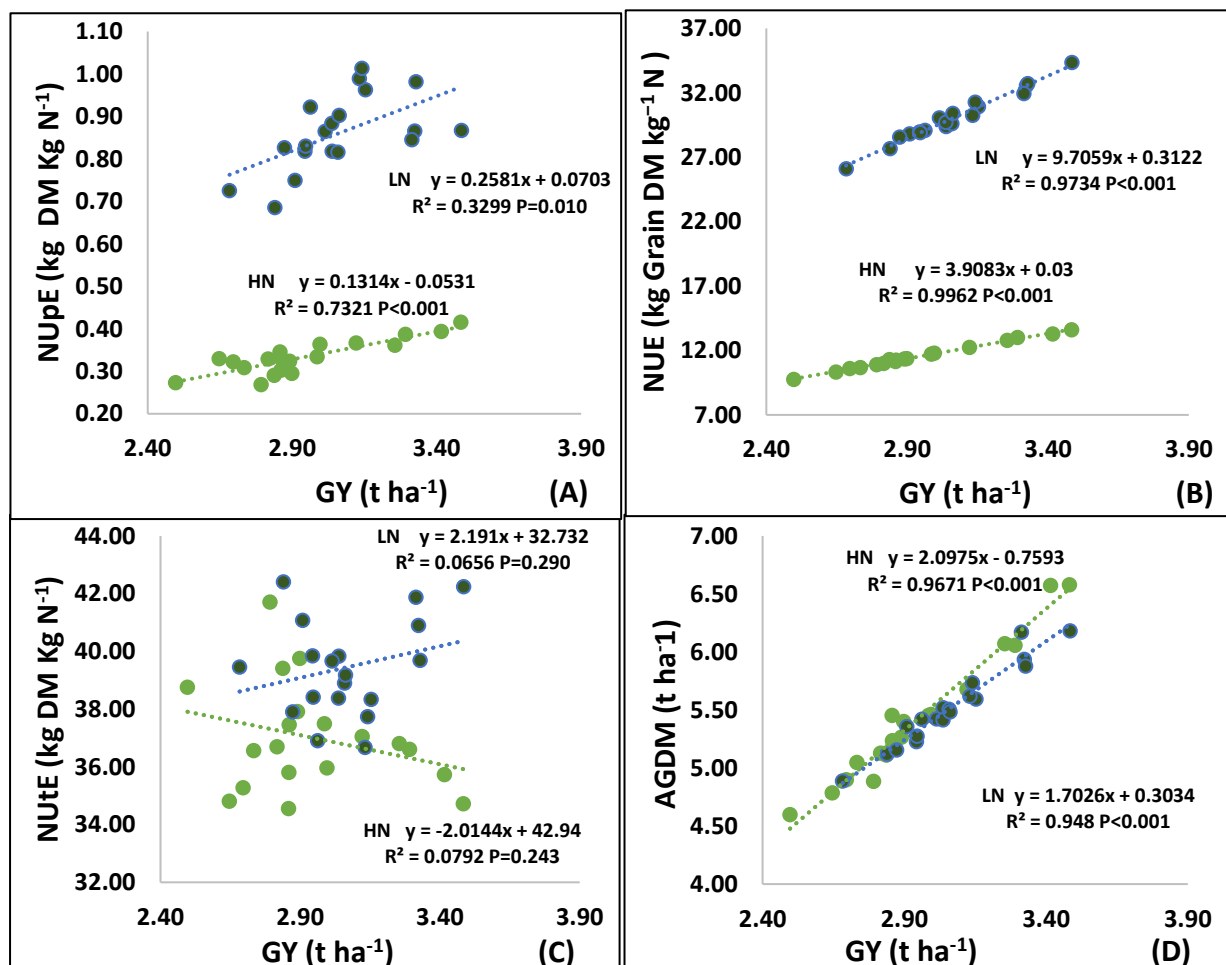


**Fig 4.3:** Linear regression of (A) GY on NUpE (B) GY on NUE and (C) GY on NUtE and (D) GY on AGDM of mean across two years of 19 NILs. Blue colour and Green colour data points represents values of mean values in 2020 and 2021 year at LN and HN respectively.

#### 4.3.5.4 Associations between GY and ears $m^{-2}$ and Grains $ear^{-1}$ across two-year mean

Across the 19 , a strong positive association was observed between GY and ears  $m^{-2}$  under high N ( $R^2 = 0.7223$   $P < 0.001$ ) and low N ( $R^2 = 0.5685$   $P < 0.001$ ) conditions (Fig 4.4 A). There was no positive linear correlation observed between GY and grains  $ear^{-1}$  under LN ( $R^2 = 0.022$ , ns) and HN ( $R^2 = 0.0068$ , ns) conditions (Fig 4.4 B).

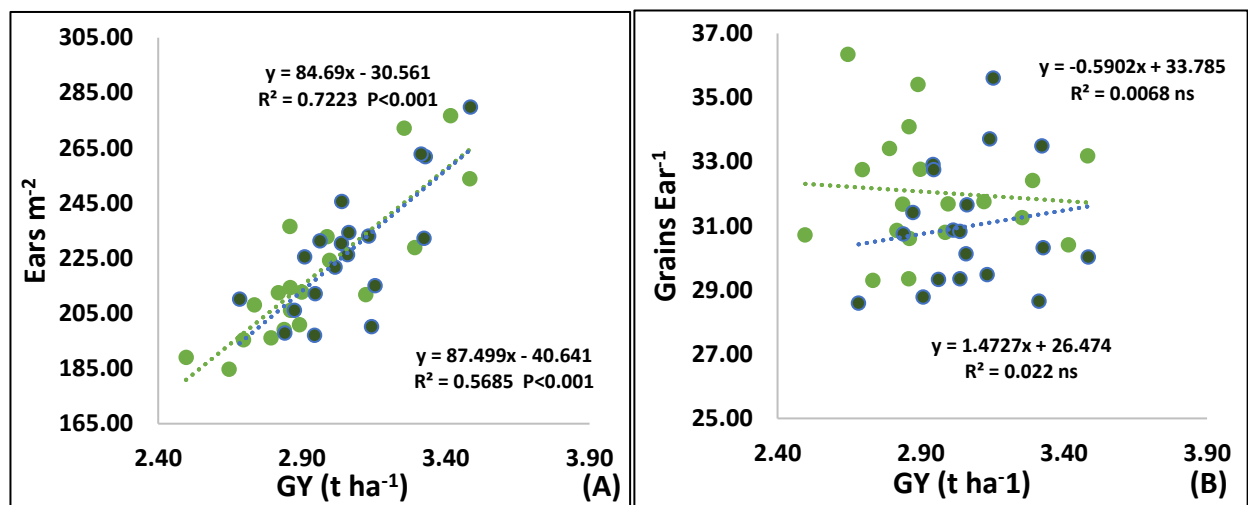


**Fig 4.4:** Linear regression of (A) GY on Ears  $m^{-2}$  and (B) GY on Grains  $Ear^{-1}$  for 19 genotypes. Blue colour and green colour data points represents values of mean in 2020 and 2021 year at LN and HN, respectively

#### 4.3.5.5 Associations between GPC, GY and NUE along with NUE and AGDM across two-year mean

No association was observed among the 19 genotypes between GPC and GY under HN ( $R^2 = 0.0292$   $P = 0.484$ ) or LN ( $R^2 = 0.0312$   $P = 0.469$ ) conditions (Fig 4.5 A). Additionally, averaging across years, GPC and NUE showed no association under LN ( $R^2 = 0.0258$   $P = 0.515$ ) or HN ( $R^2 = 0.0229$   $P = 0.491$ ) conditions (Fig 4.5 B).

Linear regression of AGDM and NUE has demonstrated positive association with high significance under high N ( $R^2 = 0.9523$ ,  $P < 0.001$ ) and low N ( $R^2 = 0.904$ ,  $P < 0.001$ ) conditions (Fig 4.5C).



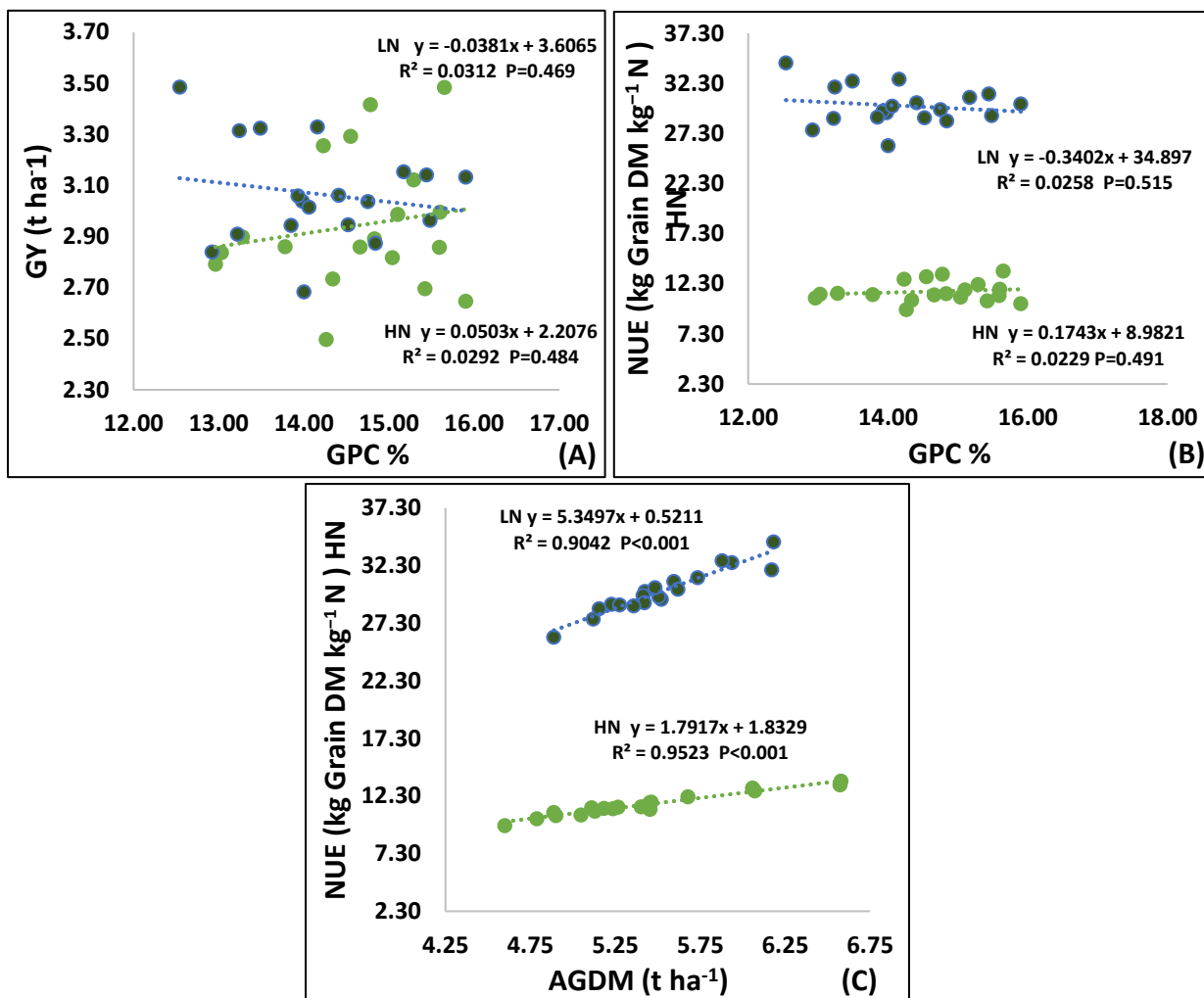


**Fig 4.5:** Linear regression of (A) GPC on GY, (B) GPC on NUE and (C) AGDM and NUE of mean across two years of 19 genotypes. Blue colour and green colour data points represents values of mean in 2020 and 2021 year at LN and HN, respectively.

#### 4.3.5.6 Correlation between traits under HN and LN conditions

The correlation matrix shows the correlations for all trait combinations under HN and LN conditions. The colour scale demonstrates the level of association with dark red being high correlation and dark blue being no correlation (Fig 4.6).

Under HN conditions, traits like GY and NUE, NUE and AGBM and, AGBM and ear m<sup>-2</sup> demonstrate positive correlation with high significance ( $p < 0.001$ ), confirming the effects described above for the linear regressions. In addition, there were a positive correlation between NHI and GPC, and a negative correlation between NUtE and GPC (Fig 4.6 A).

Similarly, under LN conditions, traits such as GY and AGBM, NUE and AGBM and, NUE and GY showed positive correlation with high significance ( $p < 0.001$ ). In addition, there were a positive correlation between NHI and GPC, and a negative correlation between NUtE and GPC. (Fig 4.6 B)

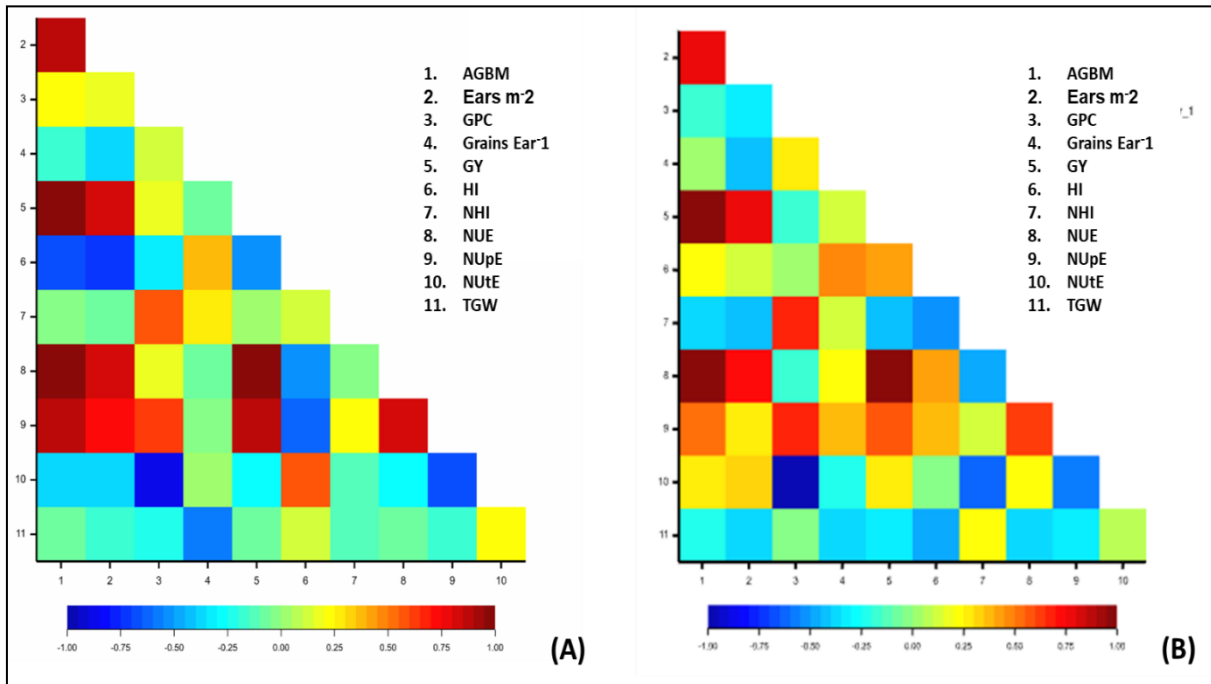


**Fig 4.6:** Correlation matrix of traits GY: Grain Yield ( $t\ ha^{-1}$ ), AGBM: Above-ground biomass ( $t\ ha^{-1}$ ), Ears  $m^{-2}$ , GPC: Grain Protein Content (%), Grains  $Ear^{-1}$ , HI: Harvest Index, NHI: Nitrogen Harvest Index, NUE, NUpE: Nitrogen-Uptake Efficiency ( $kg\ AGN\ kg^{-1}\ N$ ), NUE: Nitrogen-Use Efficiency ( $kg\ Grain\ DM\ kg^{-1}\ N$ ), NUtE: Nitrogen-Utilisation Efficiency ( $kg\ DM\ kg^{-1}\ N$ ) and TGW: Thousand Grain Weight (g) at (A) high N ( $200\ kg\ ha^{-1}$ ) (B) Low N ( $50\ kg\ ha^{-1}$ ) conditions. These values represent the mean across 2020 and 2021.

## 4.4 Discussion

The above results help understand the genetic variation occurring in NUE and related components as well the influence on physiological parameters in response to varying N supply. Further, the associations with the NUE components, biomass, Hland yield components under contrasting N conditions can be assessed and the implications for breeding for improved NUE in wheat cultivars.

### 4.4.1 Grain yield and Above-ground biomass performance of NILs under varying N condition

The variations in grain yield (GY) were distinctly seen among the 19 genotypes in the 2020 experiment, the parents Paragon and Robigus demonstrated highest GY of 4.82 and 5.08 t ha<sup>-1</sup>, respectively. Since Paragon and Robigus are adapted cultivars, high GY was expected in these two lines compared to the unadapted landrace- and synthetic-derived lines. Therefore, apart from deriving a comparison between the NILs with their respective parent, the variations between the Paragon and Watkin alleles for the QTLs was also observed. Across the years, QTLs AGDM (PW141-10-Q7D-AGDM-W, 4.59 t ha<sup>-1</sup>) and COMSTRW (PW292-8-Q3A-COMSTR-W, 4.80 t ha<sup>-1</sup>) have also shown relatively high GY compared to other NILs. The PW141-10-Q7D-AGDM-W showed high GY than the Paragon allele under LN in 2020. In 2021, GY was slightly lower under LN conditions than HN conditions and the GY value was also relatively low. This was likely a result of delay in the spring sowing in March month of 2021. Also, there was a relatively high soil mineral N content in the 2021 site (88 kg N ha<sup>-1</sup> N). Under LN conditions, a cumulative N of >135 kg N ha<sup>-1</sup> of N was available to the plant which may have reduced differences in GY compared to the HN treatment. This led to reduced NUE and reduced GY in that year. Additionally, lack of rain at pre-anthesis stage resulted in reduced N uptake in both the N treatments.

In case of Above-ground biomass, a similar trend was observed in 2020 across all the 19 NILs. The parents Paragon and Robigus again demonstrated high AGDM of 8.35 and 8.79 t ha<sup>-1</sup> respectively, as expected. Additionally, the AGDM was notably higher under LN conditions than HN conditions for most of the genotypes. The QTLs COMSTRW (PW292-8-Q3A-COMSTR-W, 8.25 t ha<sup>-1</sup>; PW292-19-Q3A-COMSTR-P, 8.08 t ha<sup>-1</sup>) and AGDM (PW729-1-Q6B-AGDM-W, 7.84 t ha<sup>-1</sup>) showed high AGDM, comparative to Paragon, and compared to respective Paragon alleles under LN conditions. The lines PW292-18-Q4B-GFPTT-P and PW292-7-Q3A-

COMSTR-W showed higher biomass HN conditions than LN conditions partly due to high NUtE.

Results in 2021 showed a trend for lower AGDM under LN conditions than HN conditions in all the genotypes. The small difference is again likely due to difference in relatively high soil mineral N content. However, the mean of the two years did not show an overall increase in AGDM under HN (5.39 t ha<sup>-1</sup>) compared to LN (5.51 t ha<sup>-1</sup>). The genotype effect, and Year effect, was significant.

The response of GY to LN conditions is associated with genotype and year components and possibly their interaction as well. Other studies have also showed the correlation of grain yield with year and cultivar (Moradi *et al.*, 2022). The high GY in parent lines, Robigus and Paragon, as well as the lines PW141-10-Q7D-AGDM-W and PW292-8-Q3A-COMSTR-W was associated with high NUpE and NUE. As can be seen in correlation matrix and the regression analysis, the association between GY and NUE, and GY and NUpE was highly significant ( $p < 0.001$ ) with positive correlation under both HN and LN conditions. Whereas the correlations with NUtE were much weaker. The present study showed that genetic variation in GY was associated strongly ( $p < 0.001$ ) with AGBM at all sites under both LN and HN conditions; and not associated with HI.

Previous studies have demonstrated that GY and GPC have an inversely proportional relationship (Triboi *et al.*, 2006; Haile *et al.*, 2012; Gaju *et al.*, 2011). This is attributed to dilution of protein at high yield and variation in accumulation rate of proteins during grain filling (de Oliveira Silva *et al.*, 2020). In the present study, however, although negative slopes were observed between GPC and GY under LN and HN conditions these slopes were not statistically significant. NHI is generally observed to have an inverse relationship with GY and NUE but a positive association with GPC (Hawkesford, 2012). In the present study, NHI showed a positive association with GY under HN but no association under LN.

#### **4.4.2 Genetic variation in NUE in relation to NUpE and NUtE components**

Genetic variation in NUE was observed amongst the genotypes under both LN and HN conditions. As expected NUE was greater under low N conditions than under HN conditions. However, it was observed that while the NUE followed a similar trend across the two years NUE was reduced in 2021 as compared to 2020. Since the soil type was consistent in the 2

years, the soil mineral N content which varied across years might partly explain this variation in the two years.

In the case of N-utilisation efficiency, overall, there was no significant effect of N treatment. However, the NUpE was enhanced under LN (1.43 kg AGN kg<sup>-1</sup> N) than HN (0.45 kg AGN kg<sup>-1</sup> N), as it was for the two-year mean: LN (0.86 kg AGN kg<sup>-1</sup> N) as compared to HN (0.33 kg AGN kg<sup>-1</sup> N). A similar pattern was observed (Gaju *et al.*, 2011) wherein under LN conditions the NUE, NUtE and NUpE are significantly higher than HN conditions.

The present study demonstrated that genetic variation in NUE was more closely associated with NUpE than NUtE. The correlation matrix also corroborates the finding as NUE and NUpE under both HN and LN; but for NUE and NUtE showed no association. Similar findings have been recorded in previous studies wherein association of NUE to NUpE at varying N conditions was stronger than that of NUE and NUtE (Le *et al.*, 2000; Barraclough *et al.*, 2010; Gaju *et al.*, 2011; Xu *et al.*, 2012; Liang *et al.*, 2014; Han *et al.*, 2015; Monostori *et al.*, 2017). However, some studies under high N conditions found NUtE was more strongly correlated with NUE than NUpE (Monostori *et al.*, 2017).

The highest NUE recorded between both the years was in 2020 in the line PW292-8-Q3A-COMSTR-W (52.06 kg Grain DM kg<sup>-1</sup> N) among the PxW lines. Among the SHW lines, the parent Robigus had highest NUE of 55.11 kg Grain DM kg<sup>-1</sup> N. Additionally, the highest NUpE was also found to be in the PxW line PW292-8-Q3A-COMSTR-W (1.67 kg AGN kg<sup>-1</sup> N) and in the SHW SEL 63 (1.78 kg AGN kg<sup>-1</sup> N). Incidentally, the highest NUtE was also found to be in the NILS PxW line PW292-8-Q3A-COMSTR-W of 46.68 kg DM kg N<sup>-1</sup> and in the SHW line SEL53 with NUtE of 47.73 kg DM kg N<sup>-1</sup>. These cultivars demonstrated higher absolute values than their parents, Paragon and Robigus (although differences were not statistically significant), which suggests some potential for improved N status.

Across the years, a significant correlation was seen between NHI and NUtE as well as between GPC and NUtE amongst the genotypes under HN and LN conditions. A genotype having a high NHI and a low GPC should have a high NUtE (Hawkesford and Riche, 2020). The NHI is highly dependent on the total amount of grain produced and the N concentration; therefore, enhancing the HI would subsequently elevate NHI, grain N uptake and NUE (Chakwizira *et al.*, 2016). Since most of the N is mobilized from canopy to the grain during grain filling; very

minute amount remains in the straw for recovery. Thereby, in some cases a high NHI may be associated with more rapid canopy senescence and lower canopy photosynthesis during grain filling and grain yield (Hawkesford, 2017b).

#### **4.5 Summary**

The screening experiment in 2018-2019 with 66 genotypes at two sites helped to shortlist 19 for further study in 2020 and 2021. These experiments at the RRes site, then helped to shortlist 5 genotypes for a RNAseq-based transcriptomics field study. As one of the objectives of the present study is to identify novel candidate genes and associated markers for NUE and related traits the following five lines were shortlisted, which includes NILs for three QTLs with Watkins alleles for above-ground dry matter (PW141-10-Q7D-AGDM-W), Grain Yield (PW468-1-Q5A-COMGRWT-W), Straw Yield (PW292-1-Q3A-COMSTR-W), the Paragon parent and one synthetic hexaploid-derived wheat line. The three NILs were shortlisted as they showed significant correlation with NUE and NUE traits. Additionally, these three NILs showed high values for NHI, NUpE, GPC and NUtE traits when compared with the NIL with the corresponding Paragon allele. Additionally, as the genetic variation for these traits might be due to Watkins landrace alleles, the three lines may represent novel variation. Since, Paragon was used as background line to generate P X W crosses, 87.5% of its background is added by the Paragon cultivar. Hence Paragon would be used to compare differential gene expression of W allele lines. For PxW lines, we will have two levels of comparison for differential expression gene analysis, viz, comparison with high and low N treatment, and comparing Watkin allele with Paragon allele. For synthetic line, SEL58, there will be only one level of comparison, i.e., HN and LN condition as adding Robigus parent line would affect the cost effectiveness of the RNAseq-based transcriptomics studies. Therefore, five genotypes were selected to perform the RNAseq study.

**Table 4.8:** 5 Shortlisted NILs and criteria used for selection

Sr No	NILs	Trait /Background	Rationale for Selection
1	PW141-10-Q7D-AGDM-W (Above-ground Dry Matter QTL on chromosome 7D)	Above-ground matter (W allele) dry	↑NUpE, ↑NUE, ↓NUE, ↑GY, ↑AGBM, ↑HI, ↑GPC and ↑NHI as compared to corresponding Paragon allele line
2	PW468-1-Q5A-COMGRWT-W (Combine Grain Weight i.e., Grain Yield QTL on chromosome 5A)	Grain Yield (W allele)	↑NUE, ↑NUE, ↑GY, ↑AGBM, ↑HI, ↓GPC and ↑NHI as compared to corresponding Paragon allele line
3	PW292-1-Q3A-COMSTR-W (Combine Straw Weight i.e., Straw Yield QTL on chromosome 3A)	Straw Yield (W allele)	↑GY, ↑AGBM, ↓GPC and ↓NHI as compared to corresponding Paragon allele line
4	Paragon	Parental Line (elite cultivar)	Parental control cultivar
5	SEL58	Synthetic Hexaploid Wheat line	↑NUE, ↓NUpE, ↑NUE, ↑GY, ↑AGBM and ↓GPC comparing to other synthetic lines but lower than Robigus

## ***Chapter 5***

***RNA-Seq-based transcriptomic analyses of wheat near isogenic lines to identify candidate genes for Nitrogen Use Efficiency and related traits***



## 5.1 Introduction

Nitrogen (N) plays a key role in the overall metabolic system of the plant system including photosynthetic activity, leaf area production, assimilation rate and subsequently biomass and grain yield. The introduction of the Haber-Bosch process, which converts atmospheric nitrogen and hydrogen gases to ammonia also facilitated the global use of synthetic nitrogen fertilisers (Javed *et al.*, 2022). The global consumption of nitrogen-based fertilisers has increased exponentially during the second half of the 20th century to 112.5 million tons in 2015 and 118.2 million tons in 2019 and is estimated to escalate to 7.9-10.5 billion tons by the year 2050 (Zhang *et al.*, 2015). The use of N fertilisers is of major concerns worldwide both from an economic and environmental point of view as the nitrogen fertiliser prices have increased. The growing demand and use of N fertilisers comes with the added cost of increased cultivation expenses, reduced soil fertility and environmental pollution. Of the total N fertilisers applied, only 30-40% are on average actually absorbed by the plant while the rest of 60% is lost in groundwater and atmosphere which can cause serious threats to the environment (Zhang *et al.*, 2021).

Nitrogen-use efficiency (NUE) which gives an estimation of the yield of grain per unit of N available to the crop from the soil and N fertilisers consists of two major components: nitrogen uptake efficiency (NUpE) and nitrogen utilisation efficiency (NUtE). These components define the efficiency of uptake of N and efficiency of assimilation and remobilisation of N, respectively (Han *et al.*, 2015). The genetic variation in these components is influenced by underlying physiological traits like root system architecture affecting N uptake at anthesis, canopy and leaf photosynthesis, N remobilisation and leaf senescence and post-anthesis N uptake (Hawkesford, 2012). While N fertilisers have been reported to enhance the NUE in plants, it is important to consider the optimum usage of N fertilisers as excessive fertiliser use can decrease the NUE as well (Javed *et al.*, 2022). On the other hand, applying less or no fertilisers would inevitably deplete the soil mineral reserve causing non-sustainable yields and erratic NUE estimation (Hawkesford, 2014). Therefore, the development of genotypes with enhanced NUE is required.

Wheat is one of the three major staple crops together with rice and maize consumed worldwide and the demand is estimated to double by 2050 (Semenov *et al.*, 2007). The global wheat land area is approximately 240 million ha (Martínez-Moreno *et al.*, 2022) with 774

million tons produced in 2021. However, the production is expected to decrease by 0.8% in 2022 (Collier, 2022) which drives the need for enhancement of NUE for better crop yield. In wheat, the NUE is estimated to be 33 kg grain DM per kg N supply which indicates a tremendous inefficiency and requirement for improvement through plant breeding (Hawkesford, 2017b).

NUE is a complex trait influenced by several physiological factors. In addition, the underlying molecular mechanisms regulating genetic variation in NUE are also complex and belong to a highly coordinated metabolic pathway. Genome-wide expression studies are an effective means to unravel these mechanisms (Zhang *et al.*, 2021). RNA-sequencing (RNA-seq) studies have been carried out in crop systems for comprehending the NUE mechanisms at the transcriptome level and identifying candidate genes involved in the regulatory network (Alvarez *et al.*, 2012). RNA-seq gives a more systematic overview of the transcript levels. Transcriptome analysis has been carried out in wheat cultivars to determine differentially expressed genes (DEGs) upregulated or downregulated during high NUE and low NUE and under varying N conditions (Sinha *et al.*, 2018; Wang *et al.*, 2019; Sultana *et al.*, 2020). These transcriptomics studies identified genes involved in photosynthesis, carbon and N metabolism which are directly associated with NUE. DEGs identified through RNA-seq studies in leaf, stem, flag leaf and spike tissues under chronic N starvation during grain filling stage in durum wheat were found to be related to N and carbon metabolism, N assimilation, photosynthesis as well as N transporters (Curci *et al.*, 2017) Zhang *et al.* (2021) performed transcriptomic profiling in two near-isogenic lines (NILs) (high NUE and low NUE) of flag leaves at anthesis under normal N conditions. The study revealed 7023 DEGs and genes belonging to Glutamine synthetase/glutamate synthase (GS and GOGAT) enzyme families, and a sub-set of transcription factors. The mechanism of NUE was found to be associated with GS/GOGAT cycle of N assimilation, photosynthetic assimilation and involvement of genes related to glycolysis, tricarboxylic acid cycle (TCA) and pentose phosphate pathway (PPP) cycle (Zhang *et al.*, 2021).

In this study, RNA-sequencing based transcriptomics approach was undertaken to investigate transcript profiling of near-isogenic lines derived from crosses between landraces and spring wheat cultivar Paragon, and between a synthetic hexaploid wheat line and winter wheat Robigus, with the flag leaf at the post-anthesis stage to identify candidate genes responsible for NUE. Additionally, transcript profiling of synthetic hexaploid wheat line of the flag leaf at

the post anthesis stage was also carried out to identify candidate genes responsible traits like stay green associated with NUE. This study was carried out in the field under two nitrogen treatments to analyse the gene expression patterns.

## 5.2 Materials and Methods

### 5.2.1 Field conditions and plant material sampling

The wheat near-isogenic lines (NILs) derived from landraces × elite cultivar crosses were a sub-set from a field experiment at Rothamsted Research, Harpenden, Hertfordshire (51° 48' 19.79" N 0° 21' 11.39" E) in 2021. These NILs contained QTLs identified for NUE-related traits like above-ground dry matter (AGDM), grain yield and straw yield. The soil type at field experiment site was a silty clay loam. The field experiment used a randomised block design with plot size of 4.15 x 1.8 m and three replicates of each NILs. Two different N treatments were given viz. N1 (50 kg ha<sup>-1</sup>) and N2 (200 kg ha<sup>-1</sup>) (Table 5.1).

**Table 5.1:** Details of the germplasm used for RNAseq experiments; nitrogen treatment (N1 (50 kg ha<sup>-1</sup>) and N2 (200 kg ha<sup>-1</sup>)), Group, Line accession and trait and background.

Treatment	Group	Genotype/QTL	Trait/Background
N1	G2	PW141-58-7-10-Q7D-AGDM-W	Above-ground dry matter
N2	G6	PW141-58-7-10-Q7D-AGDM-W	Above-ground dry matter
N1	G4	PW468-84-4-1-Q5A-COMGRWT-W	Grain Yield
N2	G9	PW468-84-4-1-Q5A-COMGRWT-W	Grain Yield
N1	G5	PW292-22-9-1-Q3A-COMSTR-W	Straw Yield
N2	G7	PW292-22-9-1-Q3A-COMSTR-W	Straw Yield
N1	G3	Paragon	Paragon Elite cultivar
N2	G8	Paragon	Paragon Elite cultivar
N1	G1	SEL58	Synthetic Hexaploid wheat
N2	G10	SEL58	Synthetic Hexaploid wheat

### 5.2.2 Growth measurements and harvest analysis

The plant height was measured manually. The visual flag-leaf senescence score was recorded every 3-4 days from GS71 to GS93 (Zadock *et al.*, 1974). The lodging score of all the lines was done at GS88. At GS94 stage, samples of 100 fertile shoots per plot was collected for analysis by cutting at ground level. Growth analysis to calculate the Nitrogen (N), N-Use Efficiency (NUE), N-Uptake Efficiency (NUpE) and N Utilisation Efficiency (NUtE), N uptake and partitioning (straw, grain) the detailed partitioning analysis as described in Chapter 4.

### 5.2.3 RNA seq experiment

The main shoot (flag leaf) was tagged at anthesis and collected at 12 days post-anthesis. The total RNA of 30 samples (5 NILs \* 2 N treatments \* 3 replicate) were isolated by using the Qiagen RNAeasy kit method. The isolated RNA was purified by using the Sodium Acetate (NaoAc) precipitation Method. The concentration of purified RNA was measured by NanoDrop™ 2000/2000c Spectrophotometer. The RNA samples with the ratio of absorbance at 260 nm and 280 nm is used to assess the purity of RNA and samples with ratio ~2.0 were run on 1% agarose gel to visualise any degradation and presence of DNA contamination.

The purified RNA samples were submitted to Novogene UK Pvt Ltd, Cambridge for Illumina next gen RNAseq Pair End 150bps (12 G raw data per sample). The samples were sequenced and analysed at the service provider facility.

Raw data (raw reads) of FASTQ format were firstly processed through Perl scripts. In this step, clean data (clean reads) were obtained by removing reads containing adapter, reads containing ploy-N and low-quality reads from raw data. At the same time, the clean data of Q20, Q30 and GC content were calculated. All the downstream analyses were based on the clean data with high quality.

### 5.2.4 Reads mapping to the reference genome

Reference genome and gene model annotation files were downloaded from NCBI. ([https://ftp.ncbi.nlm.nih.gov/genomes/all/GCF/018/294/505/GCF\\_018294505.1\\_IWGSC\\_CS\\_RefSeq\\_v2.1/GCF\\_018294505.1\\_IWGSC\\_CS\\_RefSeq\\_v2.1\\_genomic.fna.gz](https://ftp.ncbi.nlm.nih.gov/genomes/all/GCF/018/294/505/GCF_018294505.1_IWGSC_CS_RefSeq_v2.1/GCF_018294505.1_IWGSC_CS_RefSeq_v2.1_genomic.fna.gz)) Index of the reference genome was built using Hisat2 v2.0.5 and paired-end clean reads were aligned to the reference genome using Hisat2 v2.0.5.

### 5.2.5 Differential gene expression analysis and quantification

The mapped reads of each sample were assembled by StringTie (v1.3.3b) (Mihaela Pertea et al. 2015) in a reference-based approach to predict the novel transcripts. The software featureCounts v1.5.0-p3 was used to count the read numbers mapped to each gene. The FPKM (fragments per kilo base per million reads mapped) of each gene was then calculated based on the length of the gene and reads count mapped to this gene.

Differential expression analysis of two conditions/groups (two biological replicates per condition) was performed using the DESeq2Rpackage (1.20.0). DESeq2 provide statistical

routines for determining differential expression in digital gene expression data using a model based on the negative binomial distribution. The resulting P-values were adjusted using the Benjamini and Hochberg's approach for controlling the false discovery rate (Benjamini and Hochberg, 1995). Genes with an adjusted P-value  $\leq 0.05$  found by DESeq2 were reassigned as differentially expressed (for edgeR without biological replicates). Prior to differential gene expression analysis, for each sequenced library, the read counts were adjusted by edgeR program package through one scaling normalised factor. Differential expression analysis of two conditions was performed using the edgeR R package (3.22.5). The P values were adjusted using the Benjamini and Hochberg method. Corrected P-value  $\leq 0.001$  and absolute fold change of  $> 2$  was set as the threshold for significantly differential expression.

#### **5.2.6 Gene Ontology analysis and KEGG enrichment analysis**

GO (Gene ontology) and KEGG (Kyoto Encyclopedia of Genes and Genomes) enrichment analysis of differentially expressed genes was performed. GO enrichment analysis of differentially expressed genes was implemented by the cluster Profiler R package, in which gene length bias was corrected. GO terms with corrected p-value less than 0.05 were considered significantly enriched by differential expressed genes. We used cluster Profiler R package to test the statistical enrichment of differential expression genes in KEGG pathways.

#### **5.2.7 Single Nucleotide Polymorphisms (SNP)**

SNP analysis GATK (v4.1.1.0) software was used to perform SNP calling. Raw vcf files were filtered with GATK standard filter method and other parameters (cluster:3; WindowSize:35; QD 30.0; DP < 10).

## 5.3 Results

### 5.3.1 Transcriptome Summary of NILs

#### 5.3.1.1 RNA-seq data quality and mapping statistics

A total of 700 Gb 150-bp paired end (PE) reads were generated through the Illumina NextSeq500 from 30 samples (5 NILs X 2 treatments X 3 replicates). On average, 85 million reads per sample were obtained after trimming the adapter sequences (Table 5.2). The clean read percentage was approximately 97 percent and GC percentage (53) was also above standard values for all the samples. For mapping the clean reads to reference genome, recently released wheat version v2.1

([https://ftp.ncbi.nlm.nih.gov/genomes/all/GCF/018/294/505/GCF\\_018294505.1\\_IWGC\\_CS\\_RefSeq\\_v2.1/GCF\\_018294505.1\\_IWGC\\_CS\\_RefSeq\\_v2.1\\_genomic.fna.gz](https://ftp.ncbi.nlm.nih.gov/genomes/all/GCF/018/294/505/GCF_018294505.1_IWGC_CS_RefSeq_v2.1/GCF_018294505.1_IWGC_CS_RefSeq_v2.1_genomic.fna.gz))

was used (Table 5.3). Variable percentage of read mapping was observed in each sample, with the average value being 87%.

**Table 5.2:** Quality control parameters of flag tissue RNA libraries of QTLs

Genotype (QTL Name)	Nitrogen Level	Raw Read No.	Clean reads	Clean Reads Percentage	GC%
Above-ground Dry Matter	Low	85403578.67	83636319.3	97.63	53.14
Above-ground Dry Matter	High	88232406.67	87178400	97.61	53.84
Combine Grain Weight	Low	93114947.33	92046052.7	97.33	53.91
Combine Grain Weight	High	92361702.67	92167960.7	97.46	53.52
Combined straw weight	Low	91058926	90874866.7	97.45	54.06
Combined straw weight	High	83975781.33	83809997.3	97.65	54.19
Paragon	Low	86578108	84679526	97.72	54.10
Paragon	High	86103120	84179380	97.69	53.00

**Table 5.3:** Mapping statistics of RNAseq data

Genotype (QTL Name)	Nitrogen treatment	Total Mapped (%)	Perfect match (%)	Unmapped (%)
Above-ground Dry Matter	Low	89.11	80.17	5.42
Above-ground Dry Matter	High	88.30	77.44	6.25
Combine Grain Weight	Low	88.17	78.01	6.26
Combine Grain Weight	High	88.75	78.17	6.11
Combined straw weight	Low	87.64	77.04	5.97
Combined straw weight	High	88.27	79.46	5.32
Paragon	Low	88.09	76.91	6.57
Paragon	High	88.61	78.95	5.94

### 5.3.1.2 Transcriptome profiles of the NILs in response to high and low N application

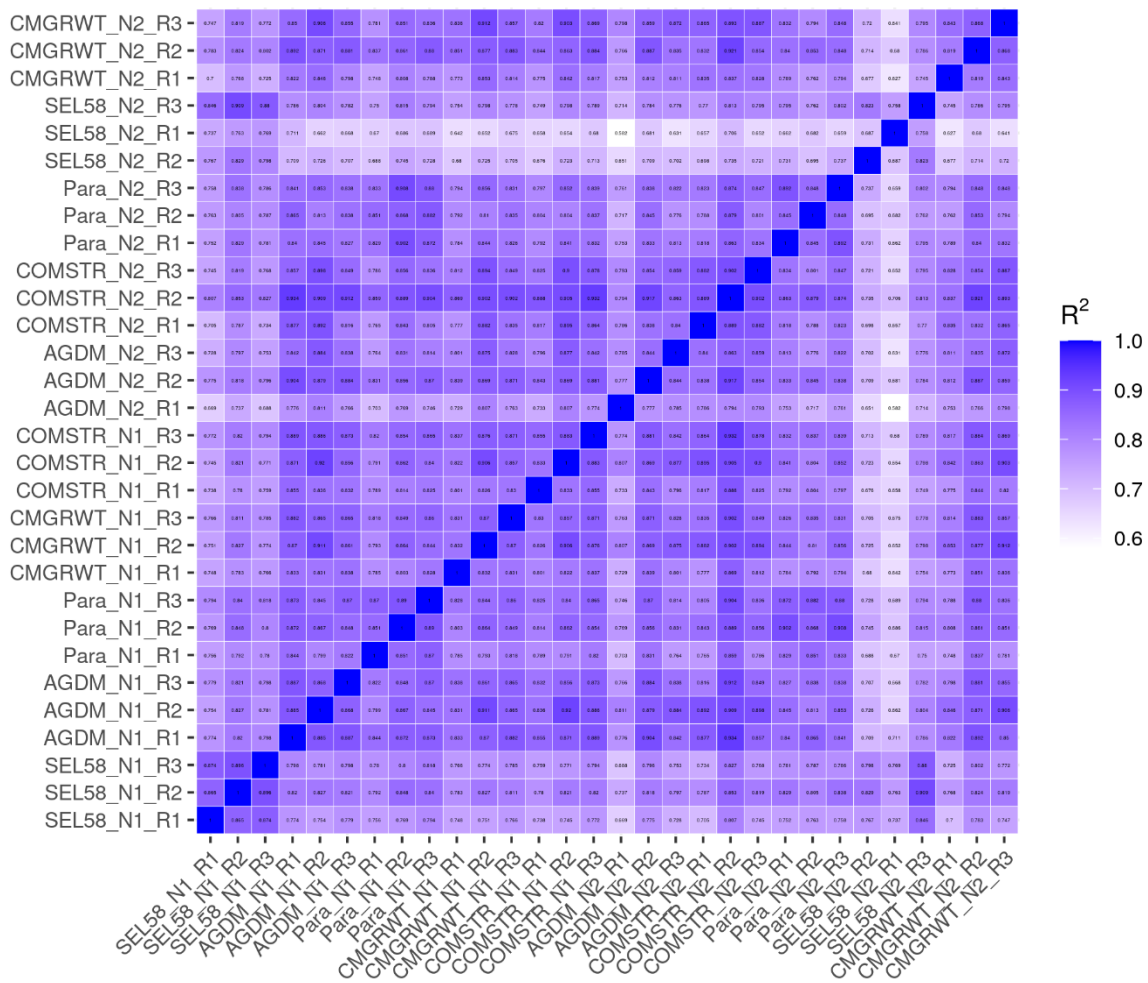


**Fig 5.1:** Co-relation matrix depicts the Pearson co-relation between 30 samples; 5 different genotypes including one synthetic hexaploid-derived wheat line, 3 landrace-derived near-isogenic lines and Paragon (a parental cultivar) under 2 nitrogen treatments (N1: low N treatment (50 kg ha<sup>-1</sup>), N2: High N treatment (200 kg ha<sup>-1</sup>) with 3 technical replicates (R1, R2 and R3).

The transcript profile of RNA seq data was analysed by calculating the read fragments per kilo base per million reads mapped (FPKM). We used FPKM to standardise the gene expression level and the Pearson correlation coefficients show that the data was highly reproducible (Fig 5.1). The Pearson coefficient for grain yield, AGDM and straw yield, as well as Paragon were evidently high with R<sup>2</sup>>0.8 implying towards high correlation while that of synthetic hexaploid is low R<sup>2</sup><0.6 indicating variables with low correlation.

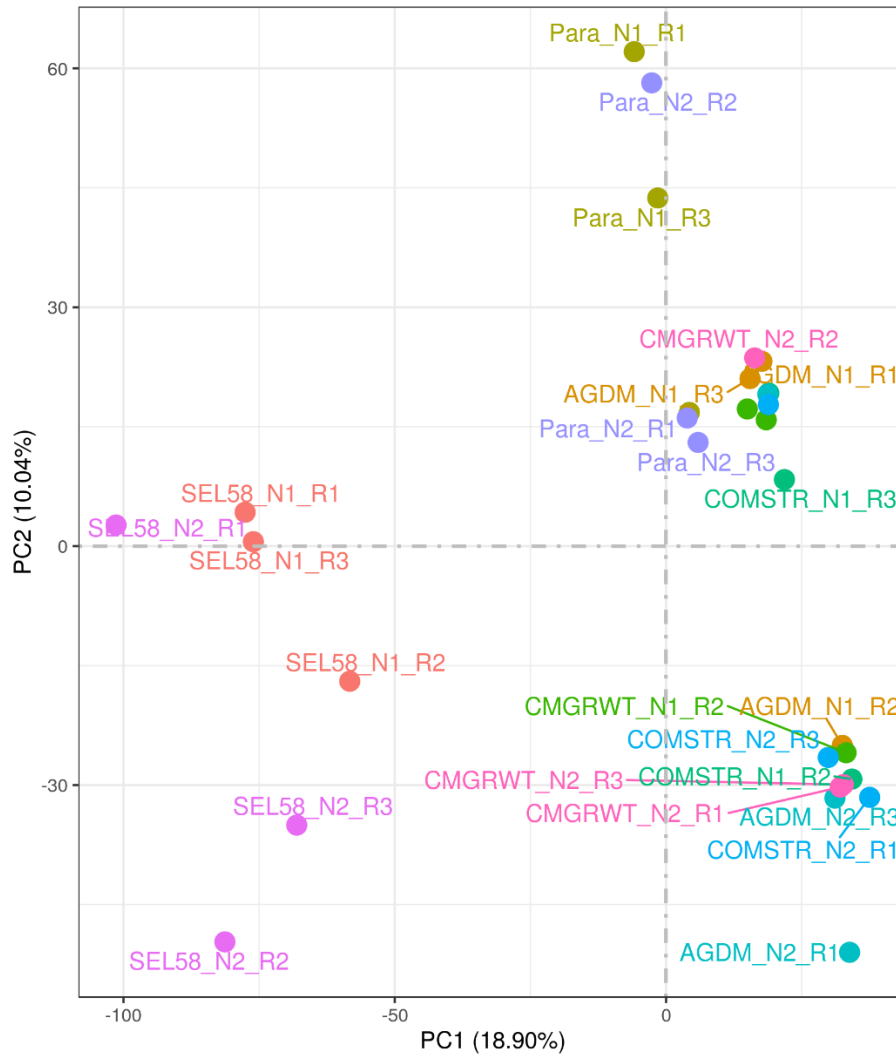


**Fig 5.2:** Principal component analysis of 30 samples from 5 different genotypes including one synthetic hexaploid-derived wheat line, 3 landrace-derived near-isogenic lines and Paragon (a parental cultivar) under 2 nitrogen treatments (N1: low N treatment (50 kg ha<sup>-1</sup>), N2: High N treatment (200 kg ha<sup>-1</sup>) with 3 technical replicates (R1, R2 and R3). Above-ground Dry Matter (AGDM), Combine Grain Weight (CMGRWT), Combined straw weight (COMSTR), Paragon (Para) and Synthetic Hexaploid line 58 (SEL58).

To evaluate intergroup difference and the intragroup sample duplication principal component analysis (PCA) was carried out on the gene expression value (FPKM) of all samples as shown in Fig 5.2. The intergroup variability is evident with the dispersed placement of samples such as Paragon with straw yield and AGDM. Additionally, the intragroup similarity can also be seen in case of SEL58\_N1 and SEL58\_N2, for example which appear to be clustered together (Fig 5.2). However, some variability can be seen within intragroup clusters as well. The gene



expression values were observed in clusters corresponding to the QTLs with their replicates. The values were therefore dispersed among the different QTL groups.

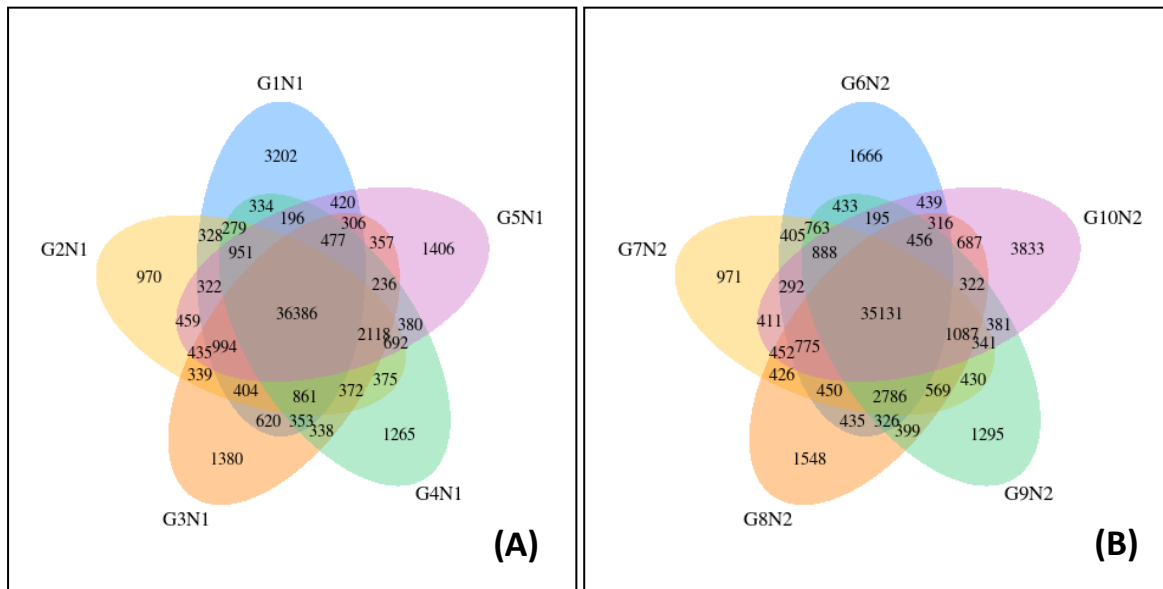


**Fig 5.3:** Venn diagram showing differential expressed genes across 5 different genotypes including one synthetic hexaploid-derived wheat line, 3 landrace-derived near-isogenic lines and Paragon (a parental cultivar) under 2 nitrogen treatments (N1: low N treatment (50 kg ha<sup>-1</sup>), N2: High N treatment (200 kg ha<sup>-1</sup>)) with 3 technical replicates (R1, R2 and R3). Two groups (G1-G5 and G6-G10) are formed for comparison among the two nitrogen treatments.

The co-expression Venn diagram was also analysed which gives the number of genes uniquely expressed within each sample along with the overlapping regions showing the number of genes that are co-expressed in two or more samples. In our study, the gene expression was studied for each sample under low (Fig 5.3 A) and high (Fig 5.3B) nitrogen levels. Under low N, a total of 36386 genes were expressed out of which the number of uniquely expressed genes were 3202 in G1N1, 1406 in G5N1, 1265 in G4N1, 1380 in G3N1 and 970 in G2N1 (Fig 5.3A). Likewise, under high N conditions, a total of 35131 genes were expressed in all the samples, with 1666 in G6N2, 3833 in G10N2, 1295 in G9N2, 1548 in G8N2 and 971 in G7N2 (Fig 5.3B).

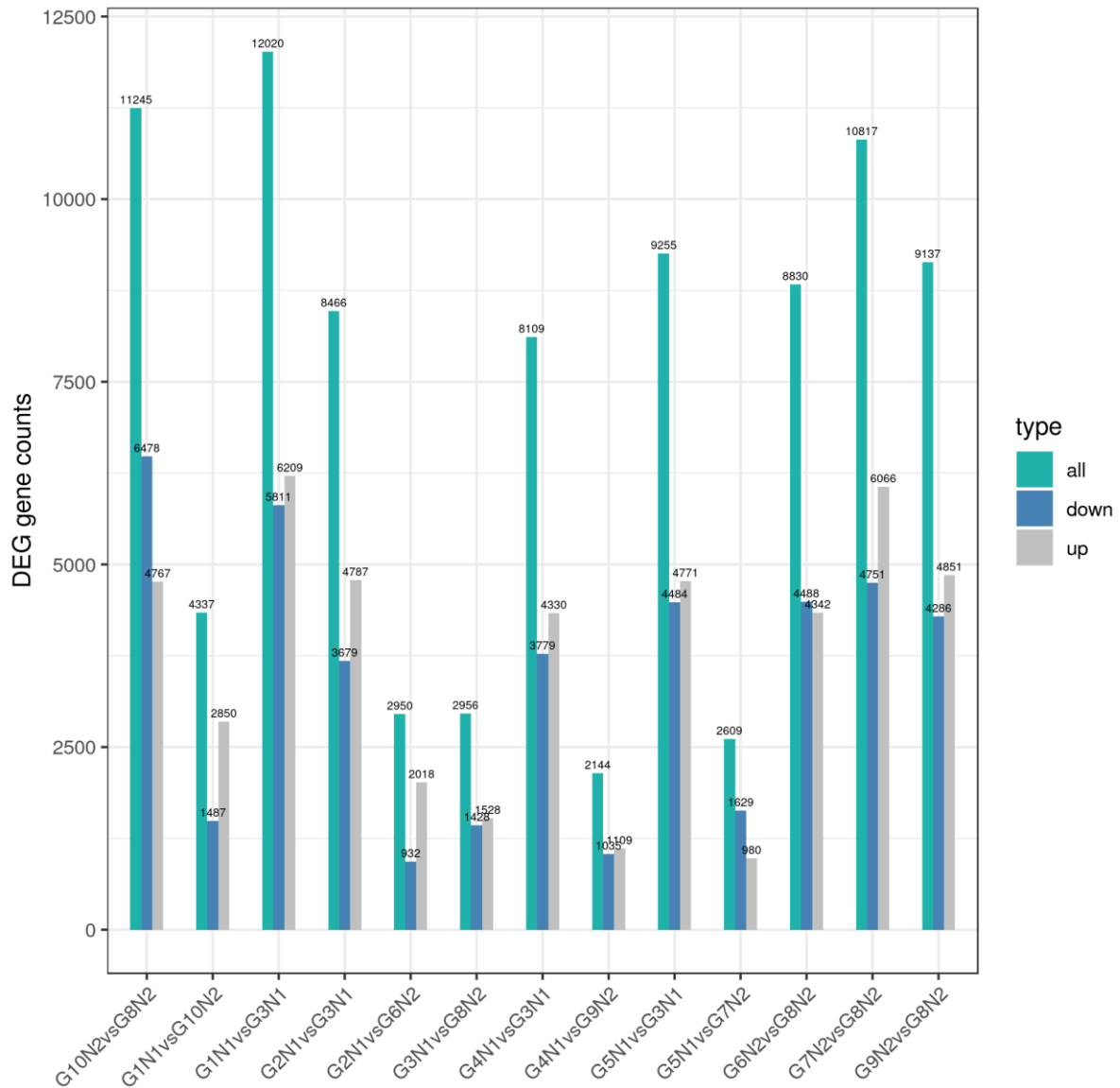


**Fig 5.4:** Bar chart representing differential expressed genes counts across 5 different genotypes including one synthetic hexaploid-derived wheat line, 3 landrace-derived near-isogenic lines and Paragon (a parental cultivar) under 2 nitrogen treatments (N1: low N treatment (50 kg ha<sup>-1</sup>), N2: High N treatment (200 kg ha<sup>-1</sup>) with 3 technical replicates (R1, R2 and R3). Two groups (G1-G5 and G6-G10) are formed for comparison among the two nitrogen treatments.

A cumulative representation of the total number of DEGs expressed along with those upregulated and downregulated for individual compare groups is shown Fig 5.4



### 5.3.2 Synthetic lines

#### 5.3.2.1 RNA-seq data quality and mapping statistics

A total of 79.84 Gb 150-bp paired end (PE) reads were generated through the Illumina NextSeq500 from 6 samples (1SEL 58-line X 2 Nitrogen treatments X 3 replicates). On average, 83 million reads per samples from low N treatment replicates and 94 million reads from high N treatment were obtained after trimming the adapter sequences (Table 5.4). The clean read percentage was approximately 99% and GC percentage was 53 also above standard values for all the samples. Q30 value (Phred values greater than 30 base number contain the percentage of total bases.  $[(\text{Base number of Phred value} > 30) / (\text{Total base number}) * 100]$  was 93 on an average which signifies the clean reads quality.

For mapping the clean reads to reference genome, recently released wheat version v2.1 ([https://ftp.ncbi.nlm.nih.gov/genomes/all/GCF/018/294/505/GCF\\_018294505.1\\_IWGSC\\_CS\\_RefSeq\\_v2.1/GCF\\_018294505.1\\_IWGSC\\_CS\\_RefSeq\\_v2.1\\_genomic.fna.gz](https://ftp.ncbi.nlm.nih.gov/genomes/all/GCF/018/294/505/GCF_018294505.1_IWGSC_CS_RefSeq_v2.1/GCF_018294505.1_IWGSC_CS_RefSeq_v2.1_genomic.fna.gz)) was used (Table 5.4). Variable percentage of read mapping was observed in each treatment, with the average value being 87.77%.

**Table 5.4:** Quality control parameters and mapping statistics of RNA-seq data of hexaploid wheat line high and low N conditions

Sample Name	Raw reads	Clean reads	Q30	GC %	Clean Reads %	Mapped Reads %	Uniquely Mapped Reads %
SEL58_N1_R1	79104498	78933044	92.75	55.36	99.78	86.64	79.36
SEL58_N1_R2	88080242	87918698	93.85	54.55	99.81	87.45	80.74
SEL58_N1_R3	82697346	82541156	93.48	54.8	99.81	87.3	80.22
SEL58_N2_R1	83379180	83184508	93.77	47.75	99.76	89.07	84.65
SEL58_N2_R2	80504026	80288650	94.08	54.18	99.73	89.13	82.81
SEL58_N2_R3	118440662	118150330	92.02	52.92	99.75	87.06	80.90

#### 5.3.2.2 Analysis of differentially expressed genes (DEGs)

A total of 86,636 genes were mapped of which 4337 genes were differentially expressed accounting for 5% of all these genes. In the present study involving SEL58, 2850 DEGs (65.71% of 4337) were upregulated and 1487 DEGs (34.28% of 4337) were downregulated. The volcano plot describes the fold change of gene expression and significant degree of results (Fig 5.6).

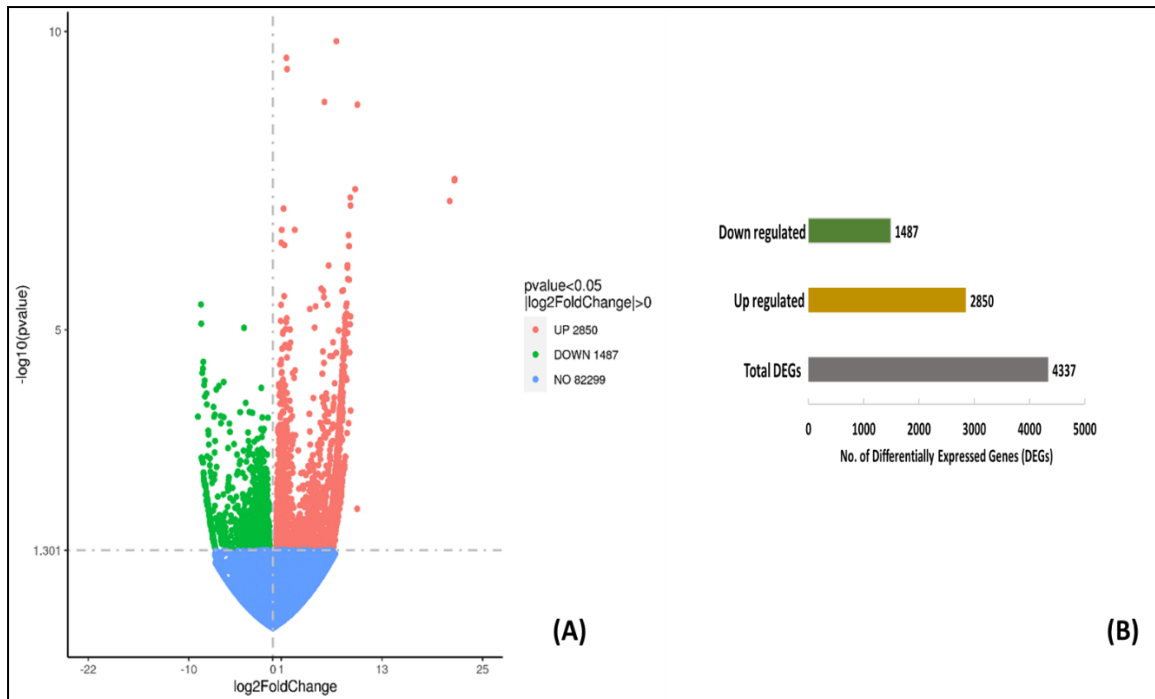


**Fig 5.6:** Details of differentially expressed genes (DEGs) (A) Volcano plot where the green colour indicates the upregulated DEGs, the red were downregulated DEGs, and the blue indicates the genes below threshold of  $-\log_{10}(\text{pvalue})$  1.3. (B) Bar chart showing significantly expressed DEGs where the green colour indicates the significantly down regulated DEGs, the red were up regulated DEGs, and the grey indicates the total DEGs.

### 5.3.2.3 GO and KEGG Analysis of DEGs in synthetic hexaploid line

Gene ontology (GO) enrichment analysis was carried out in order to determine the predominant biological functions of the identified DEGs (Fig 5.7 A). The primary GO terms with significant enrichment are shown in (Fig 5.7 B).

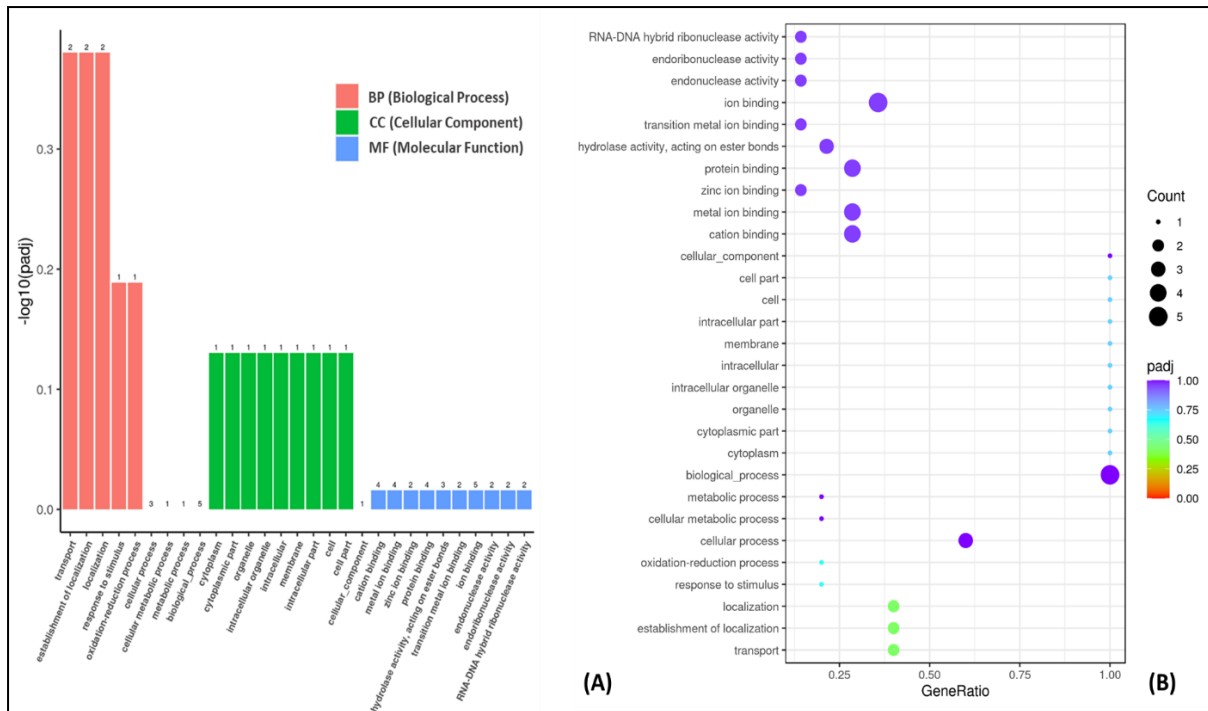


**Fig 5.7:** Gene ontology (GO) enrichment analysis ( $p < 0.05$ ) of synthetic hexaploid wheat (A) Bar chart where, the x-axis defines the name of GO terms while y-axis shows significantly enriched log base 10 padj-values. (B) Dot plot where, the x-axis indicates the gene ratio, the y-axis represents the name of the GO terms. The size of bubbles represent the number of DEGs in the corresponding GO terms, and the dot colour indicates the adjusted p value.

A total of 61 terms were annotated by GO enrichment analysis out of which 9 belonged to biological process (BP), 10 belonged to cellular component (CC) and 42 belonged to molecular function (MF). Among these, biological process (GO:0008150) and cellular process (GO:0009987) had the maximum number of genes, 5 and 3 respectively in BP; in CC category, all the components had 1 gene while in MF, molecular function (GO:0003674) and binding (GO:0005488) had maximum genes, 14 and 10 respectively.

The top GO terms with significant enrichment are depicted in Fig 5.7 (B). Among these, 15 terms were significantly enriched as can be seen through the padj value and purple shade dots. Over 11 terms are moderately enriched (blue shade dots) (Fig 5.7 B). In BP, transport (GO:0006810), establishment of localisation (GO:0051234) and localisation (GO:0051179) are the main terms. Among the CC, cellular component (GO:0005575) is the main term while in MF category, cation binding (GO:0043169), metal ion binding (GO:0046872), protein binding (GO:0005515) and ion binding (GO:0043167) are the main terms.

The biological functions of the DEGs were also explored in different metabolic pathways by mapping them to KEGG database. A total of 98 KEGG pathways were determined with 404 assigned DEGs. In the current study, significant enrichment of DEGs was observed in photosynthesis (tdc00195), carbon fixation in photosynthetic organisms (tdc00710), nitrogen metabolism (tdc00910), carbon metabolism (tdc01200) and biosynthesis of amino acids (tdc01230) (Fig 5.8).

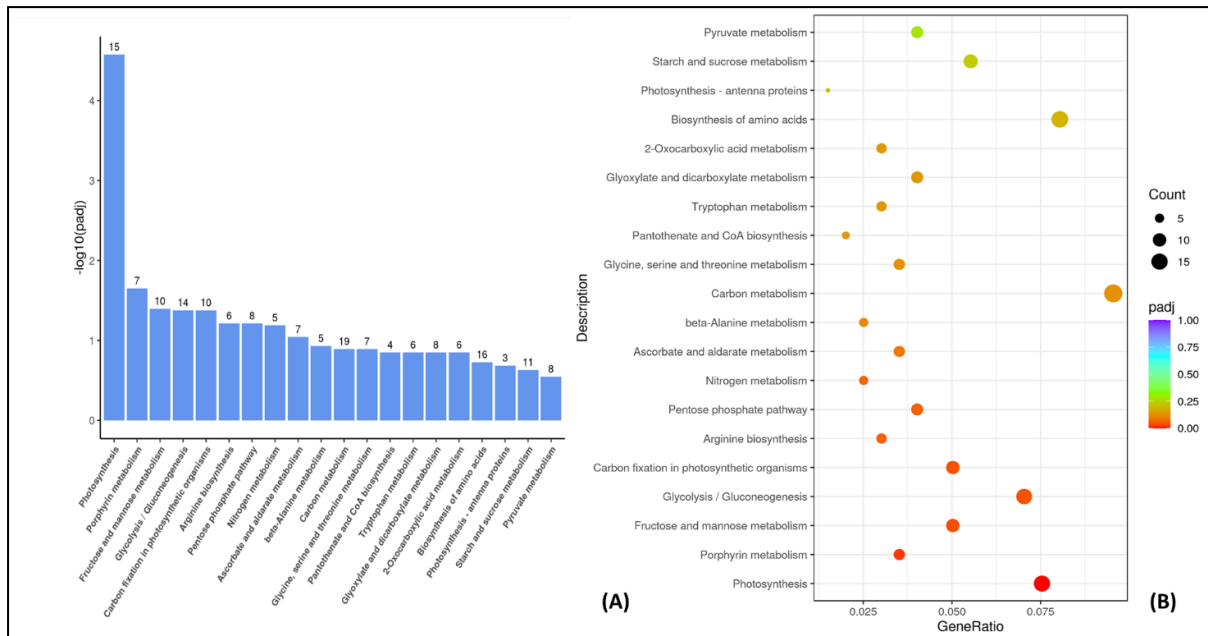


**Fig 5.8:** KEGG pathways DEGs enrichment analysis of synthetic hexaploid wheat (A) Bar chart where the x-axis indicates the x-axis defines the name of KEGG pathway while y-axis shows significantly enriched log base 10 p-adj values, the y-axis represents the name of the KEGG pathway. (B) Dot plot where, the size of bubbles represent the number of DEGs in the corresponding pathway, and the dot colour indicates the adjusted p-adj values.

In photosynthesis, out of 15 DEGs expressed, all 15 were seen to be upregulated. Similarly, 5 genes responsible for nitrogen metabolism were differentially expressed differentially among which all 5 showed upregulation. In the 10 differentially expressed genes associated with carbon fixation in photosynthetic organisms, 9 demonstrated upregulated transcript levels. 19 DEGs were found to be associated with carbon metabolism in the flag-leaves and 18 transcripts were upregulated. Finally, 15 genes were seen to be upregulated among the 16 genes which were differentially expressed during biosynthesis of amino acids.

### 5.3.3 P x W lines

#### 5.3.3.1 RNA-seq data quality and mapping statistics

A total of 80 Gb 150-bp paired end (PE) reads were generated through the Illumina NextSeq500 from 24 samples (4 lines X 2 Nitrogen treatments X 3 replicates). On average, 88 million reads per sample from low N treatment replicates and 87 million reads from high N treatment were obtained after trimming the adapter sequences (Table 5.5). The clean read percentage was approximately 97% and GC percentage was 53 also above standard values for all the samples.

**Table 5.5:** Quality control parameters and mapping statistics of RNA-seq data of PxW lines and Paragon at high and low N conditions

Sample Name	Raw reads	Clean reads	GC %	Clean Reads %	Mapped Reads %
G2_N1	85403578.67	83636319.3	53.14	97.63	89.11
G6_N2	88232406.67	87178400	53.84	97.61	88.30
G4_N1	93114947.33	92046052.7	53.91	97.33	88.17
G9_N2	92361702.67	92167960.7	53.52	97.46	88.75
G5_N1	91058926	90874866.7	54.06	97.45	87.64
G7_N2	83975781.33	83809997.3	54.19	97.65	88.27
G3_N1	86578108	84679526	54.10	97.72	88.09
G8_N2	86103120	84179380	53.00	97.69	88.61

#### 5.3.3.2 Analysis of differentially expressed genes (DEGs)

Among the PxW lines for the QTL AGDM (Above-ground dry matter) a total of 84,028 genes (Fig 5.9 A) were mapped of which 2950 DEGs were differentially expressed. 2018 DEGs were upregulated and 932 were seen to be downregulated which accounts for 68.4% and 31.5% of the total DEG respectively.



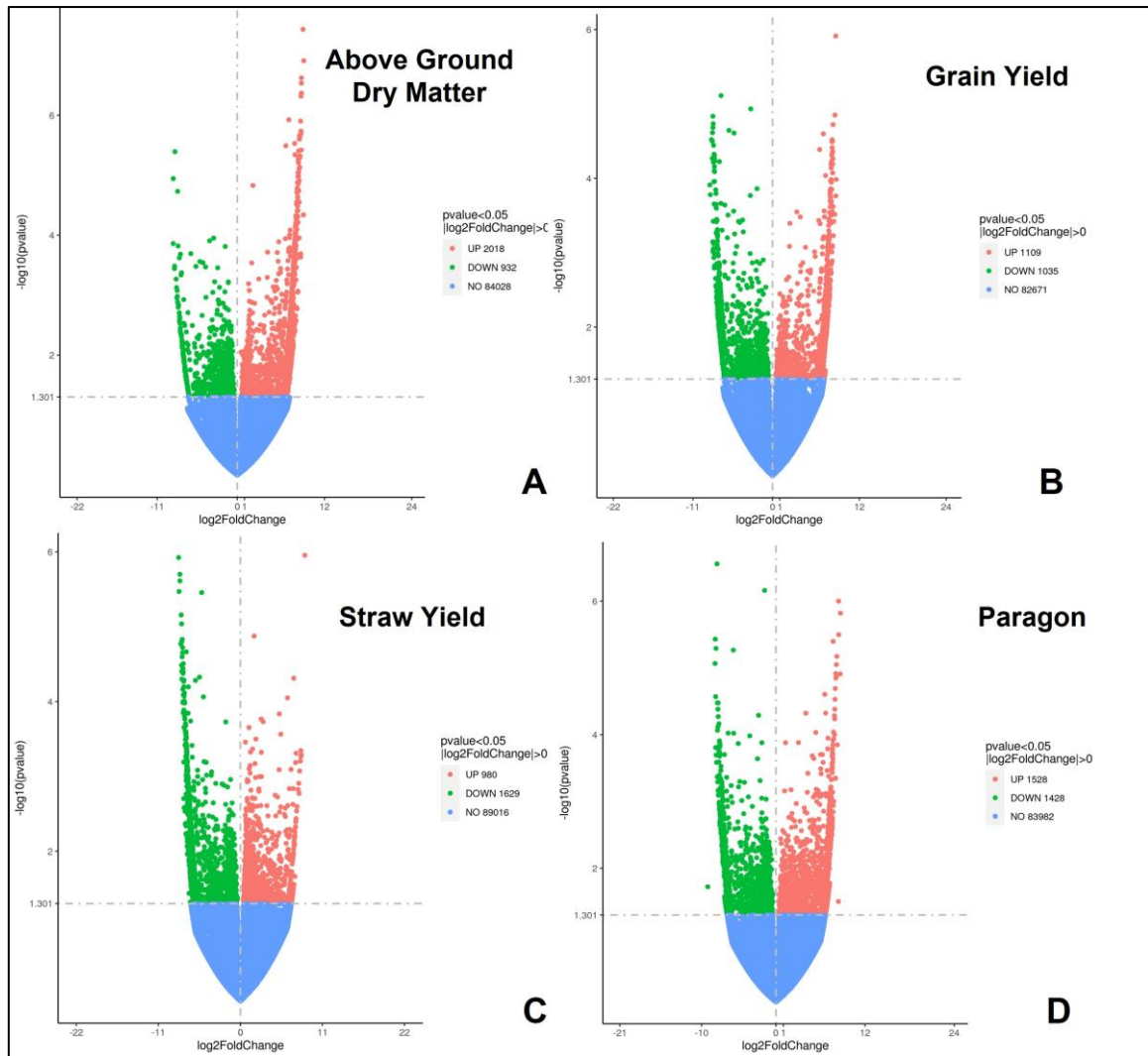


**Fig 5.9:** Volcano plot of Differentially expressed genes (DEGs) where the green colour indicates the upregulated DEGs, the red were downregulated DEGs, and the blue dots indicates the genes below threshold of  $-\log_{10}(\text{pvalue})$  1.3 for the QTLs (A) Above-ground dry matter (B) grain yield (C) straw yield and (D) parent Paragon line

Similarly, for the QTL GY (grain yield), the total number of genes was 82,671 of which 2144 were found to be DEGs (Fig 5.9 B). Among these, 1109 were upregulated DEGs (51.7%) and 1035 were downregulated DEGs (48.3%).

In the QTL straw yield, 89,016 genes were mapped of which 2609 DEGs were identified (Fig 5.9 C). Among these DEGs, 980 were found to be upregulated which accounts for 37.5% of the total; and 1629 DEGs were downregulated which is about 62.4%.

Finally, in the parent line Paragon, 83,982 genes were mapped (Fig 5.9 D) of which 2956 genes were differentially expressed accounting for 3.5% of all these genes. In the present study

involving Paragon, 1528 DEGs (51.7% of 2956) were upregulated and 1428 DEGs (48.3% of 2956) were downregulated.

The volcano plots depicted (Fig 5.9) represent the fold change in gene expression between the DEGs in each sample under N conditions.

### 5.3.3.3 GO Analysis of DEGs

The GO analysis depicts the gene properties primarily the biological functions of the identified DEGs in each QTL. From the GO enrichment analysis, the most significant 30 GO terms have been selected for display (Fig 5.10 A). The enrichment degree has been illustrated through colour shades wherein the darker shades are, the higher is the enrichment degree.

In the QTL for AGDM, a total of 94 terms were annotated by GO enrichment analysis out of which 39 belong to biological processes (BP), 12 belonged to cellular processes (CP) and the remaining 43 were from molecular function (MF). Among these, the maximum number of genes were from molecular function (GO:0003674) and binding (GO:0005488) consisting of 14 and 8 respectively. However, terms like catalytic activity (GO:0003824), biological processes (GO:0008150), metabolic processes (GO:0008152), nitrogen compound metabolic process (GO:0006807) and cellular nitrogen compound biosynthetic process (GO:0044271) organonitrogen compound metabolic process (GO:1901564) and cellular nitrogen compound metabolic process (GO:0034641) showed high number of genes ranging from 5-6. Among these, 10 GO terms were observed to be significantly enriched (purple shade) (Fig 5.10 B). In BP, organic cyclic compound biosynthetic process (GO:1901362) demonstrated high enrichment. In MF, heterocyclic compound binding (GO:1901363), nucleic acid binding (GO:0003676), transferase activity (GO:0016740), cation binding (GO:0043169) and DNA binding (GO:0003677) showed high levels of enrichment. In CC, moderate levels of enrichment were seen in cell part (GO:0044464), intracellular part (GO:0044424). Further, while terms like organonitrogen compound biosynthetic process (GO:1901566) and cellular nitrogen compound biosynthetic process (GO:0044271) showed low enrichment, they also had high number of genes annotated to these terms (Fig 5.10 B).

terms, and the dot colour indicates the adjusted p value which represents level of enrichment.

In the QTL for grain yield, a total of 41 terms were annotated by GO enrichment analysis out of which 28 belongs to BP and 13 belongs to MF. The maximum number of genes seen in BP (1) are for terms like cellular nitrogen compound metabolic process (GO:0034641), aromatic compound biosynthetic process (GO:0019438), heterocycle biosynthesis process (GO:0018130) (Fig 5.11 A). Further, in MF, maximum number of genes were observed in the

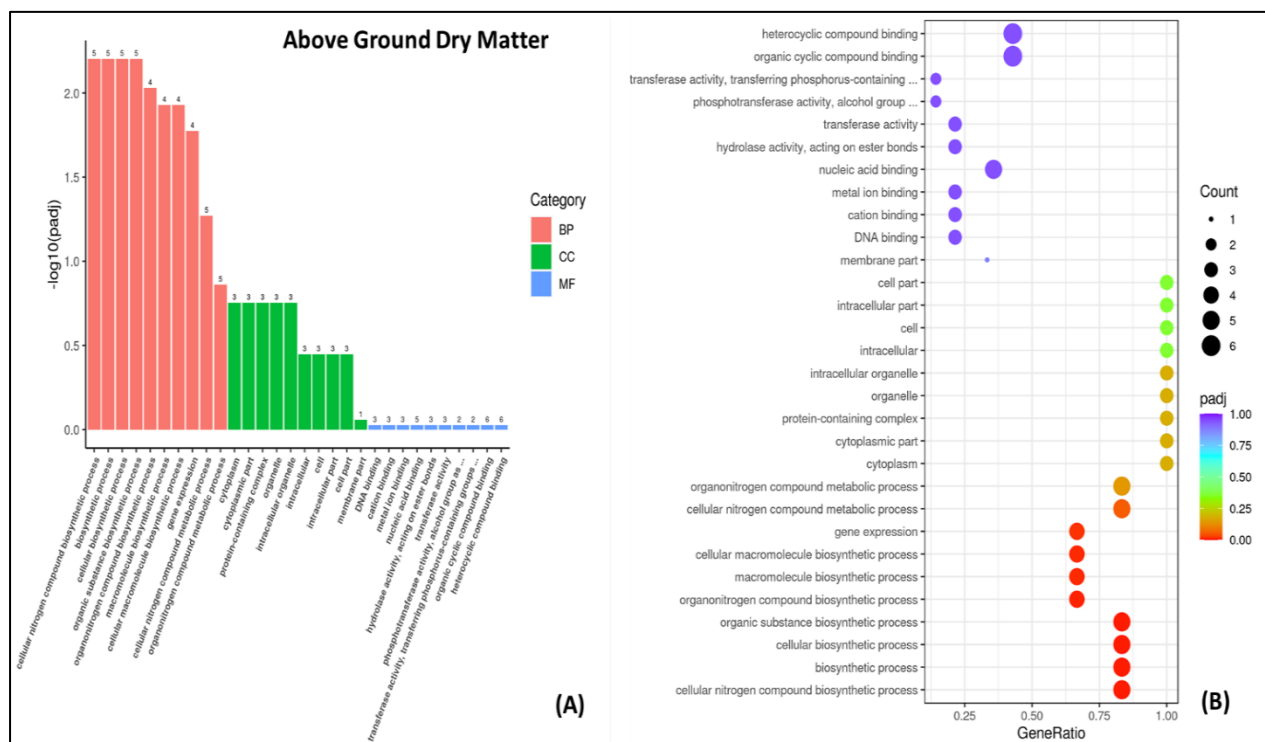


**Fig 5.10:** Gene ontology (GO) enrichment analysis (p<0.05) of QTL AGDM: (A) Bar chart where, the x-axis defines the name of GO terms while y-axis shows significantly enriched log base 10 padj-values and the most significant 30 terms have been depicted (B) Dot plot where, the x-axis indicates the gene ratio, the y-axis represents the name of the GO terms. The size of bubbles represents the number of DEGs in the corresponding GO.

terms binding (GO:0005488), DNA binding (GO:0003677), nucleic acid binding (GO:0003676) and protein binding (GO:0005515). Among these, organic cyclic compound binding (GO:0097159) belonging to MF showed highest enrichment while binding (GO:0005488), DNA binding (GO:0003677), nucleic acid binding (GO:0003676) and protein binding (GO:0005515) demonstrated high enrichment along with significant gene count. Apart from these, terms like aromatic compound biosynthetic process (GO:0019438), cellular nitrogen compound

metabolic process (GO:0034641), organic cyclic compound biosynthesis process (GO:1901362) showed high enrichment levels but with low gene count (Fig 5.11 B)

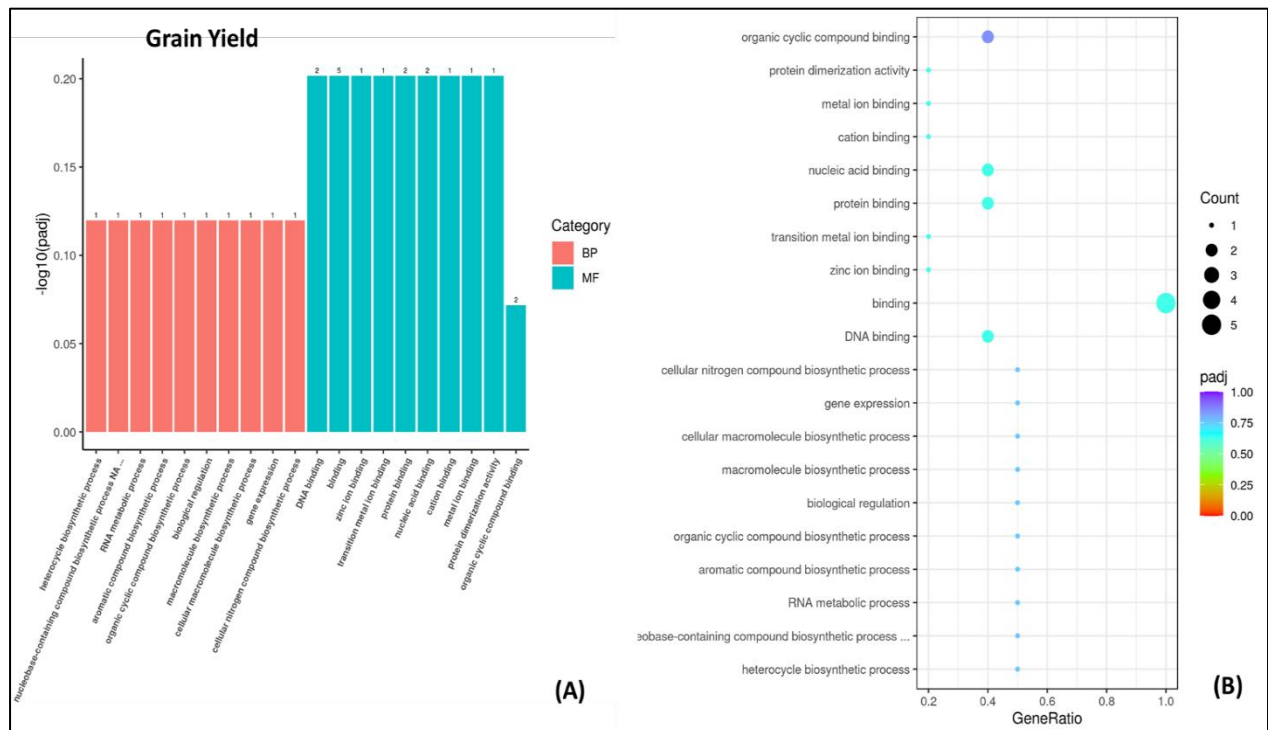


**Fig 5.11:** Gene ontology (GO) enrichment analysis ( $p < 0.05$ ) of QTL grain yield: (A) Bar chart where, the x-axis defines the name of GO terms while y-axis shows significantly enriched log base 10 padj-values and the most significant 30 terms have been depicted (B) Dot plot where, the x-axis indicates the gene ratio, the y-axis represents the name of the GO terms. The sizes of bubbles represent the number of DEGs in the corresponding GO terms, and the dot colour indicates the adjusted p value which represents level of enrichment.

In the QTL for straw yield, 75 GO terms were annotated via GO enrichment analysis out of which 30 terms belong to BP, 9 belongs to CC and 37 belongs to MF. Out of these, maximum number of genes in BP were seen for the terms primary metabolic process (GO:0044238), nitrogen compound metabolic process (GO:0006807) and protein metabolic process (GO:0019538) of 4 and 2 respectively. In CC, highest number of genes (2) were seen in the term cellular component (GO:0005575). In case of MF, the terms cation binding (GO:0043169), metal ion binding (GO:0046872) and ion binding (GO:0043167) had highest number of genes (4-5) (Fig 5.12 A). Among these terms, 19 were observed to be significantly enriched, while 10 terms were moderately enriched. The terms cellular component (GO:0005575), primary metabolic process (GO:0044238) and protein metabolic process (GO:0019538) demonstrated highest enrichment levels with high gene count. Further, the

term ion binding (GO:0043167), showed high gene count with moderate enrichment levels. The GO terms, metal ion binding (GO:0046872) and cation binding (GO:0043169) demonstrated moderate gene count as well as enrichment levels (Fig 5.12B)

In the parent Paragon, 92 terms were annotated through GO enrichment analysis of which 40 belong to BP, 11 belong to CC and the 41 belong to MF. Among these the maximum number of genes in BP were of the terms organonitrogen compound biosynthetic process

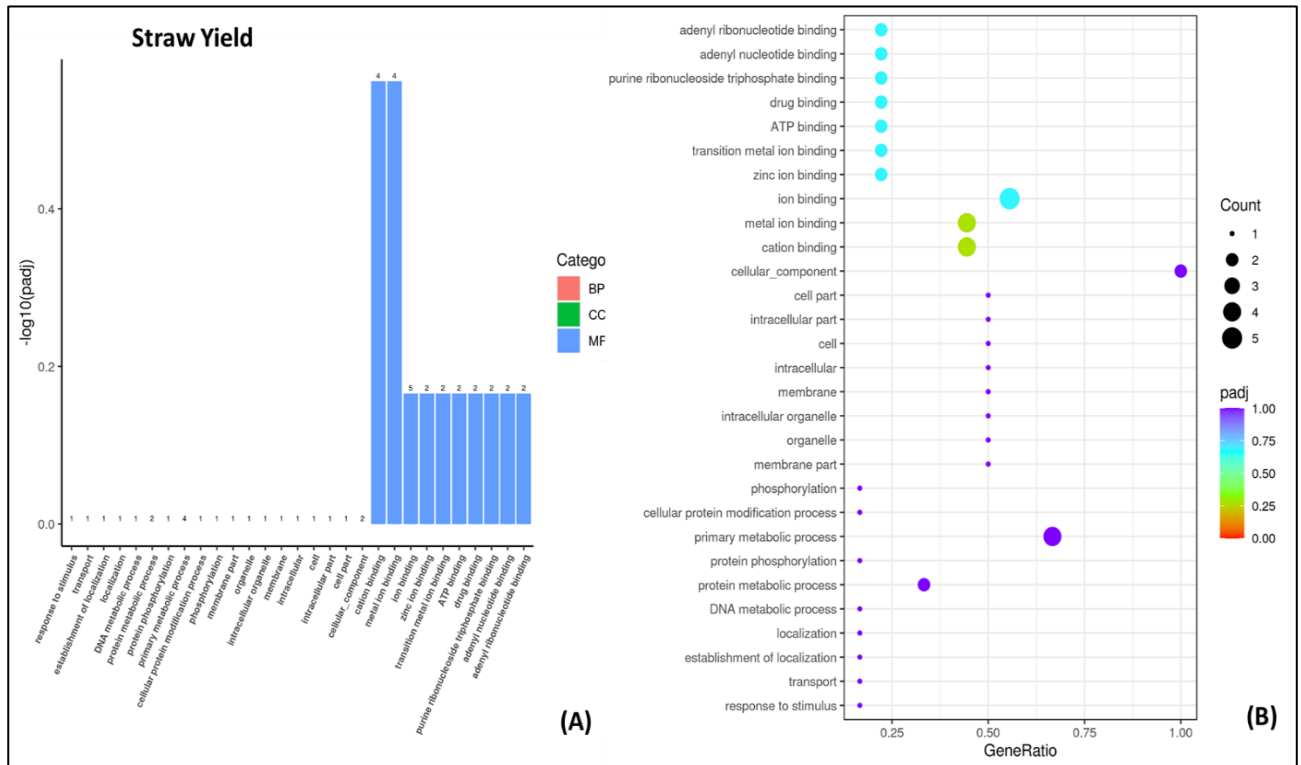


**Fig 5.12:** Gene ontology (GO) enrichment analysis ( $p < 0.05$ ) of QTL straw yield: (A) Bar chart where, the x-axis defines the name of GO terms while y-axis shows significantly enriched log base 10 padj-values and the most significant 30 terms have been depicted (B) Dot plot where, the x-axis indicates the gene ratio, the y-axis represents the name of the GO terms. The size of bubbles represents the number of DEGs in the corresponding GO terms, and the dot colour indicates the adjusted p value which represents level of enrichment.

(GO:1901566), cellular nitrogen compounds metabolic process (GO:0034641), peptide biosynthetic process (GO:0043043) nitrogen compound metabolic process (GO:0006807) consisting of 3-6 genes. In CC, maximum number of genes (2) was seen in cellular component (GO:0005575). In MF, highest number of genes were seen in the terms ion binding (GO:0043167) consisting of 7 genes and pyrophosphatase activity (GO:0016462), hydrolase activity, acting on acid anhydrides, in phosphorus-containing anhydrides (GO:0016818), nucleoside-triphosphatase activity (GO:0017111) consisting of about 4 genes (Fig 5.13 A).

Among these, 10 terms show high enrichment levels such as cell part (GO:0044464), intracellular part (GO:0044424), protein containing complex (GO:0032991). However, the gene count for these terms is the lowest. On the other hand, the terms ion binding (GO:0043167), purine ribonucleotide binding (GO:0032555), adenyly nucleotide binding (GO:0030554) have moderate enrichment with high gene count. Terms like organonitrogen compound biosynthetic process (GO:1901566) have also demonstrated moderate enrichment levels with high gene count (Fig 5.13 B).

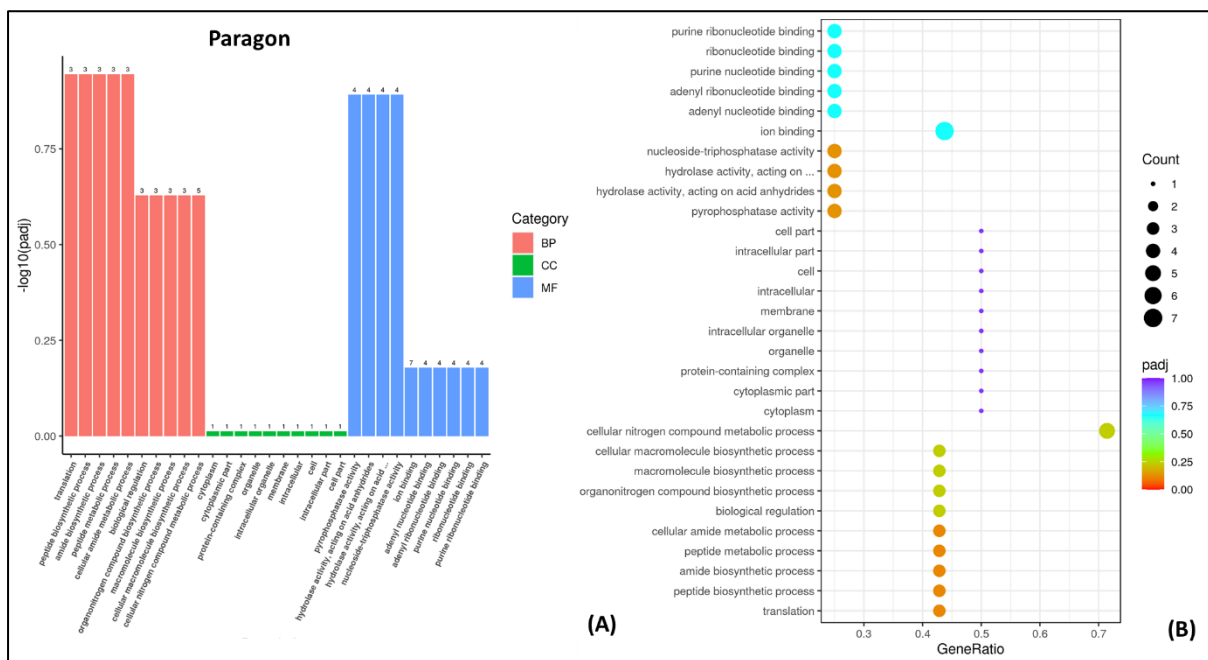


**Fig 5.13:** Gene ontology (GO) enrichment analysis ( $p < 0.05$ ) of parent Paragon: (A) Bar chart where, the x-axis defines the name of GO terms while y-axis shows significantly enriched log base 10 padj-values and the most significant 30 terms have been depicted (B) Dot plot where, the x-axis indicates the gene ratio, the y-axis represents the name of the GO terms. The size of bubbles represents the number of DEGs in the corresponding GO terms, and the dot colour indicates the adjusted p value which represents level of enrichment.

### 5.3.3.4 KEGG analysis of DEGs

The interactions of the DEGs in the biological functions and pathways has been assessed through KEGG analysis. Pathway enrichment analysis identifies significantly enriched metabolic pathways or signal transduction pathways associated with differentially expressed genes. In the KEGG analysis, the most significant 20 KEGG pathways were selected for display.

In the QTL for AGDM, 66 KEGG pathways were identified with 161 assigned DEGs. In this QTL, plant hormone signal transduction (tdc04075) and Fatty acid elongation (tdc00062), plant-

pathogen interaction (tdc04626), biosynthesis of cofactors (tdc01240) have shown high level of DEG enrichment (Fig 5.14 A). Further in the pathway plant hormone signal transduction (tdc04075), out of the 12 DEGs expressed (Fig 15.4 A), 7 were upregulated while 5 were downregulated. Similarly, out of the 9 DEGs in plant-pathogen interaction (tdc04626) (Fig 15.4 A), 3 were upregulated while 6 were downregulated. Additionally, among the 5 DEGs expressed in Fatty acid elongation (tdc00062) pathway, 3 were upregulated while 2 were downregulated. Among these, 7 genes demonstrate significant level of enrichment while 6 show moderate enrichment. Genes in pathways like phenylpropanoid biosynthesis (tdc00940), MAPK signaling pathway – plant (tdc04016) show high level of enrichment with moderate gene count. On the other hand, pathways like plant-pathogen interaction (tdc04626) demonstrate moderate enrichment with high gene count (Fig 5.14 B).

In the QTL for grain yield, 54 KEGG pathways were determined with 109 assigned DEGs. In this, the KEGG pathways fatty acid metabolism (tdc01212), protein processing in endoplasmic reticulum (tdc04141) and endocytosis (tdc04144) showed the highest number of DEG expression (Fig 5.15 A). Correspondingly, out of the 5 DEGs expressed in fatty acid metabolism pathway (Fig 5.15 A), only 1 DEG was found to be upregulated while 4 were downregulated. Furthermore, in the protein processing in endoplasmic reticulum KEGG pathway, out of the 6 DEGs (Fig 5.15 A), 5 were upregulated while 1 was downregulated. Also, in the endocytosis KEGG pathway, out of the 6 expressed DEGs (Fig 5.15 A), 3 were upregulated and the rest were downregulated. In addition to this, 13 KEGG pathways show high enrichment and 6 exhibit moderate enrichment (Fig 5.15 B). Pathways like biosynthesis of cofactors (tdc01240) and biosynthesis of amino acid (tdc01230) show high enrichment with high gene count. Further, the protein processing in endoplasmic reticulum KEGG pathway shows moderate level of enrichment with high gene count.

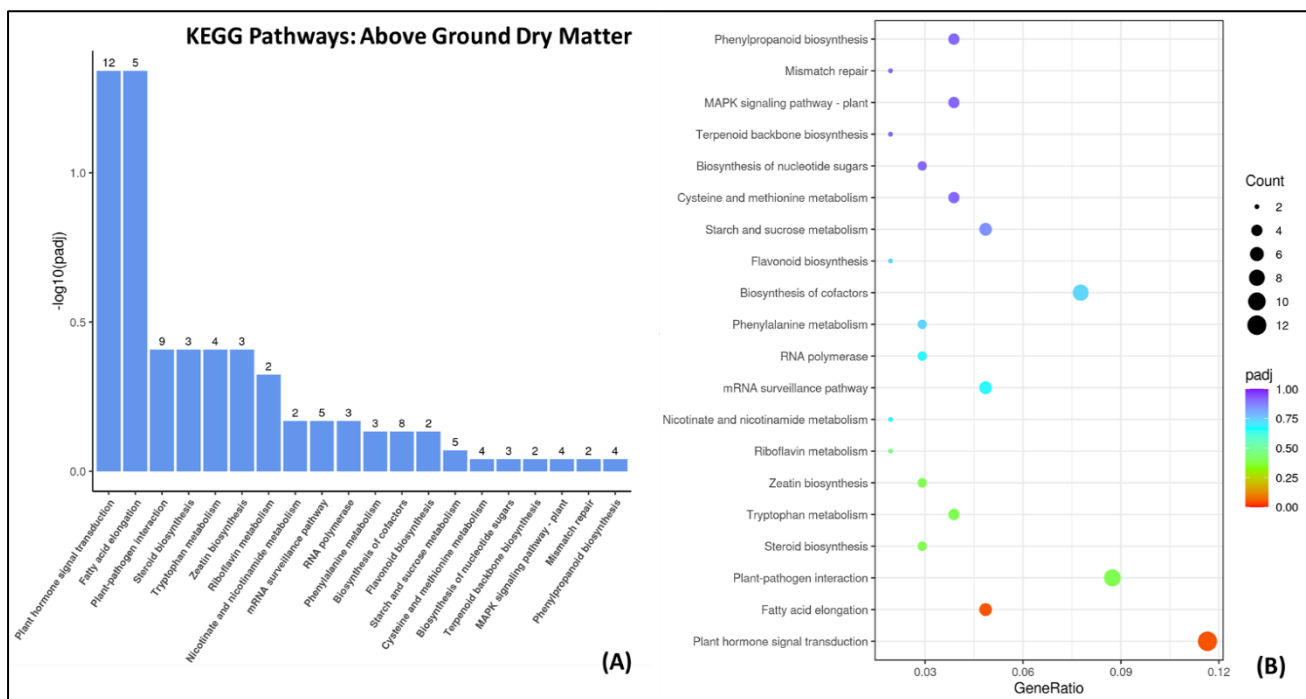


**Fig 5.14:** KEGG pathways DEGs enrichment analysis for QTL AGDM (A) Bar chart where the x-axis indicates the x-axis defines the name of KEGG pathway while y-axis shows significantly enriched log base 10 p-adj values, (B) Dot plot where, the sizes of bubbles represent the number of DEGs in the corresponding pathway, and the dot colour indicates the adjusted p-adj values.

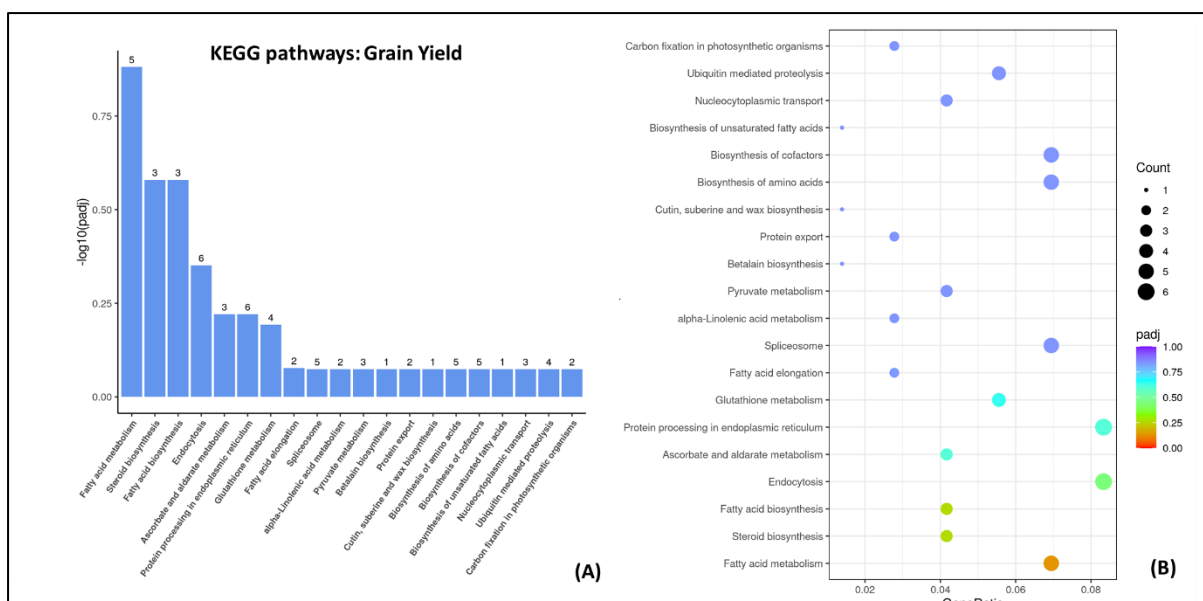




**Fig 5.15:** KEGG pathways DEGs enrichment analysis for QTL grain yield (A) Bar chart where the x-axis indicates the name of KEGG pathway while y-axis shows significantly enriched log base 10 p-adj values (B) Dot plot where, the size of bubbles represents the number of DEGs in the corresponding pathway, and the dot colour indicates the adjusted p-adj values.

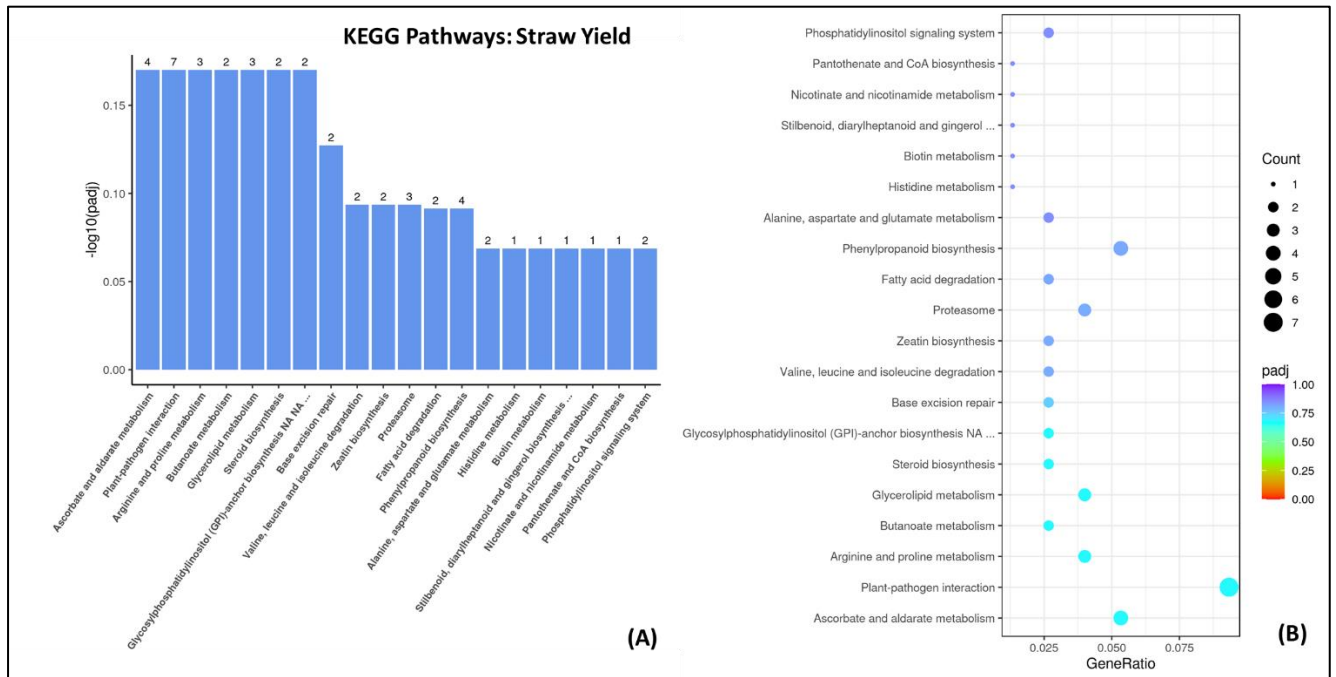


**Fig 5.16:** KEGG pathways DEGs enrichment analysis for QTL straw yield (A) Bar chart where the x-axis indicates the name of KEGG pathway while y-axis shows significantly enriched log base 10 p-adj values (B) Dot plot where, the size of bubbles represents the number of DEGs in the corresponding pathway, and the dot colour indicates the adjusted p-adj values.

In the QTL for straw yield, 63 KEGG pathways were determined with 114 expressed DEGs. Among these, the plant-pathogen interaction (tdc04626) pathway and ascorbate and aldarate metabolism (tdc00053) pathway show highest DEG expression of 7 and 4 respectively (Fig 5.16 A). Correspondingly, in the plant-pathogen interaction pathway, out of the 7 DEGs expressed, 4 were upregulated and 3 DEGs were downregulated; and in the ascorbate and aldarate metabolism pathway, out of the 4 expressed DEGs, 3 DEGs were upregulated and 1 was downregulated. The enrichment analysis shows that the DEGs of 12 pathways are highly enriched while 7 demonstrate moderate enrichment. Pathways like phenylpropanoid biosynthesis (tdc00940) demonstrate high enrichment with high gene count. Further, pathways like ascorbate and aldarate metabolism (tdc00053) and plant-pathogen interaction (tdc04626) show moderate enrichment with high gene count (Fig 5.16 B).

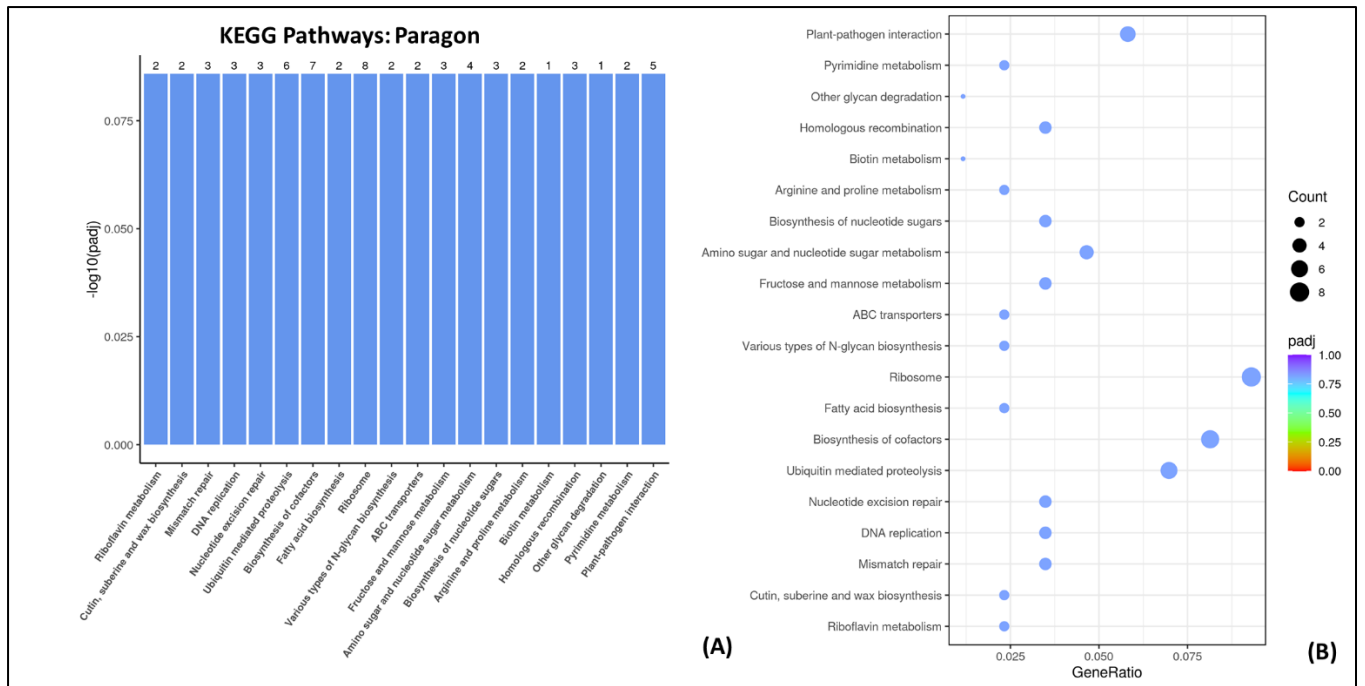


**Fig 5.17:** KEGG pathways DEGs enrichment analysis for Paragon (A) Bar chart where the x-axis indicates the name of KEGG pathway while y-axis shows significantly enriched log base 10 p-adj values B) Dot plot where, the size of bubbles represent the number of DEGs in the corresponding pathway, and the dot colour indicates the adjusted p-adj values.

In the parent Paragon, 73 KEGG pathways were identified consisting of 138 expressed DEGs. In this, the pathways, biosynthesis of cofactors (tdc01240) and ubiquitin mediated proteolysis (tdc04120) show highest number of DEG expression. Among these, in the biosynthesis of cofactors pathway, out of the 7 DEGs expressed, 4 were upregulated while 3 were seen to be downregulated (Fig 5.17 A). Likewise, in the ubiquitin mediated proteolysis pathway, of the 6 expressed DEGs, 5 were upregulated while 1 was downregulated. In terms of enrichment, most of the pathways were observed to have high enrichment levels with DEGs of pathways like biosynthesis of cofactors (tdc01240), ubiquitin mediated proteolysis (tdc04120), plant-pathogen interaction (tdc04626) showing high enrichment levels as well as high gene count (Fig 5.17 B).

### 5.3.4 Identification of candidate DEG transcripts for improved NUE

To identify candidate genes, DEG transcripts controlling NUE under HN and LN conditions for 5 genotypes using flag leaf tissues were studied. Absolute value of log<sub>2</sub> (Fold change) ≥ 1 and Padj < 0.001 has been taken as thresholds to judge the significance of differences in transcript abundance.

The 5 genotypes used for RNA-seq based transcriptomics studies are synthetic-derived lines, Paragon, grain yield QTL line, straw yield QTL line and Above-ground dry matter QTL line. In the SHW derived lines, a total of 165 DEGs were identified (Appendix table 1) and after subjecting to high stringency, 21 genes have been identified (Table 5.6). These genes are found to be associated with phosphoenolpyruvate carboxylase, glyceraldehyde-3-phosphate dehydrogenase which are directly associated with carbon metabolism. Apart from these, genes related to chlorophyll a-b binding protein and photosystem I reaction center subunit VI have been annotated which are associated with the photosynthetic pathway.

In AGDM QTL, when compared with HN and LN treatment, a total of 66 DEGs were found (Appendix table 2) out of which 6 CGs (Table 5.7) were determined based on high stringency. These CGs were observed to be associated with Cytochrome P450 which is an integral component of the photosystem regulating photosynthesis.

In the GY QTL, a total of 103 DEGs were found (Appendix table 3) and among these 20 CGs were shortlisted (Table 5.8). The genes were seen to be related to zinc finger proteins which are key players of stress adaptation, Bidirectional sugar transporter SWEET1a, which is known to improve NUE in *Arabidopsis* (Klemens *et al.*, 2013) and the ATP synthase subunit which is again associated with photosynthesis.

In the case of the straw yield QTL, 27 CGs (Table 5.9) were found after subjecting to high stringency. The CGs were related to protein kinase and zinc finger proteins which are known to be associated with stress adaptation as well as hormone signalling (Kaur *et al.*, 2022). Additionally, gene associated with mitochondrial import inner membrane translocase subunit which forms a part of the photosynthesis regulatory pathway.

Finally, in Paragon, 92 DEGs were identified (Appendix table 4) out of which 67 CGs were shortlisted (Table 5.10) based on threshold stringency. Among these CGs, genes governing senescence (MADS-box transcription factor), photosynthesis (ATP synthase subunit alpha chloroplastic, Cytochrome P450, photosynthetic NDH subunit of lumenal location chloroplastic), carbon metabolism (Glyceraldehyde-3-phosphate dehydrogenase), stress adaptation (zinc finger protein ZAT1, FBD-associated F-box protein and F-box protein, Heat stress transcription factor) have been found.

**Table 5.6:** Differentially Expressed Genes in SHW derived lines when compared with high and low N treatment. LFC: log2fold change was >1.

<b>Sr No.</b>	<b>Gene name</b>	<b>LFC</b>	<b>Chromosome</b>	<b>Gene Start</b>	<b>Gene End</b>	<b>Gene Description</b>
1	LOC123168800	7.57	7D	608483274	608484794	50S ribosomal protein
2	LOC123068639	1.62	1A	569744535	569745597	chlorophyll a-b binding protein of LHCII type 1
3	LOC123128382	1.70	6A	544675935	544678511	geranylgeranyl diphosphate reductase
4	LOC123112894	10.08	5B	519686920	519688204	probable aquaporin PIP2-7
5	LOC123183068	6.15	1D	469095049	469095895	photosystem I reaction center subunit VI protein
6	LOC100049048	21.67	2B	252473648	252474747	oxygen-evolving enhancer protein
7	LOC123164058	21.67	7D	427540322	427547561	phosphoenolpyruvate carboxylase 1
8	LOC123053529	21.65	2D	417207181	417209161	glyceraldehyde-3-phosphate dehydrogenase A
9	LOC123143070	21.65	6D	12449151	12451086	chloroplast stem-loop binding protein
10	LOC123165261	21.64	7D	186825841	186831165	trigger factor-like protein TIG
11	LOC123047424	9.81	1A	307318983	307321072	protochlorophyllide reductase B
12	LOC123098537	9.24	4D	451259850	451261385	protein PAM68
13	LOC123189421	21.08	2A	561390396	561392334	glyceraldehyde-3-phosphate dehydrogenase
14	LOC100125708	9.26	5D	527531801	527533497	tricitin-O-trimethyltransferase
15	LOC123122527	1.28	5D	441158812	441159948	chlorophyll a-b binding protein of LHCII type 1
16	LOC123121683	2.61	5D	349643203	349644533	chlorophyll a-b binding protein 1B
17	LOC123145507	1.07	1B	650625015	650625875	photosystem I reaction center subunit VI
18	LOC123187682	9.03	2A	85265337	85270911	magnesium-chelatase subunit ChIh
19	LOC123104728	1.01	5A	554070619	554071833	chlorophyll a-b binding protein of LHCII type 1
20	LOC123148365	9.09	1B	677486967	677488084	chlorophyll a-b binding protein of LHCII type III
21	LOC123044442	1.39	2B	218703119	218704562	chlorophyll a-b binding protein 7

**Table 5.7:** Differentially Expressed Genes in AGDM QTL when compared with high and low N treatment. LFC: log2fold change was >1.

Sr No	Gene name	LFC	Chromosome	Gene Start	Gene End	Gene Description
1	LOC123168472	9.042895201	7D	488165316	488168102	pentatricopeptide repeat-containing protein
2	LOC123136829	9.150332476	6B	253166866	253225437	vacuolar-processing enzyme beta-isozyme 1
3	LOC123189867	8.826288651	2A	626460939	626463152	uncharacterised Protein
4	LOC123181976	8.823151364	1D	347748455	347757351	Cytochrome P450
5	LOC123105694	8.828945944	5A	656042680	656049067	Methyltransferase C9orf114
6	LOC123060985	8.767856068	3A	208158589	208161318	uncharacterised protein

**Table 5.8:** Differentially Expressed Genes in GY QTL when compared in high and low N treatment. LFC: log2fold change was >1

Sr No	Gene name	LFC	Chromosome	Gene Start	Gene End	Gene Description
1	LOC123099896	8.72	4D	258968546	258969521	Proline-rich receptor-like protein kinase
2	LOC123140724	6.51	6D	8445864	8447420	Bisdemethoxycurcumin synthase
3	Novel Gene	8.31	5A	90239711	90240573	BED zinc finger
4	LOC123134402	8.62	6B	553498317	553501265	Mannose-P-dolichol utilisation defect 1 protein
5	LOC123145518	8.30	6D	420560798	420563029	Alpha-arabinosyltransferase
6	LOC123071827	8.36	3B	696039269	696042312	Bidirectional sugar transporter SWEET1a
7	LOC123054981	8.28	1A	444295703	444301366	Nodulation protein H
8	LOC123151220	8.33	7A	26998363	26998896	Uncharacterised Protein
9	LOC123131054	8.24	6A	565273608	565274691	Auxin-responsive protein
10	LOC123143074	7.02	1B	622051263	622052611	Methyltransferase
11	LOC123155760	8.18	7B	612737805	612739940	FBD-associated F-box protein
12	LOC123151151	8.22	7A	20370750	20373292	Uncharacterised Protein
13	LOC123066178	8.30	3B	718035739	718037126	CRIB domain-containing protein RIC4-like
14	LOC123080127	8.15	3D	516615048	516620236	Methyltransferase
15	Novel Gene	8.10	3A	741030254	741032700	ARATH Uncharacterised mitochondrial protein
16	LOC123128894	8.23	6A	600702383	600704376	Uncharacterised Protein
17	Novel Gene	8.10	7B	335917034	335919292	
18	Novel Gene	8.10	2B	278951235	278962856	
19	LOC123094421	8.32	4B	61366272	61367892	Putative pentatricopeptide repeat-containing protein
20	LOC123068902	7.32	3B	113663101	113664860	ATP synthase subunit

**Table 5.9:** Differentially Expressed Genes in straw yield QTL when compared in high and low N treatment. LFC: log2fold change was >1

Sr No	Gene name	LFC	Chromosome	Gene Start	Gene End	Gene Description
1	LOC123061040	8.640038	3A	221752658	221755249	Zinc finger CCCH domain-containing protein like OsC3H22
2	Novel Gene	8.177514	3A	42098756	42104419	ARATH Retrovirus-related Pol polyprotein from transposon RE1
3	LOC123071022	8.109673	3B	576894740	576898132	uncharacterised transcript variant
4	LOC123042038	8.10713	2B	679200677	679201311	Putative invertase inhibitor
5	LOC123102051	8.038393	5A	20732453	20736151	beta -xylosyltransferase XYXT1
6	LOC123072074	7.946632	3B	735764150	735767646	Protein S-acyltransferase 7
7	LOC123078777	7.473882	3D	342899502	342902212	Putative receptor protein kinase ZmPK1
8	LOC123050393	7.40028	2D	611685030	611686042	VQ motif-containing protein 31
9	LOC123139515	7.156892	6B	699902697	699907189	uncharacterised Protein
10	LOC123058502	6.79167	3A	504164657	504166165	Purine permease 4
11	Novel Gene	6.325299	5D	382910594	382911646	
12	Novel Gene	5.415881	7A	547745243	547745442	
13	LOC123054368	5.219692	2D	542769675	542773183	Cation transporter HKT4
14	LOC123116997	5.189485	1B	223533560	223564378	uncharacterised transcript
15	LOC123136411	3.054179	6B	171506733	171565831	Disease resistance protein RPM1
16	LOC123074049	2.811214	1A	336083	339452	28S ribosomal RNA Putative uncharacterised protein ART2
17	LOC123152715	2.779106	1B	117334299	117337687	28S ribosomal RNA Protein TAR1
18	LOC123137265	2.07297	6B	400063730	400069459	Cellulose synthase A catalytic subunit 3
19	LOC123172688	1.955549	Unplaced Scaffold	6895	10283	28S ribosomal RNA Protein TAR1
20	LOC123160849	1.84351	7B	73464855	73465398	Pathogenesis-related protein PRB1-3
21	LOC123125626	1.630045	5D	483975370	483977046	mitochondrial import inner membrane translocase subunit TIM14-3
22	LOC123068467	1.353227	3B	43482477	43483216	Lipid-transfer protein 4.1
23	LOC123165932	1.309684	7D	459100250	459101081	Multiprotein-bridging factor 1

24	LOC123070619	1.30076	3B	506939464	506940613	MPK3/6-targeted VQ-motif-containing protein
25	LOC123079516	1.168746	3D	443708026	443709486	RETICULATA-RELATED chloroplastic-Protein 3
26	LOC123158491	1.153402	1A	496806374	496807287	non-specific lipid-transfer protein RVE transcription factor family

**Table 5.10:** Differentially Expressed Genes in Paragon when compared with high and low N treatment. LFC: log<sub>2</sub>fold change was >1

Sr No	Gene name	LFC	Chromosome	Gene Start	Gene End	Gene Description
1	LOC123103037	7.62121307	1A	101370000	101371161	glutathione S-transferase 4
2	LOC123149878	7.491049151	1B	694500304	694501645	translation initiation factor IF-2
3	LOC123126988	7.302717756	1B	395539404	395585631	MADS-box transcription factor 56
4	LOC123126320	1.174229836	1B	388260594	388262451	Probable inactive shikimate kinase
5	LOC123181305	6.575432443	1D	255055275	255058454	protein ROOT PRIMORDIUM DEFECTIVE 1
6	LOC123180527	6.078419359	1D	92272958	92274360	Serpin-Z5
7	LOC123186211	6.118923972	2A	722602051	722604369	anthocyanidin reductase
8	LOC123046757	8.650301675	2B	691781179	691782909	ATP synthase subunit alpha chloroplastic
9	LOC123046909	7.765439882	2B	715284421	715285205	Cytochrome P450
10	LOC123039230	7.353490513	2B	393289400	393301746	Glyceraldehyde-3-phosphate dehydrogenase
11	Novel Gene	8.267956563	2D	334111085	334111961	
12	LOC123051779	7.584694674	2D	82405854	82408522	beta-glucosidase
13	LOC123052934	7.567621336	2D	320414305	320417719	DNA methylation 1
14	LOC123054368	7.557480619	2D	542769675	542773183	Cation transporter HKT4; OsHKT4
15	Novel Gene	7.381700569	2D	399341387	399342052	
16	LOC123050389	7.337312326	2D	611517116	611518895	tryptophan decarboxylase 1
17	LOC123058669	8.449380922	3A	570547819	570549275	salicylic acid-binding protein 2
18	LOC123057393	7.461611928	3A	26104	30516	Cellulose synthase-like protein H1



19	LOC123070699	7.99829062	3B	520777309	520783924	FBD-associated F-box protein
20	LOC123070578	7.674984879	3B	500002880	500010154	aspartic proteinase
21	LOC123069176	7.661832368	3B	163993563	163995816	double-strand break repair protein MRE11
22	LOC123070395	5.945405063	3B	465546370	465549801	nucleobase-ascorbate transporter LPE1-
23	Novel Gene	5.900557478	3B	15343862	15345258	
24	LOC123075066	7.315128093	3D	497692278	497693462	cytosolic sulfotransferase 5
25	LOC123076851	6.897696273	3D	10411946	10415066	beta xylosyltransferase XAX1
26	Novel Gene	7.615513707	4A	661788577	661789346	
27	LOC123086509	7.282915664	4A	484359355	484364867	putative HVA22-like protein
28	LOC123087289	7.265740383	4A	592847656	592852507	Ribosome biogenesis protein RPF2 homolog 1-aminocyclopropane-1-carboxylate oxidase homolog 1
29	LOC123087412	5.682855699	4A	601059230	601060976	
30	LOC123087663	1.298529071	4A	621208121	621209122	Thiocyanate methyltransferase
31	Novel Gene	7.974405381	4B	120056859	120066538	
32	LOC123093942	7.411822731	4B	657890783	657893314	formyltetrahydrofolate deformylase
33	LOC123107029	7.897005738	5A	415462720	415465012	probable inactive receptor kinase RLK902
34	Novel Gene	7.578290142	5A	608451809	608452848	
35	Novel Gene	6.673341757	5A	81958348	81959648	
36	LOC123102474	6.252235059	5A	97590134	97592214	dof zinc finger protein DOF5.1
37	LOC123105515	5.296278638	5A	637256447	637262851	UDP-glucose flavonoid 3-O-glucosyltransferase
38	LOC123111380	7.567856026	5B	279729561	279732166	pentatricopeptide repeat-containing protein
39	LOC123111465	4.027506662	5B	292748068	292758683	RNA pseudouridine synthase
40	LOC123122714	8.428794867	5D	455547112	455548219	nuclear receptor corepressor 2-like && - && -
41	LOC123121925	7.869720868	5D	378659824	378662599	IRK-interacting protein
42	LOC123121752	5.431828321	5D	358774854	358777250	tuliposide A-converting enzyme amyloplastic
43	LOC123130755	7.7684232	6A	464058390	464059732	zinc finger protein ZAT1 photosynthetic NDH subunit of lumenal location chloroplastic
44	LOC123127700	7.638672481	6A	414393040	414396327	
45	LOC123132420	7.002314091	6A	119394896	119400291	Urease accessory protein F-like Protein
46	LOC123130163	6.76685514	6A	34456683	34461555	Ubiquitin thioesterase otubain-like
47	LOC123134647	7.92069687	6B	639380787	639381565	auxin-responsive protein SAUR32

48	LOC123136894	7.632545477	6B	266371695	266378626	ATP-dependent RNA helicase DEAH13
49	LOC123135850	6.963964511	6B	70038876	70042341	LRR receptor-like serine/threonine-protein kinase
50	LOC123138978	6.34669563	6B	668215724	668217918	RING-H2 finger protein ATL13
51	LOC123140810	8.148034534	6D	16940521	16943270	mitochondrial amidoxime reducing component 2
52	Novel Gene	8.067569867	6D	337342493	337342792	- && - && -
53	LOC123145992	7.365034774	6D	470782973	470785287	FBD-associated F-box protein pentatricopeptide repeat-containing protein
54	LOC123143193	5.393769102	6D	25382626	25384662	At2g22410
55	LOC123142120	5.092907084	6D	475171633	475176845	cysteine-rich receptor-like protein kinase
56	LOC123143626	4.301123649	6D	74631408	74635255	Heat stress transcription factor
57	LOC123144219	4.232241569	6D	150668615	150670299	protein FAR1-RELATED SEQUENCE
58	LOC123146968	7.946706891	7A	387796233	387810946	Cingulin
59	Novel Gene	7.659820012	7A	452498930	452502027	
60	LOC123154099	7.563563644	7A	57796110	57802074	phosphomannomutase pentatricopeptide repeat-containing protein
61	LOC123148489	7.349169449	7A	592950321	592952774	At1g03540-like
62	LOC123153506	7.320334211	7A	579140725	579141925	Retrovirus-related Pol polyprotein from
63	Novel Gene	7.745559619	7B	721254587	721255769	ARATH Putative F-box protein PP2
64	LOC123159447	7.312992294	7B	666645146	666649887	Vacuolar-sorting receptor 6
65	LOC123159852	6.006110163	7B	599984875	599986286	E3 ubiquitin-protein ligase
66	LOC123164659	6.031460153	7D	583455888	583457571	F-box protein
67	Novel Gene	5.366966163	Unplaced Scaffold	987	2140	

### 5.3.5 SNP analysis

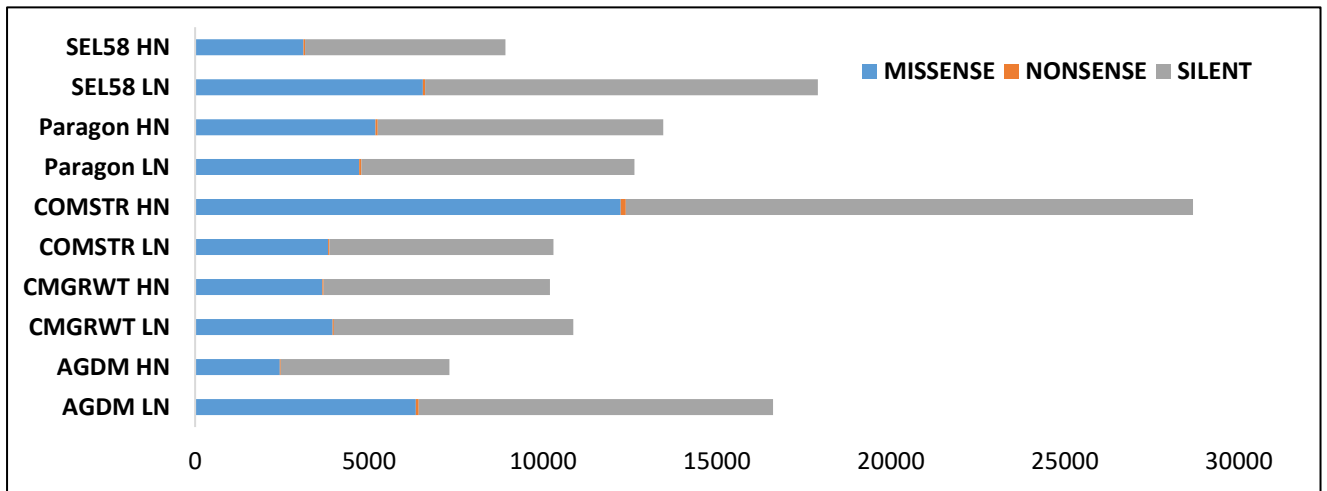


**Fig 5.18:** SNP function of 5 genotypes with MISSENSE (a single nucleotide changes that missense mutation), NONSENSE (a single nucleotide change that does not cause mutation) and SILENT (a single nucleotide changes that synonymous mutation).

Combine straw weight (Straw Yield) QTL at high N treatment showed the highest no of missense and silent mutations i.e., 12229 and 16311 respectively, whereas Above-ground Dry Matter QTL at high N exhibited the least missense and silent mutations viz. 2431.33 and 4850.67 respectively. In total 51994 missense, 617.68 nonsense and 84262 silent SNPs were observed during SNP calling analysis (Fig 5.11).

## 5.4 Discussion

The aim of our study was to analyse the transcriptomic response of PxW lines and synthetically derived wheat under high N and low N conditions in flag-leaves in the post-anthesis stage.

Deficiency of N is of major concern in agricultural production and therefore, development of high-NUE genotypes is crucial. Genotypic variations occurring in wheat has led to the need to determine underlying regulatory mechanisms of N response. Studies indicating novel variations in NUE and associated traits have been previously done in synthetically-derived (SD) hexaploid wheat lines and modern cultivars in cv. Paragon background under varying N conditions (Gaju *et al.*, 2016). TheSHW derived lines showed greater photosynthetic rate, biomass and grain yield than modern cultivars (Gaju *et al.*, 2016) implying the importance of utilising and studying SHW derived lines for NUE. Nitrogen accumulation and assimilation occurs across the wheat plant in various parts, but predominantly in leaf from which maximum N remobilisation occurs (Curci *et al.*, 2017).

Unlike most studies which focus on N deficiency response, the transcriptomic variation was presently studied under normal N conditions as well, in the five genotypes to identify key regulatory genes. The study has shown that the genes which have been most highly expressed are associated with photosynthesis, carbon and N metabolism and biosynthesis of amino acids and are discussed in detail below.

### 5.4.1 Photosynthesis

Effects of photosynthesis are directly correlated with grain yield and nitrogen-use efficiency. An increase in CO<sub>2</sub> fixation and N assimilation would eventually contribute to improving NUE. Canopy structure is one of the major contributing factors for enhanced photosynthetic activity through maximum light interception at anthesis stage (Hawkesford, 2014). In previous studies in landraces, modern and synthetic-derived wheat cultivars, genetic variations in hexaploid wheat associated with SHW under varying N conditions showed improved leaf photosynthesis rates (Gaju *et al.*, 2016). In achieving stay-green traits, physiological parameters like chlorophyll metabolism and nutrient remobilisation play an important role along with maintaining photosynthetic activity leading to increased NUE (Hawkesford, 2014). Genetic variation in flag-leaf photosynthesis has also been reported previously in landrace-derived

genotypes under HN and LN (Kareem *et al.*, 2022). Under HN and LN conditions, enhanced flag-leaf photosynthesis rate along with increased biomass and yield, respectively, has been observed in a synthetically-derived line as compared to Paragon indicating the importance of trait introgression from SD genotypes (Gaju *et al.*, 2016).

In the present study, DEGs associated with photosynthesis were observed to be greatly upregulated along with metabolic pathways associated with photosynthesis such as oxidative phosphorylation, photosynthesis antenna protein and chloroplast ribosomal activity, pyruvate metabolism and carbon fixation.

#### **5.4.2 Carbon metabolism**

In the present study, DEGs were observed to be associated with carbon fixation in photosynthetic organisms, carbon metabolism and glyoxylate and dicarboxylate metabolism which showed significant enrichment. Nitrogen metabolism is associated with photorespiration at various levels including glyoxylate metabolism (Canvin, 1981) as well as in dicarboxylic acid synthesis in C4 plants.

Alanine is essential for carbon metabolism and alanine aminotransferase (AlaAt) plays a key role in N metabolism (Miyashita *et al.*, 2007). Expression of AlaAt also impacts the TCA cycle and glycolysis promotes N assimilation and utilisation subsequently improving NUE (Tiong *et al.*, 2021). However, in our study have not demonstrated differential expression in AlaAt in given selection parameters ( $\text{Log}_{10}$  padj-value).

#### **5.4.3 Nitrogen metabolism**

Nitrogen metabolism during the grain filling stage consists of physiological processes like N assimilation governed by key enzymes including nitrate reductase (NR), glutamate pyruvate transaminase (GPT) and glutamine synthase (GS). While a small portion of the N required for optimum grain protein quality is taken up post-anthesis from the soil, a larger portion of 60-90% is remobilized from the vegetative organs of the plant (Lyu *et al.*, 2022). The expression of the aforementioned enzymes can be utilized as potential markers for determining wheat genotypes having high NUE (Zhang *et al.*, 2021). In this study, DEGs associated with alanine, aspartate and glutamate metabolism have been expressed and corresponding transcripts were upregulated indicating the role of these enzymes in nitrogen assimilation. In the putative candidates genes amino acid biosynthesis genes like Tryptophan decarboxylase 1,

aspartic proteinase and LRR receptor-like serine/threonine-protein kinase have been identified which are associated with N assimilation.

#### **5.4.4 Biosynthesis of amino acids**

Nitrogen assimilation and photosynthetic capacity is greatly dependent on amino acid biosynthesis and leads to enhanced performance under N-limiting conditions. The assimilation of N from nitrate or ammonium is regulated by enzymes like NADH, NADPH, AlaAt, GS and GOGAT in conjunction with amino acid glutamate and alanine (Beatty *et al.*, 2013). Furthermore, photorespiration contributes to synthesis of many amino acids. Higher levels of amino acids in the leaves is known to be indicative of higher N-uptake efficiency under N-limiting conditions (Kocheva *et al.*, 2020). Additionally, greater levels of amino acids is associated with enhanced photosynthetic activity and PNUE (Perchlik and Tegeder *et al.*, 2018).

In this study, DEGs associated with amino acid biosynthesis and metabolism such as arginine, glycine, serine, tryptophan, threonine, tyrosine, phenylalanine was expressed along with associated transcripts being upregulated in the NILs.

The study revealed the association of a wide variety of DEGs associated with various processes including N metabolism and carbon metabolism. In the five genotypes the genes identified were found to be directly associated with the pathways. Since pathways like carbon metabolism and photosynthesis function in correspondence to N metabolism, the CGs are of utmost importance. Several transcription factors (TFs) have been found which are known to play a crucial role in stress adaptation, in this case, N deficit. Protein kinases (PKs) and zinc finger proteins are also known to be associated with N stress response. PKs are also involved in nutrient signalling and can therefore be actively participating in N uptake and transport. Additionally, carbon metabolism genes like phosphoenolpyruvate carboxylase 1 and glyceraldehyde-3-phosphate dehydrogenase A are upregulated which are components of carbohydrate metabolism. C metabolism and N metabolism are closely associated as the former is dependent on N assimilation (Foyer *et al.*, 2001) and therefore the CGs are significant.

The SNPs associated with the DEGs are highly reliable markers to select haplotypes for pre-breeding and breeding technologies. SNP calling was performed, and missense, nonsense and

silence SNP mutations were observed in all 5 genotypes. SNP markers derived from sequencing have the ability to enhance the marker density which in turn improves the quality and accuracy of QTLs associated with complex traits like NUE (Brasier *et al.*, 2020).

## 5.5 Summary

Identification of DEGs in landrace- and synthetically derived wheat genotypes under contrasting N conditions allows for a better understanding of the genetic basis of remobilisation of N and NUE. In this study, RNA-seq analysis using post-anthesis flag leaves of low and high N treatments demonstrated that genes associated with photosynthesis, amino acid biosynthesis, carbon and nitrogen metabolism were highly expressed.

RNA sequencing of the five genotypes (Paragon, SD line, QTL AGDM, QTL, GY and QTL straw yield) for NUE resulted in identification of candidate genes which could be utilized for future NUE breeding programs. Most of the genes were found to be associated with photosynthesis like photosystem I reaction center subunit VI, Cytochrome P450, ATP synthase subunit, mitochondrial import inner membrane translocase subunit, ATP synthase subunit alpha chloroplastic, Cytochrome P450, photosynthetic NDH subunit of lumenal location chloroplastic and geranylgeranyl diphosphate reductase, protochlorophyllide reductase B which regulate the photosystem. Additionally, several genes associated with chlorophyll generation in a light dependent manner were also found like chlorophyll a-b binding protein 1B, chlorophyll a-b binding protein of LHCII type 1, chlorophyll a-b binding protein of LHCII type 1, chlorophyll a-b binding protein of LHCII type III and chlorophyll a-b binding protein 7. Furthermore, several genes associated with carbon metabolism especially glycolysis and TCA cycle were found such as phosphoenolpyruvate carboxylase 1 and glyceraldehyde-3-phosphate dehydrogenase A. Stress-response genes which are associated with stress conditions like drought, heat and nutrient deficiency (like N deficiency) were observed such as Proline-rich receptor-like protein kinase, F-box protein, FBD-associated F-box protein, heat stress TF, methyltransferase, zinc finger protein, Zinc finger CCCH domain-containing protein like OsC3H22, MADS-box transcription factor 56. Finally, amino-acid biosynthesis related genes correlated with N assimilation were identified. A total of 67 genes in Paragon, 26 genes in straw yield QTL, 20 genes in GY QTL, 6 genes in AGDM QTL and 21 genes in SHW derived lines were identified which are related to N-use efficiency in one way or the other. Since NUE is a complex trait, studying variations in its associated traits is of utmost importance. The

transcriptomics study of NILs for important QTLs as well as the synthetic-derived line and Paragon gave a substantial list of candidate genes which can help regulate and subsequently improve NUE in wheat. Furthermore, the expression level of these transcripts can be analysed through expression studies using quantitative RT-PCR. This would give a clearer idea of the highly upregulated genes which can be functionally validated in crop systems using a genetic engineering approach or alternatively mutants having improved NUE can be generated using genome editing.



## ***Chapter 6***

### ***General Discussion***

## 6.1 Hypothesis validation

In the first part of the study, 55 NILs were selected based on QTL related to NUE and associated traits from 289 genotypes. These NILs were derived from Watkins collection landraces crossed with spring wheat Paragon background. The NILs comprised allelic contrasts of QTLs for the NUE-related traits grain yield (GY), above-ground biomass (AGDM), thousand grain weight (TGW), combined straw weight (COMSTR), combined grain weight (COMGRWT), Normalised Difference Vegetative Index (NDVI). Apart from these 55, 7 SHW-derived lines were also taken which were in a Robigus background. These NILs were studied, along with their parent, in two different sites having varying soil type. Based on these variations and QTL performance, 19 lines were shortlisted for further evaluation under high N and low N conditions. Analysis of two-year harvest data and NUE related traits data then led to determination of 4 lines which showed distinct and significant genetic variation favouring NUE traits and Paragon. These genotypes were further analysed in a transcriptomics-based study to determine candidate genes for NUE and related traits.

The main aim of the study was to assess genetic variation of NUE as well as its genetic and physiological basis in wider wheat cultivars and to identify novel NUE traits and candidate genes. The first hypothesis was to establish that genetic variation for NUE and its component traits is related to NUpE and NUtE in the landrace-derived lines (Paragon x Watkin landrace) above the parent Paragon. The study quantified the genetic variation occurring between the PxW lines compared to Paragon in traits like NUE, NUtE and NUpE. Additionally, genetic variation was also observed between individual alleles of Paragon and Watkins of each QTL implying towards allelic diversity as well. Among these 55 NILs, significant genetic variation was observed for GY, NUE and TGW along with photosynthesis-related traits like photosynthesis rate, stomatal conductance and SPAD at GS61. Further, under HN and LN conditions, cross-year analysis suggested that the mean NUtE and NUpE were higher under LN conditions as compared to HN. In these situations, the N supply and year component had a significant impact. The parent line, Paragon, performed better in traits like NUE, NUtE. However, overall, no PxW line showed enhanced GY above the Paragon parent likely due to the presence of many unadapted genes in the PxW lines.

The study also investigated NUE and its component traits in synthetic hexaploid (SHW)-derived lines compared to their parent Robigus, and its relation to NUpE and NUtE. While

Robigus was observed to be high performing for most of the traits. Some variation in some trends were observed for higher levels of GY, NUpE and NUE than the parent Robigus in one of the sites. The SHW-derived lines also exhibited genetic variation in flag-leaf leaf photosynthesis rate which was positively associated with GY and NUE.

The third major hypothesis investigated related to the physiological basis of genetic variation in grain yield and NUE. Genetic variation in NUE and GY was observed for all the 19 NILs under HN and LN conditions in 2020 and 2021. A high association of GY with NUE was observed under HN and LN conditions. In the present study, under both HN and LN conditions, GY and NUE showed strong association with NUpE and AGDM and was found to be most strongly correlated with these traits.

The relation between photosynthesis traits like flag-leaf photosynthesis rate and grain yield has been established before in wheat (Carmo-Silva *et al.*, 2017). Landraces and synthetic-derived hexaploid lines are known to exhibit wider genetic variation compared to modern wheat cultivars. Previous studies have also shown that SHW lines demonstrate elevated levels of GY and biomass under varying N conditions (Nehe *et al.*, 2022). Another of the present hypotheses was that there are candidate genes which are expressed in the flag-leaf during the post-anthesis period will positively influence NUpE, NUE and GY.

In the present study, among the PxW lines, 9 NILs (PW141-58-7-10-Q7D-AGDM-W, PW292-22-9-1-Q3A-COMSTR-W, PW292-22-9-19-Q3A-COMSTR-P, PW292-22-9-7-Q3A-COMSTR-W, PW292-9-5-18-Q4B-GFPTT-P, PW468-77-3-20-Q7B-AGDM-P, PW468-84-4-12-Q5A-COMGRWT-P, PW729-55-3-1-Q6B-AGDM-W, PW729-55-3-15-Q6B-AGDM-P) have demonstrated significant positive genetic variation for NUE traits and higher flag-leaf photosynthesis rate and the SHW-derived line DFW SEL 58 has also demonstrated positive variation. Similarly, in the case of stomatal conductance (gs), the following 9 NILs have shown significant positive genetic variation (PW141-58-7-10-Q7D-AGDM-W, PW141-58-7-20-Q7D-AGDM-P, PW292-22-9-19-Q3A-COMSTR-P, PW468-77-3-10-Q7B-AGDM-W, PW468-77-3-14-Q7B-AGDM-W, PW468-77-3-20-Q7B-AGDM-P, PW468-84-4-12-Q5A-COMGRWT-P, PW729-55-3-1-Q6B-AGDM-W, PW729-55-3-15-Q6B-AGDM-P) along with SHW-derived line DFW SEL 63. Most of these NILs are for the QTLs for AGDM and COMGRWT suggesting their potential value for use in NUE breeding programs. The genetic variation observed in these NILs at GS61 was positively correlated with grain yield. Further, evaluation of allelic variation in the PxW

NILs for QTL for AGDM on chromosome 7B has shown that Paragon allele has conferred higher  $A_{max}$ ; and similarly for the QTL for COMGRWT on chromosome 5A and for COMSTR on chromosome 3A as compared to its Watkins counterpart. Similar results were observed for stomatal conductance for QTLs for AGDM on chromosome 6B, 7D and 7B and COMGRWT on chromosome 5A. Previous results have also exhibited positive correlation between GY and  $A_{max}$  in wheat cultivars (Gaju *et al.*, 2016). This also lays the foundation for identification of genes associated with flag-leaf photosynthesis traits to improve NUE.

The final hypothesis focuses on identification of candidate genes with potential SNP markers associating with NUE and NUE traits. Sequencing derived SNPs has been utilised in order to detect marker-trait associations for NUE and related traits in wheat leading to identification of specific genes (Brasier *et al.*, 2020). In the present study, DEGs in SHW derived lines, AGDM QTL, GY QTL, COMSTR QTL, and Paragon (5 NILs) were identified when comparing HN with LN conditions. High stringency was applied in terms of  $p_{adj}$  and log2fold change values in order to mine genes among these DEGs specifically associated with processes related to NUE. Additionally, SNP function of these 5 genotypes with missense, nonsense and silent mutations was also analysed. In a previous study in recombinant inbred lines (RILs) of wheat, genetic map consisting of 456 SNP markers associated with QTLs of NUE, NUpE and NUtE was determined in order to validate phenotypic variation (Singh *et al.*, 2023). A total of 737 candidate genes (CGs) were mined from these QTL regions of which 83 were differentially expressed in root and shoot for various metabolic and cellular processes. The genes identified were found to be associated with transcription factors and transporters which have a function in NUE (Singh *et al.*, 2023). Comparative transcriptomics studies in different wheat cultivars under HN and LN conditions using root and shoot tissue has also been carried out which found 13 potential CGs associated with transcription factors, transporters, protein kinases as well as genes involved in N metabolism and transportation (Kaur *et al.*, 2022). In the present study, transporters, zinc finger proteins, cytochrome proteins, transferases and various transporters have been identified in the 5 NILs. Therefore, the hypothesis with regard to candidate genes was supported.

## 6.2 Validation of QTLs for target traits and improved NUE (QTLs performance)

An important aspect of our study was to assess the heritability and genetic variability under varying N conditions. QTL mapping allows for a more detailed understanding of qualitative and quantitative traits and presents the genes governing them. Several studies have been carried out in wheat which analysed the effects of genetic variation at varying levels of N to determine regions associated with NUE (Quarrie *et al.*, 2005; An *et al.*, 2006; Laperche *et al.*, 2007; Guo *et al.*, 2012). Previous studies based on determination of genomic regions has shown genetic variability is lowest under low N (Mahjourimajd *et al.*, 2016). These genomic regions will provide genes underlying the QTLs associated with NUE. However, these QTLs have also been known to be associated with adaptation to environmental stress conditions and not N uptake alone. In our study, the NILs having Watkins allele for QTLs like GY, AGBM, COMGRWT, COMSTR and GFPTT demonstrated higher values than the Paragon allele in some cases. Further, QTLs associated with flag-leaf  $A_{max}$  and  $gs$  were also identified directly influencing NUE and GY. Based on these parameters, 19 genotypes were shortlisted to evaluate their performance under HN and LN conditions.

The impact of HN and LN conditions on the genetic variability of the genotypes was studied. In case of GY, the parents, Paragon ( $3.32 \text{ t ha}^{-1}$ ) and Robigus ( $3.49 \text{ t ha}^{-1}$ ) demonstrated high GY under LN conditions as expected, which can be attributed to these being adapted cultivars under varying N conditions. In 2020, the line PW292-8-Q3A-COMSTR-W showed highest GY ( $4.80 \text{ t ha}^{-1}$ ) among the PxW lines compared to Paragon ( $4.82 \text{ t ha}^{-1}$ ) while among the SHW-derived lines, SEL63 showed relatively high GY ( $4.76 \text{ t ha}^{-1}$ ) compared to Robigus ( $5.08 \text{ t ha}^{-1}$ ) under LN conditions. Other lines like PW292-19-Q3A-COMSTR-P ( $4.66 \text{ t ha}^{-1}$ ) also showed comparable GY. However, none of these were significantly above Paragon. In 2021 the line PW292-18-Q4B-GFPTT-P showed high significance with GY of ( $2.69 \text{ t ha}^{-1}$ ) compared to Paragon which had GY of  $2.14 \text{ t ha}^{-1}$  under LN conditions. Further, the SHW-derived line SEL58 showed higher (LSD=0.33) GY of  $2.76 \text{ t ha}^{-1}$  as compared to Robigus which had GY of  $2.17 \text{ t ha}^{-1}$ . Finally, the cross-year analysis revealed the NIL PW292-8-Q3A-COMSTR-W had comparable GY of  $3.33 \text{ t ha}^{-1}$  compared to Paragon ( $3.32 \text{ t ha}^{-1}$ ). In addition, in case of GY, the QTL for GFPTT showed significant positive variation under HN conditions compared to its parent.

In 2020, AGBM was found to be higher overall under LN conditions. However, this was not the case for all cultivars. While under LN conditions, Paragon had highest AGDM of 8.35 t ha<sup>-1</sup>, lines like PW292-8-Q3A-COMSTR-W were comparable (8.25 t ha<sup>-1</sup>). However, these lines were not significantly above Paragon. In the case of Robigus, the AGBM was higher (5.08 t ha<sup>-1</sup>) than the two SHW-derived lines. Under HN conditions in 2020, the NIL PW292-7-Q3A-COMSTR-W showed positive variation (LSD=0.62) for AGDM of 8.27 t ha<sup>-1</sup> compared to Paragon (6.75 t ha<sup>-1</sup>). In 2021, the PxW line, PW292-18-Q4B-GFPTT-P showed positive variation for AGDM of 5.24 t ha<sup>-1</sup> compared to Paragon (4.06 t ha<sup>-1</sup>). On the other hand, compared to Robigus (4.41 t ha<sup>-1</sup>), the SHW line SEL58 showed positive variation (LSD=0.62) with AGDM of 5.69 t ha<sup>-1</sup>.

For NUE, in both years genotypes demonstrated higher NUE under LN conditions as compared to HN. In the cross-year analysis, the parent lines had highest NUE. While the NILs, PW141-20-Q7D-AGDM-P (13.08 kg Grain DM kg<sup>-1</sup> N), PW292-1-Q3A-COMSTR-W (13.04 kg Grain DM kg<sup>-1</sup> N), PW292-8-Q3A-COMSTR-W (13.37 kg Grain DM kg<sup>-1</sup> N) and PW468-10-Q7B-AGDM-W (13.89 kg Grain DM kg<sup>-1</sup> N) demonstrated a trend for higher NUE, under LN conditions, compared to Paragon (12.85 kg Grain DM kg<sup>-1</sup> N), but they were not significantly higher (LSD=2.5 kg Grain DM kg<sup>-1</sup> N). Similarly, the SHW line SEL58 showed relatively higher NUE under LN of 15.71 kg Grain DM kg<sup>-1</sup> N compared to Robigus (13.59 kg Grain DM kg<sup>-1</sup> N). However, again this increase was non-significant (LSD=2.5 kg Grain DM kg<sup>-1</sup> N).

In the case of NUpE, the values were higher under LN conditions for the genotypes in both the years as well as the cross-year analysis. In 2020, the lines PW141-10-Q7D-AGDM-W (1.65 kg AGN kg<sup>-1</sup> N), PW292-19-Q3A-COMSTR-P (1.49 kg AGN kg<sup>-1</sup> N), PW292-7-Q3A-COMSTR-W (1.47 kg AGN kg<sup>-1</sup> N), PW292-8-Q3A-COMSTR-W (1.67 kg AGN kg<sup>-1</sup> N), PW292-18-Q4B-GFPTT-P (1.58 kg AGN kg<sup>-1</sup> N), PW468-10-Q7B-AGBM-W (1.65 kg AGN kg<sup>-1</sup> N) and PW729-1-Q6B-AGDM-W (1.55 kg AGN kg<sup>-1</sup> N) all showed significantly higher NUpE (LSD=0.10), under LN conditions, compared to Paragon (1.43 kg Grain DM kg<sup>-1</sup> N). Additionally, SEL63 showed higher NUpE (LSD=0.10) of 1.78 kg AGN kg<sup>-1</sup> N compared to Robigus (1.42 kg AGN kg<sup>-1</sup> N). In 2021, the lines PW141-20-Q7D-AGDM-P (0.31 kg AGN kg<sup>-1</sup> N), PW292-1-Q3A-COMSTR-W (0.32 kg AGN kg<sup>-1</sup> N) and PW468-10-Q7B-AGDM-W (0.33 kg AGN kg<sup>-1</sup> N) showed significantly higher NUpE compared to Paragon (0.30 kg AGN kg<sup>-1</sup> N) under LN conditions. Also, SEL58 showed significantly higher NUpE of 0.34 kg AGN kg<sup>-1</sup> N compared to parent Robigus (0.31 kg

AGN kg<sup>-1</sup> N). Therefore, the QTLs for COMSTR, AGBM and GFPTT demonstrated significant impact on NUpE under LN conditions.

In case of NUtE, the cultivars also demonstrated higher values under LN conditions as compared to HN conditions across both the years as expected. In 2020, while cultivars like PW468-20-Q7B-AGDM-P showed a trend for higher NUtE of 40.60 kg DM kg N<sup>-1</sup> compared to Paragon (37.54 kg DM kg N<sup>-1</sup>), the increase was not significant (LSD=3.27). Similarly, 2021, the PxW line PW292-8-Q3A-COMSTR-W showed higher NUpE of 46.68 kg DM kg N<sup>-1</sup> compared to Paragon (44.25 kg DM kg N<sup>-1</sup>), but not significantly so (LSD = 3.27).

Previous studies in wheat have determined NUE traits and alleles in landraces and wild relatives along with identification of QTLs associated with them (Fontaine *et al.*, 2009; Bogard *et al.*, 2013; Hu *et al.*, 2015; Pozzo *et al.*, 2018; Van Deynze *et al.*, 2018). For a complex trait like NUE it is imperative to carry out QTL mapping studies with suitable elite parents in multiple environments. Additionally, detection of single nucleotide polymorphism (SNPs) markers derived from sequencing aligned to available reference genome would improve marker density and facilitate increased accuracy of QTL associated with NUE and its related traits (Brasier *et al.*, 2020). In the present study, the QTLs for AGDM, COMSTR, COMGRWT as well as the synthetic-derived lines have shown impact on NUE and GY. Therefore, NILs having these QTLs can be used as primary germplasm in pre-breeding and have been utilised for identification of candidate gene markers associated with NUE and its related components in the present study.

### **6.3 Genetic diversity in traits and its association with NUE**

The domestication of landraces and selective breeding has led to constraints in genetic diversity in crop species including wheat. Therefore, evaluation of a wider diversity of germplasm is crucial in order to fish out alleles or genes associated with NUE (Hawkesford, 2017a).

In the present study, variation was seen for QTLs between Paragon and Watkins alleles in the 55 NILs. For grain yield, the QTLs for AGDM on chromosome 7B and 7D showed significant positive variation for the Paragon compared to the Watkins allele. However, on chromosome 6B, the QTL for AGDM showed a higher value for the Watkins allele compared to Paragon.

Apart from this a QTL for GFPTT on chromosome 4B also showed significant variation for the Paragon compared to the Watkins allele.

For NUE, a QTL for AGDM on chromosome 7D showed significantly higher (LSD (5%) = 4.262) value Watkins allele, while on chromosome 7B that of Paragon was greater.

In the case of grain protein content, the Watkins allele showed a significantly higher value for the COMSTRW QTL on chromosome 3A, the NDVI QTL on chromosome 1A, and the GRYLD QTL on chromosome 1B; while the Paragon allele showed a higher value for a AGDM QTL on chromosome 7D and a AGBM QTL on chromosome 7B.

In the synthetic-derived lines, significant genetic variation was observed for traits like GY, GNUP, NUE and GPC. In GY, none of the SHW-derived lines displayed values higher than Robigus. Additionally, However, while the SHW lines did not show elevated NUE levels, genetic variation was seen within the lines ( $p < 0.001$ ). Finally, in case of GPC, all the lines (SEL63, SEL64, SEL56, SEL69, SEL58, SEL57 and SEL6) demonstrated high genetic variation and improved GPC levels from parent Robigus.

Previous studies have established that variations in NUE are influenced mainly by NUpE under LN conditions, while under HN conditions, variations in NUE is attributed more to NUtE (Han *et al.*, 2015). This was corroborated in our study as well wherein the relative influence of NUpE and NUtE varies under varying N conditions. This also indicates the additive nature of traits which perform in a combined manner to improve NUE rather than demonstrating trade-offs. The present study also demonstrated the site variation (RRes and SB) which occurred in terms of GY and NUE, NUpE, NUtE, photosynthesis traits and NUE. As evident, much genetic variation was seen among the NILs. According to previous studies, landraces have low GY leading due a low HI which makes achieving high NUE a challenge (Hawkesford and Griffiths, 2019). Thereby, combining high N uptake and biomass from landraces with high HI for improved NUE at optimum N conditions as well as for optimum GPC is a future challenge for pre-breeding for NUE (Hawkesford and Griffiths, 2019).

#### **6.4 Discovery of candidate gene markers**

Grain yield can be improved by harnessing the genetic variation occurring in NUE which is in turn dependent on factors like the interaction between environment and genotype (Xu *et al.*, 2012). Identification of genes involved in NUE, and its associated regulator pathways will



provide a foundation for determination of N-stress condition effects on different genotypes. The omics-based approach allows for identification of such genes. In wheat, several attempts have been made to study N metabolism used RNA-seq based transcriptomic studies. These studies have been carried out in different tissue samples such as root, shoot, flag leaf in different cultivars as well (Sultana *et al.*, 2021; Tiong *et al.*, 2021). Comparative transcriptomics studies have also been carried out under varying N conditions in contrasting cultivars in terms of NUE (Kaur *et al.*, 2022).

In the present study, comparative transcriptomics studies were carried out in five genotypes under HN and LN conditions. In SHW derived lines, a total of 165 DEGs were shortlisted out of which 21 genes were considered as candidate genes after subjecting to stringent selection criteria of  $P_{adj} < 0.001$  and  $\log_2\text{foldchange} > 1$ . Similarly, in the AGDM QTL, 6 genes were shortlisted, in the GY QTL, 20 genes were shortlisted; the straw yield QTL had 26 CGs and Paragon had 67 CGs. These CGs were found to be associated with transporters, transcription factors (TFs), transferases like methyltransferase and acyltransferase, protein kinases and synthases. Most of these pathways are associated with carbon and N metabolism, photosynthesis and also biosynthesis of amino acids. Transcription factors are crucial for adaptation under stress conditions (Shahzad *et al.*, 2020) and govern genes associated with regulation of N metabolism, uptake and transport (Liu *et al.*, 2022). The present study has identified several TFs like MADS-box transcription factor 56, Heat stress transcription factor etc. Additionally, transporters have been identified in the present study including the Bidirectional sugar transporter SWEET1a under GY QTL. Previous studies in *Arabidopsis* have suggested the role of *SWEET16* in improving NUE (Klemens *et al.*, 2013). Apart from this, genes associated with Cytochrome P450 have also been identified which are directly associated with photosynthesis. Also zinc finger proteins which are key players under stress conditions like N deficit and protein kinases which have a central role in environmental stress as well as hormone signalling (Kaur *et al.*, 2022) have been determined among the DEGs in the present study.

### **6.5 Application of traits and candidate genes for plant breeding for N-uptake efficiency and N-utilisation efficiency**

NUE is a complex trait and comprehension of its genetic variations and physiology is crucial for its improvement in wheat. Previous studies have demonstrated that genetic variation in

NUE and GY is associated more with NUpE than NUtE (Peng *et al.*, 2022). This is more prominent under low N conditions. In the present study also NUE was found to be highly associated with NUpE under both HN and LN conditions. On the other hand, the correlation between NUE and NUtE was extremely low under both conditions and more so under HN conditions.

The NUtE component has been found to be dependent on photosynthesis rate of the canopy, N assimilation and N remobilisation capacity which in turn impacts the canopy senescence (Good *et al.*, 2004). N assimilation also determines grain yield and GPC through affecting N-remobilisation efficiency. Previous studies have demonstrated that genes related to amino acid biosynthesis and N transporters play a crucial role in N assimilation. NADPH-GOGAT enzyme, for instance, regulates N assimilation which impacts the N uptake (Quraishi *et al.*, 2011; Beatty *et al.*, 2013). Apart from this glutamine synthase, and NADH are also important for N assimilation. In the present study amino acid biosynthesis genes including tryptophan decarboxylase 1, LRR receptor-like serine/threonine-protein kinase were identified as candidate genes which can behave as important markers for N assimilation and eventually NUE.

In this study there were QTLs for above-ground dry matter and straw yield at chromosome 7D and 3A, respectively. These traits can be phenotyped using NDVI and subsequently markers for these traits can be determined. Under the QTL on chromosome 7D, genes associated with zinc finger proteins and F box protein are present which are associated with stress adaptations such as N deficit. Additionally, genes associated with phosphoenolpyruvate carboxylase 1 which is associated with carbon metabolism which is turn is correlated with N assimilation were identified. In addition, under chromosome 3A, genes associated with mitochondrial protein which governs photosynthesis, and the photosystem complex were found along with zinc finger proteins.

Combine 1,000 grain weight pertains to the QTL chromosome 5A which was found to contain genes for chlorophyll a-b binding protein corresponding to photosynthesis, methyltransferase, zinc finger proteins and protein kinases which are activated during stress conditions and UDP-glucose flavonoid 3-O-glucosyltransferase which participates in flavonoids biosynthesis which, in turn, causes formation of anthocyanin. Furthermore, the

BED zinc finger protein was also identified which is related to plant growth and development. This has been previously identified in *Arabidopsis* (Knip *et al.*, 2012).

Since the chromosome number and genes under it are known, SNP markers can be detected which can help determine marker-trait association with NUE.

In the present study, the photosynthesis rate of flag-leaf was positively correlated with grain yield in the NILs. So high-throughput measurements of leaf photosynthesis rate are required in wheat breeding. The stay green trait at the canopy level which affects photosynthesis efficiency can also be monitored through NDVI, including the use of unmanned aerial vehicles. Furthermore, leaf chlorophyll content assessed using a SPAD meter has been used as a relatively high-throughput parameter to assess leaf N content in wheat and may be related to leaf photosynthesis rate and grain yield (Xiong *et al.*, 2015). SPAD is highly influenced by environmental factors along with N application and genetic variation has been observed to be associated with GY (Islam *et al.*, 2021). This can be an important perspective for studying photosynthesis rate wherein cultivar-specific SPAD and its relation with  $A_{max}$  and GY can be assessed for a more detailed analysis of NUE and related components. Also, accelerated senescence causes reduced photosynthetic activity and subsequently reduced yield (Hawkesford, 2017b). In the present study, genes associated with senescence (MADS-box transcription factor) and several genes corresponding to photosynthetic activity (ATP synthase subunit alpha chloroplastic, Cytochrome P450, photosynthetic NDH subunit of lumenal location chloroplastic, chlorophyll a-b binding protein and photosystem I reaction center subunit VI) have been identified which can be directly targeted for improved NUE.

In summary, selected QTL regions were introgressed by Marker Assisted Selection (MAS) into UK reference cultivar Paragon. After performing two backcrosses, BC2F2 were produced; NILs are BC3 equivalents and have approximately 87% Paragon background. To capture the complete picture, the Watkins allele NILs were used along with Paragon for a RNA-seq based transcriptomics experiment. Using this approach, maximum differentially expressed genes were identified to reveal unique DEGs from the Watkins alleles and from background Paragon allele for the NUE traits for the deployment in wheat breeding for enhanced NUE.

## ***Chapter 7***

### ***Conclusion and future prospect***

## 7.1 Conclusion and Summary

Among the numerous candidate genes which were found to be significant, there are a few genes which are directly associated with photosynthesis, carbon metabolism, N assimilation and biosynthesis of amino acids which could be strong potential candidates. A list of the shortlisted genes based on their function is given below and which will be taken forward for future expression studies and functional validation studies for developing elite wheat lines with improved NUE.

Sr. No	QTL	Gene description
1	Synthetic-derived line	<i>Photosynthesis:</i> Geranylgeranyl diphosphate reductase (LOC123128382), chlorophyll a-b binding protein of LHCII type 1 (LOC123068639), chlorophyll a-b binding protein of LHCII type 1 (LOC123122527), chlorophyll a-b binding protein 1B (LOC123121683), photosystem I reaction center subunit IV (LOC123145507) chlorophyll a-b binding protein of LHCII type 1 (LOC123104728), chlorophyll a-b binding protein of LHCII type III (LOC123148365), chlorophyll a-b binding protein 7 (LOC123044442) <i>Carbohydrate metabolism:</i> phosphoenolpyruvate carboxylase 1 (LOC123164058), glyceraldehyde-3-phosphate dehydrogenase A (LOC123053529), glyceraldehyde-3-phosphate dehydrogenase (LOC123189421),
2	AGDM QTL	<i>Photosynthesis:</i> Cytochrome P450 (LOC123181976) <i>Stress response:</i> Methyltransferase C9orf114 (LOC123105694)
3	GY QTL	<i>Stress response:</i> Proline-rich receptor-like protein kinase (LOC123099896), BED zinc finger (Novel Gene), Methyltransferase (LOC123143074), FBD-associated F-box protein (LOC123155760) <i>Photosynthesis:</i> ATP synthase subunit (LOC123068902)

		<i>NUE improvement</i> : Bidirectional sugar transporter SWEET1a (LOC123145518)
4	Straw yield QTL	<i>Stress response</i> : Zinc finger CCCH domain-containing protein like OsC3H22 (LOC123061040), <i>Photosynthesis</i> : Mitochondrial import inner membrane translocase subunit TIM14-3 (LOC123125626)
5	Paragon	<i>Stress response</i> : MADS-box transcription factor 56 (LOC123126988), FBD-associated F-box protein (LOC123070699), dof zinc finger protein DOF5.1 (LOC123102474), zinc finger protein ZAT1 (LOC123130755), FBD-associated F-box protein (LOC123145992), F-box protein (LOC123164659) <i>Photosynthesis</i> : ATP synthase subunit alpha chloroplastic (LOC123046757), UDP-glucose flavonoid 3-O-glucosyltransferase (LOC123105515), photosynthetic NDH subunit of lumenal location chloroplastic (LOC123127700) <i>Carbohydrate metabolism</i> : Glyceraldehyde-3-phosphate dehydrogenase (LOC123039230) <i>Amino acid biosynthesis</i> : Tryptophan decarboxylase 1 (LOC123050389), aspartic proteinase (LOC123070578), LRR receptor-like serine/threonine-protein kinase (LOC123135850)

## **7.2 Ongoing work**

Based on RNA-seq data of the flag leaf collected from the five genotypes, SNPs for the QTLs for further validation were acquired. The effect of the SNP markers is being analysed and a score for missense, nonsense or silent mutation will be generated which will give the predicted effect of the SNP on the corresponding gene function. Hypothetically, the SNPs which have a larger impact are located on the putative candidate genes. Furthermore, the gene functions can also be validated by determining homologous genes in related cereals and crop systems.

### 7.3 Future work

In the present investigation, genetic diversity was identified in wheat landrace and synthetic derivatives for NUE and its components (N uptake and NUtE). Genotypes selected for study in these experiments were developed at John Innes Centre, UK (landrace derivatives) and NIAB, UK (synthetic derivatives); a wider range of genotypes should be screened in future work including other wheat germplasm collections and panels worldwide (e.g., CIMMYT wheat diversity panel) to identify further for diversity for NUE traits.

To understand the genetic variation for NUE, QTL analysis based on sets of NILs was carried out. Additionally, the chromosomal location of these QTLs was determined followed by identification of putative candidate genes using a RNA-seq based transcriptomics study. Further validation of these major QTLs can be done by developing Kompetitive Allele Specific PCR (KASP) markers based on sequencing data and predicted candidate genes for NUE, GY, AGDM, straw yield according to gene annotation as well as SNP analysis. Utilisation of KASP markers would facilitate determination of specific and accurate QTL regions associated with a chromosome number and physical region corresponding to a particular trait. The linked KASP markers identified from this study will help in breeding for improving NUE in wheat.

Functional validation of candidate genes is crucial for determining the utility and importance of a gene. Induced mutational studies in novel genes of interest can be accessed via Targeting Induced Local Lesion IN Genomes (TILLING) and CRISPR/Cas9 (Clustered regularly interspaced short palindromic repeats/Cas9) based genome editing approaches. TILLING is a reverse genetics approach which allows for detection of useful mutant lines in a sub-set of induced mutant lines. Mutational studies can also be done via genome editing through knockout and knockdown of relevant genes which is also an effective non-transgenic approach for crop improvement.

Evaluation of phenotypes distinct of the generated mutants from wild type, as well as novel morphological features, would be done for parameters like tillering type, senescence timing, plant height etc which are directly correlated with N uptake. Determination of frequency of the various mutations exhibited phenotypically in the mutant population will help in developing a repository of significant mutations for future forwards and reverse genetic studies.



Finally, another technique to obtain improved NUE in wheat is genetic engineering. The identified genes associated with NUE can first be analysed for their expression profiles using q-RTPCR analysis. This would narrow down the CGs for further validation studies. Over-expression of the gene using recombinant DNA technology in model crop systems followed by over-expression in specific crop systems would provide lines with improved NUE. Considering NUE is a highly complex trait, using modern techniques like mutation generation, genetic engineering and genome editing will enable a fast and efficient means of achieving this goal.

## References

- Ahmed, O.H., Hussin, A., Ahmad, H.M., Rahim, A.A. and Majid, N.M.A., 2008. Enhancing the urea-N use efficiency in maize (*Zea mays*) cultivation on acid soils amended with zeolite and TSP. *The scientific world journal*, 8, pp.394-399.
- Alvarez, J.M.; Vidal, E.A.; and Gutiérrez, R.A. (2012) Integration of local and systemic signaling pathways for plant N responses. *Curr. Opin. Plant Biology*. 15, pp. 185–191.
- An, D., Su, J., Liu, Q., Zhu, Y., Tong, Y., Li, J., Jing, R., Li, B. and Li, Z., 2006. Mapping QTLs for nitrogen uptake in relation to the early growth of wheat (*Triticum aestivum* L.). *Plant and Soil*, 284, pp.73-84.
- Atkinson, J.A., Wingen, L.U., Griffiths, M., Pound, M.P., Gaju, O., Foulkes, M.J., Le Gouis, J., Griffiths, S., Bennett, M.J., King, J. and Wells, D.M., 2015. Phenotyping pipeline reveals major seedling root growth QTL in hexaploid wheat. *J. Exp. Bot.* 66(8), pp.2283-2292.
- Austin, R.B., Morgan, C.L., Ford, M.A. and Bhagwat, S.G., 1982. Flag leaf photosynthesis of *Triticum aestivum* and related diploid and tetraploid species. *Annals of Botany*, 49(2), pp.177-189.
- Babar, M.A., Reynolds, M.P., Van Ginkel, M., Klatt, A.R., Raun, W.R., and Stone, M.L., 2006. Spectral reflectance indices as a potential indirect selection criterion for wheat yield under irrigation. *Crop Sci.* 46, pp.578–588.
- Bancal, P., 2009. Decorrelating source and sink determinism of nitrogen remobilisation during grain filling in wheat. *Ann. Bot.* 103, pp. 1315–1324.
- Banerjee, B.P., Joshi, S., Thoday-Kennedy, E., Pasam, R.K., Tibbits, J., Hayden, M., Spangenberg, G., and Kant, S., 2020. High-throughput phenotyping using digital and hyperspectral imaging-derived biomarkers for genotypic nitrogen response. *J. Exp. Bot.* 71, pp. 4604–4615.
- Bansiwal, A.K., Rayalu, S.S., Labhasetwar, N.K., Juwarkar, A.A. and Devotta, S., 2006. Surfactant-modified zeolite as a slow release fertiliser for phosphorus. *J. Agric. Food Chem.* 54(13), pp.4773-4779.
- Barbottin, A., Lecomte, C., Bouchard, C. and Jeuffroy, M.H., 2005. Nitrogen remobilisation during grain filling in wheat: Genotypic and environmental effects. *Crop Sci.* 45, 1141–1150.
- Barraclough, P.B., Howarth, J.R., Jones, J., Lopez-Bellido, R., Parmar, S., Shepherd, C.E., and Hawkesford, M.J., 2010. Nitrogen efficiency of wheat: Genotypic and environmental variation and prospects for improvement. *Eur. J. Agron.* 33, pp. 1–11.
- Barraclough, P.B., Lopez-Bellido, R. and Hawkesford, M.J., 2014. Genotypic variation in the uptake, partitioning and remobilisation of nitrogen during grain-filling in wheat. *Field Crops Research*, 156, pp.242-248.

- Barutçular, C., Yildirim, M., Koc, M., Akinci, C., Toptas, I., Albayrak, O., Tanrikulu, A., and Ayman, S.E., 2016. Evaluation of Spad Chlorophyll in Spring Wheat Genotypes Under Different. *Fresenius Environ. Bull.* 25, pp. 1258–1266.
- Beatty, P.H., Carroll, R.T., Shrawat, A.K., Guevara, D., and Good, A.G., 2013. Physiological analysis of nitrogen-efficient rice over-expressing alanine aminotransferase under different N regimes. *Botany* 91, pp. 866–883.
- Benjamini, Y. and Hochberg, Y., 1995. Controlling the false discovery rate: a practical and powerful approach to multiple testing. *Journal of the Royal statistical society: series B (Methodological)*, 57(1), pp.289-300.
- Bhattacharyya, P.N. and Jha, D.K., 2012. Plant growth-promoting rhizobacteria (PGPR): emergence in agriculture. *World J. Microbiol. Biotechnol.* 28, pp.1327-1350.
- Bogard, M., Allard, V., Brancourt-Hulmel, M., Heumez, E., MacHet, J.M., Jeuffroy, M.H., Gate, P., Martre, P., and Le Gouis, J., 2010. Deviation from the grain protein concentration-grain yield negative relationship is highly correlated to post-anthesis N uptake in winter wheat. *J. Exp. Bot.* 61, pp. 4303–4312.
- Bogard, M., Allard, V., Martre, P., Heumez, E., Snape, J.W., Orford, S., Griffiths, S., Gaju, O., Foulkes, J. and Le Gouis, J., 2013. Identifying wheat genomic regions for improving grain protein concentration independently of grain yield using multiple inter-related populations. *Mol. Plant Breed.* 31, pp.587-599.
- Bouchet, A.S., Laperche, A., Bissuel-Belaygue, C., Snowdon, R., Nesi, N. and Stahl, A., 2016. Nitrogen use efficiency in rapeseed. A review. *Agron. Sustain. Dev.* 36, pp.1-20.
- Boussadia, O., Steppe, K., Zgallai, H., El Hadj, S.B., Braham, M., Lemeur, R. and Van Labeke, M.C., 2010. Effects of nitrogen deficiency on leaf photosynthesis, carbohydrate status and biomass production in two olive cultivars 'Meski' and 'Koroneiki'. *Sci. Hortic.* 123(3), pp.336-342.
- Brasier, K., Ward, B., Smith, J., Seago, J., Oakes, J., Balota, M., Davis, P., Fountain, M., Brown-Guedira, G., Sneller, C., Thomason, W., and Griffey, C., 2020. Identification of quantitative trait loci associated with nitrogen use efficiency in winter wheat. *PLoS One.* 15, pp. 1–23.
- Canvin, D. T. 1981. Photorespiration and nitrogen metabolism. In *Nitrogen and Carbon Metabolism: Proceedings of a Symposium on the Physiology and Biochemistry of Plant Productivity*, held in Calgary, Canada, July 14–17, 1980 (pp. 178-194). Springer Netherlands.
- Carmo-Silva, E., Scales, J.C., Madgwick, P.J. and Parry, M.A., 2015. Optimizing Rubisco and its regulation for greater resource use efficiency. *Plant Cell Environ.* 38(9), pp.1817-1832.
- Carmo-Silva, E., Andralojc, P.J., Scales, J.C., Driever, S.M., Mead, A., Lawson, T., Raines, C.A. and Parry, M.A., 2017. Phenotyping of field-grown wheat in the UK highlights contribution of

light response of photosynthesis and flag leaf longevity to grain yield. *J Exp Bot.* 68(13), pp.3473-3486.

Carvalho, P., and Foulkes, M.J., 2018. Roots and uptake of water and nutrients. *Encyclopedia of sustainability science and technology*, pp.1-24

Cassán, F., Perrig, D., Sgroj, V., Masciarelli, O., Penna, C. and Luna, V., 2009. *Azospirillum brasilense* Az39 and *Bradyrhizobium japonicum* E109, inoculated singly or in combination, promote seed germination and early seedling growth in corn (*Zea mays* L.) and soybean (*Glycine max* L.). *Eur. J. Soil Biol.*, 45(1), pp.28-35.

Chakwizira, E., Teixeira, E.I., Ruitter, J.M. De, Maley, S., and George, M.J., 2016. Harvest index for biomass and nitrogen in maize crops limited by nitrogen and water. *Int. Nitrogen Initiat. Conf.* 4–8.

Charousová, I., Javoreková, S., Medo, J. and Schade, R., 2016. Characteristic of selected soil Streptomycetes with antimicrobial potential against phytopathogenic microorganisms. *J. Microbiol. Biotechnol. Food Sci.* 5, pp.64.

Colla, G., Rouphael, Y., Canaguier, R., Svecova, E. and Cardarelli, M., 2014. Biostimulant action of a plant-derived protein hydrolysate produced through enzymatic hydrolysis. *Front. Plant Sci.* 5, pp.448.

Collier, E., 2022. Wheat production, utilisation and stocks (FAO report). *Food Outlook 2022*.

Congreves, K.A., Otchere, O., Ferland, D., Farzadfar, S., Williams, S., and Arcand, M.M., 2021. Nitrogen Use Efficiency Definitions of Today and Tomorrow. *Front. Plant Sci.* 12, pp. 1–10.

Cormier, F., Foulkes, J., Hirel, B., Gouache, D., Moëgne-Loccoz, Y., and Le Gouis, J., 2016. Breeding for increased nitrogen-use efficiency: A review for wheat (*T. aestivum* L.). *Plant Breed.* 135, pp. 255–278.

Cormier, F., Le Gouis, J., Dubreuil, P., Lafarge, S. and Praud, S., 2014. A genome-wide identification of chromosomal regions determining nitrogen use efficiency components in wheat (*Triticum aestivum* L.). *Theor. Appl. Genet.* 127, pp.2679-2693.

Curci, P.L., Aiese Cigliano, R., Zuluaga, D.L., Janni, M., Sanseverino, and W., Sonnante, G., 2017. Transcriptomic response of durum wheat to nitrogen starvation. *Sci. Rep.* 7, pp. 1–14.

de Oliveira Silva, A., Ciampitti, I.A., Slafer, G.A., and Lollato, R.P., 2020. Nitrogen utilisation efficiency in wheat: A global perspective. *Eur. J. Agron.* 114.

Del Blanco, I.A., Rajaram, S., Kronstad, W.E. and Reynolds, M.P., 2000. Physiological performance of synthetic hexaploid wheat-derived populations. *Crop Sci.* 40(5), pp.1257-1263.

Desai, R.M., and Bhatia, C.R., 1978. Nitrogen uptake and nitrogen harvest index in durum wheat cultivars varying in their grain protein concentration. *Euphytica* 27, 561–566.

Di Benedetto, N.A., Corbo, M.R., Campaniello, D., Cataldi, M.P., Bevilacqua, A., Sinigaglia, M. and Flagella, Z., 2017. The role of plant growth promoting bacteria in improving nitrogen use efficiency for sustainable crop production: a focus on wheat. *AIMS Microbiol.* 3(3), p.413.

Dobermann, A. and Cassman, K.G., 2005. Cereal area and nitrogen use efficiency are drivers of future nitrogen fertiliser consumption. *Science in China Series C: Life Sciences*, 48, pp.745-758.

Dobermann, A.R., 2005. Nitrogen use efficiency-state of the art. *Agronomy--Faculty Publications*, p.316.

Dreccer, F., Ogbonnaya, G., Borgognone, J. and Wilson, J., 2004, September. Variation in shoot and root growth in primary synthetic wheats—implications for overcoming water deficits in marginal environments. In *Proceedings of the 4th international crop science congress, Brisbane (Vol. 26)*.

Duncan, E.G., O'Sullivan, C.A., Roper, M.M., Palta, J., Whisson, K. and Peoples, M.B., 2018. Yield and nitrogen use efficiency of wheat increased with root length and biomass due to nitrogen, phosphorus, and potassium interactions. *J Plant Nutr Soil. Sci* 181(3), pp.364-373.

Fageria, N.K. and Baligar, V.C., 2005. Enhancing nitrogen use efficiency in crop plants. *Adv. Agron.* 88, pp.97-185.

Fageria, N.K., 2010, August. Optimal nitrogen fertilization timing for upland rice. In *19th World Congress of Soil Science, Soil Solutions for a Changing World (pp. 1-6)*.

Fageria, N.K., 2014. Nitrogen Harvest Index and Its Association With Crop Yields. *J. Plant Nutr.* 37, pp. 795–810.

Fan, X., Zhang, W., Zhang, N., Chen, M., Zheng, S., Zhao, C., Han, J., Liu, J., Zhang, X., Song, L., Ji, J., Liu, X., Ling, H., Tong, Y., Cui, F., Wang, T., and Li, J., 2018. Identification of QTL regions for seedling root traits and their effect on nitrogen use efficiency in wheat (*Triticum aestivum* L.). *Theor. Appl. Genet.* 131, pp. 2677–2698.

Fan, Xiaorong, Naz, M., Fan, Xiaoru, Xuan, W., Miller, A.J., and Xu, G., 2017. Plant nitrate transporters: From gene function to application. *J. Exp. Bot.* 68, pp. 2463–2475.

FAO, Wheat production, 2022. <https://www.fao.org/faostat/en/#data/QCL>

Fernando, K.M.C., Ehoche, O.G., Atkinson, J.A. and Sparkes, D.L., 2021. Root System Architecture and Nitrogen Uptake Efficiency of Wheat Species. *J Agric Sci (Sri Lanka)*. 16(1).

Fischer, A.M., 2012. The complex regulation of senescence. *Crit. Rev. Plant Sci* .31(2), pp.124-147.

Fontaine, J.X., Ravel, C., Pageau, K., Heumez, E., Dubois, F., Hirel, B. and Le Gouis, J., 2009. A quantitative genetic study for elucidating the contribution of glutamine synthetase,

glutamate dehydrogenase and other nitrogen-related physiological traits to the agronomic performance of common wheat. *Theor. Appl. Genet.* 119(4), pp.645-662.

Foulkes, M.J., Hawkesford, M.J., Barraclough, P.B., Holdsworth, M.J., Kerr, S., Kightley, S., and Shewry, P.R., 2009. Identifying traits to improve the nitrogen economy of wheat: Recent advances and future prospects. *F. Crop. Res.* 114, pp. 329–342.

Foyer, C.H., Ferrario-Méry, S. and Noctor, G., 2001. Interactions between carbon and nitrogen metabolism. In *Plant nitrogen* (pp. 237-254). Berlin, Heidelberg: Springer Berlin Heidelberg.

Fradgley, N., Evans, G., Biernaskie, J.M., Cockram, J., Marr, E.C., Oliver, A.G., Ober, E., Jones, and H., 2020. Effects of breeding history and crop management on the root architecture of wheat. *Plant Soil* 452, pp. 587–600.

Fujinuma, R., Balster, N.J. and Hyung-Kyung, L., 2011, January. Reduced rates of controlled-release fertiliser lower potential nitrogen leaching from a Wisconsin bare-root tree nursery. In *Proceedings of the 17th Central Hardwood Forest Conference GTR-NRS-P-78* (pp. 347-357).

Gaju, O., Allard, V., Martre, P., Le Gouis, J., Moreau, D., Bogard, M., Hubbart, S. and Foulkes, M.J., 2014. Nitrogen partitioning and remobilisation in relation to leaf senescence, grain yield and grain nitrogen concentration in wheat cultivars. *Field Crops Research*, 155, pp.213-223.

Gaju, O., Allard, V., Martre, P., Snape, J.W., Heumez, E., LeGouis, J., Moreau, D., Bogard, M., Griffiths, S., Orford, S., Hubbart, S., and Foulkes, M.J., 2011. Identification of traits to improve the nitrogen-use efficiency of wheat genotypes. *F. Crop. Res.* 123, pp. 139–152.

Gaju, O., DeSilva, J., Carvalho, P., Hawkesford, M.J., Griffiths, S., Greenland, A., and Foulkes, M.J., 2016. Leaf photosynthesis and associations with grain yield, biomass and nitrogen-use efficiency in landraces, synthetic-derived lines and cultivars in wheat. *F. Crop. Res.* 193, pp.1–15.

Galloway, J.N., Schlesinger, W.H., Levy, H., Michaels, A. and Schnoor, J.L., 1995. Nitrogen fixation: Anthropogenic enhancement-environmental response. *Global biogeochemical cycles*, 9(2), pp.235-252.

Ghafoor, I., Habib-ur-Rahman, M., Ali, M., Afzal, M., Ahmed, W., Gaiser, T., Ghaffar, A., 2021. Slow-release nitrogen fertilisers enhance growth, yield, NUE in wheat crop and reduce nitrogen losses under an arid environment. *Environ. Sci. Pollut. Res.* 28, pp.43528–43543.

Giehl, R.F., Gruber, B.D. and von Wirén, N., 2014. It's time to make changes: modulation of root system architecture by nutrient signals. *J. Exp. Bot.* 65(3), pp.769-778.

Givaty Rapp, Y., Ransbotyn, V. and Grafi, G., 2015. Senescence meets dedifferentiation. *Plants*, 4(3), pp.356-368.

Glass, A.D.M., 2003. Nitrogen Use Efficiency of Crop Plants: Physiological Constraints upon Nitrogen Absorption. *CRC. Crit. Rev. Plant Sci.* 22, pp.453–470.

- Good, A.G. and Beatty, P.H., 2011. Biotechnological approaches to improving nitrogen use efficiency in plants: alanine aminotransferase as a case study. The molecular and physiological basis of nutrient use efficiency in crops, pp.165-191.
- Good, A.G., Shrawat, A.K. and Muench, D.G., 2004. Can less yield more? Is reducing nutrient input into the environment compatible with maintaining crop production? Trends Plant Sci. 9(12), pp.597-605.
- Gruber, B.D., Giehl, R.F., Friedel, S. and von Wirén, N., 2013. Plasticity of the *Arabidopsis* root system under nutrient deficiencies. Plant Physiol. 163(1), pp.161-179.
- Guo M., Wang Q., Zong Y., Nian J., Li H., Li J., Wang T., Gao C., and Zuo J. 2021. Genetic manipulations of TaARE1 boost nitrogen utilisation and grain yield in wheat. JGG= Yi chuan xue bao 48(10), pp.950-3
- Guo, Y., Kong, F.M., Xu, Y.F., Zhao, Y., Liang, X., Wang, Y.Y., An, D.G. and Li, S.S., 2012. QTL mapping for seedling traits in wheat grown under varying concentrations of N, P and K nutrients. Theor. Appl. Genet. 124, pp.851-865.
- Guttieri, M.J., Frels, K., Regassa, T., Waters, B.M., and Baenziger, P.S., 2017. Variation for nitrogen use efficiency traits in current and historical great plains hard winter wheat. Euphytica 213, pp.1–18.
- Habash, D.Z., Bernard, S., Schondelmaier, J., Weyen, J. and Quarrie, S.A., 2007. The genetics of nitrogen use in hexaploid wheat: N utilisation, development and yield. Theor. Appl. Genet. 114, pp.403-419.
- Habash, D.Z., Massiah, A.J., Rong, H.L., Wallsgrove, R.M. and Leigh, R.A., 2001. The role of cytosolic glutamine synthetase in wheat. Ann. Appl. Biol. 138(1), pp.83-89.
- Haile, D., Nigussie, D., and Ayana, A., 2012. Nitrogen use efficiency of bread wheat: Effects of nitrogen rate and time of application. J. Soil Sci. Plant Nutr. 12, pp.389–409.
- Halloran, G.M., Ogbonnaya, F.C. and Lagudah, E.S., 2008. *Triticum* (*Aegilops*) *tauschii* in the natural and artificial synthesis of hexaploid wheat. Australian journal of agricultural research, 59(5), pp.475-490.
- Han, M., Okamoto, M., Beatty, P. H., Rothstein, S. J., and Good, A. G., 2015. The Genetics of Nitrogen Use Efficiency in Crop Plants. Annu. Rev. Genet. 49, pp.269–289.
- Hassan, T.U. and Bano, A., 2016. Biofertiliser: a novel formulation for improving wheat growth, physiology and yield. Pak. J. Bot, 48(6), pp.2233-2241.
- Häusler, R.E., Rademacher, T., Li, J., Lipka, V., Fischer, K.L., Schubert, S., Kreuzaler, F. and Hirsch, H.J., 2001. Single and double over-expression of C4-cycle genes had differential effects on the pattern of endogenous enzymes, attenuation of photorespiration and on contents of UV protectants in transgenic potato and tobacco plants. J. Exp. Bot. 52(362), pp.1785-1803.

- Hawkesford, M., 2012. The diversity of nitrogen use efficiency for wheat varieties and the potential for crop improvement. *Better Crop. with Plant Food* 96, pp.10–12.
- Hawkesford, M.J., 2011. An overview of nutrient use efficiency and strategies for crop improvement. *The molecular and physiological basis of nutrient use efficiency in crops*, pp.3-19.
- Hawkesford, M.J., 2014. Reducing the reliance on nitrogen fertiliser for wheat production. *J. Cereal Sci.* 59, pp.276–283.
- Hawkesford, M.J., 2017. Genetic variation in traits for nitrogen use efficiency in wheat. *J. Exp. Bot.* 68, pp.2627–2632.
- Hawkesford, M.J., and Griffiths, S., 2019. Exploiting genetic variation in nitrogen use efficiency for cereal crop improvement. *Curr. Opin. Plant Biol.* 49, pp.35–42.
- Hawkesford, M.J., Riche, A.B., 2020. Impacts of G x E x M on Nitrogen Use Efficiency in Wheat and Future Prospects. *Front. Plant Sci.* 11, pp.1–9.
- He, X., Qu, B., Li, W., Zhao, X., Teng, W., Ma, W., Ren, Y., Li, B., Li, Z. and Tong, Y., 2015. The nitrate-inducible NAC transcription factor TaNAC2-5A controls nitrate response and increases wheat yield. *Plant Physiol.* 169(3), pp.1991-2005.
- Hirel, B., Le Gouis, J., Ney, B. and Gallais, A., 2007. The challenge of improving nitrogen use efficiency in crop plants: towards a more central role for genetic variability and quantitative genetics within integrated approaches. *J. Exp. Bot.* 58(9), pp.2369-2387.
- Holman, F.H., Riche, A.B., Michalski, A., Castle, M., Wooster, M.J., and Hawkesford, M.J., 2016. High throughput field phenotyping of wheat plant height and growth rate in field plot trials using UAV based remote sensing. *Remote Sens.* 8.
- Hu, B., Wang, W., Ou, S., Tang, J., Li, H., Che, R., Zhang, Z., Chai, X., Wang, H., Wang, Y. and Liang, C., 2015. Variation in NRT1. 1B contributes to nitrate-use divergence between rice subspecies. *Nat. Gen.* 47(7), pp.834-838.
- Hu, M., Zhao, X., Liu, Q., Hong, X., Zhang, W., Zhang, Y., Sun, L., Li, H., and Tong, Y., 2018. Transgenic expression of plastidic glutamine synthetase increases nitrogen uptake and yield in wheat. *Plant Biotechnol. J.* 16, pp.1858–1867.
- Inman, D., Khosla, R., Reich, R.M. and Westfall, D.G., 2007. Active remote sensing and grain yield in irrigated maize. *Precision Agriculture*, 8, pp.241-252.
- Islam, M.R., Haque, K.S., Akter, N. and Karim, M.A., 2014. Leaf chlorophyll dynamics in wheat based on SPAD meter reading and its relationship with grain yield. *Sci. Agric.* 8(1), pp.13-18.
- Islam, S., Zhang, J., Zhao, Y., She, M., and Ma, W., 2021. Genetic regulation of the traits contributing to wheat nitrogen use efficiency. *Plant Sci.* 303, pp.110759.



- Jaradat, A.A., 2013. Wheat landraces: A mini review. *Emirates J. Food Agric.* 25, pp.20–29.
- Javed, T., Singhal, R.K., Shabbir, R., Shah, A.N., Kumar, P., Jinger, D., Dharmappa, P.M., Shad, M.A., Saha, D., Anuragi, H. and Adamski, R., 2022. Recent advances in agronomic and physio-molecular approaches for improving nitrogen use efficiency in crop plants. *Front. Plant Sci.*, 13, p.877544.
- Jha, C.K., Ghosh, R.K., Saxena, S., Singh, V., Mosnier, A., Guzman, K.P., Stevanović, M., Popp, A., and Lotze-Campen, H., 2023. Pathway to achieve a sustainable food and land-use transition in India. *Sustain. Sci.* 18, pp.457–468.
- Jimenez-Berni, J.A., Deery, D.M., Rozas-Larraondo, P., Condon, A.T.G., Rebetzke, G.J., James, R.A., Bovill, W.D., Furbank, R.T., and Sirault, X.R.R., 2018. High throughput determination of plant height, ground cover, and above-ground biomass in wheat with LiDAR. *Front. Plant Sci.* 9, pp.1–18.
- Jin, X., Zarco-Tejada, P.J., Schmidhalter, U., Reynolds, M.P., Hawkesford, M.J., Varshney, R.K., Yang, T., Nie, C., Li, Z., Ming, B. and Xiao, Y., 2020. High-throughput estimation of crop traits: A review of ground and aerial phenotyping platforms. *IEEE Trans. Geosci. Remote Sens.* 9(1), pp.200-231.
- Justes, E., Mary, B., Meynard, J.M., Machet, J.M. and Thelier-Huché, L., 1994. Determination of a critical nitrogen dilution curve for winter wheat crops. *Annals of botany*, 74(4), pp.397-407.
- Kareem, S.H., Hawkesford, M.J., DeSilva, J., Weerasinghe, M., Wells, D.M., Pound, M.P., Atkinson, J.A. and Foulkes, M.J., 2022. Root architecture and leaf photosynthesis traits and associations with nitrogen-use efficiency in landrace-derived lines in wheat. *Eur. J. Agron.* 140, pp.126603.
- Kaur, S., Shamshad, M., Jindal, S., Kaur, A., Singh, S. and Kaur, S., 2022. RNA-seq-based transcriptomics study to investigate the genes governing nitrogen use efficiency in indian wheat cultivars. *Front. Geneti*, 13, pp.1-15
- Kenobi, K., Atkinson, J.A., Wells, D.M., Gaju, O., De Silva, J.G., Foulkes, M.J., Dryden, I.L., Wood, A.T. and Bennett, M.J., 2017. Linear discriminant analysis reveals differences in root architecture in wheat seedlings related to nitrogen uptake efficiency. *J. Exp. Bot.* 68(17), pp.4969-4981.
- Kiba, T., Krapp, A., 2016. Plant nitrogen acquisition under low availability: Regulation of uptake and root architecture. *Plant Cell Physiol.* 57, pp.707–714.

- Kichey, T., Hirel, B., Heumez, E., Dubois, F. and Le Gouis, J., 2007. In winter wheat (*Triticum aestivum* L.), post-anthesis nitrogen uptake and remobilisation to the grain correlates with agronomic traits and nitrogen physiological markers. *Field Crops Res.* 102(1), pp.22-32.
- Klemens, P.A., Patzke, K., Deitmer, J., Spinner, L., Le Hir, R., Bellini, C., Bedu, M., Chardon, F., Krapp, A. and Neuhaus, H.E., 2013. Over-expression of the vacuolar sugar carrier *AtSWEET16* modifies germination, growth, and stress tolerance in *Arabidopsis*. *Plant Physiol.* 163(3), pp.1338-1352.
- Knip, M., de Pater, S. and Hooykaas, P.J., 2012. The SLEEPER genes: a transposase-derived angiosperm-specific gene family. *BMC Plant Biol.* 12, pp.1-15.
- Kocheva, K., Kartseva, T., Nenova, V., Georgiev, G., Brestič, M., and Misheva, S., 2020. Nitrogen assimilation and photosynthetic capacity of wheat genotypes under optimal and deficient nitrogen supply. *Physiol. Mol. Biol. Plants* 26, pp.2139–2149.
- Kong, L., Xie, Y., Hu, L., Feng, B. and Li, S., 2016. Remobilisation of vegetative nitrogen to developing grain in wheat (*Triticum aestivum* L.). *Field Crops Res.* 196, pp.134-144.
- Kuhlmann, H. and Barraclough, P.B., 1987. Comparison between the seminal and nodal root systems of winter wheat in their activity for N and K uptake. *Zeitschrift für Pflanzenernährung und Bodenkunde*, 150(1), pp.24-30.
- Laperche, A., Brancourt-Hulmel, M., Heumez, E., Gardet, O., Hanocq, E., Devienne-Barret, F. and Le Gouis, J., 2007. Using genotypex nitrogen interaction variables to evaluate the QTL involved in wheat tolerance to nitrogen constraints. *Theor. Appl. Genet.* 115(3), pp.399-415.
- Latshaw, S.P., Vigil, M.F., and Haley, S.D., 2016. Genotypic differences for nitrogen use efficiency and grain protein deviation in hard winter wheat. *Agron. J.* 108, pp.2201–2213.
- Le Gouis, J., Béghin, D., Heumez, E. and Pluchard, P., 2000. Genetic differences for nitrogen uptake and nitrogen utilisation efficiencies in winter wheat. *Eur. J. Agron.* 12(3-4), pp.163-173.
- Lea, P.J. and Azevedo, R.A.D., 2007. Nitrogen use efficiency. 2. Amino acid metabolism. *Annals of Applied Biology*, 151(3), pp.269-275.
- Lei, L., Li, G., Zhang, H., Powers, C., Fang, T., Chen, Y., Wang, S., Zhu, X., Carver, B.F., and Yan, L., 2018. Nitrogen use efficiency is regulated by interacting proteins relevant to development in wheat. *Plant Biotechnol. J.* 16, pp.1214–1226.
- Li, G.Q., Li, Z.F., Yang, W.Y., Zhang, Y., He, Z.H., Xu, S.C., Singh, R.P., Qu, Y.Y. and Xia, X.C., 2006. Molecular mapping of stripe rust resistance gene *YrCH42* in Chinese wheat cultivar Chuanmai 42 and its allelism with *Yr24* and *Yr26*. *Theor. Appl. Genet.* 112, pp.1434-1440.
- Li, J., WAN, H.S. and YANG, W.Y., 2014. Synthetic hexaploid wheat enhances variation and adaptive evolution of bread wheat in breeding processes. *J Syst Evol.* 52(6), pp.735-742.

- Liang, Z., Bronson, K.F., Thorp, K.R., Mon, J., Badaruddin, M. and Wang, G., 2014. Cultivar and N fertiliser rate affect yield and N use efficiency in irrigated durum wheat. *Crop Sci.* 54(3), pp.1175-1183.
- Lima, J.E., Kojima, S., Takahashi, H. and von Wirén, N., 2010. Ammonium triggers lateral root branching in *Arabidopsis* in an AMMONIUM TRANSPORTER1; 3-dependent manner. *The Plant Cell*, 22(11), pp.3621-3633.
- Liu, X., Hu, B. and Chu, C., 2022. Nitrogen assimilation in plants: current status and future prospects. *J Genet. Genomics.* 49(5), pp.394-404.
- Liu, X.M., Feng, Z.B., Zhang, F.D., Zhang, S.Q., and He, X.S., 2006. Preparation and testing of cementing and coating nano-subnanocomposites of slow/controlled-release fertiliser. *Agr. Sci. China.* 5(9), pp.700-706.
- Liu, Y., Li, Y., Li, S. and Motesharrei, S., 2015. Spatial and temporal patterns of global NDVI trends: correlations with climate and human factors. *Remote Sens.* 7(10), pp.13233-13250.
- López-Bucio, J., Cruz-Ramirez, A. and Herrera-Estrella, L., 2003. The role of nutrient availability in regulating root architecture. *Curr. Opin. Plant Biol.* 6(3), pp.280-287.
- Lukina, E.V., Freeman, K.W., Mullen, R.W., Wynn, K.J., Thomason, W.E., Teal, R., Mosali, J., Feng, T., Needham, D.E., Washmon, C.N. and Solie, J.B., Soil Fertility Research Report 2000.
- Lynch, J.P., 2013. Steep, cheap and deep: an ideotype to optimize water and N acquisition by maize root systems. *Annals of botany*, 112(2), pp.347-357.
- Lyu X., Liu Y., Li N., Ku L., Hou Y., and Wen X. 2022. Foliar applications of various nitrogen (N) forms to winter wheat affect grain protein accumulation and quality via N metabolism and remobilisation. *Crop J.* 10, pp.1165–1177.
- Maccaferri, M., El-Feki, W., Nazemi, G., Salvi, S., Canè, M.A., Colalongo, M.C., Stefanelli, S. and Tuberosa, R., 2016. Prioritizing quantitative trait loci for root system architecture in tetraploid wheat. *J. Exp. Bot.* 67(4), pp.1161-1178.
- Mahjourimajd, S., Taylor, J., Sznajder, B., Timmins, A., Shahinnia, F., Rengel, Z., Khabaz-Saberi, H., Kuchel, H., Okamoto, M., and Langridge, P., 2016. Genetic basis for variation in wheat grain yield in response to varying nitrogen application. *PLoS One.* 11, pp.1–18.
- Mairhofer, S., Zappala, S., Tracy, S., Sturrock, C., Bennett, M.J., Mooney, S.J. and Pridmore, T.P., 2013. Recovering complete plant root system architectures from soil via X-ray  $\mu$ -computed tomography. *Plant methods.* 9(1), pp.1-7.
- Majeed, A., Muhammad, Z. and Ahmad, H., 2018. Plant growth promoting bacteria: role in soil improvement, abiotic and biotic stress management of crops. *Plant Cell Rep.* 37, pp.1599-1609.

- Mallmann, J., Heckmann, D., Bräutigam, A., Lercher, M.J., Weber, A.P., Westhoff, P. and Gowik, U., 2014. The role of photorespiration during the evolution of C4 photosynthesis in the genus *Flaveria*. *Elife*. 3, p.e02478.
- Martin, A., Lee, J., Kichey, T., Gerentes, D., Zivy, M., Tatout, C., Dubois, F., Balliau, T., Valot, B., Davanture, M. and Terce-Laforgue, T., 2006. Two cytosolic glutamine synthetase isoforms of maize are specifically involved in the control of grain production. *Plant Cell* .18(11), pp.3252-3274.
- Martínez-Moreno F., Ammar K., and Solís I. 2022. Global Changes in Cultivated Area and Breeding Activities of Durum Wheat from 1800 to Date: A Historical Review. *Agron*. 12, pp.1–17.
- Martre, P., Porter, J.R., Jamieson, P.D. and Triboï, E., 2003. Modeling grain nitrogen accumulation and protein composition to understand the sink/source regulations of nitrogen remobilisation for wheat. *Plant Physiol*. 133(4), pp.1959-1967.
- Masclaux-Daubresse, C., Daniel-Vedele, F., Dechorgnat, J., Chardon, F., Gaufichon, L. and Suzuki, A., 2010. Nitrogen uptake, assimilation and remobilisation in plants: challenges for sustainable and productive agriculture. *Ann. Bot.* 105(7), pp.1141-1157.
- Masumoto, C., Miyazawa, S.I., Ohkawa, H., Fukuda, T., Taniguchi, Y., Murayama, S., Kusano, M., Saito, K., Fukayama, H. and Miyao, M., 2010. Phospho enol pyruvate carboxylase intrinsically located in the chloroplast of rice plays a crucial role in ammonium assimilation. *Proc. Natl. Acad. Sci. U.S.A* 107(11), pp.5226-5231.
- Mifflin, B.J. and Habash, D.Z., 2002. The role of glutamine synthetase and glutamate dehydrogenase in nitrogen assimilation and possibilities for improvement in the nitrogen utilisation of crops. *J. Exp. Bot.* 53(370), pp.979-987.
- Miyashita, Y., Dolferus, R., Ismond, K.P. and Good, A.G., 2007. Alanine aminotransferase catalyses the breakdown of alanine after hypoxia in *Arabidopsis thaliana*. *Plant J.* 49(6), pp.1108-1121.
- Moll, R.H., Kamprath, E.J. and Jackson, W.A., 1982. Analysis and interpretation of factors which contribute to efficiency of nitrogen utilisation 1. *Agron J.* 74(3), pp.562-564.
- Monostori, I., Árendás, T., Hoffman, B., Galiba, G., Gierczik, K., Szira, F., and Vágújfalvi, A., 2016. Relationship between SPAD value and grain yield can be affected by cultivar, environment and soil nitrogen content in wheat. *Euphytica* 211, pp.103–112.
- Monostori, I., Szira, F., Tondelli, A., Árendás, T., Gierczik, K., Cattivelli, L., Galiba, G. and Vágújfalvi, A., 2017. Genome-wide association study and genetic diversity analysis on nitrogen use efficiency in a Central European winter wheat (*Triticum aestivum* L.) collection. *PLoS One*, 12(12), p.e0189265.

- Mooney, S.J., Pridmore, T.P., Helliwell, J. and Bennett, M.J., 2012. Developing X-ray computed tomography to non-invasively image 3-D root systems architecture in soil. *Plant Soil* .352, pp.1-22.
- Moradi, L., Siosemardeh, A., Sohrabi, Y., Bahramnejad, B., and Hosseinpanahi, F., 2022. Dry matter remobilisation and associated traits, grain yield stability, N utilisation, and grain protein concentration in wheat cultivars under supplemental irrigation. *Agric. Water Manag.* 263, pp. 107449.
- Moubayidin, L., Di Mambro, R. and Sabatini, S., 2009. Cytokinin–auxin crosstalk. *Trends Plant Sci.* 14(10), pp.557-562.
- Murchie, E.H., Pinto, M., and Horton, P., 2009. Agriculture and the new challenges for photosynthesis research. *New Phytol.* 181, pp. 532–552.
- Myles, C. and Wayne, M., 2008. Quantitative trait locus (QTL) analysis. *Nature Education* 1 (1), pp. 208.
- Nagel, K.A., Putz, A., Gilmer, F., Heinz, K., Fischbach, A., Pfeifer, J., Faget, M., Blossfeld, S., Ernst, M., Dimaki, C. and Kastenholz, B., 2012. GROWSCREEN-Rhizo is a novel phenotyping robot enabling simultaneous measurements of root and shoot growth for plants grown in soil-filled rhizotrons. *Funct. Plant Biol.* 39(11), pp.891-904.
- Naiman, A.D., Latrónico, A. and de Salamone, I.E.G., 2009. Inoculation of wheat with *Azospirillum brasilense* and *Pseudomonas fluorescens*: impact on the production and culturable rhizosphere microflora. *Eur. J. Soil Biol.* 45(1), pp.44-51.
- Nauš, J., Prokopová, J., Řebíček, J. and Špundová, M., 2010. SPAD chlorophyll meter reading can be pronouncedly affected by chloroplast movement. *Photosynth. Res.*105, pp.265-271.
- Nehe, A., King, J., King, I.P., Murchie, E.H., and Foulkes, M.J., 2022. Identifying variation for N-use efficiency and associated traits in amphidiploids derived from hybrids of bread wheat and the genera *Aegilops*, *Secale*, *Thinopyrum* and *Triticum*. *PLoS One* 17, pp. 1–19.
- O’Sullivan, C.A., Fillery, I.R.P., Roper, M.M., and Richards, R.A., 2016. Identification of several wheat landraces with biological nitrification inhibition capacity. *Plant Soil.* 404, pp. 61–74.
- Ogbonnaya, C.I., Sarr, B., Brou, C., Diouf, O., Diop, N.N. and Roy-Macauley, H., 2003. Selection of cowpea genotypes in hydroponics, pots, and field for drought tolerance. *Crop Sci.* 43(3), pp.1114-1120.
- Ogbonnaya, F.C., Abdalla, O., Mujeeb-Kazi, A., Kazi, A.G., Xu, S.S., Gosman, N., Lagudah, E.S., Bonnett, D., Sorrells, M.E. and Tsujimoto, H., 2013. Synthetic hexaploids: harnessing species of the primary gene pool for wheat improvement. *Plant Breed. Rev.* 37, pp.35-122.
- Otteson, B.N., Mergoum, M. and Ransom, J.K., 2007. Seeding rate and nitrogen management effects on spring wheat yield and yield components. *Agron.J.* 99(6), pp.1615-1621.

Parry, M.A. and Hawkesford, M.J., 2010. Food security: increasing yield and improving resource use efficiency. *Proc. Nutr. Soc.* 69(4), pp.592-600.

Parry, M.A.J., Andralojc, P.J., Mitchell, R.A., Madgwick, P.J. and Keys, A.J., 2003. Manipulation of Rubisco: the amount, activity, function and regulation. *J. Exp. Bot.* 54(386), pp.1321-1333.

Pask, A.J.D., Sylvester-Bradley, R., Jamieson, P.D., and Foulkes, M.J., 2012. Quantifying how winter wheat crops accumulate and use nitrogen reserves during growth. *F. Crop. Res.* 126, pp. 104–118.

Peng, C., Zhang, Z., Li, Y., Zhang, Y., Dong, H., Fang, Y., Han, L.P., Xu, W., and Hu, L., 2022. Genetic improvement analysis of nitrogen uptake, utilisation, translocation, and distribution in Chinese wheat in Henan Province. *F. Crop. Res.* 277, pp. 108406.

Peng, Y., Li, X. and Li, C., 2012. Temporal and spatial profiling of root growth revealed novel response of maize roots under various nitrogen supplies in the field. *PLoS One*, 7(5), p.e37726.

Perchlik M., and Tegeder M., 2018. Leaf amino acid supply affects photosynthetic and plant nitrogen use efficiency under nitrogen stress. *Plant Physiol.* 178, pp. 174–188.

Pertea, M., Pertea, G.M., Antonescu, C.M., Chang, T.C., Mendell, J.T. and Salzberg, S.L., 2015. StringTie enables improved reconstruction of a transcriptome from RNA-seq reads. *Nature biotechnol.* (3), pp.290-295.

Piccinin, G.G., Braccini, A.L., Dan, L.G., Scapim, C.A., Ricci, T.T. and Bazo, G.L., 2013. Efficiency of seed inoculation with *Azospirillum brasilense* on agronomic characteristics and yield of wheat. *Industrial Crops and Products*, 43, pp.393-397.

Poorter, H., Bühler, J., van Dusschoten, D., Climent, J. and Postma, J.A., 2012. Pot size matters: a meta-analysis of the effects of rooting volume on plant growth. *Funct. Plant Biol.* 39(11), pp.839-850.

Pozzo T., Higdon S.M., Pattathil S., Hahn M.G. and Bennett A.B., 2018. Characterization of novel glycosyl hydrolases discovered by cell wall glycan directed monoclonal antibody screening and metagenome analysis of maize aerial root mucilage. *PloS One*. 13: e0204525. pmid:30256843

Quarrie, S.A., Steed, A., Calestani, C., Semikhodskii, A., Lebreton, C., Chinoy, C., Steele, N., Pljevljakusić, D., Waterman, E., Weyen, J. and Schondelmaier, J., 2005. A high-density genetic map of hexaploid wheat (*Triticum aestivum* L.) from the cross Chinese Spring× SQ1 and its use to compare QTLs for grain yield across a range of environments. *Theor. Appl. Genet.* 110, pp.865-880.

Quraishi, U.M., Abrouk, M., Murat, F., Pont, C., Foucrier, S., Desmaizieres, G., Confolent, C., Riviaère, N., Charmet, G., Paux, E., Murigneux, A., Guerreiro, L., Lafarge, S., Le Gouis, J., Feuillet, C., and Salse, J., 2011. Cross-genome map based dissection of a nitrogen use

efficiency ortho-metaQTL in bread wheat unravels concerted cereal genome evolution. *Plant J.* 65, pp. 745–756.

Ranjan, R., Yadav, R., Jain, N., Sinha, N., Bainsla, N.K., Gaikwad, K.B., and Kumar, M., 2021. QTLs play a major role in nitrogen use efficiency and its component traits in Indian spring wheat. *Agric.* 11, pp.1–20.

Rastogi and Ang, 2022. These are the top 10 countries that produce the most wheat. <https://www.weforum.org/agenda/2022/08/top-10-countries-produce-most-wheat/#:~:text=China%20is%20the%20world%27s%20largest,around%2017%25%20of%20total%20production>

Raun, W.R. and Johnson, G.V., 1999. Improving nitrogen use efficiency for cereal production. *Agron J.* 91(3), pp.357-363.

Ravier, C., Meynard, J.M., Cohan, J.P., Gate, P. and Jeuffroy, M.H., 2017. Early nitrogen deficiencies favor high yield, grain protein content and N use efficiency in wheat. *Eur. J. Agron.* 89, pp.16-24.

Reynolds, M.P., Pellegrineschi, A., and Skovmand, B., 2005. Sink-limitation to yield and biomass: A summary of some investigations in spring wheat. *Ann. Appl. Biol.* 146, pp. 39–49.

Richards, R.A., Cavanagh, C.R., and Riffkin, P., 2019. Selection for erect canopy architecture can increase yield and biomass of spring wheat. *F. Crop. Res.* 244, pp. 107649.

Saia, S., Rappa, V., Ruisi, P., Abenavoli, M.R., Sunseri, F., Giambalvo, D., Frenda, A.S. and Martinelli, F., 2015. Soil inoculation with symbiotic microorganisms promotes plant growth and nutrient transporter genes expression in durum wheat. *Front. Plant Sci.* p.815.

Saini, D.K., Chopra, Y., Pal, N., Chahal, A., Srivastava, P., and Gupta, P.K., 2021. Meta-QTLs, ortho-MQTLs and candidate genes for nitrogen use efficiency and root system architecture in bread wheat (*Triticum aestivum* L.). *Physiol. Mol. Biol. Plants* 27, pp. 2245–2267.

Salamini, F., Özkan, H., Brandolini, A., Schäfer-Pregl, R. and Martin, W., 2002. Genetics and geography of wild cereal domestication in the near east. *Nat. Rev. Genet.* 3(6), pp.429-441.

Sathisha, T.N. and Desai, S.A., 2016. Genetic variability for nitrogen use efficiency (NUE) and yield attributing traits in wheat. *Int. J. Agric. Sci.* ISSN, pp.0975-3710.

Schjoerring, J.K., Möllers, C. and Finnemann, J., 2001. Cytosolic glutamine synthetase (GS 1): posttranslational regulation and role in nitrogen remobilisation from leaves of non-transgenic and GS1-over-expressing oilseed rape plants. *Plant Nutrition: Food security and sustainability of agro-ecosystems through basic and applied research*, pp.120-121.

Schmittgen, S., Metzner, R., Van Dusschoten, D., Jansen, M., Fiorani, F., Jahnke, S., Rascher, U. and Schurr, U., 2015. Magnetic resonance imaging of sugar beet taproots in soil reveals

growth reduction and morphological changes during foliar *Cercospora beticola* infestation. *J. Exp. Bot.* 66(18), pp.5543-5553.

Semenov, M.A., Jamieson, P.D., and Martre, P., 2007. Deconvoluting nitrogen use efficiency in wheat: A simulation study. *Eur. J. Agron.* 26, pp. 283–294.

Shahzad, R., Jamil, S., Ahmad, S., Nisar, A., Amina, Z., Saleem, S., Iqbal, M.Z., Atif, R.M. and Wang, X., 2021. Harnessing the potential of plant transcription factors in developing climate resilient crops to improve global food security: Current and future perspectives. *Saudi J. Biol. Sci.* 28(4), pp.2323-2341.

Sharma, A., Garg, S., Sheikh, I., Vyas, P., and Dhaliwal, H.S., 2020. Effect of wheat grain protein composition on end-use quality. *J. Food Sci. Technol.* 57, pp. 2771–2785.

Sharma, S., Kumar, T., Foulkes, M.J., Orford, S., Singh, A.M., Wingen, L.U., Karnam, V., Nair, L.S., Mandal, P.K., Griffiths, S. and Hawkesford, M.J., 2023. Nitrogen uptake and remobilisation from pre-and post-anthesis stages contribute towards grain yield and grain protein concentration in wheat grown in limited nitrogen conditions. *CABI Agric Biosci.* 4(1), pp.1-20.

Shewry, P.R., 2009. Wheat. *J. Exp. Bot.*60(6), pp.1537-1553.

Shi, H., Chen, M., Gao, L., Wang, Y., Bai, Y., Yan, H., Xu, C., Zhou, Y., Xu, Z., Chen, J. and Tang, W., 2022. Genome-wide association study of agronomic traits related to nitrogen use efficiency in wheat. *Theor. Appl. Genet.* 135(12), pp.4289-4302.

Shi, J. and Tong, Y., 2021. TaLAMP1 plays key roles in plant architecture and yield response to nitrogen fertiliser in wheat. *Front. Plant Sci.* 11, p.598015.

Shrawat, A.K., Carroll, R.T., DePauw, M., Taylor, G.J. and Good, A.G., 2008. Genetic engineering of improved nitrogen use efficiency in rice by the tissue-specific expression of alanine aminotransferase. *Plant Biotechnol. J.*6(7), pp.722-732.

Singh, R., Saripalli, G., Kumar, A., Gautam, T., Singh, S.K., Gahlaut, V., Kumar, S., Meher, P.K., Mishra, R.P., Singh, V.K., Sharma, P.K., Balyan, H.S., and Gupta, P.K., 2023. QTL analysis for nitrogen use efficiency in wheat (*Triticum aestivum* L.). *Euphytica.* 219, pp. 1–22.

Sinha, S.K., V, A.M.S., Chaudhary, S., Tyagi, P., Venkadesan, S., Rani, M. and Mandal, P.K., 2018. Transcriptome analysis of two rice varieties contrasting for nitrogen use efficiency under chronic N starvation reveals differences in chloroplast and starch metabolism-related genes. *Genes.* 9(4), p.206.

Slimane, R.B., Bancal, P. and Bancal, M.O., 2013. Down-regulation by stems and sheaths of grain filling with mobilized nitrogen in wheat. *Field Crops Res.*140, pp.59-68.



- Song, X., Yang, G., Yang, C., Wang, J., and Cui, B., 2017. Spatial variability analysis of within-field winter wheat nitrogen and grain quality using canopy fluorescence sensor measurements. *Remote Sens.* 9, pp. 1–18.
- Sozzi, M., Kayad, A., Gobbo, S., Cogato, A., Sartori, L., and Marinello, F., 2021. Economic Comparison of Satellite, Plane and UAV-Acquired NDVI Images for Site-Specific Nitrogen Application: Observations from Italy. *Agronomy.* 11, pp. 2098.
- Subramanian, K.S. and Sharma, R.E., 2009. Nanofertiliser formulations for balanced fertilization of crops paper presented at the platinum Jubilee celebrations of Iss. New Delhi, pp.2-25.
- Subramanian, K.S. and Thirunavukkarasu, M., 2017. Nano-fertilisers and nutrient transformations in soil. *Nanoscience and Plant–Soil Systems*, pp.305-319.
- Sultana, N., Islam, S., Juhasz, A., and Ma, W., 2021. Wheat leaf senescence and its regulatory gene network. *Crop J.* 9, pp. 703–717.
- Sultana, N., Islam, S., Juhasz, A., Yang, R., She, M., Alhabbar, Z., Zhang, J., and Ma, W., 2020. Transcriptomic study for identification of major nitrogen stress responsive genes in Australian bread wheat cultivars. *Front. Genet.* 11, pp.583785.
- Sultana, S.R., Ali, A., Ahmad, A., Mubeen, M., Zia-Ul-Haq, M., Ahmad, S., Ercisli, S. and Jaafar, H.Z., 2014. Normalized difference vegetation index as a tool for wheat yield estimation: a case study from Faisalabad, Pakistan. *The Scientific World Journal*, 2014.
- Tabuchi M., Sugiyama K., Ishiyama K., Inoue E., Sato T., Takahashi H., and Yamaya T., 2005. Severe reduction in growth rate and grain filling of rice mutants lacking *OsGS1;1*, a cytosolic glutamine synthetase1;1. *Plant J.*42, pp. 641–651
- Talebna, F., Karakashev, D., and Angelidaki, I., 2010. Production of bioethanol from wheat straw: An overview on pretreatment, hydrolysis and fermentation. *Bioresour. Technol.* 101, pp. 4744–4753.
- Tanaka, R. and Tanaka, A., 2011. Chlorophyll cycle regulates the construction and destruction of the light-harvesting complexes. *Biochimica et Biophysica Acta (BBA)-Bioenergetics*, 1807(8), pp.968-976.
- Terasaka, K., Blakeslee, J.J., Titapiwatanakun, B., Peer, W.A., Bandyopadhyay, A., Makam, S.N., Lee, O.R., Richards, E.L., Murphy, A.S., Sato, F. and Yazaki, K., 2005. PGP4, an ATP binding cassette P-glycoprotein, catalyzes auxin transport in *Arabidopsis thaliana* roots. *Plant Cell.* 17(11), pp.2922-2939.
- Thind, H.S., Singh, B., Pannu, R.P.S., Singh, Y., Singh, V., Gupta, R.K., Singh, G., Kumar, A. and Vashistha, M., 2010. Managing neem (*Azadirachta indica*)-coated urea and ordinary urea in wheat (*Triticum aestivum*) for improving nitrogen-use efficiency at high yields. *Indian J. Agric. Sci.* 80(11), p.960.

- Thomas, H. and Ougham, H., 2014. The stay-green trait. *J. Exp. Bot.* 65(14), pp.3889-3900.
- Tiong, J., Sharma, N., Sampath, R., MacKenzie, N., Watanabe, S., Metot, C., Lu, Z., Skinner, W., Lu, Y., Kridl, J., Baumann, U., Heuer, S., Kaiser, B., and Okamoto, M., 2021. Improving nitrogen use efficiency through over-expression of alanine aminotransferase in rice, wheat, and barley. *Front. Plant Sci.* 12, pp.1–18.
- Triboï, E., Martre, P., Girousse, C., Ravel, C., and Triboï-Blondel, A.M., 2006. Unravelling environmental and genetic relationships between grain yield and nitrogen concentration for wheat. *Eur. J. Agron.* 25, pp.108–118
- Trnka, M., Feng, S., Semenov, M.A., Olesen, J.E., Kersebaum, K.C., Rötter, R.P., Semerádová, D., Klem, K., Huang, W., Ruiz-Ramos, M., Hlavinka, P., Meitner, J., Balek, J., Havlík, P., and Büntgen, U., 2019. Mitigation efforts will not fully alleviate the increase in water scarcity occurrence probability in wheat-producing areas. *Sci. Adv.* 5, 1–12.
- Van Deynze, A., Zamora, P., Delaux, P.M., Heitmann, C., Jayaraman, D., Rajasekar, S., Graham, D., Maeda, J., Gibson, D., Schwartz, K.D. and Berry, A.M., 2018. Nitrogen fixation in a landrace of maize is supported by a mucilage-associated diazotrophic microbiota. *PLoS biology*, 16(8), p.e2006352.
- Venieraki, A., Dimou, M., Vezyri, E., Kefalogianni, I., Argyris, N., Liara, G., Pergalis, P., Chatzipavlidis, I. and Katinakis, P., 2011. Characterization of nitrogen-fixing bacteria isolated from field-grown barley, oat, and wheat. *J. Microbiol.* 49, pp.525-534.
- Vergara-Díaz, O., Zaman-Allah, M.A., Masuka, B., Hornero, A., Zarco-Tejada, P., Prasanna, B.M., Cairns, J.E., and Araus, J.L., 2016. A novel remote sensing approach for prediction of maize yield under different conditions of nitrogen fertilization. *Front. Plant Sci.* 7, pp. 1–13.
- VSN International (2020). *Genstat Reference Manual (Release 21), Part 1 Summary*. VSN International, Hemel Hempstead, UK.
- VSN International (2021). *Genstat for Windows 21<sup>st</sup> Edition*. VSN International, Hemel Hempstead, UK.
- VSN International (2022). *Genstat for Windows 22<sup>nd</sup> Edition*. VSN International, Hemel Hempstead, UK.
- Walter, B.N., Huang, Z., Jakobi, R., Tuazon, P.T., Alnemri, E.S., Litwack, G. and Traugh, J.A., 1998. Cleavage and activation of p21-activated protein kinase  $\gamma$ -PAK by *CPP32 (caspase 3)*: effects of autophosphorylation on activity. *J. Biol. Chem.* 273(44), pp.28733-28739.
- Wang, J., Song, K., Sun, L., Qin, Q., Sun, Y., Pan., Xue, Y., 2019. Morphological and transcriptome analysis of wheat seedlings response to low nitrogen stress. *Plants.* 8, pp. 98.

- Wang, Q., Nian, J., Xie, X., Yu, H., Zhang, J., Bai, J., Dong, G., Hu, J., Bai, B., Chen, L. and Xie, Q., 2018. Genetic variations in *ARE1* mediate grain yield by modulating nitrogen utilisation in rice. *Nat. Commun.* 9(1), p.735.
- Waters, B.M., Uauy, C., Dubcovsky, J. and Grusak, M.A., 2009. Wheat (*Triticum aestivum*) NAM proteins regulate the translocation of iron, zinc, and nitrogen compounds from vegetative tissues to grain. *J. Exp. Bot.* 60(15), pp.4263-4274.
- Whalley, W.R., Binley, A., Watts, C.W., Shanahan, P., Dodd, I.C., Ober, E.S., Ashton, R.W., Webster, C.P., White, R.P. and Hawkesford, M.J., 2017. Methods to estimate changes in soil water for phenotyping root activity in the field. *Plant Soil.* 415, pp.407-422.
- White, C.A., Sylvester-Bradley, R. and Berry, P.M., 2015. Root length densities of UK wheat and oilseed rape crops with implications for water capture and yield. *J. Exp. Bot.* 66(8), pp.2293-2303.
- Winfield, M.O., Allen, A.M., BurrIDGE, A.J., Barker, G.L., Benbow, H.R., Wilkinson, P.A., Coghill, J., Waterfall, C., Davassi, A., Scopes, G. and Pirani, A., 2016. High-density SNP genotyping array for hexaploid wheat and its secondary and tertiary gene pool. *Plant Biotechnol. J.*, 14(5), pp.1195-1206.
- Winfield, M.O., Allen, A.M., Wilkinson, P.A., BurrIDGE, A.J., Barker, G.L., Coghill, J., Waterfall, C., Wingen, L.U., Griffiths, S. and Edwards, K.J., 2018. High-density genotyping of the AE Watkins Collection of hexaploid landraces identifies a large molecular diversity compared to elite bread wheat. *Plant Biotechnol. J.* 16(1), pp.165-175.
- Wingen, L.U., Orford, S., Goram, R., Leverington-Waite, M., Bilham, L., Patsiou, T.S., Ambrose, M., Dicks, J., and Griffiths, S., 2014. Establishing the A. E. Watkins landrace cultivar collection as a resource for systematic gene discovery in bread wheat. *Theor. Appl. Genet.* 127, pp. 1831–1842.
- Wingen, L.U., West, C., Leverington-Waite, M., Collier, S., Orford, S., Goram, R., Yang, C.Y., King, J., Allen, A.M., BurrIDGE, A. and Edwards, K.J., 2017. Wheat landrace genome diversity. *Genet.* 205(4), pp.1657-1676.
- Xie, W. and Nevo, E., 2008. Wild emmer: genetic resources, gene mapping and potential for wheat improvement. *Euphytica.* 164, pp.603-614.
- Xiong, D., Chen, J., Yu, T., Gao, W., Ling, X., Li, Y., Peng, S. and Huang, J., 2015. SPAD-based leaf nitrogen estimation is impacted by environmental factors and crop leaf characteristics. *Sci. Rep.* 5(1), p.13389.
- Xu, G., Fan, X. and Miller, A.J., 2012. Plant nitrogen assimilation and use efficiency. *Annu. Rev. Plant Biol.* 63, pp.153-182.

- Xu, Y., Wang, R., Tong, Y., Zhao, H., Xie, Q., Liu, D., Zhang, A., Li, B., Xu, H., and An, D., 2014. Mapping QTLs for yield and nitrogen-related traits in wheat: Influence of nitrogen and phosphorus fertilization on QTL expression. *Theor. Appl. Genet.* 127, pp. 59–72.
- Yang, M., Hassan, M.A., Xu, K., Zheng, C., Rasheed, A., Zhang, Y., Jin, X., Xia, X., Xiao, Y., and He, Z., 2020. Assessment of Water and Nitrogen Use Efficiencies Through UAV-Based Multispectral Phenotyping in Winter Wheat. *Front. Plant Sci.* 11, pp. 1–16.
- Yang, W., Liu, D., Li, J., Zhang, L., Wei, H., Hu, X., Zheng, Y., He, Z. and Zou, Y., 2009. Synthetic hexaploid wheat and its utilisation for wheat genetic improvement in China. *J Genet Genomics.* 36(9), pp.539-546.
- Zadoks, J.C., Chang, T.T., and Konzak, C.F., 1974. A decimal code for the growth stages of cereals. *Weed Res.* 14, pp. 415-421.
- Zhang, M., Gao, M., Zheng, H., Yuan, Y., Zhou, X., Guo, Y., Zhang, G., Zhao, Y., Kong, F., An, Y., and Li, S., 2019. QTL mapping for nitrogen use efficiency and agronomic traits at the seedling and maturity stages in wheat. *Mol. Breed.* 39.
- Zhang, X., Davidson, E. A., Mauzerall, D. L., Searchinger, T. D., Dumas, P., and Shen, Y., 2015. Managing nitrogen for sustainable development. *Nat.* 528, pp. 51–59.
- Zhang, X., Li, F., Ding, Y., Ma, Q., Yi, Y., Zhu, M., Ding, J., Li, C., Guo, W., and Zhu, X., 2021. Transcriptome analysis of two near-isogenic lines with different NUE under normal nitrogen conditions in wheat. *Biology (Basel).* 10, pp.1–16.
- Zhao, D., Derkx, A.P., Liu, D.C., Buchner, P. and Hawkesford, M.J., 2015. Over-expression of a NAC transcription factor delays leaf senescence and increases grain nitrogen concentration in wheat. *Plant Biol.* 17(4), pp.904-913.
- Zhou, B., Elazab, A., Bort, J., Vergara, O., Serret, M.D., and Araus, J.L., 2015. Low-cost assessment of wheat resistance to yellow rust through conventional RGB images. *Comput. Electron. Agric.* 116, pp.20–29.
- Ziadi, N., Bélanger, G., Claessens, A., Lefebvre, L., Cambouris, A.N., Tremblay, N., Nolin, M.C. and Parent, L.É., 2010. Determination of a critical nitrogen dilution curve for spring wheat. *Agron J.* 102(1), pp.241-250.
- Zörb, C., Ludewig, U. and Hawkesford, M.J., 2018. Perspective on wheat yield and quality with reduced nitrogen supply. *Trends Plant Sci.* 23(11), pp.1029-1037.

## Appendix Tables

### 1

**Appendix Table 1:** Differentially Expressed Genes in SHW58 line when compared with high and low N treatment. log2fold change was >1 and Padj value <0.05. This list is obtained when less stringent log2fold change and Padj value threshold criteria are used.

Gene_Name	log2FoldChange	Padj	Gene_chr	Gene_start	Gene_end	Gene_description
LOC123168800	7.572809549	9.16E-06	NC_057814.1	60848327 4	60848479 4	50S ribosomal protein L35%2C chloroplastic-like && Q8VZ55.1 RecName: Full=50S ribosomal protein L35, chloroplastic; Flags: Precursor && -
LOC123068639	1.616552177	9.16E-06	NC_057794.1	56974453 5	56974559 7	chlorophyll a-b binding protein of LHCII type 1-like && P04784.1 RecName: Full=Chlorophyll a-b binding protein, chloroplastic; AltName: Full=LHCII type I CAB; Short=LHCP; Flags: Precursor && -
LOC123128382	1.699929215	9.42E-06	NC_057809.1	54467593 5	54467851 1	geranylgeranyl diphosphate reductase%2C chloroplastic-like && Q6Z2T6.1 RecName: Full=Geranylgeranyl diphosphate reductase, chloroplastic; AltName: Full=Geranylgeranyl reductase; Flags: Precursor && -
LOC123112894	10.07723558	2.23E-05	NC_057807.1	51968692 0	51968820 4	probable aquaporin PIP2-7 && Q651D5.2 RecName: Full=Probable aquaporin PIP2-7; AltName: Full=OsPIP2;7; AltName: Full=Plasma membrane intrinsic protein 2-7 && -
LOC123183068	6.154181408	2.23E-05	NC_057796.1	46909504 9	46909589 5	photosystem I reaction center subunit VI%2C chloroplastic-like && P20143.1 RecName: Full=Photosystem I reaction center subunit VI, chloroplastic; Short=PSI-H; AltName: Full=Light-harvesting complex I 11 kDa protein; Flags: Precursor && -
LOC100049048	21.67031234	0.000208 062	NC_057798.1	25247364 8	25247474 7	oxygen-evolving enhancer protein 3%2C chloroplastic && Q0D5P8.1 RecName: Full=Oxygen-evolving enhancer protein 3, chloroplastic; Short=OEE3; AltName: Full=LP02; Flags: Precursor >P83646.2 RecName: Full=Oxygen-evolving

LOC123164058	21.67031234	0.000208062	NC_057814.1	427540322	427547561	enhancer protein 3, chloroplastic; Short=OEE3; AltName: Full=LPO2; Flags: Precursor && - phosphoenolpyruvate carboxylase 1-like && P29195.1 RecName: Full=Phosphoenolpyruvate carboxylase 1; Short=PEPC 1; Short=PEPCase 1; AltName: Full=CP21 && -
LOC123053529	21.65411043	0.000208062	NC_057799.1	417207181	417209161	glyceraldehyde-3-phosphate dehydrogenase A%2C chloroplastic && P09315.1 RecName: Full=Glyceraldehyde-3-phosphate dehydrogenase A, chloroplastic; AltName: Full=NADP-dependent glyceraldehydephosphate dehydrogenase subunit A; Flags: Precursor && -
LOC123143070	21.65411043	0.000208062	NC_057811.1	12449151	12451086	chloroplast stem-loop binding protein of 41 kDa a%2C chloroplastic-like && Q9LYA9.1 RecName: Full=Chloroplast stem-loop binding protein of 41 kDa a, chloroplastic; Short=CSP41-a; Flags: Precursor && -
LOC123165261	21.63535426	0.000208062	NC_057814.1	186825841	186831165	trigger factor-like protein TIG%2C Chloroplastic && Q8S9L5.1 RecName: Full=Trigger factor-like protein TIG, Chloroplastic; AltName: Full=Immunophilin TIG; AltName: Full=Peptidyl-prolyl cis-trans isomerase TIG; Short=PPlase TIG; AltName: Full=Rotamase; Flags: Precursor && -
LOC123047424	9.812687703	0.000264806	NC_057794.1	307318983	307321072	protochlorophyllide reductase B%2C chloroplastic && Q42850.1 RecName: Full=Protochlorophyllide reductase B, chloroplastic; Short=PCR B; AltName: Full=NADPH-protochlorophyllide oxidoreductase B; Short=POR B; Flags: Precursor && -
LOC123098537	9.235176516	0.000334875	NC_057805.1	451259850	451261385	protein PAM68%2C chloroplastic-like && O49668.1 RecName: Full=Protein PAM68, chloroplastic; AltName: Full=PHOTOSYNTHESIS AFFECTED MUTANT 68; Flags: Precursor && -
LOC123189421	21.08265041	0.000355083	NC_057797.1	561390396	561392334	glyceraldehyde-3-phosphate dehydrogenase A%2C chloroplastic-like && P09315.1 RecName: Full=Glyceraldehyde-3-phosphate dehydrogenase A, chloroplastic; AltName: Full=NADP-dependent

LOC100125708	9.255240426	0.000391 063	NC_057808.1	52753180 1	52753349 7	glyceraldehydephosphate dehydrogenase subunit A; Flags: Precursor && - trictetin 3'-O-trimethyltransferase-like && Q38J50.1 RecName: Full=Trictetin 3',4',5'-O-trimethyltransferase; Short=TaOMT2; AltName: Full=Caffeic acid 3-O-methyltransferase; Short=TaCM; AltName: Full=Flavone O-methyltransferase 2 && -
LOC123122527	1.279630396	0.000411 179	NC_057808.1	44115881 2	44115994 8	chlorophyll a-b binding protein of LHCII type 1-like && P12329.1 RecName: Full=Chlorophyll a-b binding protein 1, chloroplastic; AltName: Full=LHCII type I CAB-1; Short=LHCP; Flags: Precursor && -
LOC123121683	2.612193568	0.000825 846	NC_057808.1	34964320 3	34964453 3	chlorophyll a-b binding protein 1B-20 chloroplastic-like && Q36718.1 RecName: Full=Chlorophyll a-b binding protein 1B-20, chloroplastic; AltName: Full=LHCI type I CAB-1B-20; AltName: Full=Light-harvesting complex I 20 kDa protein; Flags: Precursor && -
LOC123145507	1.066206189	0.000825 846	NC_057795.1	65062501 5	65062587 5	photosystem I reaction center subunit VI chloroplastic && P20143.1 RecName: Full=Photosystem I reaction center subunit VI, chloroplastic; Short=PSI-H; AltName: Full=Light-harvesting complex I 11 kDa protein; Flags: Precursor && -
LOC123187682	9.031651579	0.000956 103	NC_057797.1	85265337	85270911	magnesium-chelatase subunit ChIH chloroplastic-like && B8ANF1.1 RecName: Full=Magnesium-chelatase subunit ChIH, chloroplastic; Short=Mg-chelatase subunit H; AltName: Full=Mg-protoporphyrin IX chelatase subunit ChIH; Flags: Precursor && -
LOC123104728	1.008420103	0.001214 504	NC_057806.1	55407061 9	55407183 3	chlorophyll a-b binding protein of LHCII type 1-like && P12329.1 RecName: Full=Chlorophyll a-b binding protein 1, chloroplastic; AltName: Full=LHCII type I CAB-1; Short=LHCP; Flags: Precursor && -
LOC123148365	9.085377538	0.001250 813	NC_057795.1	67748696 7	67748808 4	chlorophyll a-b binding protein of LHCII type III chloroplastic && P27523.1 RecName: Full=Chlorophyll a-b binding protein of LHCII type III, chloroplastic; Short=CAB; Flags: Precursor && -

LOC123044442	1.3912471	0.001250 813	NC_057798.1	21870311 9	21870456 2	chlorophyll a-b binding protein 7%2C chloroplastic-like && P10708.1 RecName: Full=Chlorophyll a-b binding protein 7, chloroplastic; AltName: Full=LHCI type II CAB-7; Flags: Precursor && -
LOC123183260	8.896219466	0.002413 737	NC_057796.1	48313080 4	48313197 6	chlorophyll a-b binding protein of LHCII type III%2C chloroplastic && P27523.1 RecName: Full=Chlorophyll a-b binding protein of LHCII type III, chloroplastic; Short=CAB; Flags: Precursor && -
LOC123088383	6.648152721	0.002413 737	NC_057803.1	72492280 5	72492806 2	ruBisCO large subunit-binding protein subunit beta%2C chloroplastic-like && P21240.3 RecName: Full=Chaperonin 60 subunit beta 1, chloroplastic; Short=CPN-60 beta 1; AltName: Full=60 kDa chaperonin subunit beta 1; AltName: Full=RuBisCO large subunit-binding protein subunit beta, chloroplastic; Flags: Precursor && -
LOC123166407	8.900116112	0.002510 837	NC_057814.1	32854039	32854512	uncharacterised LOC123166407 && - && -
LOC123113017	9.087989483	0.003687 725	NC_057807.1	53601302 2	53601413 7	chlorophyll a-b binding protein of LHCII type 1-like && P12329.1 RecName: Full=Chlorophyll a-b binding protein 1, chloroplastic; AltName: Full=LHCII type I CAB-1; Short=LHCP; Flags: Precursor && -
LOC123051777	8.933216324	0.003687 725	NC_057799.1	82351579	82357227	magnesium-chelatase subunit ChI%2C chloroplastic-like && B8ANF1.1 RecName: Full=Magnesium-chelatase subunit ChIH, chloroplastic; Short=Mg-chelatase subunit H; AltName: Full=Mg-protoporphyrin IX chelatase subunit ChIH; Flags: Precursor && -
LOC123112836	8.389679733	0.004956 423	NC_057807.1	51077409 5	51077532 9	chlorophyll a-b binding protein%2C chloroplastic && Q10HD0.1 RecName: Full=Chlorophyll a-b binding protein, chloroplastic; AltName: Full=LHCII type I CAB; Short=LHCP; Flags: Precursor >A2XJ35.1 RecName: Full=Chlorophyll a-b binding protein, chloroplastic; AltName: Full=LHCII type I CAB; Short=LHCP; Flags: Precursor && -
LOC123187228	8.260069603	0.004956 423	NC_057797.1	34537439	34538087	ribulose bisphosphate carboxylase small subunit%2C chloroplastic 1 && P00871.2 RecName: Full=Ribulose



LOC123051868	6.013570587	0.004956 423	NC_057799.1	90729922	90731288	bisphosphate carboxylase small chain PWS4.3, chloroplastic; Short=Rubisco small subunit PWS4.3; Flags: Precursor && -
LOC123104110	5.771893426	0.004956 423	NC_057806.1	47283388 6	47283458 0	probable carboxylesterase 18 && Q940G6.1 RecName: Full=Gibberellin receptor GID1C; AltName: Full=AtCXE19; AltName: Full=Carboxylesterase 19; AltName: Full=GID1-like protein 3; AltName: Full=Protein GA INSENSITIVE DWARF 1C; Short=AtGID1C && -
LOC123143439	1.346127205	0.005859 072	NC_057795.1	62950950 3	62951525 8	photosystem I reaction center subunit V%2C chloroplastic-like && Q00327.1 RecName: Full=Photosystem I reaction center subunit V, chloroplastic; AltName: Full=PSI-G; AltName: Full=Photosystem I 9 kDa protein; Flags: Precursor && -
LOC123131635	6.079408421	0.005882 929	NC_057809.1	9962519	9968158	phosphomethylethanolamine N-methyltransferase-like%2C transcript variant X2 && Q944H0.2 RecName: Full=Phosphomethylethanolamine N-methyltransferase; Short=AtPMEAMT; AltName: Full=Phosphoethanolamine N-methyltransferase 2 && -
LOC123138457	8.801234801	0.007041 323	NC_057810.1	64454932 1	64455257 1	nitrate reductase [NADH]-like && P27967.1 RecName: Full=Nitrate reductase [NADH]; Short=NR && -
LOC123074117	6.508911384	0.007041 323	NC_057794.1	179918	183306	ferredoxin--nitrite reductase%2C chloroplastic-like && Q42997.1 RecName: Full=Ferredoxin--nitrite reductase, chloroplastic; Flags: Precursor && -
LOC123167588	8.722594351	0.007108 913	NC_057814.1	47601474 8	47602346 0	28S ribosomal RNA && Q6CQE5.2 RecName: Full=Protein TAR1 && -
LOC123143623	5.108143226	0.007108 913	NC_057811.1	74134111	74137432	amino acid permease 3-like && Q39134.2 RecName: Full=Amino acid permease 3; AltName: Full=Amino acid transporter AAP3 && -
						chloride channel protein CLC-b-like && P92942.1 RecName: Full=Chloride channel protein CLC-b; Short=AtCLC-b; AltName: Full=CBS domain-containing protein CBSCL7 && -

LOC123042250	4.409322045	0.007646 662	NC_057798.1	71518337 4	71518420 9	phylloplanin-like && - && -
LOC123042249	8.791650125	0.008878 129	NC_057798.1	71505212 3	71505304 8	phylloplanin-like && - && -
LOC123068541	8.653666238	0.009235 788	NC_057801.1	54181415	54183450	thylakoid lumenal 15 kDa protein 1%2C chloroplastic-like && O22160.2 RecName: Full=Thylakoid lumenal 15 kDa protein 1, chloroplastic; AltName: Full=p15; Flags: Precursor && -
LOC123138188	9.25152448	0.009451 271	NC_057810.1	58883392 5	58883492 9	PLAT domain-containing protein 3-like && O65660.1 RecName: Full=PLAT domain-containing protein 1; Short=AtPLAT1; Short=PLAT domain protein 1; Flags: Precursor && -
LOC123047575	8.667098202	0.009465 663	NC_057798.1	80483693 3	80484337 0	small glutamine-rich tetratricopeptide repeat-containing protein-like%2C transcript variant X1 && O13797.1 RecName: Full=Small glutamine-rich tetratricopeptide repeat-containing protein 2 && -
LOC123051265	8.572225993	0.009465 663	NC_057799.1	29864287	29865766	ribulose biphosphate carboxylase small subunit%2C chloroplastic 2-like && P26667.1 RecName: Full=Ribulose biphosphate carboxylase small chain PW9, chloroplastic; Short=RuBisCO small subunit PW9; Flags: Precursor && -
LOC123154092	1.655433197	0.009465 663	NC_057812.1	11718100 7	11718227 0	inositol-tetrakisphosphate 1-kinase 4-like && Q7XBW0.1 RecName: Full=Inositol-tetrakisphosphate 1-kinase 5; AltName: Full=Inositol 1,3,4-trisphosphate 5/6-kinase 5; Short=Inositol-triphosphate 5/6-kinase 5; Short=Ins(1,3,4)P(3) 5/6-kinase 5; Short=OsITP5/6K-5; Short=OsITPK5; AltName: Full=OsITL3 >AOJJZ6.1 RecName: Full=Inositol-tetrakisphosphate 1-kinase 5; AltName: Full=Inositol 1,3,4-trisphosphate 5/6-kinase 5; Short=Inositol-triphosphate 5/6-kinase 5; Short=Ins(1,3,4)P(3) 5/6-kinase 5; Short=OsITP5/6K-5; Short=OsITPK5 && -
LOC123080518	8.603786756	0.010385 913	NC_057802.1	56389405 8	56389980 7	uncharacterised LOC123080518%2C transcript variant X2 && - && -

LOC123097432	1.602879118	0.010385 913	NC_057805.1	26557330 0	26557611 0	50S ribosomal protein L6%2C chloroplastic-like && O23049.1 RecName: Full=50S ribosomal protein L6, chloroplastic; AltName: Full=Protein EMBRYO DEFECTIVE 2394; Flags: Precursor && -
LOC123148794	9.198199602	0.010740 762	NC_057812.1	63087585 4	63088066 5	uncharacterised LOC123148794%2C transcript variant X1 && - && -
LOC123145630	8.639227513	0.011365 107	NC_057811.1	43305238 7	43305313 5	uncharacterised LOC123145630 && - && -
LOC123175189	4.986515487	0.011620 764	NW_025229832. 1	9318	10360	senescence-specific cysteine protease SAG39-like && A2XQE8.1 RecName: Full=Senescence-specific cysteine protease SAG39; AltName: Full=Cysteine proteinase SAG39; AltName: Full=Protein SENESENCE-ASSOCIATED GENE 39; Flags: Precursor && -
LOC123079290	8.600238402	0.011918 261	NC_057802.1	41925218 6	41925638 0	uncharacterised LOC123079290 && - && -
LOC123152730	8.556781755	0.011918 261	NC_057812.1	5779839	5794367	uncharacterised LOC123152730 && - && -
-	7.848078275	0.011918 261	NC_057799.1	39020546 4	39020901 7	- && - && -
LOC123065910	2.045266695	0.011918 261	NC_057794.1	54898888 3	54898996 0	chlorophyll a-b binding protein of LHCI type 1-like && P07369.1 RecName: Full=Chlorophyll a-b binding protein 3C, chloroplastic; AltName: Full=LHCI type I CAB-3C; Short=LHCP; Flags: Precursor && -
LOC123041551	1.523961584	0.011918 261	NC_057794.1	14871553 4	14872047 0	peroxidase 42-like%2C transcript variant X5 && P84516.2 RecName: Full=Cationic peroxidase SPC4; Flags: Precursor && -
LOC123071148	8.915045252	0.012083 602	NC_057801.1	59443295 2	59443717 4	probable arabinosyltransferase ARAD1 && Q6DBG8.1 RecName: Full=Probable arabinosyltransferase ARAD1; AltName: Full=Arabinan alpha-1,5-arabinosyltransferase; AltName: Full=L-Arabinosyltransferase; AltName: Full=Protein ARABINAN DEFICIENT 1 && -
LOC123110767	8.792006693	0.012083 602	NC_057807.1	12659957 0	12660203 1	uncharacterised LOC123110767 && - && -

LOC123110766	8.643022651	0.012083 602	NC_057807.1	12658710 5	12659073 9	putative pentatricopeptide repeat-containing protein At3g16890%2C mitochondrial && Q9LSQ2.1 RecName: Full=Putative pentatricopeptide repeat-containing protein At3g16890, mitochondrial; AltName: Full=Protein PENTATRICOPEPTIDE REPEAT 40; Flags: Precursor && -
LOC123083519	8.637895659	0.012083 602	NC_057803.1	73979224 1	73979506 6	homeobox protein BEL1 homolog && Q38897.2 RecName: Full=Homeobox protein BEL1 homolog && -
LOC123057039	8.551848333	0.012083 602	NC_057800.1	61088081 3	61088589 8	- && - && -
LOC123069326	1.23570692	0.012083 602	NC_057794.1	57771812 9	57772240 9	protein FAR1-RELATED SEQUENCE 7-like%2C transcript variant X1 && Q9LIE5.1 RecName: Full=Protein FAR-RED ELONGATED HYPOCOTYL 3 && -
LOC123164083	1.197118709	0.012083 602	NC_057814.1	76328917	76336049	MADS-box transcription factor 5-like && Q10PZ9.1 RecName: Full=MADS-box transcription factor 1; AltName: Full=OsMADS1; AltName: Full=Protein LEAFY HULL STERILE 1; AltName: Full=Protein SEPALLATA-like >A2XDY1.2 RecName: Full=MADS-box transcription factor 1; AltName: Full=OsMADS1; AltName: Full=Protein LEAFY HULL STERILE 1; AltName: Full=Protein SEPALLATA-like && -
LOC123121350	8.455592547	0.014559 463	NC_057808.1	30355119 2	30355514 7	uncharacterised LOC123121350%2C transcript variant X1 && - && -
LOC123068653	8.578080125	0.015008 239	NC_057801.1	71379362	71383371	uncharacterised LOC123068653 && - && -
LOC123161432	8.535533766	0.015008 239	NC_057813.1	17172459 2	17172808 8	proline-rich receptor-like protein kinase PERK12 && Q9ZUE0.2 RecName: Full=Proline-rich receptor-like protein kinase PERK12; AltName: Full=Proline-rich extensin-like receptor kinase 12; Short=AtPERK12; AltName: Full=Protein INFLORESCENCE GROWTH INHIBITOR 1 && -
LOC123127719	8.498190227	0.015008 239	NC_057809.1	42223457 3	42224573 7	ubiquitin carboxyl-terminal hydrolase 19-like%2C transcript variant X7 && - && -
LOC123106896	8.468178714	0.015008 239	NC_057806.1	34212182 2	34212430 2	uncharacterised LOC123106896 && Q9SAF5.1 RecName: Full=Probable phospholipid-transporting ATPase 11;

LOC123135450	8.450205496	0.015008 239	NC_057810.1	21393795	21398216	Short=AtALA11; AltName: Full=Aminophospholipid flippase 11 && - disease resistance protein RPM1-like%2C transcript variant X2 && Q39214.1 RecName: Full=Disease resistance protein RPM1; AltName: Full=Resistance to Pseudomonas syringae protein 3 && -
LOC123059107	7.175170509	0.015008 239	NC_057800.1	68760324 5	68760477 4	uncharacterised LOC123059107 && - && -
LOC123162355	2.099895616	0.015008 239	NC_057813.1	72584002 7	72584384 5	putrescine hydroxycinnamoyltransferase 1-like && Q5SMM6.1 RecName: Full=Hydroxycinnamoyltransferase 4; Short=OsHCT4; AltName: Full=BAHD-like hydroxycinnamoyl transferase HCT4; AltName: Full=Glycerol hydroxycinnamoyl transferase && -
LOC123111386	8.470627177	0.015265 185	NC_057807.1	28031544 1	28031799 4	probable protein phosphatase 2C 73 && Q2RBJ6.1 RecName: Full=Probable protein phosphatase 2C 73; Short=OsPP2C73 && -
LOC123143820	8.454267592	0.015267	NC_057795.1	63328628 8	63328856 3	protein PLASTID MOVEMENT IMPAIRED 15-like && Q9C9N6.1 RecName: Full=Protein PLASTID MOVEMENT IMPAIRED 2; AltName: Full=Protein WEAK CHLOROPLAST MOVEMENT UNDER BLUE LIGHT 2; Short=Protein WEB2 && -
LOC123070844	1.477654434	0.015613 105	NC_057801.1	55163150 2	55163562 1	- && - && -
LOC123104003	8.68738741	0.015898 32	NC_057806.1	45810112 7	45810329 1	UDP-glycosyltransferase 73C12-like && Q9ZQ95.1 RecName: Full=UDP-glycosyltransferase 73C6; AltName: Full=Flavonol-3-O-glycoside-7-O-glucosyltransferase 1; AltName: Full=Zeatin O-glucosyltransferase 2 && -
LOC123142121	8.632285205	0.015898 32	NC_057795.1	60941833 1	60942093 7	uncharacterised LOC123142121 && - && -
LOC123077998	8.461268077	0.015898 32	NC_057802.1	15378665 0	15379077 0	serine carboxypeptidase-like 26 && Q9LSM9.2 RecName: Full=Serine carboxypeptidase-like 33; Flags: Precursor && -
LOC123105161	8.438316244	0.015898 32	NC_057806.1	59847453 0	59847871 9	RNA-binding protein 1-like && Q9C652.1 RecName: Full=RNA-binding protein 1; Short=AtRBP1 && -

LOC123093397	1.834457188	0.015898 32	NC_057795.1	50709015 8	50709132 8	uncharacterised LOC123093397 && - && -
LOC123145030	1.401494229	0.015898 32	NC_057811.1	34526892 4	34527281 4	probable trehalose-phosphate phosphatase 1 && Q75WV3.1 RecName: Full=Probable trehalose-phosphate phosphatase 1; Short=OsTPP1; AltName: Full=Trehalose 6- phosphate phosphatase && -
LOC123062997	1.331989758	0.015898 32	NC_057800.1	65892420 7	65892670 3	uncharacterised LOC123062997 && - && -
LOC123086273	1.94662764	0.015994 14	NC_057803.1	44620855 8	44621897 9	filaggrin-like%2C transcript variant X11 && Q9LHP2.1 RecName: Full=Serine/arginine-rich SC35-like splicing factor SCL30A; Short=At-SCL30A; Short=AtSCL30A; AltName: Full=SC35-like splicing factor 30A; AltName: Full=Serine/arginine-rich splicing factor 30A && -
LOC123076949	8.488129899	0.016027 489	NC_057802.1	17651845	17655098	uncharacterised LOC123076949 && - && -
LOC123136344	8.403899852	0.016027 489	NC_057810.1	16246793 1	16247137 4	tyrosine-sulfated glycopeptide receptor 1-like && Q9C7S5.1 RecName: Full=Tyrosine-sulfated glycopeptide receptor 1; AltName: Full=PSY1 receptor && -
LOC123113933	1.1041938	0.016027 489	NC_057807.1	65500803 9	65501385 1	uncharacterised LOC123113933 && Q5FPX9.1 RecName: Full=Probable GTP-binding protein EngB && -
LOC123178512	5.959466423	0.017438 321	NW_025281071. 1	9	1200	uncharacterised LOC123178512%2C transcript variant X1 && - && -
LOC123040026	8.493748753	0.017486 609	NC_057798.1	19050012	19052090	probable amidase At4g34880 && Q9URY4.1 RecName: Full=Putative amidase C869.01; Flags: Precursor && -
LOC123078634	9.158097159	0.017516 349	NC_057802.1	31917185 5	31917744 7	protein RAE1-like && Q38942.2 RecName: Full=Protein RAE1; AltName: Full=RNA export factor 1 && -
LOC123184683	8.469545478	0.017516 349	NC_057797.1	56716338	56717358	calmodulin-binding protein 25-like && - && -
LOC123181029	7.56099954	0.017577 905	NC_057796.1	20952757 6	20952920 1	uncharacterised LOC123181029 && - && -
LOC123186972	8.620594237	0.018043 28	NC_057797.1	9870674	9873094	uncharacterised LOC123186972 && - && -

LOC123145119	8.383586019	0.019210 04	NC_057811.1	36563300 9	36564122 7	uncharacterised LOC123145119%2C transcript variant X6 && Q9FE20.1 RecName: Full=Serine/threonine-protein kinase PBS1; AltName: Full=AvrPphB susceptible protein 1 && -
LOC123072128	7.118320305	0.019210 04	NC_057801.1	74351622 6	74351997 3	probable LRR receptor-like serine/threonine-protein kinase At3g47570 && COLGP4.1 RecName: Full=Probable LRR receptor-like serine/threonine-protein kinase At3g47570; Flags: Precursor && -
LOC123049180	6.836309298	0.019210 04	NC_057794.1	33599906 0	33600145 1	L-type lectin-domain containing receptor kinase SIT2-like && O80939.1 RecName: Full=L-type lectin-domain containing receptor kinase IV.1; Short=Arabidopsis thaliana lectin-receptor kinase e; Short=AthlecRK-e; Short=LecRK-IV.1; AltName: Full=Lectin Receptor Kinase 1; Flags: Precursor && -
LOC123122607	8.366342337	0.019718 101	NC_057795.1	33736898 8	33738218 2	FBD-associated F-box protein At3g52670-like && Q9LSJ3.2 RecName: Full=Putative F-box/LRR-repeat protein At3g28410 && -
LOC123114388	1.698375853	0.019718 101	NC_057807.1	70422130 1	70422531 1	putative pentatricopeptide repeat-containing protein At1g03510%2C transcript variant X2 && Q9LR72.1 RecName: Full=Putative pentatricopeptide repeat-containing protein At1g03510 && -
LOC123102115	8.327427385	0.019758 04	NC_057806.1	31429119	31431231	pentatricopeptide repeat-containing protein At1g11290%2C chloroplastic-like && Q9SS60.1 RecName: Full=Pentatricopeptide repeat-containing protein At3g03580 && -
LOC123160164	8.414196554	0.019892 645	NC_057813.1	59295606 8	59296233 7	probable F-box protein At4g22060 && - && -
LOC123164030	8.428976205	0.020587 765	NC_057814.1	56881679 1	56881781 4	probable phospholipase A2 homolog 2 && Q9XG81.1 RecName: Full=Probable phospholipase A2 homolog 2; Flags: Precursor && -
LOC123149185	6.087356665	0.022990 75	NC_057795.1	68472591 5	68473177 0	trimethylguanosine synthase-like && P85107.1 RecName: Full=Trimethylguanosine synthase; AltName: Full=Nuclear receptor coactivator 6-interacting protein; AltName:

LOC123143805	8.284978102	0.024436 256	NC_057811.1	95026090	95029100	Full=PRIP-interacting protein with methyltransferase motif; Short=PIMT; Short=PIPMT && - protein At-4/1-like && Q1PE49.1 RecName: Full=Protein At-4/1; AltName: Full=Tomato spotted wilt virus movement protein-interacting protein 4/1; Short=At-4/1 && -
LOC123165973	8.549784426	0.025081 636	NC_057814.1	33798764 7	33799126 8	cinamoyl-CoA reductase 1-like && Q500U8.1 RecName: Full=Tetraketide alpha-pyrone reductase 1; AltName: Full=Protein DIHYDROFLAVONOL 4-REDUCTASE-LIKE 1 && -
LOC123083133	8.510186977	0.025987 282	NC_057803.1	68610532 3	68610741 9	cytochrome P450 711A1-like && B9DFU2.1 RecName: Full=Cytochrome P450 711A1; AltName: Full=Protein MORE AXILLARY BRANCHES 1 && -
LOC123127655	8.367695144	0.027971 919	NC_057794.1	35287642 5	35287743 1	uncharacterised LOC123127655%2C transcript variant X1 && - && -
LOC123098918	2.64970031	0.028356 64	NC_057805.1	48841060 7	48841461 8	uncharacterised LOC123098918%2C transcript variant X6 && - && -
-	8.243951012	0.028492 685	NC_057809.1	57507673 1	57507710 2	- && - && -
LOC123121653	8.318023202	0.029479 826	NC_057808.1	34574144 2	34574307 3	myb-related protein 306-like && P81392.1 RecName: Full=Myb-related protein 306 && -
LOC123094411	1.085813171	0.029479 826	NC_057804.1	60390357	60390907	uncharacterised LOC123094411 && - && -
LOC123137640	8.495173661	0.029844 583	NC_057810.1	49178534 4	49179057 5	RING-H2 finger protein ATL73-like && Q5EAE9.2 RecName: Full=RING-H2 finger protein ATL43; AltName: Full=RING-type E3 ubiquitin transferase ATL43; Flags: Precursor && -
LOC123088012	1.033484459	0.029844 583	NC_057803.1	67005384 5	67005841 6	wall-associated receptor kinase 3-like && Q9LMP1.1 RecName: Full=Wall-associated receptor kinase 2; Flags: Precursor && -
LOC123182265	8.283948684	0.029854 815	NC_057796.1	38440690 6	38440806 2	chitinase 1-like && Q9SLP4.1 RecName: Full=Chitinase 1; AltName: Full=Tulip bulb chitinase-1; Short=TBC-1; Flags: Precursor && -
LOC123042989	2.370885896	0.029854 815	NC_057794.1	18908151 5	18908363 5	uncharacterised LOC123042989 && - && -



LOC123041568	5.895921262	0.029971 49	NC_057798.1	52900418 7	52900593 1	- && O80518.1 RecName: Full=Galactinol synthase 3; Short=AtGolS3; Short=GolS-3 && -
LOC123148659	8.220115847	0.032117 595	NC_057812.1	71392557	71402797	disease resistance protein RGA5-like%2C transcript variant X1 && PODI17.1 RecName: Full=Probable disease resistance protein RF9 >PODI18.1 RecName: Full=Probable disease resistance protein RDL6 && -
LOC123125690	8.21655571	0.032117 595	NC_057808.1	49351664 0	49351797 3	probable carboxylesterase 15 && Q9FG13.1 RecName: Full=Probable carboxylesterase 15; AltName: Full=AtCXE15 && -
LOC123123102	8.33695835	0.032413 096	NC_057808.1	49123329 1	49123584 9	- && - && -
LOC123190028	8.256623463	0.032413 096	NC_057797.1	65703469 8	65703950 9	E3 ubiquitin ligase BIG BROTHER-related-like && Q8L649.1 RecName: Full=E3 ubiquitin ligase BIG BROTHER; AltName: Full=Protein ENHANCER OF DA1-1; AltName: Full=RING- type E3 ubiquitin transferase BIG BROTHER && -
LOC123053864	8.28934482	0.032430 315	NC_057799.1	46620969 3	46621277 1	uncharacterised LOC123053864 && Q0J CZ4.1 RecName: Full=Auxin response factor 9 && -
-	8.719218892	0.033193 677	NC_057812.1	36133362	36137421	- && sp P10978 POLX_TOBAC Retrovirus-related Pol polyprotein from transposon TNT 1-94 OS=Nicotiana tabacum OX=4097 PE=2 SV=1 && -
LOC123167397	8.247246359	0.033193 677	NC_057814.1	88870943	88874181	uncharacterised LOC123167397 && - && -
LOC123119944	2.540223321	0.033193 677	NC_057808.1	15849152 3	15849566 8	uncharacterised LOC123119944%2C transcript variant X2 && - && -
LOC123054279	8.258101489	0.033401 534	NC_057799.1	53378379 1	53378535 9	uncharacterised LOC123054279 && F4JZL7.1 RecName: Full=Heavy metal-associated isoprenylated plant protein 33; Short=AtHIP33; Flags: Precursor && -
LOC123066761	1.215373854	0.034503 224	NC_057801.1	80967397 7	80967916 5	uncharacterised LOC123066761%2C transcript variant X2 && Q9FM19.1 RecName: Full=Hypersensitive-induced response protein 1; Short=AtHIR1 && -
LOC123052792	8.794367961	0.034819 905	NC_057799.1	28932724 7	28933047 6	uncharacterised LOC123052792 && - && -

LOC123152173	1.205578855	0.035937 719	NC_057812.1	27339224 9	27339585 1	transcription factor RF2a-like%2C transcript variant X1 && Q69IL4.1 RecName: Full=Transcription factor RF2a && -
LOC123046651	8.255312525	0.035939 11	NC_057798.1	67579528 1	67579874 3	uncharacterised LOC123046651 && - && -
LOC123189596	8.206697206	0.035939 11	NC_057797.1	58897436 4	58897787 9	protein FAR1-RELATED SEQUENCE 7-like%2C transcript variant X1 && Q9M8J3.1 RecName: Full=Protein FAR1-RELATED SEQUENCE 7 && -
LOC123167676	1.128276241	0.035939 11	NC_057814.1	54420604	54422436	probable receptor-like protein kinase At5g20050 && Q94C25.1 RecName: Full=Probable receptor-like protein kinase At5g20050; Flags: Precursor && -
LOC123107860	8.27620838	0.036080 365	NC_057806.1	59402111 0	59402294 3	cytochrome P450 81Q32-like && P93147.2 RecName: Full=Isoflavone 2'-hydroxylase; AltName: Full=CYP GE-3; AltName: Full=Cytochrome P450 81E1; AltName: Full=Cytochrome P450 91A4 && -
LOC123080504	7.373125628	0.037489 215	NC_057802.1	56237649 8	56238303 9	uncharacterised LOC123080504%2C transcript variant X2 && - && -
LOC123096400	1.237352924	0.037627 315	NC_057805.1	87921544	87925852	uncharacterised LOC123096400%2C transcript variant X2 && - && -
LOC123072913	8.216924743	0.038560 405	NC_057801.1	85146369 5	85147136 5	disease resistance protein RPM1-like && Q9FJB5.1 RecName: Full=Disease resistance RPP8-like protein 3 && -
LOC123072238	8.202888878	0.038560 405	NC_057801.1	75659793 5	75659965 4	protein SRG1-like && Q39224.1 RecName: Full=Protein SRG1; Short=AtSRG1; AltName: Full=Protein SENESCENCE-RELATED GENE 1 && -
LOC123153341	1.471096739	0.038560 405	NC_057812.1	36043259 5	36043666 4	vegetative cell wall protein gp1-like && - && -
LOC123157595	1.009420919	0.038560 405	NC_057813.1	28584583	28595433	F-box protein At5g67140-like && Q9FH99.1 RecName: Full=F-box protein At5g67140 && -
LOC123168862	8.226761462	0.039030 273	NC_057814.1	25299161 6	25299429 2	F-box/FBD/LRR-repeat protein At5g56420-like && Q8GXW6.1 RecName: Full=F-box/LRR-repeat protein At3g58930 && -
LOC123046469	8.175284393	0.039043 644	NC_057798.1	64530828 6	64531079 6	vegetative cell wall protein gp1-like && Q00451.1 RecName: Full=36.4 kDa proline-rich protein && -

LOC123161868	8.195164514	0.040524 087	NC_057813.1	89772345	89773808	probable carboxylesterase 12 && Q9SMN0.1 RecName: Full=Probable carboxylesterase 12; AltName: Full=AtCXE12 && -
LOC123126294	8.161018764	0.041995 527	NC_057808.1	56681133 8	56681251 4	mucin-1-like && - && -
LOC123113558	8.157649962	0.042261 76	NC_057807.1	60245699 8	60246080 1	chaperone protein ClpB1-like%2C transcript variant X1 && P42730.2 RecName: Full=Chaperone protein ClpB1; AltName: Full=ATP-dependent Clp protease ATP-binding subunit ClpB homolog 1; AltName: Full=Casein lytic proteinase B1; AltName: Full=Heat shock protein 101; AltName: Full=Protein DEFECTIVE IN LONG-TERM ACQUIRED THERMOTOLERANCE && -
-	8.192016289	0.043839 959	NC_057803.1	27051951 9	27052174 5	- && - && -
LOC123105552	8.126307675	0.044234 225	NC_057806.1	64184767 9	64185069 8	uncharacterised LOC123105552%2C transcript variant X5 && - && -
LOC123143010	8.108613755	0.044234 225	NC_057811.1	9310944	9312686	7-deoxyloganetin glucosyltransferase-like && F8WKW1.1 RecName: Full=7-deoxyloganetin glucosyltransferase; AltName: Full=Genipin glucosyltransferase; AltName: Full=UDP-glucose glucosyltransferase 2; Short=GjUGT2; AltName: Full=UDP-glycosyltransferase 85A24 && -
LOC123097596	1.403036536	0.044450 508	NC_057805.1	30662628 9	30663202 7	uncharacterised LOC123097596%2C transcript variant X2 && Q9BRT9.1 RecName: Full=DNA replication complex GINS protein SLD5; AltName: Full=GINS complex subunit 4; Contains: RecName: Full=DNA replication complex GINS protein SLD5, N-terminally processed && -
LOC123095080	8.352647654	0.045796 459	NC_057804.1	51671599 0	51671685 6	uncharacterised LOC123095080 && - && -
LOC123124347	8.16817854	0.045867 919	NC_057808.1	63446581	63448494	zealexin A1 synthase-like && Q6YV88.1 RecName: Full=Ent-cassadiene C2-hydroxylase; AltName: Full=Cytochrome P450 71Z7 && -
-	1.685805929	0.045867 919	NC_057807.1	16822468 3	16822700 3	- && - && -

LOC123133502	1.023275127	0.045867 919	NC_057810.1	66741534	66742188	histone H2B.2-like && Q6ZBP3.1 RecName: Full=Histone H2B.2 >A2YWI3.1 RecName: Full=Histone H2B.2 && -
LOC123052651	6.355612924	0.045978 172	NC_057794.1	39447105 6	39447526 4	TATA box-binding protein-associated factor RNA polymerase I subunit B-like && Q5W770.2 RecName: Full=TATA box-binding protein-associated factor RNA polymerase I subunit B; AltName: Full=TATA box-binding protein-associated factor 1B; Short=TBP-associated factor 1B && -
LOC123125311	1.313160775	0.046277 6	NC_057808.1	43380839 4	43381004 3	putrescine hydroxycinnamoyltransferase-like && Q7XXN4.1 RecName: Full=Putrescine hydroxycinnamoyltransferase && -
LOC123102486	8.088050521	0.046828 722	NC_057806.1	10080431 6	10080629 3	xyloglucan galactosyltransferase KATAMARI1 homolog && Q8H038.1 RecName: Full=Xyloglucan galactosyltransferase KATAMARI1 homolog && -
LOC123131696	8.088633226	0.048891 723	NC_057809.1	16092365	16108348	uncharacterised LOC123131696%2C transcript variant X2 && Q9S775.1 RecName: Full=CHD3-type chromatin-remodeling factor PICKLE; AltName: Full=Protein CHROMATIN REMODELING 6; Short=AtCHR6; AltName: Full=Protein GYMNOS && -
LOC123139977	1.199696629	0.048957 617	NC_057810.1	71807249 7	71807819 5	uncharacterised LOC123139977%2C transcript variant X3 && B4KKN5.1 RecName: Full=Protein SMG8; AltName: Full=Protein smg-8 homolog && -
LOC123141981	8.115733192	0.049000 219	NC_057811.1	45732646 8	45732744 5	dehydrin DHN3-like && P12948.1 RecName: Full=Dehydrin DHN3; AltName: Full=B17 && -
LOC123092265	8.325144378	0.049255 591	NC_057804.1	38482386 6	38482954 1	probable ADP-ribosylation factor GTPase-activating protein AGD14 && Q8RXE7.2 RecName: Full=Probable ADP-ribosylation factor GTPase-activating protein AGD14; Short=ARF GAP AGD14; AltName: Full=Protein ARF-GAP DOMAIN 14; Short=AtAGD14; AltName: Full=Protein ZIGA4 && -
LOC123043078	8.309669892	0.049482 33	NC_057798.1	7488632	7503008	ABC transporter B family member 4-like && Q9FWX7.1 RecName: Full=ABC transporter B family member 11; Short=ABC transporter ABCB.11; Short=AtABCB11;

-	8.16909545	0.049482 33	NC_057810.1	76303973	76304444	AltName: Full=Multidrug resistance protein 8; AltName: Full=P-glycoprotein 11 && - - && - && PF00280:Potato inhibitor I family
-	8.109201689	0.049482 33	NC_057796.1	79080370	79081432	- && - && -
LOC123151128	8.096893209	0.049482 33	NC_057812.1	16677645 8	16677726 6	pathogenesis-related protein PRB1-2-like && P35792.1 RecName: Full=Pathogenesis-related protein PRB1-2; Flags: Precursor && -
LOC123176816	8.089692555	0.049482 33	NC_057794.1	52965545 0	52965635 2	non-symbiotic hemoglobin 1-like && O04986.1 RecName: Full=Non-symbiotic hemoglobin 1; AltName: Full=ORYsa GLB1a; AltName: Full=rHb1 && -
LOC123052496	8.085645166	0.049482 33	NC_057799.1	19111076 5	19111234 6	probable long-chain-alcohol O-fatty-acyltransferase 5 && Q9FJ76.1 RecName: Full=Probable long-chain-alcohol O-fatty-acyltransferase 5; AltName: Full=Wax synthase 5 && -
LOC123137523	8.085477336	0.049482 33	NC_057795.1	54919340 2	54919447 0	chlorophyll a-b binding protein of LHCII type 1-like && P07369.1 RecName: Full=Chlorophyll a-b binding protein 3C, chloroplastic; AltName: Full=LHCII type I CAB-3C; Short=LHCP; Flags: Precursor && -
LOC123150954	7.310469593	0.049482 33	NC_057812.1	1705172	1706788	protein ENHANCED PSEUDOMONAS SUSCEPTIBILITY 1-like && Q9SND9.1 RecName: Full=Uncharacterised acetyltransferase At3g50280 && -
LOC123161966	5.877557348	0.049482 33	NC_057813.1	69351229 4	69351321 3	alpha-amylase/trypsin inhibitor-like && P81370.2 RecName: Full=Thaumatococcus-like protein; AltName: Allergen=Act d 2; Flags: Precursor && -
-	4.829115781	0.049482 33	NC_057798.1	38573978 6	38574216 1	- && - && -
LOC123090384	8.202341695	0.049706 565	NC_057804.1	65742918 1	65743158 3	transcription factor GHD7-like && E5RQA1.1 RecName: Full=Transcription factor GHD7; AltName: Full=Protein GRAIN NUMBER PLANT HEIGHT AND HEADING DATE 7 && -
LOC123039308	6.447920076	0.050496 236	NC_057798.1	58011459 4	58011767 0	uncharacterised LOC123039308 && - && -

LOC123168272 8.093588811 0.050725 678 NC\_057814.1 90902389 90909334 uncharacterised LOC123168272%2C transcript variant X1 && - && -

2

**Appendix Table 2:** Differentially Expressed Genes in AGDM QTL when compared with high and low N treatment. log2fold change was >1 and Padj value <0.05. This list is obtained when less stringent log2fold change and Padj value threshold criteria is used.

Gene_Name	log2FoldChange	Padj	Gene_chr	Gene_start	Gene_end	Gene_description
LOC123168472	9.042895	0.002414	NC_057814.1	4.88E+08	4.88E+08	pentatricopeptide repeat-containing protein At1g18485-like && QOWN60.2 RecName: Full=Penatricopeptide repeat-containing protein At1g18485 && -
LOC123136829	9.150332	0.004031	NC_057810.1	2.53E+08	2.53E+08	vacuolar-processing enzyme beta-isozyme 1-like%2C transcript variant X7 && B8ASK4.1 RecName: Full=Vacuolar-processing enzyme beta-isozyme 1; Short=Beta-VPE 1; Short=OsVPE1; AltName: Full=Asparaginyl endopeptidase VPE1; Flags: Precursor && -
LOC123189867	8.826289	0.00477	NC_057797.1	6.26E+08	6.26E+08	uncharacterised LOC123189867 && - && -
LOC123181976	8.823151	0.00477	NC_057796.1	3.48E+08	3.48E+08	- && H2DH21.1 RecName: Full=Cytochrome P450 CYP72A219; AltName: Full=Cytochrome P450 CYP72A129 [Panax ginseng] && -
LOC123105694	8.828946	0.005229	NC_057806.1	6.56E+08	6.56E+08	putative methyltransferase C9orf114 && Q5T280.3 RecName: Full=Putative methyltransferase C9orf114 && -
LOC123060985	8.767856	0.005229	NC_057800.1	2.08E+08	2.08E+08	uncharacterised LOC123060985 && - && -
LOC123180086	8.702931	0.010261	NC_057794.1	5.41E+08	5.41E+08	&& P17801.2 RecName: Full=Putative receptor protein kinase ZmPK1; Flags: Precursor && -
LOC123127992	7.101246	0.010261	NC_057809.1	4.81E+08	4.81E+08	uncharacterised LOC123127992%2C transcript variant X3 && - && -
-	8.777464	0.011685	NC_057811.1	4.04E+08	4.04E+08	- && - && -
LOC123168840	8.763817	0.011685	NC_057814.1	4.16E+08	4.16E+08	NDR1/HIN1-like protein 1 && Q9SJ54.1 RecName: Full=NDR1/HIN1-like protein 12 && -
LOC123191087	8.647363	0.011685	NC_057797.1	7.7E+08	7.7E+08	uncharacterised LOC123191087 && - && -
-	8.594831	0.011685	NC_057812.1	3.69E+08	3.69E+08	- && sp A1EA09 YCF3_AGRST Photosystem I assembly protein Ycf3 OS=Agrostis stolonifera OX=63632 GN=ycf3 PE=3 SV=1 && -

LOC123085526	8.558643	0.011685	NC_057803.1	1.19E+08	1.19E+08	elongator complex protein 6-like && Q8L9Y2.1 RecName: Full=Elongator complex protein 6; Short=AtELP6; AltName: Full=Elongator component 6; AltName: Full=UPF0405 protein ELP6 && -
LOC123053392	8.545655	0.011685	NC_057799.1	3.98E+08	3.98E+08	protein phosphatase methylesterase 1-like && Q8BVQ5.5 RecName: Full=Protein phosphatase methylesterase 1; Short=PME-1 && -
LOC123105106	7.898283	0.012874	NC_057806.1	5.94E+08	5.94E+08	aspartate-semialdehyde dehydrogenase-like && Q55512.2 RecName: Full=Aspartate-semialdehyde dehydrogenase; Short=ASA dehydrogenase; Short=ASADH; AltName: Full=Aspartate-beta-semialdehyde dehydrogenase && -
LOC123167394	6.673676	0.01318	NC_057814.1	1.44E+08	1.44E+08	uncharacterised LOC123167394 && - && -
LOC123128139	8.806477	0.01396	NC_057809.1	5.02E+08	5.02E+08	zinc-finger homeodomain protein 7-like && Q8S3Q9.1 RecName: Full=Zinc-finger homeodomain protein 7; Short=OsZHD7 && -
LOC123142873	8.448734	0.01396	NC_057795.1	6.2E+08	6.2E+08	uncharacterised LOC123142873 && - && -
LOC123061066	-8.55736	0.01396	NC_057794.1	5.07E+08	5.07E+08	serine/threonine-protein kinase Aurora-3-like%2C transcript variant X6 && O64629.1 RecName: Full=Serine/threonine-protein kinase Aurora-3; Short=AtAur3; AltName: Full=Aurora-like kinase 3 && -
-	8.635561	0.014614	NC_057805.1	2.75E+08	2.75E+08	- && - && -
LOC123086239	8.602726	0.014614	NC_057803.1	4.38E+08	4.38E+08	uncharacterised LOC123086239%2C transcript variant X2 && - && -
LOC123126443	8.440109	0.014614	NC_057808.1	5.23E+08	5.23E+08	small nucleolar RNA snoR99 && - && -
LOC123188307	7.946394	0.014614	NC_057797.1	1.97E+08	1.97E+08	uncharacterised LOC123188307 && - && -
LOC123185291	8.415947	0.014828	NC_057797.1	3.84E+08	3.84E+08	uncharacterised LOC123185291 && - && -
LOC123142031	8.428623	0.014918	NC_057811.1	4.67E+08	4.67E+08	uncharacterised LOC123142031 && - && -
LOC123065622	8.405683	0.014918	NC_057801.1	5.16E+08	5.16E+08	RING-H2 finger protein ATL67-like && O82353.1 RecName: Full=RING-H2 finger protein ATL67; AltName: Full=RING-type E3 ubiquitin transferase ATL67 && -
LOC123080638	8.405021	0.014918	NC_057802.1	5.79E+08	5.79E+08	hexokinase-3-like && Q2KNB4.1 RecName: Full=Hexokinase-3; AltName: Full=Hexokinase-8 && -
LOC123189528	8.597548	0.01714	NC_057797.1	5.78E+08	5.78E+08	NAC domain-containing protein 73-like%2C transcript variant X1 && Q6NQK2.1 RecName: Full=NAC domain-containing protein 8; Short=ANAC008 && -
LOC123159059	8.506102	0.017603	NC_057813.1	4.28E+08	4.28E+08	chromatin assembly factor 1 subunit FAS2 homolog%2C transcript variant X2 && Q6ZD63.1 RecName: Full=Chromatin assembly factor 1 subunit FAS2

LOC123053679	8.445595	0.019134	NC_057799.1	4.38E+08	4.38E+08	homolog; Short=CAF-1 subunit FAS2 homolog; AltName: Full=CAF-1 p60 homolog; AltName: Full=Protein FASCIATA 2 homolog && - uncharacterised LOC123053679 && - && - bHLH transcription factor RHL1-like%2C transcript variant X1 && Q9ZUG9.1 RecName: Full=Transcription factor bHLH66; AltName: Full=Basic helix-loop-helix protein 66; Short=AtbHLH66; Short=bHLH 66; AltName: Full=Transcription factor EN 95; AltName: Full=bHLH transcription factor
LOC123103878	8.368735	0.019134	NC_057806.1	4.42E+08	4.42E+08	bHLH066 && -
LOC123074993	8.42717	0.020808	NC_057802.1	4.78E+08	4.78E+08	- && - && -
LOC123160410	8.342232	0.020808	NC_057813.1	7E+08	7E+08	uncharacterised LOC123160410 && - && - zinc finger protein ZAT5-like && Q681X4.1 RecName: Full=Zinc finger
LOC123184132	-8.79136	0.021947	NC_057797.1	1422772	1424345	protein ZAT5 && -
LOC123125285	8.505781	0.022927	NC_057808.1	4.28E+08	4.28E+08	uncharacterised LOC123125285%2C transcript variant X2 && - && -
LOC123062753	8.393982	0.023888	NC_057800.1	6.33E+08	6.33E+08	uncharacterised LOC123062753%2C transcript variant X1 && - && - cytochrome b5-like && Q42342.2 RecName: Full=Cytochrome b5 isoform E; Short=AtCb5-E; AltName: Full=Cytochrome b5 isoform 1; AltName: Full=Cytochrome b5 isoform A; Short=AtCb5-A && -
LOC123127869	8.381061	0.023888	NC_057809.1	4.54E+08	4.54E+08	uncharacterised LOC123086808%2C transcript variant X2 && Q17QN8.1 RecName: Full=UPF0454 protein C12orf49 homolog; Flags: Precursor && - beta-1%2C3-galactosyltransferase 7-like && Q6NQB7.1 RecName: Full=Beta-1,3-galactosyltransferase 7 && -
LOC123086808	8.296482	0.023888	NC_057803.1	5.41E+08	5.41E+08	uncharacterised LOC123185364 && - && -
LOC123127507	2.159024	0.024867	NC_057809.1	3.33E+08	3.33E+08	protein XRI1-like && Q6NLW5.2 RecName: Full=Protein XRI1; AltName: Full=Protein X-RAY INDUCED 1 && -
LOC123185364	8.475024	0.026015	NC_057797.1	4.27E+08	4.27E+08	4%2C5:9%2C10-diseco-3-hydroxy-5%2C9%2C17-trioxoandrosta-1(10)%2C2-diene-4-oate hydrolase-like%2C transcript variant X1 && - && -
-	8.295143	0.026015	NC_057804.1	3.64E+08	3.64E+08	reticulon-like protein B12 && Q9M392.1 RecName: Full=Reticulon-like protein B12; Short=AtRTNLB12 && -
LOC123071973	8.29325	0.026015	NC_057801.1	7.18E+08	7.18E+08	uncharacterised LOC123048221 && - && - expansin-like A4 && Q5Z980.1 RecName: Full=Expansin-like A4; AltName: Full=OsEXLA4; AltName: Full=OsEXPL4; Flags: Precursor && -
LOC123098643	8.262764	0.026015	NC_057805.1	4.64E+08	4.64E+08	
LOC123150158	8.259576	0.026015	NC_057795.1	6.98E+08	6.98E+08	
LOC123048221	8.252957	0.026015	NC_057799.1	10305413	10307095	
LOC123147128	8.250248	0.026015	NC_057812.1	7.28E+08	7.28E+08	



LOC123076973	8.233404	0.026015	NC_057802.1	19564558	19568170	L-Ala-D/L-amino acid epimerase-like && B9I2J6.2 RecName: Full=L-Ala-D/L-amino acid epimerase; AltName: Full=L-Ala-D/L-Xxx epimerase && - transcription factor BIM2-like && Q9CAA4.1 RecName: Full=Transcription factor BIM2; AltName: Full=BES1-interacting Myc-like protein 2; AltName: Full=Basic helix-loop-helix protein 102; Short=AtbHLH102; Short=bHLH 102; AltName: Full=Transcription factor EN 125; AltName: Full=bHLH
LOC123147839	8.22065	0.026015	NC_057812.1	5.03E+08	5.03E+08	transcription factor bHLH102 && -
LOC123151856	-8.19208	0.026015	NC_057812.1	69357004	69359239	anti-sigma-I factor RsgI2-like && - && - probable LRR receptor-like serine/threonine-protein kinase At3g47570%2C transcript variant X2 && COLGP4.1 RecName: Full=Probable LRR receptor-like serine/threonine-protein kinase At3g47570; Flags: Precursor && - mitogen-activated protein kinase kinase kinase 17-like && Q9CAD5.1 RecName: Full=Mitogen-activated protein kinase kinase kinase YODA; AltName: Full=YODA MAPKK kinase && -
LOC123054814	8.329751	0.029934	NC_057799.1	5.96E+08	5.96E+08	uncharacterised LOC123127600%2C transcript variant X4 && - && - uncharacterised LOC123128442%2C transcript variant X3 && - && - - && - && -
LOC123045998	8.320406	0.030182	NC_057794.1	5.47E+08	5.47E+08	protein ROLLING AND ERECT LEAF 2-like%2C transcript variant X1 && - && - probable dual-specificity RNA methyltransferase RlmN && Q3AHX9.1 RecName: Full=Probable dual-specificity RNA methyltransferase RlmN; AltName: Full=23S rRNA (adenine(2503)-C(2))-methyltransferase; AltName: Full=23S rRNA m2A2503 methyltransferase; AltName: Full=Ribosomal RNA large subunit methyltransferase N; AltName: Full=tRNA (adenine(37)-C(2))-methyltransferase; AltName: Full=tRNA m2A37 methyltransferase && -
LOC123127600	8.524345	0.034055	NC_057809.1	3.85E+08	3.85E+08	uncharacterised LOC123078187 && - && -
LOC123128442	8.371287	0.034055	NC_057809.1	5.54E+08	5.54E+08	pentatricopeptide repeat-containing protein At1g73710-like && Q9C9U0.1 RecName: Full=Pentatricopeptide repeat-containing protein At1g73710 && -
-	8.187582	0.034055	NC_057799.1	6.56E+08	6.56E+08	-
LOC123168084	8.220778	0.034304	NC_057814.1	2.26E+08	2.26E+08	fasciclin-like arabinogalactan protein 15 && Q66GR0.1 RecName: Full=Fasciclin-like arabinogalactan protein 17; Flags: Precursor && - splicing factor U2af large subunit A-like%2C transcript variant X2 && Q2R0Q1.2 RecName: Full=Splicing factor U2af large subunit A; AltName: Full=U2 auxiliary factor 65 kDa subunit A; AltName: Full=U2 small nuclear
LOC123072851	8.186933	0.034304	NC_057801.1	8.42E+08	8.42E+08	
LOC123078187	8.157662	0.034907	NC_057802.1	1.85E+08	1.85E+08	
LOC123170031	8.293284	0.037113	NC_057814.1	4.98E+08	4.98E+08	
LOC100037584	8.347126	0.042633	NC_057797.1	3.77E+08	3.77E+08	
LOC123122652	8.255236	0.042633	NC_057808.1	4.51E+08	4.51E+08	

						ribonucleoprotein auxiliary factor large subunit A; Short=U2 snRNP auxiliary factor large subunit A && -
LOC123115969	9.110673	0.048197	NC_057807.1	2.74E+08	2.74E+08	uncharacterised LOC123115969 && - && -
LOC123134157	8.175831	0.048197	NC_057810.1	3.89E+08	3.89E+08	uncharacterised LOC123134157%2C transcript variant X1 && - && -
-	8.114316	0.048197	NC_057812.1	5.81E+08	5.81E+08	- && - && - - && Q0D5R3.1 RecName: Full=Cysteine-rich receptor-like protein kinase 6;
LOC123057965	8.063366	0.048197	NC_057800.1	71065024	71068840	Short=Cysteine-rich RLK6; Flags: Precursor && -
LOC123076277	8.328286	0.049158	NC_057802.1	3.14E+08	3.14E+08	uncharacterised LOC123076277 && - && -

### 3

**Appendix Table 3:** Differentially Expressed Genes in GY QTL when compared with high and low N treatment. log2fold change was >1 and Padj value <0.05. This list is obtained when less stringent log2fold change and Padj value threshold criteria is used.

Gene_Name	log2FoldChange	Padj	Gene_chr	Gene_start	Gene_end	Gene_description
LOC123099896	8.723599	0.102562	NC_057805.1	2.59E+08	2.59E+08	proline-rich receptor-like protein kinase PERK10 && - && - bisdemethoxycurcumin synthase-like && Q8LIL0.2 RecName: Full=Bisdemethoxycurcumin synthase; AltName: Full=Curcuminoid
LOC123140724	6.506292	0.149349	NC_057811.1	8445864	8447420	synthase && -
-	8.305068	0.149349	NC_057806.1	90239711	90240573	- && - && PF02892:BED zinc finger mannose-P-dolichol utilisation defect 1 protein homolog 2- like%2C transcript variant X3 && Q8VY63.1 RecName: Full=Mannose-P-dolichol utilisation defect 1 protein homolog 2
LOC123134402	8.619432	0.149349	NC_057810.1	5.53E+08	5.54E+08	&& - alpha-1%2C3-arabinosyltransferase XAT3-like && Q5NDE4.1 RecName: Full=Protein O-linked-mannose beta-1,4-N- acetylglucosaminyltransferase 2; Short=POMGnT2; AltName: Full=Extracellular O-linked N-acetylglucosamine transferase-like; AltName: Full=Glycosyltransferase-like domain-containing protein
LOC123145518	8.297055	0.149349	NC_057811.1	4.21E+08	4.21E+08	2 && -

LOC123071827	8.357907	0.149349	NC_057801.1	6.96E+08	6.96E+08	bidirectional sugar transporter SWEET1a-like && P0DKJ3.1 RecName: Full=Bidirectional sugar transporter SWEET1a; Short=SbSWEET1a && - nodulation protein H-like%2C transcript variant X2 && O24303.1 RecName: Full=Protein TIC110, chloroplastic; AltName: Full=Chloroplast inner envelope protein, 110 kDa; Short=psIEP110; AltName: Full=IAP100; AltName: Full=Translocon at the inner envelope membrane of chloroplasts 110; Flags: Precursor && - uncharacterised LOC123151220 && - && - - && Q9ZUZ3.1 RecName: Full=Auxin-responsive protein SAUR32; AltName: Full=Protein ABOLISHED APICAL HOOK MAINTENANCE 1; AltName: Full=Protein SMALL AUXIN UP RNA 32 && - probable methyltransferase At1g27930 && Q9LQ32.1 RecName: Full=Glucuronoxylan 4-O-methyltransferase 3 && - putative FBD-associated F-box protein At3g50710%2C transcript variant X2 && Q9FWZ1.1 RecName: Full=F-box/LRR-repeat protein 13 && - uncharacterised LOC123151151 && - && - CRIB domain-containing protein RIC4-like && Q9FFD5.1 RecName: Full=CRIB domain-containing protein RIC4; AltName: Full=ROP- interactive CRIB motif-containing protein 4; AltName: Full=Target of ROP protein RIC4 && - probable methyltransferase PMT26 && Q8L7V3.1 RecName: Full=Probable methyltransferase PMT26 && - - && sp P93295 M310_ARATH Uncharacterised mitochondrial protein AtMg00310 OS=Arabidopsis thaliana OX=3702 GN=AtMg00310 PE=4 SV=1 && - uncharacterised LOC123128894%2C transcript variant X1 && - &&
LOC123054981	8.277876	0.149349	NC_057794.1	4.44E+08	4.44E+08	
LOC123151220	8.333261	0.149349	NC_057812.1	26998363	26998896	
LOC123131054	8.244081	0.149349	NC_057809.1	5.65E+08	5.65E+08	
LOC123143074	7.018058	0.149349	NC_057795.1	6.22E+08	6.22E+08	
LOC123155760	8.18494	0.149349	NC_057813.1	6.13E+08	6.13E+08	
LOC123151151	8.218442	0.149349	NC_057812.1	20370750	20373292	
LOC123066178	8.302481	0.149349	NC_057801.1	7.18E+08	7.18E+08	
LOC123080127	8.152533	0.149349	NC_057802.1	5.17E+08	5.17E+08	
-	8.104484	0.149349	NC_057800.1	7.41E+08	7.41E+08	
LOC123128894	8.225079	0.149349	NC_057809.1	6.01E+08	6.01E+08	
-	8.102941	0.149349	NC_057813.1	3.36E+08	3.36E+08	- && - && -
-	8.102013	0.156166	NC_057798.1	2.79E+08	2.79E+08	- && - && -

LOC123094421	8.315969	0.169092	NC_057804.1	61366272	61367892	putative pentatricopeptide repeat-containing protein At3g28640 && Q9LJJ1.1 RecName: Full=Putative pentatricopeptide repeat-containing protein At3g28640 && - ATP synthase subunit a%2C chloroplastic-like && Q9XPT0.1 RecName: Full=ATP synthase subunit a, chloroplastic; AltName: Full=ATP synthase F0 sector subunit a; AltName: Full=F-ATPase subunit IV >A1E9I5.1 RecName: Full=ATP synthase subunit a, chloroplastic; AltName: Full=ATP synthase F0 sector subunit a; AltName: Full=F-ATPase subunit IV && -
LOC123068902	7.32197	0.179352	NC_057801.1	1.14E+08	1.14E+08	- && - && -
-	8.795999	0.193434	NC_057811.1	3.37E+08	3.37E+08	UDP-glycosyltransferase 88B1-like && Q4R1I9.1 RecName: Full=Anthocyanidin 5,3-O-glucosyltransferase; AltName: Full=UDP-glucose: anthocyanidin 5,3-O-glucosyltransferase && - receptor-like serine/threonine-protein kinase NCRK && Q8VYY5.1 RecName: Full=Receptor-like serine/threonine-protein kinase NCRK; Flags: Precursor && -
LOC123119480	8.125608	0.193434	NC_057808.1	65178501	65181183	WAS/WASL-interacting protein family member 1-like && - && - copper-transporting ATPase PAA1%2C chloroplastic-like && Q9SZC9.1 RecName: Full=Copper-transporting ATPase PAA1, chloroplastic; AltName: Full=Protein HEAVY METAL ATPASE 6; AltName: Full=Protein glucose insensitive root 1; Flags: Precursor && -
LOC123135516	8.096305	0.193434	NC_057810.1	28390626	28393301	protein Rf1%2C mitochondrial-like%2C transcript variant X1 && Q76C99.1 RecName: Full=Protein Rf1, mitochondrial; AltName: Full=Fertility restorer; AltName: Full=Protein PPR; AltName: Full=Restorer for CMS; Flags: Precursor && -
LOC123120456	8.017793	0.193434	NC_057808.1	2.31E+08	2.31E+08	uncharacterised LOC123107735 && - && - uncharacterised LOC123080474 && - && -
LOC123124203	8.187054	0.216447	NC_057808.1	37487798	37491382	- && - && - transcription factor EMB1444-like%2C transcript variant X5 && POC7P8.1 RecName: Full=Transcription factor EMB1444; AltName: Full=Basic helix-loop-helix protein EMB1444; AltName: Full=LONESOME HIGHWAY-like protein 1; AltName: Full=Protein
LOC123188503	8.048342	0.216447	NC_057794.1	39035497	39042096	
LOC123107735	8.005117	0.216447	NC_057806.1	5.68E+08	5.68E+08	
LOC123080474	7.955909	0.216447	NC_057802.1	5.59E+08	5.59E+08	
-	8.015677	0.216447	NC_057795.1	3.83E+08	3.83E+08	
LOC123188784	7.946655	0.229846	NC_057797.1	3.96E+08	3.96E+08	

						EMBRYO DEFECTIVE 1444; AltName: Full=bHLH transcription factor EMB1444 && -
LOC123169670	8.740243	0.23343	NC_057814.1	2.04E+08	2.04E+08	protein RAFTIN 1B-like && Q70KG3.1 RecName: Full=Protein RAFTIN 1B; Short=TaRAFTIN1b; AltName: Full=BURP domain-containing protein 1B; Flags: Precursor && -
LOC123113694	8.019606	0.233946	NC_057807.1	6.22E+08	6.22E+08	receptor-like protein EIX2 && - && -
LOC123130806	7.9912	0.233946	NC_057809.1	4.88E+08	4.88E+08	FCS-Like Zinc finger 2-like && - && -
-	8.02178	0.233946	NC_057805.1	3.57E+08	3.57E+08	- && - && -
						60 kDa jasmonate-induced protein-like%2C transcript variant X1 && Q00531.1 RecName: Full=60 kDa jasmonate-induced protein; AltName: Full=rRNA N-glycosidase && -
LOC123159163	8.12695	0.254195	NC_057813.1	6.09E+08	6.09E+08	zinc finger CCCH domain-containing protein 43-like%2C transcript variant X1 && Q5Z5Q3.1 RecName: Full=Zinc finger CCCH domain-containing protein 43; Short=OsC3H43 && -
LOC123103297	7.960234	0.254195	NC_057795.1	9356653	9363048	U-box domain-containing protein 39-like && Q9STT1.1 RecName: Full=U-box domain-containing protein 39; AltName: Full=Plant U-box protein 39 && -
LOC123111877	8.086906	0.261185	NC_057807.1	3.64E+08	3.64E+08	uncharacterised LOC123053971 && - && -
LOC123053971	8.350453	0.267834	NC_057799.1	4.82E+08	4.82E+08	- && Q7F1M0.1 RecName: Full=ATP-dependent DNA helicase 2 subunit KU70; Short=OsKU70; AltName: Full=ATP-dependent DNA helicase 2 subunit 1; AltName: Full=ATP-dependent DNA helicase II 70 kDa subunit && -
LOC123069529	7.961253	0.267834	NC_057801.1	2.42E+08	2.42E+08	uncharacterised LOC123106811 && - && -
LOC123106811	3.359379	0.293295	NC_057806.1	2.84E+08	2.84E+08	uncharacterised LOC123054495%2C transcript variant X1 && Q67A25.1 RecName: Full=S-norococlaurine synthase; Flags: Precursor && -
LOC123054495	8.269017	0.293295	NC_057799.1	5.59E+08	5.59E+08	- && - && PF05699:hAT family C-terminal dimerisation region bZIP transcription factor 46-like && Q9M7Q4.1 RecName: Full=ABSCISIC ACID-INSENSITIVE 5-like protein 5; AltName: Full=ABA-responsive element-binding protein 1; AltName: Full=Abscisic acid responsive elements-binding factor 2; Short=ABRE-binding factor 2; AltName: Full=bZIP transcription factor 36; Short=AtbZIP36 && -
-	7.133842	0.293295	NC_057800.1	57966294	57967088	
LOC123157113	7.871051	0.295905	NC_057813.1	87817822	87823485	

LOC123117718	8.603882	0.308879	NC_057807.1	6.92E+08	6.92E+08	probable polyamine transporter At3g13620%2C transcript variant X1 && Q9LHN7.1 RecName: Full=Probable polyamine transporter At3g13620 && -
LOC123095540	8.100654	0.310176	NC_057805.1	463562	465621	probable serine/threonine-protein kinase PBL7 && Q9SFT7.1 RecName: Full=Serine/threonine-protein kinase At3g07070 && -
LOC123145925	3.833407	0.318889	NC_057811.1	4.65E+08	4.65E+08	uncharacterised LOC123145925 && - && -
LOC123164989	7.180336	0.318889	NC_057814.1	4.02E+08	4.02E+08	protein IQ-DOMAIN 17-like && Q8LPG9.1 RecName: Full=Protein IQ-DOMAIN 14 && -
LOC123188077	7.967634	0.327783	NC_057797.1	1.48E+08	1.48E+08	zinc finger protein 7-like && Q39266.1 RecName: Full=Zinc finger protein 7 && -
LOC123188466	6.387966	0.327783	NC_057797.1	2.38E+08	2.38E+08	mitotic checkpoint serine/threonine-protein kinase BUB1-like%2C transcript variant X2 && F4IVIO.1 RecName: Full=Mitotic checkpoint serine/threonine-protein kinase BUB1; Short=AtBUB1; AltName: Full=Protein BUDDING UNINHIBITED BY BENZYMIDAZOL 1 && -
LOC123041198	7.808925	0.327783	NC_057798.1	2.81E+08	2.81E+08	- && - && -
-	7.790728	0.327783	NC_057794.1	4.38E+08	4.38E+08	- && - && -
LOC123130259	8.470232	0.327783	NC_057809.1	55784669	55785808	uncharacterised LOC123130259 && - && -
-	8.111893	0.333321	NC_057813.1	3.46E+08	3.46E+08	- && - && -
LOC123117648	2.395708	0.335399	NC_057807.1	6.84E+08	6.84E+08	phosphoglycerate mutase-like protein AT74H && Q9MAA2.1 RecName: Full=Phosphoglycerate mutase-like protein AT74; Short=At-74 && -
LOC123137168	6.567878	0.335973	NC_057810.1	3.63E+08	3.63E+08	uncharacterised LOC123137168%2C transcript variant X1 && - && -
LOC123190824	7.771501	0.350833	NC_057797.1	7.48E+08	7.48E+08	-
LOC123112103	7.780638	0.397312	NC_057807.1	4.02E+08	4.02E+08	uncharacterised LOC123190824 && - && -
LOC123040204	8.401409	0.416213	NC_057798.1	34685926	34688100	bHLH transcription factor RHL1-like%2C transcript variant X1 && Q9ZUG9.1 RecName: Full=Transcription factor bHLH66; AltName: Full=Basic helix-loop-helix protein 66; Short=AtbHLH66; Short=bHLH 66; AltName: Full=Transcription factor EN 95; AltName: Full=bHLH transcription factor bHLH066 && -
						uncharacterised LOC123040204 && - && -

LOC123186893	7.836113	0.416213	NC_057797.1	2382671	2390405	putative disease resistance protein RGA3%2C transcript variant X6 && Q9LRR5.1 RecName: Full=Putative disease resistance protein At3g14460 && -
LOC123083068	7.765231	0.416213	NC_057803.1	6.78E+08	6.78E+08	uncharacterised LOC123083068 && - && -
LOC123053266	7.702668	0.416213	NC_057794.1	4.05E+08	4.05E+08	- && - && -
LOC123079098	7.738632	0.416213	NC_057802.1	3.9E+08	3.9E+08	respiratory burst oxidase homolog protein A-like && O48538.1 RecName: Full=Respiratory burst oxidase homolog protein F; AltName: Full=Cytochrome b245 beta chain homolog RbohAp108; AltName: Full=NADPH oxidase RBOHF; Short=AtRBOHF && - putative pentatricopeptide repeat-containing protein At3g23330 && Q9LW63.1 RecName: Full=Putative pentatricopeptide repeat-
LOC123044129	7.734312	0.416213	NC_057798.1	1.69E+08	1.69E+08	containing protein At3g23330 && -
LOC123090443	7.082701	0.416213	NC_057804.1	6.69E+08	6.69E+08	uncharacterised LOC123090443 && - && -
LOC123126491	7.715128	0.416213	NC_057808.1	4.87E+08	4.87E+08	small nucleolar RNA SNOR75 && - && -
LOC123142919	7.829631	0.4259	NC_057811.1	3461732	3462540	thiosulfate sulfurtransferase 16%2C chloroplastic-like && - && - cold shock protein CS66 && P46526.1 RecName: Full=Cold shock protein CS66 && -
LOC123138917	6.956578	0.433083	NC_057810.1	6.66E+08	6.66E+08	uncharacterised LOC123105976%2C transcript variant X3 && Q9FYT6.1 RecName: Full=Chloroplastic group IIA intron splicing facilitator CRS1, chloroplastic; AltName: Full=Chloroplastic RNA splicing factor 1; AltName: Full=Protein CHLOROPLAST RNA SPLICING 1; Flags: Precursor && -
LOC123105976	7.655811	0.433083	NC_057795.1	46653801	46657133	proteasome subunit beta type-6-like && P93395.1 RecName: Full=Proteasome subunit beta type-6; AltName: Full=Proteasome delta chain; AltName: Full=Tobacco cryptogein-induced protein 7; Short=tcl 7; Flags: Precursor && -
LOC123082518	7.817502	0.436732	NC_057795.1	6.84E+08	6.84E+08	CSC1-like protein At3g54510 && F4JCY2.1 RecName: Full=CSC1-like protein At3g54510 && -
LOC123075652	7.708166	0.444328	NC_057802.1	5.85E+08	5.85E+08	chaperone protein dnaJ 10-like && Q8GYX8.2 RecName: Full=Chaperone protein dnaJ 10; Short=AtDjC10; Short=AtJ10 && -
LOC123150887	7.75848	0.450675	NC_057812.1	4.34E+08	4.34E+08	glycine-rich protein DOT1-like && - && -
LOC123185788	7.680417	0.475688	NC_057797.1	6.42E+08	6.42E+08	glycine-rich protein DOT1-like && - && -
LOC123052306	7.6869	0.475688	NC_057799.1	1.55E+08	1.55E+08	cilia- and flagella-associated protein 251-like && - && -

LOC123185756	2.338113	0.480613	NC_057797.1	6.29E+08	6.29E+08	mitochondrial import receptor subunit TOM9-2-like && Q9FNC9.3 RecName: Full=Mitochondrial import receptor subunit TOM9-2; AltName: Full=Mitochondrial import receptor subunit TOM22 homolog 2; AltName: Full=Translocase of outer membrane 22 kDa subunit homolog 2; AltName: Full=Translocase of outer membrane 9 kDa subunit TOM9-2 && -
LOC123071367	8.009272	0.480613	NC_057801.1	6.31E+08	6.31E+08	heat shock cognate 70 kDa protein-like && P09189.1 RecName: Full=Heat shock cognate 70 kDa protein && -
LOC123085359	8.261598	0.480613	NC_057803.1	93710620	93711839	uncharacterised LOC123085359 && - && - - && Q76C99.1 RecName: Full=Protein Rf1, mitochondrial; AltName: Full=Fertility restorer; AltName: Full=Protein PPR; AltName: Full=Restorer for CMS; Flags: Precursor && -
LOC123106907	8.251943	0.480613	NC_057795.1	61987932	61993146	pentatricopeptide repeat-containing protein At5g46100-like%2C transcript variant X1 && Q9FNL2.1 RecName: Full=Pentatricopeptide repeat-containing protein At5g46100 && -
LOC123070321	7.662567	0.480613	NC_057801.1	4.54E+08	4.54E+08	uncharacterised LOC123166932 && - && -
LOC123166932	8.26513	0.480613	NC_057814.1	5.98E+08	5.98E+08	uncharacterised LOC123096393 && - && -
LOC123096393	7.635395	0.480613	NC_057805.1	86696919	86698511	uncharacterised LOC123160739%2C transcript variant X1 && Q8LPT3.1 RecName: Full=Membrane protein of ER body-like protein && -
LOC123160739	6.90489	0.480613	NC_057813.1	4.9E+08	4.9E+08	putative tRNA (cytidine(32)/guanosine(34)-2'-O)- methyltransferase%2C transcript variant X2 && Q9UET6.2 RecName: Full=Putative tRNA (cytidine(32)/guanosine(34)-2'-O)- methyltransferase; AltName: Full=2'-O-ribose RNA methyltransferase TRM7 homolog; AltName: Full=Protein ftsJ homolog 1 && -
LOC123051523	4.555658	0.481805	NC_057799.1	54934913	54945151	serpin-Z1-like && Q9ST57.1 RecName: Full=Serpin-Z2A; AltName: Full=TriaeZ2a; AltName: Full=WSZ2a && -
LOC123083299	7.71813	0.481805	NC_057803.1	7.1E+08	7.1E+08	- && - && -
-	7.583362	0.481805	NC_057799.1	1.85E+08	1.85E+08	
LOC123070265	7.655401	0.501123	NC_057801.1	4.43E+08	4.43E+08	uncharacterised LOC123070265 && - && -
LOC123181873	7.616677	0.502684	NC_057796.1	3.36E+08	3.36E+08	uncharacterised LOC123181873 && - && -
LOC123062689	7.930723	0.504037	NC_057800.1	6.24E+08	6.24E+08	reticuline oxidase-like && P93479.1 RecName: Full=Reticuline oxidase; AltName: Full=Berberine bridge-forming enzyme;



LOC123051304	7.656182	0.504037	NC_057799.1	31140440	31147799	Short=BBE; AltName: Full=Tetrahydroprotoberberine synthase; Flags: Precursor && -
LOC123096727	8.200015	0.50618	NC_057805.1	1.21E+08	1.21E+08	disease resistance protein RGA5-like%2C transcript variant X3 && Q9STE5.1 RecName: Full=Putative disease resistance RPP13-like protein 2 && -
LOC123104927	5.802077	0.50618	NC_057806.1	5.76E+08	5.76E+08	acyl-coenzyme A thioesterase 13-like && - && - uncharacterised LOC123104927%2C transcript variant X2 && - && -
LOC123175826	8.238001	0.612192	NW_025231539.1	7950	9839	-
LOC123073146	8.170947	0.620392	NC_057801.1	6.05E+08	6.05E+08	18S ribosomal RNA && - && -
LOC123134872	8.10838	0.620392	NC_057810.1	6.86E+08	6.86E+08	small nucleolar RNA Z122 && - && -
-	8.103068	0.620392	NC_057801.1	7.48E+08	7.48E+08	- && - && -
LOC123130624	8.104025	0.632267	NC_057809.1	3.38E+08	3.38E+08	- && - && - uncharacterised LOC123130624%2C transcript variant X1 && - && -
LOC123049875	8.037154	0.683165	NC_057799.1	5.43E+08	5.43E+08	-
LOC123156021	7.798576	0.687545	NC_057813.1	16798271	16798928	probable cation transporter HKT7 && Q7XPF7.2 RecName: Full=Probable cation transporter HKT7; Short=OsHKT7 && - histone H3.2-like && P68427.2 RecName: Full=Histone H3.2 >P68428.2 RecName: Full=Histone H3.2 >P68429.2 RecName: Full=Histone H3.2; AltName: Full=Histone H3.1; AltName: Full=Major histone H3 >P68430.2 RecName: Full=Histone H3.2 && -
LOC123095697	8.043412	0.694342	NC_057805.1	11107779	11110683	protein NRT1/ PTR FAMILY 8.3-like && P46032.1 RecName: Full=Protein NRT1/ PTR FAMILY 8.3; Short=AtNPF8.3; AltName: Full=Histidine-transporting protein; AltName: Full=Peptide transporter PTR2 && -
LOC123168692	8.120003	0.705507	NC_057814.1	4.52E+08	4.52E+08	cytochrome P450 734A4-like && Q69XM6.1 RecName: Full=Cytochrome P450 734A4 && -
-	8.08929	0.705507	NC_057804.1	5.16E+08	5.16E+08	- && - && - uncharacterised LOC123161202%2C transcript variant X2 && - && -
LOC123161202	7.982186	0.705507	NC_057813.1	2.11E+08	2.11E+08	-
-	7.99874	0.705507	NC_057805.1	2.93E+08	2.93E+08	- && - && -
LOC123168135	7.632208	0.708476	NC_057796.1	2.56E+08	2.56E+08	uncharacterised LOC123168135 && - && -

## 4

**Appendix Table 4:** Differentially Expressed Genes in Paragon parent line when compared with high and low N treatment. log2fold change was >1 and Padj value <0.05. This list is obtained when less stringent log2fold change and Padj value threshold criteria is used.

Gene_Name	log2FoldChange	Padj	Gene_chr	Gene_start	Gene_end	Gene_description
LOC123096427	8.674048	0.024507	NC_057805.1	92412883	92414993	uncharacterised LOC123096427 && - && -
LOC123046757	8.650302	0.056207	NC_057798.1	6.92E+08	6.92E+08	ATP synthase subunit alpha%2C chloroplastic-like && P12112.2 RecName: Full=ATP synthase subunit alpha, chloroplastic; AltName: Full=ATP synthase F1 sector subunit alpha; AltName: Full=F-ATPase subunit alpha && - salicylic acid-binding protein 2-like && Q6RYA0.1
LOC123058669	8.449381	0.037134	NC_057800.1	5.71E+08	5.71E+08	RecName: Full=Salicylic acid-binding protein 2; Short=NtSABP2; AltName: Full=Methyl salicylate esterase && -
LOC123122714	8.428795	0.021598	NC_057808.1	4.56E+08	4.56E+08	nuclear receptor corepressor 2-like && - && -
-	8.267957	0.179849	NC_057799.1	3.34E+08	3.34E+08	- && - && -
LOC123185354	8.199563	0.043532	NC_057797.1	4.23E+08	4.23E+08	uncharacterised LOC123185354 && - && -
LOC123140810	8.148035	0.056207	NC_057811.1	16940521	16943270	mitochondrial amidoxime reducing component 2-like%2C transcript variant X2 && - && -
LOC123161904	8.12803	0.048108	NC_057813.1	2.88E+08	2.88E+08	uncharacterised LOC123161904 && - && -
-	8.06757	0.057476	NC_057811.1	3.37E+08	3.37E+08	- && - && -
LOC123135750	8.053904	0.056207	NC_057810.1	57399050	57400458	uncharacterised LOC123135750 && - && -
LOC123091550	7.998787	0.295482	NC_057804.1	1.49E+08	1.49E+08	uncharacterised LOC123091550%2C transcript variant X2 && - && -

LOC12307069 9	7.998291	0.29403 4	NC_057801.1	5.21E+08	5.21E+08	FBD-associated F-box protein At4g10400-like && Q9LXJ7.2 RecName: Full=FBD-associated F-box protein At3g52670 && -
-	7.974405	0.07745 2	NC_057804.1	1.20E+08	1.20E+08	- && - && -
LOC12314696 8	7.946707	0.09576 5	NC_057812.1	3.88E+08	3.88E+08	cingulin-like && - && -
LOC12313464 7	7.920697	0.11207 2	NC_057810.1	6.39E+08	6.39E+08	auxin-responsive protein SAUR32-like && Q9ZUZ3.1 RecName: Full=Auxin-responsive protein SAUR32; AltName: Full=Protein ABOLISHED APICAL HOOK MAINTENANCE 1; AltName: Full=Protein SMALL AUXIN UP RNA 32 && -
LOC12310702 9	7.897006	0.12495 4	NC_057806.1	4.15E+08	4.15E+08	probable inactive receptor kinase RLK902 && Q9LVI6.1 RecName: Full=Probable inactive receptor kinase RLK902; AltName: Full=Receptor-like kinase 902; Flags: Precursor && -
LOC12307157 3	7.894915	0.17051 3	NC_057801.1	6.66E+08	6.66E+08	uncharacterised LOC123071573 && - && -
LOC12312192 5	7.869721	0.11940 4	NC_057808.1	3.79E+08	3.79E+08	IRK-interacting protein-like && Q9LXU9.1 RecName: Full=IRK-interacting protein && -
LOC12313075 5	7.768423	0.38975 8	NC_057809.1	4.64E+08	4.64E+08	zinc finger protein ZAT1-like && Q9M202.1 RecName: Full=Zinc finger protein ZAT9 && -
LOC12304690 9	7.76544	0.17984 9	NC_057798.1	7.15E+08	7.15E+08	- && O04790.1 RecName: Full=Flavonoid 3',5'-hydroxylase; Short=F3'5'H; AltName: Full=Cytochrome P450 75A7 && -
-	7.74556	0.16643 4	NC_057813.1	7.21E+08	7.21E+08	- && sp Q9ZVR5 PP2B2_ARATH Putative F-box protein PP2-B2 OS=Arabidopsis thaliana OX=3702 GN=PP2B2 PE=4 SV=2 && -
LOC12306511 9	7.699723	0.03713 4	NC_057801.1	1.61E+08	1.61E+08	uncharacterised LOC123065119 && - && -
LOC12307057 8	7.674985	0.17984 9	NC_057801.1	5.00E+08	5.00E+08	aspartic proteinase NANA%2C chloroplast-like && Q766C2.1 RecName: Full=Aspartic proteinase nepenthesin-2; AltName: Full=Nepenthesin-II; Flags: Precursor && -

LOC12306917 6	7.661832	0.20608 2	NC_057801.1	1.64E+08	1.64E+08	double-strand break repair protein MRE11-like%2C transcript variant X2 && Q7XQR9.2 RecName: Full=Double-strand break repair protein MRE11; Short=OsMre11 >Q25AA3.1 RecName: Full=Double-strand break repair protein MRE11; Short=OsMre11 && -
-	7.65982	0.17984 9	NC_057812.1	4.52E+08	4.53E+08	- && - && -
LOC12312770 0	7.638672	0.21851 9	NC_057809.1	4.14E+08	4.14E+08	photosynthetic NDH subunit of lumenal location 3%2C chloroplastic-like%2C transcript variant X1 && - && - ATP-dependent RNA helicase DEAH13-like%2C transcript variant X2 && Q9C813.1 RecName: Full=ATP-dependent RNA helicase DEAH13; AltName: Full=Protein FASCIATED STEM 4; Short=AtFAS4 && -
LOC12313689 4	7.632545	0.21851 9	NC_057810.1	2.66E+08	2.66E+08	
TRNAG-CCC	7.624768	0.36819 7	NC_057798.1	1.08E+08	1.08E+08	tRNA-Gly && - && -
LOC12310303 7	7.621213	0.19706 3	NC_057794.1	1.01E+08	1.01E+08	glutathione S-transferase 4-like && P46420.2 RecName: Full=Glutathione S-transferase 4; AltName: Full=GST class-phi member 4; AltName: Full=GST-27; AltName: Full=GST-IV && -
-	7.615514	0.18532 7	NC_057803.1	6.62E+08	6.62E+08	- && - && -
LOC12312077 1	7.60256	0.19706 3	NC_057795.1	3.03E+08	3.03E+08	uncharacterised LOC123120771%2C transcript variant X2 && - && -
LOC12310692 6	7.601041	0.19706 3	NC_057806.1	3.65E+08	3.65E+08	uncharacterised LOC123106926%2C transcript variant X1 && - && -
LOC12304431 3	7.589825	0.23847 1	NC_057798.1	1.95E+08	1.95E+08	uncharacterised LOC123044313 && - && -
LOC12305177 9	7.584695	0.23847 1	NC_057799.1	82405854	82408522	beta-glucosidase 26-like && A3BMZ5.1 RecName: Full=Beta-glucosidase 26; Short=Os7bglu26; Flags: Precursor && -
-	7.57829	0.26276 5	NC_057806.1	6.08E+08	6.08E+08	- && - && -

LOC12305832 2	7.57797	0.22448 2	NC_057800.1	3.45E+08	3.45E+08	uncharacterised LOC123058322 && - && - pentatricopeptide repeat-containing protein
LOC12311138 0	7.567856	0.23847 1	NC_057807.1	2.80E+08	2.80E+08	At3g09040%2C mitochondrial-like && Q9FWA6.2 RecName: Full=Pentatricopeptide repeat-containing protein At3g02330 && -
LOC12305293 4	7.567621	0.24313 4	NC_057799.1	3.20E+08	3.20E+08	factor of DNA methylation 1-like && Q9SAI1.1 RecName: Full=Factor of DNA methylation 5 && -
LOC12315409 9	7.563564	0.19706 3	NC_057812.1	57796110	57802074	phosphomannomutase-like && Q1W374.1 RecName: Full=Phosphomannomutase; AltName: Full=TaPMM && -
LOC12318925 8	7.557919	0.23847 1	NC_057797.1	5.31E+08	5.31E+08	uncharacterised LOC123189258 && - && -
LOC12305436 8	7.557481	0.22448 2	NC_057799.1	5.43E+08	5.43E+08	- && Q7XPF8.2 RecName: Full=Cation transporter HKT4; Short=OsHKT4 && -
LOC12314987 8	7.491049	0.24313 4	NC_057795.1	6.95E+08	6.95E+08	translation initiation factor IF-2-like && - && -
LOC12309959 6	7.46743	0.37029 8	NC_057805.1	55241090	55242986	uncharacterised LOC123099596 && - && -
LOC12305739 3	7.461612	0.30146 9	NC_057800.1	26104	30516	- && Q339N5.2 RecName: Full=Cellulose synthase-like protein H1; AltName: Full=OsCslH1 && -
LOC12309394 2	7.411823	0.35060 3	NC_057804.1	6.58E+08	6.58E+08	formyltetrahydrofolate deformylase 2%2C mitochondrial- like && F4JP46.1 RecName: Full=Formyltetrahydrofolate deformylase 2, mitochondrial; Flags: Precursor && -
-	7.381701	0.35060 3	NC_057799.1	3.99E+08	3.99E+08	- && - && PF14372:Domain of unknown function (DUF4413)
LOC12314599 2	7.365035	0.37029 8	NC_057811.1	4.71E+08	4.71E+08	putative FBD-associated F-box protein At5g38570 && Q9FJT2.1 RecName: Full=Putative F-box/FBD/LRR-repeat protein At5g56810 && -
LOC12313024 9	7.354548	0.36501 5	NC_057809.1	53770191	53771364	uncharacterised LOC123130249 && - && -
LOC12303923 0	7.353491	0.38479 7	NC_057798.1	3.93E+08	3.93E+08	- && P08477.1 RecName: Full=Glyceraldehyde-3- phosphate dehydrogenase 2, cytosolic && -

LOC12314848 9	7.349169	0.36819 7	NC_057812.1	5.93E+08	5.93E+08	pentatricopeptide repeat-containing protein At1g03540-like && Q9LR69.1 RecName: Full=Pentatricopeptide repeat-containing protein At1g03540 && -
LOC12305038 9	7.337312	0.37029 8	NC_057799.1	6.12E+08	6.12E+08	tryptophan decarboxylase 1-like && P17770.1 RecName: Full=Aromatic-L-amino-acid decarboxylase; Short=AADC; AltName: Full=DOPA decarboxylase; AltName: Full=Tryptophan decarboxylase && -
LOC12315350 6	7.320334	0.36819 7	NC_057812.1	5.79E+08	5.79E+08	uncharacterised mitochondrial protein AtMg00810-like && P10978.1 RecName: Full=Retrovirus-related Pol polyprotein from transposon TNT 1-94; Includes: RecName: Full=Protease; Includes: RecName: Full=Reverse transcriptase; Includes: RecName: Full=Endonuclease && -
LOC12307506 6	7.315128	0.37029 8	NC_057802.1	4.98E+08	4.98E+08	cytosolic sulfotransferase 5-like && Q8RV79.1 RecName: Full=Cytosolic sulfotransferase 11; Short=AtSOT11 && -
LOC12315944 7	7.312992	0.36819 7	NC_057813.1	6.67E+08	6.67E+08	uncharacterised LOC123159447%2C transcript variant X5 && Q9FYH7.3 RecName: Full=Vacuolar-sorting receptor 6; Short=AtVSR6; AltName: Full=BP80-like protein d; Short=AtBP80d; AltName: Full=Epidermal growth factor receptor-like protein 6; Short=AtELP6; Flags: Precursor && -
LOC12312698 8	7.302718	0.38479 7	NC_057795.1	3.96E+08	3.96E+08	MADS-box transcription factor 56-like%2C transcript variant X2 && A2Z9Q7.2 RecName: Full=MADS-box transcription factor 56; AltName: Full=FDRMADS8; AltName: Full=OsMADS56; AltName: Full=RMADS214 && -
LOC12312418 6	7.284266	0.37347 3	NC_057808.1	31348768	31350433	uncharacterised LOC123124186 && - && -
LOC12308650 9	7.282916	0.38479 7	NC_057803.1	4.84E+08	4.84E+08	putative HVA22-like protein g && Q8GXE9.2 RecName: Full=HVA22-like protein j; Short=AtHVA22j && -
LOC12310020 9	7.269707	0.38479 7	NC_057805.1	4.35E+08	4.35E+08	uncharacterised LOC123100209 && - && -
LOC12308728 9	7.26574	0.37630 8	NC_057803.1	5.93E+08	5.93E+08	uncharacterised LOC123087289%2C transcript variant X3 && Q9AWM9.1 RecName: Full=Ribosome production factor 2 homolog; AltName: Full=Brix domain-containing

LOC12313800 2	7.091934	0.28460 4	NC_057810.1	5.61E+08	5.61E+08	protein 1 homolog; AltName: Full=Ribosome biogenesis protein RPF2 homolog && -
LOC12313242 0	7.002314	0.17984 9	NC_057809.1	1.19E+08	1.19E+08	uncharacterised LOC123138002 && - && - urease accessory protein F-like%2C transcript variant X2 && E0ZS46.1 RecName: Full=Urease accessory protein F; Short=AtUREF >Q0E3L5.2 RecName: Full=Urease accessory protein F; Short=AtUREF && -
LOC12313585 0	6.963965	0.18532 7	NC_057810.1	70038876	70042341	probable LRR receptor-like serine/threonine-protein kinase At3g47570 && Q2R2D5.1 RecName: Full=Receptor kinase-like protein Xa21; Contains: RecName: Full=Receptor kinase-like protein Xa21, processed; Flags: Precursor && -
LOC12307685 1	6.897696	0.24771 3	NC_057802.1	10411946	10415066	beta-1%2C2-xylosyltransferase XAX1-like && - && -
LOC12313016 3	6.766855	0.37029 8	NC_057809.1	34456683	34461555	uncharacterised LOC123130163%2C transcript variant X2 && Q8LG98.2 RecName: Full=Ubiquitin thioesterase otubain-like; AltName: Full=Deubiquitinating enzyme otubain-like; AltName: Full=Ubiquitin-specific-processing protease otubain-like && -
LOC12318524 2	6.691794	0.11855 8	NC_057797.1	3.08E+08	3.08E+08	uncharacterised LOC123185242 && - && -
-	6.673342	0.36819 7	NC_057806.1	81958348	81959648	- && - && -
LOC12318130 5	6.575432	0.08955 1	NC_057796.1	2.55E+08	2.55E+08	protein ROOT PRIMORDIUM DEFECTIVE 1-like%2C transcript variant X2 && Q689D6.1 RecName: Full=Protein ROOT PRIMORDIUM DEFECTIVE 1 && -
LOC12313897 8	6.346696	0.21851 9	NC_057810.1	6.68E+08	6.68E+08	RING-H2 finger protein ATL13-like && Q940Q4.2 RecName: Full=RING-H2 finger protein ATL13; AltName: Full=RING-type E3 ubiquitin transferase ATL13 && -
LOC12310247 4	6.252235	0.19706 3	NC_057806.1	97590134	97592214	dof zinc finger protein DOF5.1-like && Q9LZ56.1 RecName: Full=Dof zinc finger protein DOF5.1; Short=AtDOF5.1 && -

LOC12318621 1	6.118924	0.37029 8	NC_057797.1	7.23E+08	7.23E+08	anthocyanidin reductase ((2S)-flavan-3-ol-forming)-like && D7U6G6.1 RecName: Full=Anthocyanidin reductase ((2S)-flavan-3-ol-forming); Short=VvANR && -
LOC12309197 7	6.083705	0.37029 8	NC_057804.1	2.74E+08	2.74E+08	uncharacterised LOC123091977 && - && -
LOC12318052 7	6.078419	0.26705 8	NC_057796.1	92272958	92274360	putative serpin-Z5 && Q53MD3.1 RecName: Full=Putative serpin-Z5; AltName: Full=OrysaZ5 && -
LOC12316465 9	6.03146	0.24313 4	NC_057814.1	5.83E+08	5.83E+08	F-box protein At5g07610-like && Q9FLS0.1 RecName: Full=F-box protein At5g07610 && -
LOC12315985 2	6.00611	0.19706 3	NC_057813.1	6.00E+08	6.00E+08	E3 ubiquitin-protein ligase BOI-like && Q9LDD1.1 RecName: Full=Probable BOI-related E3 ubiquitin-protein ligase 3; AltName: Full=RING-type E3 ubiquitin transferase BRG3 && -
LOC12307039 5	5.945405	0.37029 8	NC_057801.1	4.66E+08	4.66E+08	nucleobase-ascorbate transporter LPE1-like && Q41760.2 RecName: Full=Nucleobase-ascorbate transporter LPE1; AltName: Full=Leaf permease protein 1 && -
-	5.900557	0.37029 8	NC_057801.1	15343862	15345258	- && - && -
LOC12309067 4	5.78897	0.37029 8	NC_057804.1	21649814	21654040	uncharacterised LOC123090674 && - && -
LOC12308741 2	5.682856	0.36819 7	NC_057803.1	6.01E+08	6.01E+08	1-aminocyclopropane-1-carboxylate oxidase homolog 1-like && Q84MB3.1 RecName: Full=1-aminocyclopropane-1-carboxylate oxidase homolog 1 && -
LOC12312175 2	5.431828	0.36562 8	NC_057808.1	3.59E+08	3.59E+08	tuliposide A-converting enzyme b1%2C amyloplastic-like && R4X244.1 RecName: Full=Tuliposide A-converting enzyme b1, amyloplastic; Short=TgTCEA-b1; Flags: Precursor && -
LOC12314319 3	5.393769	0.37029 8	NC_057811.1	25382626	25384662	pentatricopeptide repeat-containing protein At2g22410%2C mitochondrial-like && Q9FIF7.1 RecName: Full=Putative pentatricopeptide repeat-containing protein At5g59200, chloroplastic; AltName: Full=Protein ORGANELLE TRANSCRIPT PROCESSING 80; Flags: Precursor && -



-	5.366966	0.16643 4	NW_025250379. 1	987	2140	- && - && -
LOC12310551 5	5.296279	0.37029 8	NC_057806.1	6.37E+08	6.37E+08	uncharacterised LOC123105515%2C transcript variant X6 && Q2V6J9.1 RecName: Full=UDP-glucose flavonoid 3-O-glucosyltransferase 7; AltName: Full=Flavonol 3-O-glucosyltransferase 7; Short=FaGT7 && - cysteine-rich receptor-like protein kinase 10%2C transcript variant X2 && Q8GWJ7.2 RecName: Full=Cysteine-rich receptor-like protein kinase 19; Short=Cysteine-rich RLK19; Flags: Precursor && -
LOC12314212 0	5.092907	0.20608 2	NC_057811.1	4.75E+08	4.75E+08	uncharacterised LOC123185058 && - && -
LOC12318505 8	5.044181	0.37029 8	NC_057797.1	1.61E+08	1.61E+08	uncharacterised LOC123064312 && - && -
LOC12306431 2	4.882561	0.19706 3	NC_057801.1	11594982	11595965	heat stress transcription factor A-5-like && Q6K6S5.1 RecName: Full=Heat stress transcription factor A-5; AltName: Full=Heat stress transcription factor 6; Short=OsHsf-06 && -
LOC12314362 6	4.301124	0.26592 9	NC_057811.1	74631408	74635255	protein FAR1-RELATED SEQUENCE 6-like && - && -
LOC12314421 9	4.232242	0.36819 7	NC_057811.1	1.51E+08	1.51E+08	RNA pseudouridine synthase 4%2C mitochondrial-like && Q69K07.1 RecName: Full=RNA pseudouridine synthase 4, mitochondrial; AltName: Full=RNA pseudouridylate synthase 4; AltName: Full=RNA-uridine isomerase 4; Flags: Precursor && -
LOC12311146 5	4.027507	0.11855 8	NC_057807.1	2.93E+08	2.93E+08	uncharacterised LOC123105458 && - && -
LOC12310545 8	3.034807	0.17984 9	NC_057806.1	6.28E+08	6.28E+08	uncharacterised LOC123120074%2C transcript variant X3 && - && -
LOC12312007 4	2.036179	0.36819 7	NC_057795.1	2.92E+08	2.92E+08	- && Q93V78.1 RecName: Full=Thiocyanate methyltransferase 1 && -
LOC12308766 3	1.298529	0.17984 9	NC_057803.1	6.21E+08	6.21E+08	probable inactive shikimate kinase like 2%2C chloroplastic && O82290.2 RecName: Full=Probable inactive shikimate
LOC12312632 0	1.17423	0.36819 7	NC_057795.1	3.88E+08	3.88E+08	

kinase like 2, chloroplastic; Short=AtSKL2; Flags: Precursor  
&& -

5

Appendix Table 5: Weather data Temperature (Min) °C, Temperature(Max) °C, Rain (mm), Relative Humidity (%), Solar Radiation (J cm<sup>-2</sup>) at Rothamsted Research, site, year 2018-19

2018-19 Month	Temperature (Max) °C	Temperature (Min) °C	Rain (mm)	Solar Radiation (J cm <sup>-2</sup> )	Relative Humidity (%)
October	14.96	7.24	2.21	706.92	86.17
November	10.78	4.93	2.13	331.10	91.60
December	9.29	3.54	2.50	193.29	92.27
January	6.30	0.90	1.01	285.78	87.40
February	10.91	1.85	1.55	597.35	92.37
March	11.37	4.27	2.01	901.91	81.80
April	13.94	3.62	0.44	1395.93	75.57
May	16.23	6.22	1.42	1718.24	71.30
June	19.30	10.16	2.36	1672.52	74.13
July	23.16	12.90	1.50	1762.71	69.07
August	23.21	12.38	1.51	1615.25	72.17
September	19.47	10.32	2.50	1180.49	74.97

## 6

Appendix Table 6: Weather data Temperature (Min) °C, Temperature(Max) °C, Rain (mm), Relative Humidity (%), Solar Radiation (J cm<sup>-2</sup>) at Sutton Bonington, site, year 2018-19

<b>2018-19 Month</b>	<b>Temperature (Mean) °C</b>	<b>Rain (mm)</b>	<b>Relative Humidity (%)</b>	<b>Irradiance MJ/m2</b>
October	10.89	1.15	80.87	6.59
November	8.31	1.01	86.09	2.93
December	7.10	2.42	88.02	1.87
January	4.42	0.63	82.98	2.57
February	6.57	1.07	82.09	5.87
March	7.99	1.83	77.54	9.97
April	8.44	1.06	77.20	14.93
May	11.29	1.32	76.07	17.97
June	14.25	4.21	80.85	15.72
July	17.80	2.83	76.51	17.54
August	17.59	2.31	74.51	16.06